

Structural and mechanistic studies of post-translationally modified peptides and proteins

A thesis submitted for the degree of Doctor of Philosophy

by Thi Thanh Nha Tran

M.Sc.(Chemistry)

from the

Department of Chemistry



September 2014

CONTENTS

Acknowledgments	i
Statement Of Originality	ii
Abstract	iii
Chapter 1: Mass spectrometry based proteomics: an overview	1
1.1 Introduction to mass spectrometry based proteomics	1
1.2 Mass spectrometry of peptides and proteins	2
1.3 Electrospray ionisation	4
1.4 Nanospray	7
1.5 Q-TOF 2 mass spectrometer	8
1.6 Peptide/protein preparation for mass spectrometry	11
1.6.1 Protein separation	12
1.6.2 Protein digestion	13
1.6.3 Peptide clean up prior to MS	14
1.7 Peptide/protein sequencing by mass spectrometry	14
1.8 Positive ion mass spectrometry	15
1.8.1 Proton mobility and fragmentation pathways of low-energy collision-induced dissociation	15
1.8.2 Positive ion fragmentations for peptide sequencing	17
1.9 Negative ion mass spectrometry	19
1.9.1 Amide backbone cleavages.....	19
1.9.2 Side-chain induced backbone cleavages	21
1.9.3 β' (beta prime) fragmentation	23
1.9.4 Characteristic side-chain fragmentations	24
1.10 Post-translational modification	25
Chapter 2: Investigation of phosphorylated peptides by negative ion mass spectrometry	29
2.1 Introduction to phosphoproteome analysis by mass spectrometry	29
2.2 Tandem mass spectrometry and dissociation techniques for phosphoproteome analysis	30

2.2.1 Phosphopeptide detection	30
2.2.2 Phosphorylation site localization and peptide sequencing by positive ion mass spectrometry	33
2.2.3 Peptide/protein phosphorylation under investigation of negative CID mass spectrometry	36
2.3 Results and discussion	39
2.3.1 pTyr containing peptides: phosphate rearrangement to the C-terminal carboxylate anion followed by cyclisation/cleavage reactions of the resultant (M-H) ⁻ anions	39
2.3.2 pTyr rearrangement to an internal carboxylate anion of Asp or Glu	45
2.3.3 Phosphate rearrangement from pSer/Thr to carboxylate anion centres	53
2.3.4 Phosphate migration between modified and unmodified amino acid residues of Tyr, Ser and Thr in monophospho-peptides (M-H) ⁻ anions	60
2.3.5 Phosphate rearrangement between two serine residues in the (M-H) ⁻ of monophosphorylated peptides	63
2.3.6 Migration behaviour of the phosphate group in di- and tri-phosphorylated serine containing peptides	67
2.4 Summary and conclusions	71
2.5 Experimental	72
2.5.1 Peptide synthesis	72
2.5.2 Mass spectra	72
Chapter 3: Investigation of sulfated peptides by negative ion mass spectrometry.....	73
3.1 Introduction to sulfoproteome	73
3.2 Mass spectrometry based methods for analysis of sulfation	74
3.2.1 Detection of sulfation in sulfated peptides/proteins	75
3.2.2 Differentiation of sulfation and phosphorylation modifications	76
3.2.3 Localization of sulfation sites by mass spectrometry	77
3.3 Results and discussion	79
3.3.1 Formation of deprotonated ions of sulfated peptides	79
3.3.2 Loss of SO ₃ from sulfated Tyr	80
3.3.3 Sulfate rearrangement from sulfate Tyr (sTyr) to a C-terminal carboxylate anion	84
3.3.4 Sulfate rearrangement from sTyr to Ser	86

3.3.5 Fragmentations of (M-H) ⁻ ions of peptides with Ser(SO ₃ H) in the C-terminal position. Formation of HOSO ₃ ⁻ and [(M-H) - H ₂ SO ₄] ⁻	89
3.3.6 Fragmentations of (M-H) ⁻ ions of peptides with Ser(SO ₃ H) in the C-terminal position. The formation of [(M-H) - SO ₃] ⁻	93
3.3.7 The formation of [(M-H) - SO ₃] ⁻ from a non-C-terminal Ser(SO ₃ H)	95
3.3.8 Fragmentation of a sulfated Ser peptide also containing Asp.....	96
3.3.9 Fragmentation of a disulfate peptide	97
3.4. Summary and conclusion	98
3.5 Experimental	99
3.5.1 Peptides	99
3.5.2 Mass spectra	99

Chapter 4: Identification of disulfide bonds in ricin by negative ion mass spectrometry

.....	101
4.1 Disulfide linkage in peptides and proteins	101
4.2 Positive ion mass spectrometry of disulfide linkages	101
4.3. Negative ion mass spectrometry of disulfide linkages	104
4.3.1 Intramolecular disulfide linkages.....	105
4.3.2 Intermolecular disulfides	106
4.4 Ricin: structure and bioactivity	107
4.4.1 Biosynthesis of ricin	107
4.4.2 Three dimensional structure of ricin	109
4.4.3 Ricin activity	110
4.4.4 Ricin detection and identification	111
4.5 Results and discussion	112
4.5.1 Sequencing data obtained from proteolytic digest of ricin	112
4.5.2 Identification of disulfide containing peptides from proteolytic digestion of ricin	116
4.5.3 Fragment peptides not containing disulfides	127
4.6. Summary and conclusions	132
4.7 Experimental	133
4.7.1 Materials	133
4.7.2 Digests	133
4.7.3 Synthesis of disulfide containing peptides from cysteine precursors	133

4.7.4 High performance liquid chromatography	134
4.7.5 Nanospray ionisation mass spectrometry	134
Chapter 5: Peptides from the skin glands of <i>Litoria rubella</i>	136
5.1 Peptides from amphibian skin secretions	136
5.1.1 Overview	136
5.1.2 Peptides from Australian anurans	138
5.1.3 Production of glandular peptides	140
5.1.4 Collecting skin secretions	141
5.1.5 Peptide sequencing by mass spectrometry and Edman degradation	142
5.2 <i>Litoria rubella</i> , the Red-tree frog	143
5.3 Results and discussion	147
5.3.1 HPLC separation of the skin secretions	147
5.3.2 Peptide sequence determination	149
5.3.3 Evolutionary significance of peptides from <i>L. rubella</i>	159
5.3.4 Opioid activity	160
5.4 Summary and conclusion	161
5.5 Experimental	161
5.5.1 Peptide secretion collection	161
5.5.2 HPLC separation of the skin secretions	162
5.5.3 Mass spectra	162
5.5.4 Solid state synthesis of FP-Kyn-L(NH ₂)	163
5.5.5 Biological testing	163
Chapter 6: Do neuropeptides “park” on the lipid bilayer of a membrane before moving to an adjacent active receptor site? A QCM investigation	164
6.1 Introduction	164
6.1.1 Membrane-bound pathway of receptor binding of neuropeptides	164
6.1.2 Peptides to be studied	167
6.1.3 Biomimetic membranes	170
6.1.4 Peptides/protein-membrane interactions	173
6.2 Theory of quartz crystal microbalance-dissipation	176
6.2.1 Quartz crystal microbalance: basic components and operation	176
6.2.2 Quartz crystal microbalance-dissipation in liquid phase	178

6.2.3 Measurement of resonant frequency in QCM	181
6.2.4 Measurement of the dissipation factor	183
6.3 Results and discussion	185
6.3.1 Riparin 1 and signiferin 1	185
6.3.2 Tryptophyllin 3.1 [FPWP(NH ₂)] and kynurenine-tetrapeptide [FPKynL(NH ₂)]	190
6.3.3 Tachykinin peptides: <i>iso</i> -Asp uperin 1.1 [pEA <i>iso</i> -DPNAFYGLM(NH ₂)] and uperolein [pEPDPNAFYGLM(NH ₂)]	192
6.3.4 Rothein 1 and its synthetic modifications	195
6.4 Discussion and conclusion	195
6.5 Experimental	199
6.5.1 Peptides	199
6.5.2 Buffers and solvents	199
6.5.3 Liposome preparation	200
6.5.4 Chip cleaning and modification	200
6.5.5 QCM experiments	201
Reference	203
Appendix: The 20 amino acid	249
Publications	251

ACKNOWLEDGMENTS

First and foremost I would like to thank my supervisor, Prof. John Bowie, for giving me the opportunity to work on such an interesting and diverse project, and for all his guidance and considerate advice throughout my course of PhD.

Special thanks go to my co-supervisor, Dr. Tara Pukala, for being a supportive supervisor who is willing to listen and give useful advice.

I gratefully acknowledge the Vietnamese government and the University of Adelaide for the VIET-MOET PhD scholarship, which provided financial support during my PhD course.

I would also like to recognise the help of a number of collaborators. Much appreciation goes to Prof. Michael Tyler from the Department of Zoology at the University of Adelaide for assistance in collecting the frog secretions. Many thanks must go to Prof. Lisa Martin of Monash University for providing the resources and guidance during my time doing QCM work. Thanks also to Dr. Ian Musgrave from the Department of Clinical and Experimental Pharmacology for assistance with opioid testing of tryptophyllin peptides. Appreciation must go to Dr. Craig Brinkworth from Defence Science and Technology Organisation, Melbourne, Vic., for providing peptides and advice related to ricin project.

Many thanks to the past and present members of the Bowie group for all the help they provided. Particular mention goes to Dr. Anton Calabrese and Dr. Yanqin Liu, and especially, Dr. Daniel Bilusich for help with proofreading.

Finally, I would like to thank my family for their emotional support throughout my Ph.D journey. Thanks to Mon, Dad and my little sister who have shown continuous interest in my research progress and encouraged me to finish it.

STATEMENT OF ORIGINALITY

I certify that this work contains no material which has been accepted for the award of any other degree or diploma in my name, in any university or other tertiary institution and, to the best of my knowledge and belief, contains no material previously published or written by another person, except where due reference has been made in the text.

I give consent to this copy of my thesis when deposited in the University Library, being made available for loan and photocopying, subject to the provisions of the Copyright Act 1968.

Thi Thanh Nha Tran

Date

ABSTRACT

In mass spectrometry (MS), negative ions can be formed by many ion sources, and although sometimes less predominant than their cationic counterparts, they can be observed and studied to provide complementary molecular, ionic structure and mechanistic information. The research presented in this thesis investigates the production and use of negative ions for the structural determination of underivatised peptides and proteins and some post-translationally modified peptides and proteins. An additional application of this research is to determine the structure and membrane interaction of some peptides isolated from Australian amphibians.

Phosphorylated Tyr (pTyr) containing peptides undergo S_Ni cyclisation of the C-terminal carboxylate anion at the P of the pTyr to effect transfer of PO_3H_2 to the C-terminal position. (A similar phosphate rearrangement from pTyr to side-chain carboxylate sites or to the side chains of Ser/Thr also occurs). Following proton transfer, several rearrangements initiated by this phosphate anion can occur, including a specific cyclisation to, and cleavage of, the peptide backbone at the central C of the penultimate amino acid residue. When a peptide contains two/three phosphate side chains, phosphate groups undergo phosphate/phosphate cyclisation to form characteristic di-/tri-phosphate anions. The mechanisms of all fragmentation processes are suggested with the assistance of *ab initio* theoretical calculations.

The major negative-ion fragmentation of Tyr sulfate containing peptides is $[(M-H) - SO_3]^-$ and this process normally yields the base peak of the spectrum. Rearrangement reactions involving the formation of $HOSO_3^-$ and $[(M-H) - H_2SO_4]^-$ yield minor peaks with relative abundances $\leq 10\%$ and $\leq 2\%$ respectively. A Ser sulfate containing peptide, in contrast, shows pronounced peaks due to cleavage product anions $[(M-H) - SO_3]^-$ and $HOSO_3^-$. Theoretical calculations at the CAM-B3LYP/6-311++g(d,p) level of theory suggest that rearrangement of a Ser sulfate to give C-terminal CO_2SO_3H is energetically unfavourable in comparison with fragmentation of the intact Ser sulfate to yield $[(M-H) - SO_3]^-$ and $HOSO_3^-$. $[(M-H) - H_2SO_4]^-$ anions are not observed in the spectra of peptides containing Ser sulfate, presumably because $HOSO_3^-$ is a relatively weak gas-phase base ($\Delta G_{acid} = 1265 \text{ kJ mol}^{-1}$). The peaks corresponding to anions formed following cyclisation of the sulfate groups are not detected in the spectra of energised $(M-H)^-$ ions of Ser disulfate containing peptides.

Proteolytic digest/negative ion nanospray MS was used to determine the five disulfide units and much of the amino acid sequence of ricin, addressing both ricin detection and structural confirmation. Negative ion MS is found to be more effective than positive ion MS in identification and sequencing disulfide bridged peptides. While positive ion MS only provides partial sequences of disulfide containing peptides and often does not specify the positions of disulfide residues, negative ion MS gives clear evidence for the presence and positions of disulfide linkages via characteristic fragmentations.

The skin peptide profiles of the red tree frog *Litoria rubella* (*L. rubella*) from three locations, namely Flinders Ranges, a region of south-western Queensland and Longreach (Queensland), have been investigated in an eight-month survey. Nine peptides were identified primarily using MS. While the secretion from the *L. rubella* frogs from Flinders Ranges consists of only the major peptide, tryptophyllin L1.2; the *L. rubella* frogs from the south-western Queensland and Longreach (Queensland) produce a number of small tryptophyllin peptides and two rubellidins (caeridin type). The primary structures of the major peptide tryptophyllin L1.2 and the two rubellidins (caeridin type) 4.1 and 4.2 were determined previously. The noticeable findings were the discovery of three tryptophyllin metabolite containing peptides including tryptophyllin L1.6, 1.7 and 1.8. The peptide profiles of these frog populations added more information about the evolutionary divergence of this genus.

Schwyzler and Zerbe have proposed that certain neuropeptides can transfer from extracellular fluid to attach to a cell membrane prior to moving from that membrane to the adjacent active site of a transmembrane receptor. There are differences in the detailed mechanisms proposed but the key feature is the initial addition of the neuropeptide to the membrane. The Quartz Crystal Microbalance technique with Dissipation (QCM-D) was used to see whether certain amphibian neuropeptides are able to add to a mammalian model bilayer without destroying that membrane. It appears that the peptides may have different modes of interaction with the membrane depending upon overall charges, the charge densities, the secondary structures and the free energies of transferring (to water-membrane interface and to membrane interior), and that the membrane binding may take part but not play a requisite role in a receptor-binding process.

CHAPTER 1

MASS SPECTROMETRY BASED PROTEOMICS: AN OVERVIEW

1.1 Introduction to mass spectrometry based proteomics

The fact that the human genome has barely more genes than that of the fly or worm indicates that human complexity cannot simply be rationalised by the size of the genome but rather by the way the gene products (RNA or proteins) are modified or interact [1]. The systematic study of all proteins expressed in a genome, namely proteomics, therefore becomes the focus of life science.

Unlike the relatively unchanged human genome, which consists of about 21,000 genes, the dynamic proteome with an estimated size of more than 1 million proteins keeps changing in accordance to intracellular and extracellular stress from time to time [2-4]. The increase in complexity from the level of the genome to the proteome is due to two mechanisms. The first route is by alternative mRNA splicing, resulting in the production of multiple proteins from a single gene [5]. The second route is via covalent post-translational modifications (PTMs) occurring on the side chains or peptide backbone of nascent proteins after the translation process [4, 6].

By definition, proteomics not only can provide the protein complement of a given cell at a given time but also can reflect the interaction between proteins in a cell, thus opening a window into complex cellular regulatory networks. In the biomedical field, proteomics can ideally shed light into the causes of disease or identify the initiator of a disease process [3]. In order to achieve these ambitious goals, the covalent structures of proteins in a cell must firstly be obtained. Such a task is challenging due to the complexity of the cellular proteome and the low abundance of modified proteins. In the context of the development of various techniques for protein characterisation, mass spectrometry (MS) has emerged as a major technique [7-9]. Protein analysis using MS has been rapidly advancing owing to the development of MS instrumentation and related methodologies (see section 1.2). However, proteomics still faces many technical and experimental challenges, especially related to the unambiguous identification of some PTMs (see section 1.10).

1.2 Mass spectrometry of peptides and proteins

MS is an analytical technique used to measure the molecular mass of analytes. This technique is based on the generation, separation and detection of ions in the gas phase according to their mass-to-charge ratios, providing a means for the elucidation of the chemical composition and the structure of molecules. Although the earliest concept of MS was introduced in the early 1900s, it was not until 1960s that the success of ionisation of large, polar and non-volatile molecules made MS applicable to the solution of biochemical and biological problems [10-14]. Since then, MS has become an increasingly valuable tool used to examine the structures of peptides/proteins, protein complexes, as well as protein interactions. Improvements in MS and tandem MS instrumentation have greatly advanced the selectivity, sensitivity and the mass range for peptides and proteins to be detected [15].

Peptide and protein identification using MS is determined by the interplay between MS instrumentation and gas-phase peptide chemistry. While MS instrumentation defines the ways by which peptide and protein molecules are ionised, activated and detected, factors of peptide/protein charge state, size, composition and sequence affect the bonds and the rate at which these molecules are cleaved in gas phase. Among these factors, developments in ionisation, activation methods and mass analysers have contributed significantly to the enhancement of the examination of peptide and protein structures. Ionisation techniques have progressed from “hard ionisation” to “soft ionisation” such as electrospray ionisation (ESI) and matrix assisted laser desorption ionisation (MALDI). These techniques minimise the fragmentation of parent ions within the source; allow direct analysis of large, polar and non-volatile molecules and are thus well-suited for investigation of thermally labile proteins and their complexes [9, 15].

Different types of mass analysers have evolved along with the development of ionisation methods. The early single-magnetic-sector instrument was quickly superseded by double-sector and tandem-double-sector instruments consisting of both a magnetic and an electric component. These have greatly enhanced the resolution, sensitivity and mass range of peptides and proteins studied. Four types of mass analysers commonly used now are the quadrupole mass analyser, time-of-flight (TOF), quadrupole ion-trap (Q-IT) and fourier transform ion cyclotron resonance (FTICR) [16].

Some mass analysers can be combined to generate tandem (MS/MS) or MSⁿ instruments [9, 17-19], known as tandem in space mass spectrometers, such as triple quadrupole (Q-Q-Q) [20], quadrupole time-of-flight (Q-TOF) [21], TOF-TOF [22], quadrupole linear ion trap (Q-Q-LIT) [23] and linear-trap-quadrupole Orbitrap (LTQ Orbitrap) [24-26]. In contrast, tandem in time instruments refer to mass spectrometers which isolate and fragment ions in the same mass analyser with isolation, activation and detection steps being a sequence of events separated in time. Linear-trap-quadrupole (LTQ) [27] and FTICR [16] are examples of this category. Each has its own strengths and limitations for the analysis of peptides and proteins. The characteristics of some commonly used tandem mass spectrometers are displayed in Table 1.1.

Table 1.1. Characteristics of commonly used mass spectrometers in proteomic analysis [8, 28]. Check marks indicate available, check marks in parentheses indicate optional. +, ++, and +++ indicate possible or moderate, good or high, and very high or excellent, respectively. Seq., sequential.

	IT-LIT	Q-Q-TOF	TOF-TOF	LTQ Orbitrap	FT-ICR	Q-Q-Q	Q-Q-LIT
Mass accuracy	Low	Good	Good	Excellent	Excellent	Medium	Medium
Resolving power	Low	Good	High	Very high	Very high	Low	Low
Sensitivity	Good		High	Medium	Medium	High	High
Dynamic range	Low	Medium	Medium	Medium	Medium	High	High
ESI	✓	✓		✓	✓	✓	✓
MALDI	(✓)	(✓)	✓				
MS/MS capabilities	✓	✓	✓	✓	✓	✓	✓
Additional capabilities	Seq. MS ⁿ					Precursor, neutral loss monitoring, MRM	
Identification	++	++	++	+++	+++	+	+
Quantification	+	+++	++	++	++	+++	+++
Throughput	+++	++	+++	++	++	++	++
Detection of modifications	+	++	+	+	+		+++

Proteomic analysis typically involves the isolation and gas-phase dissociation of selected precursor ions in tandem mass spectrometers. The resultant product ions can be subjected to further fragmentation reactions, which is termed MS^n ($n-1$ is the number of isolation and fragmentation rounds), so that structural information can be extracted from mass analysis. Some gas-phase dissociation methods include collision-induced dissociation (CID; also known as collision-activated dissociation CAD) [29], surface-induced dissociation [30], infrared multi-proton dissociation (IRMPD) [31], ultraviolet photodissociation (UVPD) [32], femto-second laser induced ionisation dissociation (fsLIID) [33], electron capture dissociation (ECD) [34-36], electron transfer dissociation (ETD) [37-38], electron ionisation dissociation (EID) [39], and electron-induced dissociation (eID) [40]. Of these techniques, CID, ECD and ETD are normally employed to study peptides/proteins and protein complexes, especially post-translational modified peptides/proteins [38, 41-42].

1.3 Electrospray ionisation

The idea of production of large gaseous molecular ions from highly charged droplets was first suggested by Malcolm Dole in the early 1960s [11] and developed further to the electrospray ionisation technique by John Fenn [13]. Electrospray ionisation (ESI) is a method that can transfer molecules in solution into the gas phase as ions (Figure 1.1). This provides a way to ionise high mass and non-volatile analytes such as polymers, nucleic acids and proteins [12, 43-45].

The production of isolated gaseous ions from solutes in solution at atmospheric pressure can be described as a three-step process, namely (i) formation of charged droplets at the electrospray capillary tip; (ii) reduction in size of the charged droplets by solvent evaporation to produce very small highly charged droplets; and (iii) production of gas-phase ions from very small highly charged droplets. In the first step, the sample is dissolved in a polar, volatile solvent and pumped through a narrow, stainless steel capillary (75-150 μm) at a flow rate of between 1 $\mu\text{l}/\text{min}$ and 1 ml/min . A potential difference of 2-3 kV is applied between the electrospray needle and the counter electrode. Penetration of the imposed electric field into the solution at the capillary tip causes polarisation and orientation of induced dipoles of the solvent molecules inducing the solution to conduct. This leads to the accumulation of the electrolyte ions (with the same polarity as the charge on the needle) near the surface of the meniscus, which distorts the liquid surface into a conical shape known as a

“Taylor cone”. As the charge intensity at the meniscus increases, the Taylor cone is elongated into a jet form that then produces charged droplets as the surface tension exceeds the electrostatic force. The approximate equation for the required electric field E_{on} at the onset of droplets’ formation was established by D. P. H. Smith as follows [46-48];

$$E_{\text{on}} \approx \left(\frac{2\gamma \cos \theta}{\epsilon_0 r_c} \right)^{1/2}$$

The potential V_{on} required for the onset of electrospray derived from the electric field E_{on} is given by following equation;

$$V_{\text{on}} \approx \left(\frac{r_c \gamma \cos \theta}{2\epsilon_0} \right)^{1/2} \times \ln(4d / r_c)$$

where γ is the surface tension of the solvent, ϵ_0 is the permittivity of vacuum, r_c is the radius of the capillary and θ is the half-angle for the Taylor cone.

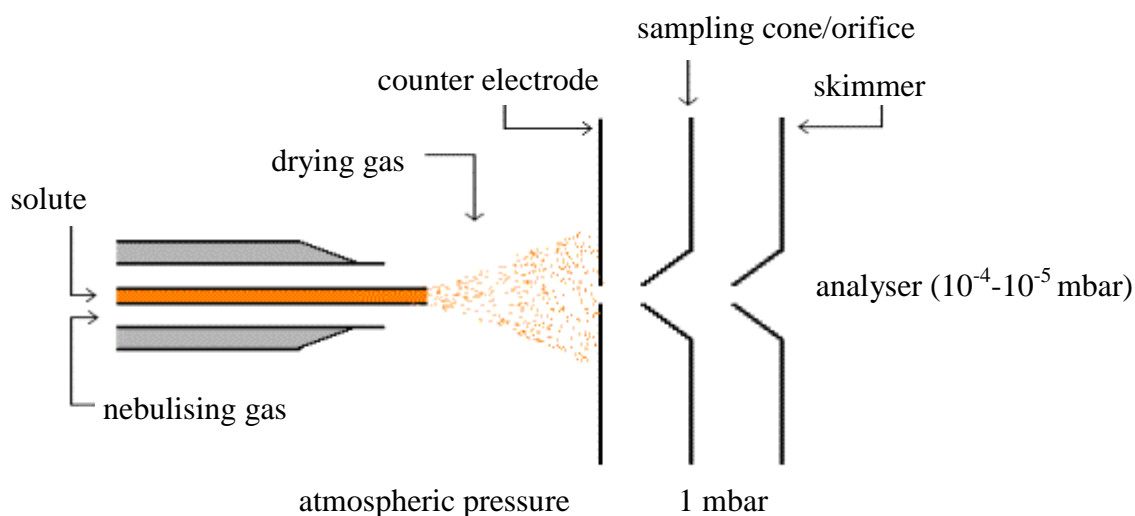


Figure 1.1. Schematic representation of the ESI process. Adapted from [46].

As the droplet travels from the needle tip to the cone, solvent evaporation occurs. The droplet shrinks until it reaches the point where the surface tension can no longer sustain the charge. At this point, the Coulombic force overcomes the cohesive surface tension force which causes the droplet to disintegrate. Fission and evaporation re-occur to produce smaller

progeny droplets until they only retain few elementary charges with radii in the nanometre range. The Rayleigh equation provides the condition for the Coulomb instability as follows;

$$Q_{Ry} = 8\pi(\epsilon_0\gamma R^3)^{1/2}$$

where Q_{Ry} is the charge on the droplet, γ is the surface tension of the solvent, R is the radius of the droplet and ϵ_0 is the permittivity of vacuum.

Two mechanisms have been suggested to explain the formation of gas-phase ions from very small and highly charged droplets. These are the charged residue model (CRM) and the ion evaporation model (IEM). The first mechanism proposed by Dole et al. [11, 49] stated that continuous solvent evaporation of the charge droplet can lead to the creation of a droplet containing one analyte molecule and some ionic charges. In contrast, the IEM suggested by Iribarne and Thomson [50] proposed that gaseous ions can be emitted directly from a highly charged droplet as soon as the droplet size is reduced to less than 10 nanometres in radius. This is due to charge repulsion among the analyte ions in the droplet. While the IEM was determined by investigation of small analyte ions such as NaCl, the validity of the CRM has been confirmed by investigation of denatured and non-denatured proteins and protein complexes [49, 51]. According to the CRM, the solvent evaporation process can result in charged droplets containing not only one protein molecule but also dimers, trimers and higher multimers of proteins. Experimental observations indicate that the monomers occur predominantly, while the abundance of dimers and trimers are much lower and decrease with an increase in multimerisation [52].

Peptides and proteins are inherently charged analytes since they contain multiple acidic and basic residues and can be deprotonated or protonated in the bulk solution or in the electrospray droplets. The charging of a protein/peptide is normally assisted by the presence of a small amount of an acid such as acetic/formic acid or a base such as ammonium hydroxide/triethylamine. Electrospray therefore serves to separate the charged peptide/protein from their counter ions and transfer them into the gas phase. However, the protonated/deprotonated ions of peptides/proteins formed in solution are not necessarily the final ion forms of peptides/protein in gas phase. This is because protons can be transferred among the analyte ions and between analytes and solvent molecules due to the difference in their gas-phase basicities [48, 53-56]. The charged peptides/proteins can also ion-pair with

impurities such as Na^+ , K^+ , Cl^- , F^- , NH_4^+ and other ions from glass containers or solvents to form adduct ions [57-60]. In the gas phase, protein- Na^+/K^+ bonding is so strong that the Na^+/K^+ forms of peptides/proteins are commonly observed if there is a trace amount of the salt present in the solution [55]. Furthermore, the electrospray response of a particular peptide/protein ion from an analyte mixture also depends on the surface activity, the ability of this peptide/protein to compete for excess charge (the charge on the surfaces of droplets) [61-63].

The choice of solvent composition has been found to have a significant effect on the electrospray process. Buffered aqueous solvents are normally the first choice for the solvent system in proteomic analysis. However, the use of only water as solvent can initiate electric discharge due to its high surface tension. The occurrence of electric discharge is manifested by the formation of the solvent cluster (e.g. $\text{H}_3\text{O}^+(\text{H}_2\text{O})_n$) which degrades the electrospray performance [64-65]. Organic solvents are commonly added to reduce this risk and to assist the spraying process. The solvents often used in ESI are a mixture of methanol-water or acetonitrile-water. Peptides/proteins which are sensitive to organic compounds can be partly denatured in these solvents [66], leading to an increase in the charge state and also a characteristic broadening of charge distribution of these peptides/proteins relative to their native states [67-68]. In addition, other factors such as the surface tension and vapour pressure of solvents have been found to affect the ESI of peptides/proteins [69-71]. A significant increase of absolute abundance of high charge states of peptides/proteins and synthetic polymer ions is normally observed when certain solvents such as glycerol and *m*-nitrobenzyl alcohol are added into the electrospray solvent. Such a supercharging phenomenon is preliminarily brought about by increasing the surface tension of the charged droplets by adding of these solvents [69, 72]. Replacement of one organic solvent by another may result in a change in the charge state; for instance, the charge state of an analyte is gradually enhanced with a change from isopropanol to acetonitrile to methanol [73].

1.4 Nanospray

Nanospray is a “microspray” version of ESI, developed by Wilm and Mann [74-75] in order to improve the sensitivity and ionisation efficiency of the electrospray technique. A spray capillary (metal-coated glass needle) with the entrance end opened is used instead of a driven syringe as in ESI. The flow is induced by the pull of the applied electric field on the

solution at the capillary tip (diameter of 1-2 μm). The droplets produced are usually 1000 times smaller than those formed by the conventional ESI and evaporate rapidly to generate gas-phase ions. The capillary tip therefore can be located close to the sampling orifice, minimizing sample loss due to travelling of spraying droplets from the capillary tip to the sampling cone. The volume of sample consumed by nanospray is much smaller than ESI in the same time period due to its low flow (nl/min). Therefore, a small volume of analyte of 0.2-10 μl is sufficient to obtain a good mass spectrum. In addition, nanospray ionisation can be performed in neat water solvent without causing electric gas discharges. It is also less affected by contaminants in the solution compared to ESI [76-80].

1.5 The Q-TOF 2 mass spectrometer

Most mass spectrometric work in this thesis was carried out using a Q-TOF 2 hybrid quadrupole time-of-flight mass spectrometer. A schematic diagram of the principal components of this instrument is presented in Figure 1.2.

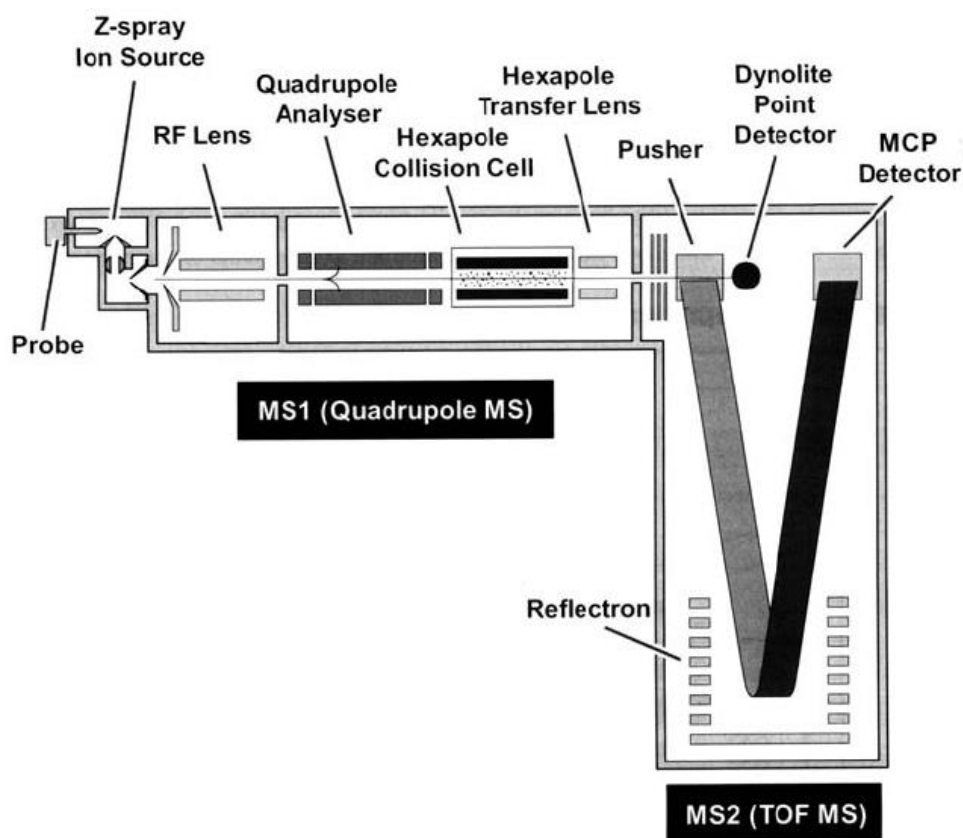


Figure 1.2. Schematic diagram of the Q-TOF 2 mass spectrometer [78].

In the Q-TOF 2, the TOF analyser that works as a mass resolving device is placed in an orthogonal position to the quadrupole mass analyser and the ion source. The quadrupole serves as an ion guide device in MS mode and as a mass selection device (mass filter) in MS/MS mode. The quadrupole and TOF analyser in the Q-TOF are separated by a hexapole collision cell. In the Z-spray ion source, ionisation in the gas phase is achieved by ESI. The resulting ions are drawn through the sample cone to the first analyser by application of an electric potential. Manipulation of the applied cone voltage can favour the selection of different mass-to-charge ratio ions. Generally, the higher the cone voltage employed, the larger the m/z ions and lower charged forms which are attracted into the analyser [81].

The quadrupole sector is comprised of four parallel rods (Figure 1.3). Fixed direct current (DC) and alternating radiofrequency (RF) potentials are applied on these rods to produce an electric field. Ions are introduced as a beam along the central axis of the rods. They experience forces from the electric field that cause them to oscillate toward and away from the rods (Figure 1.3). For a specific set of DC and RF potentials, only ions of particular m/z can have stable trajectories and are thus transmitted to the detector. All other ions with an unstable motion will be ejected from the quadrupole. Variation in the strength of DC and frequency of RF bring ions of different m/z into focus on the detector [78].

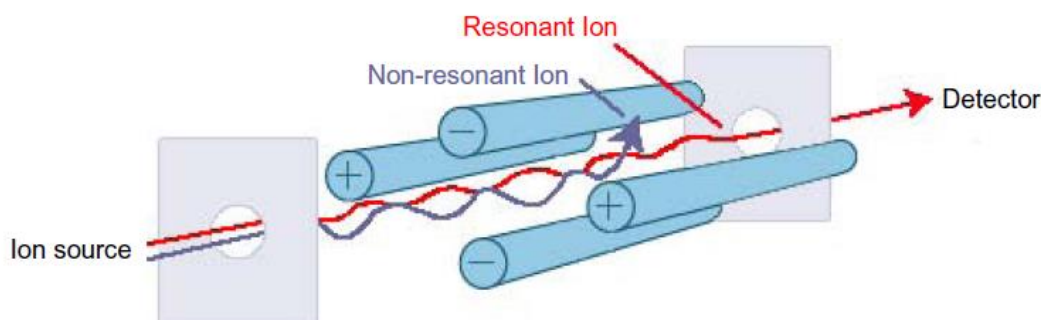


Figure 1.3. Schematic illustration for the operation of a quadrupole analyser. Adapted from [82].

In the MS mode, the quadrupole is operated in the RF-only mode, which allows ions of all m/z ratios to pass through to the pusher. The pusher accelerates ions so that they all possess identical translational energy as they enter into the TOF. The ions are pushed by an applied potential difference down the TOF tube towards the reflectron where they are

electrostatically reflected back towards the detector. All ions with common charge z leave the pusher with the same initial kinetic energy K [82].

$$K = 1/2mv^2 = zeV \quad (1) \quad (v \text{ is the velocity})$$

The velocity v is related to the time t for an ion to pass the length (d) of the tube as follows;

$$t = d/v \quad (2)$$

From (1) and (2),

$$\frac{m}{z} = \frac{2Vt^2}{d^2}$$

where m/z is the mass-to-charge ratio of the charged molecule; V is the accelerating voltage.

If the length of the flight tube and the accelerating voltage are fixed, the time it takes for an ion to reach the detector depends only on the ion mass-to-charge ratio. Thus, the ion mass-to-charge ratio can be determined via time-of-flight measurements.

An ion mirror or reflectron is built in most TOF mass analyser to reduce the effect of initial kinetic energy spread. This is due to spatial distribution of ions in the ion source or their proximity to the applied electric field which may cause poor mass resolution. A reflectron is constructed of a series of evenly spaced lenses onto which a linear electric field is applied. The ions that enter the reflectron are gradually repelled due to the potential applied across the lenses. Using the reflection can improve the mass resolution in the TOF due to the increase of the flight tube length and the decrease in arrival time distribution. For ions of the same m/z but of slightly different initial kinetic energies, the more energetic ions reach the reflectron sooner and penetrate deeper into it than the less energetic ions. Accordingly, the difference in flight path and time correct the differences in initial kinetic energies of the ions. Thus, they arrive at the detector at the same time [83].

In MS/MS mode, the ions of interest are selected by the quadrupole analyser and introduced into a hexapole collision cell where they collide with an inert gas, resulting in ion excitation and fragmentation. This process is known as CID. In a typical Q-TOF instrument, dissociation of ions is achieved by low-energy collision (20-100 eV) with heavy gases such as Ar or N₂ [84]. This normally results in backbone cleavages ions. These ions may undergo

further dissociation as they travel through the collision cell to generate internal fragment ions and immonium ions [29]. Side-chain fragments are rarely observed in the low-energy collision regime in the Q-TOF2 as they are typically formed under charge-remote conditions (see section 1.8.1). The product ions are then accelerated and collected via the pusher for subsequent mass determination in the TOF.

“MS/MS/MS” data can be achieved using the Q-TOF 2 by increasing the cone voltage to induce fragmentation of an ion (parent ion) in the ion source. The source formed fragment ion is then selected for MS/MS measurement; equivalent to an MS/MS/MS experiment. However, these data may suffer from the possibility of the selected “fragment ion” coming from a process different from the required fragmentation of the parent ion [85].

1.6 Peptide/protein preparation for mass spectrometry

The prerequisite requirement for MS analysis of peptides/proteins is to reduce the complexity of the peptide/protein sample such that the mass spectrometric response of the ions of interest are least affected by other ions in the sample. The general preparation of proteins prior to MS includes three key steps: (i) protein separation and digestion, (ii) enrichment of peptides of interest after digestion, and (iii) desalting of the peptide mixture prior to MS measurements [86]. Each of these three steps can be modified or optimized to suit the analytical purpose or strategy, the sample analyzed and the experimental setup [8] (Figure 1.4).

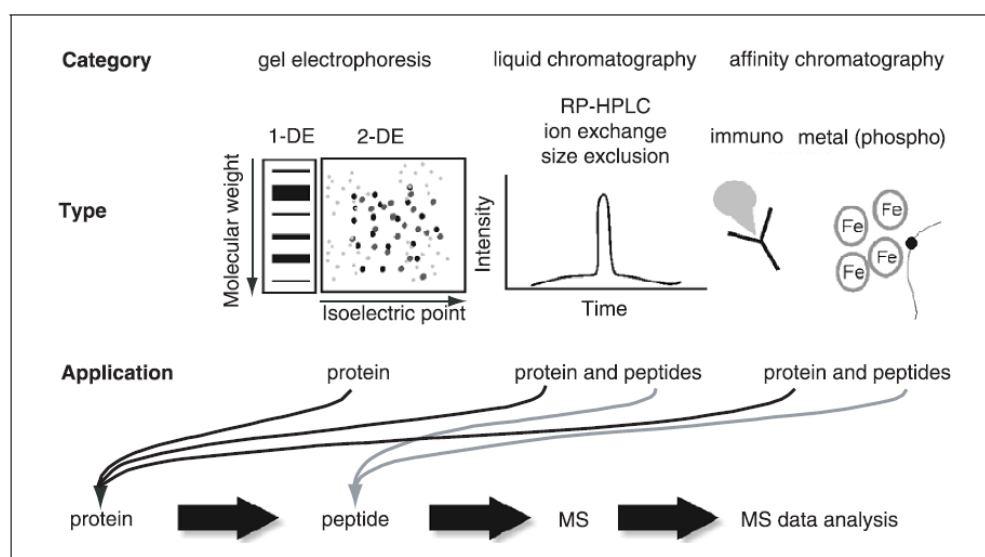


Figure 1.4. Peptide/protein separation/purification procedure for MS analysis. Adapted from [86].

1.6.1 Protein separation

Protein separation can be implemented by gel electrophoresis or high performance liquid chromatography (HPLC) techniques or less frequently by affinity capture. Belonging to the gel electrophoresis technique group, two-dimensional electrophoresis (2-DE) has been established as a robust technique to separate proteins in complex mixtures such as cellular extracts. Generally, it distributes proteins in the first dimension based on the difference in isoelectric point (pI) using a pH gradient (isoelectric focusing), and in the second dimension based on the difference in molecular weight using SDS PAGE (sodium dodecyl sulfate-polyacrylamide gel electrophoresis) [87-89]. The choice of detection method for in-gel separation is influential to the success of downstream MS analysis since different visualising dyes interact with and modify proteins differently [90-95]. Among three general classes of in-gel protein detection methods including detection with organic dyes, silver staining and fluorescence, Coomassie Blue staining and detection with fluorescence have been reported to provide good compromises between the detection sensitivity and MS compatibility [96-99].

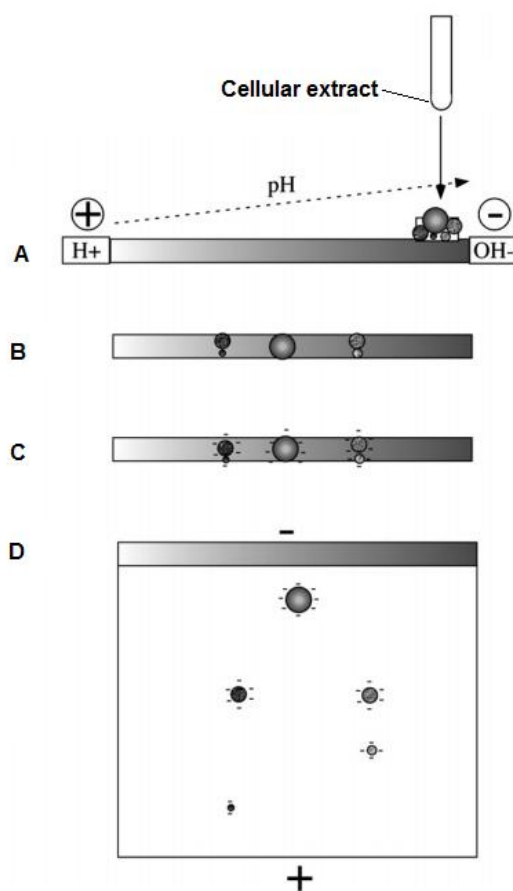


Figure 1.5. Principle of 2D gel electrophoresis separation: the sample is loaded onto a pH gradient gel (A), inducing proteins of different isoelectric points to accumulate at different distances from the OH^- side (as they reach their pI and have no remaining electrical charge) (B), the sample is then equilibrated in a SDS-containing buffer so all proteins are coated by SDS and becoming strongly negatively charged (C), finally the proteins are separated on the second dimension perpendicular to the first dimension due to differences in the molecular weights as potential difference is applied (D). Adapted from [91]

On the other hand, several types of HPLC techniques commonly used in MS based proteomics include ion exchange (IEX), reverse phase high performance liquid chromatography (RP-HPLC), hydrophilic interaction chromatography (HILIC) [28]. Among these, RP-HPLC has been recommended as the most suitable method for protein/peptide fractionation since it uses volatile solvents and results in no salt containing fractions, which is therefore compatible with protein digest or direct MS measurement [100]. The RP-HPLC separation of any peptide/protein mixture is dependent upon the strength of the hydrophobic interactions of each component in the mixture with the hydrophobic stationary phase and the elution strength of the organic solvent in the mobile phase. A gradient elution profile with concentration of organic solvents increased gradually is applied causing peptides/proteins from low to high hydrophobicity to elute [101-102]. Subtle differences in conformation and hydrophobicity of the peptides will determine the partitioning behaviour between two phases and consequently, the rate at which the peptides will move through the column [103].

The stationary phase commonly used in peptide/protein separation is a column packed with alkyl-silica sorbent which contains alkyl-terminating chains between 1 to 18 carbon atoms (C1 to C18). If carbon loading is high, smaller or more hydrophilic peptides are recovered (e.g. C18). In contrast, if carbon loading is lower, the larger or more hydrophobic peptides give higher yield, but the smaller, hydrophilic peptides do not bind [81]. Better resolution of separation can be achieved by varying the composition, pH and ionic strength of the mobile phase. A small amount of an ionic modifier (0.05-0.1% of the solvent volume) is normally added to the mobile phase to adjust the pH, solubilise the peptides and minimise ionic interactions between the peptides and the stationary phase. Trifluoroacetic acid (TFA) is commonly chosen since it gives high resolution separation and is volatile so can be easily removed. Peptides in the eluent are detected using an ultraviolet (UV) detector at a wavelength of 214 nm, corresponding to the $n-\pi^*$ transition state of the CO bond [104]. Acetonitrile is commonly used as the organic solvent due to its low viscosity and is UV transparent at 214 nm.

1.6.2 Protein digestion

The resultant protein fractions can then be digested in-gel [105] or in-solution [106] depending on the previous protein separation method. Alternatively, proteins can be transferred from a gel associated state to solution for in-solution digest by electroelution [107-109]. However, the removal of SDS by organic solvents or chromatographic techniques

normally results in significant sample loss [106]. The common endoprotease used is trypsin, which cleaves proteins mainly at the carboxyl side of the amino acids lysine or arginine, except when either is followed by proline. Some other proteases such as chymotrypsin, Lys-C, and Arg-C can also be utilized to deliberately break certain peptide bonds in order to improve sequence coverage and generate overlapping peptide fragments [110-112]. For instance, Lys-C can be used to differentiate between isobaric Lys and Gln and to determine the number and positions of Lys residues in the sequence [113]. Chymotrypsin cleavage at hydrophobic residues (Tyr, Phe and Trp) can provide complementary peptides to the tryptic digest [114]. Most digest protocols require protein denaturation to facilitate protease access to cleavage sites. Denaturants such as urea, guanidine hydrochloride, disulfide reducing agents or organic solvents such as acetonitrile or methanol are preferably used. However, these agents have to be removed prior to mass spectrometric analysis to avoid signal suppression.

1.6.3 Peptide clean-up prior to mass spectrometry

The digested peptide mixture is fractionated by HPLC and subjected to MS either online or offline. In online mode, where a HPLC device is coupled with a mass spectrometric detector (e.g. LC-MS or LC-MS/MS), a filter is fitted prior to the analytical column to remove salt excess. TFA commonly used in LC as an ion-pairing reagent is replaced by formic acid to eliminate interference with peptide ionisation [115]. Alternatively, offline purification employs a pipette tip, spin column, or syringe column to desalt the peptide sample [116]. Some commercial devices available for peptide offline clean-up include Millipore ZipTips and Nest Group UltraMicrospin columns [86].

1.7 Peptide/protein sequencing by mass spectrometry

Characterisation of proteins and protein complexes can be carried out using two mass spectrometric approaches including top-down and bottom-up sequencing. While top-down sequencing involves direct protein sequencing of an intact protein in the gas phase [117-122], bottom-up sequencing is a more popular approach that sequences peptide fragments formed by protein digestion [9, 19, 120]. In principle, the mass differences of a series of consecutive fragments from the N-terminus (e.g. b-ion series; see section 1.8.2) or C-terminus (e.g. y-ion series; see section 1.8.2) indicate the amino acid content of a peptide/protein [123]. This method is known as de novo sequencing, typically performed

without prior knowledge of the sequences of peptides and post-translational modifications involved [124-126].

In most cases of proteomic analysis, sequence assignment of a peptide/protein is not always unambiguous due to poor fragmentation and missed cleavages. In addition, with high throughput MS/MS where many MS/MS spectra can be produced from the digested peptides of a protein sample, manual interpretation of all MS/MS data is not feasible. Computer software called tandem mass spectrometry search engine is therefore normally utilised to assist peptide/protein identification [124, 127-130]. This software matches the experimental spectra with peptide sequences from a protein sequence database using different algorithms/approaches such as peptide sequence tag [131], cross-correlation [132] and probability based matching [133-134]. Each correlation results in a score reflecting the statistical significance of the match between the experimental spectrum and the sequences in a database. The correlated peptides will then be used to infer the protein content of the sample. The choice of protein database thus impacts the sensitivity, specificity and speed of the search. Among many commercial search engines available, only a few have become commonly used, including Mascot [133], SEQUEST [135-138], X!Tandem [127] and OMSSA [139]. Regardless of the increasing expansion of the protein database and the software for MS interpretation, peptide/protein sequencing can be difficult sometimes because of poor peptide fragmentation, cleavage abnormalities, low mass accuracy and poor resolution [124].

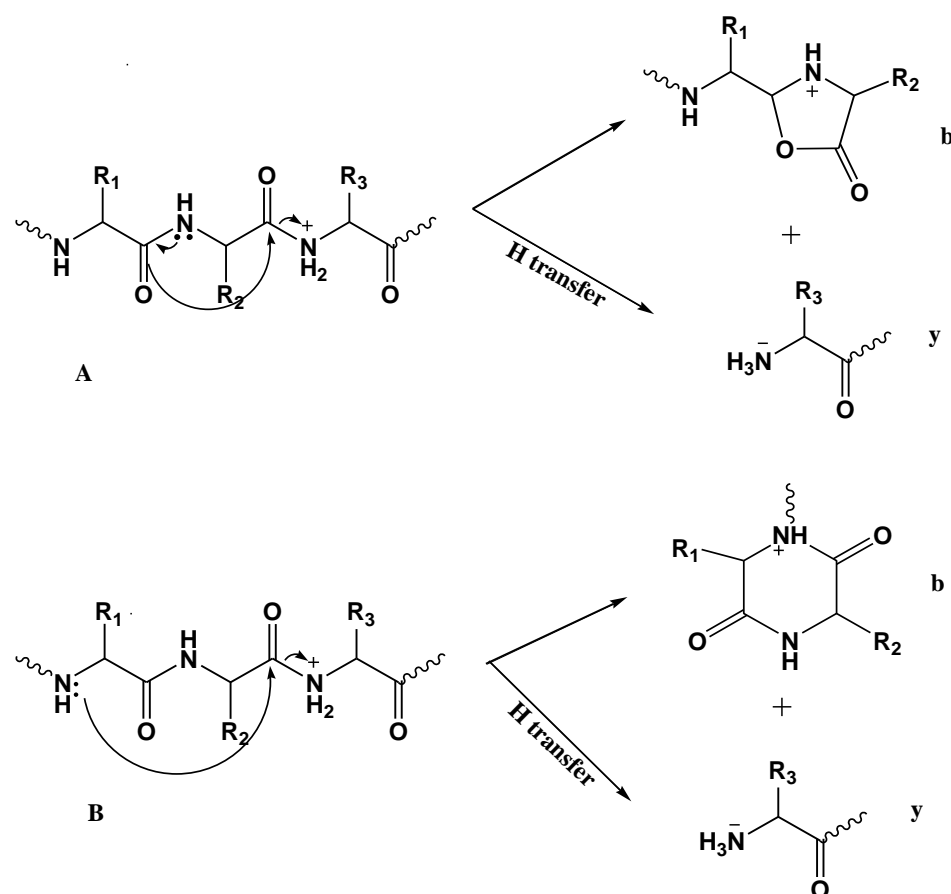
1.8 Positive ion mass spectrometry

1.8.1 Proton mobility and fragmentation pathways of low-energy collision-induced dissociation

In contrast with high-energy CID (> 1000 eV) which results in the production of all types of fragment ions (by both charge-remote and charge-directed reactions), low-energy CID (< 100 eV) produces cleavage ions in a more specific manner, mainly by fragmentations along the backbone at the amide bonds [140]. Other non-sequence ions such as the loss of a small molecule (water, ammonia...) or side-chain cleavage ions (known to be formed via charged-remote mechanisms) are rarely observed in low-energy MS/MS mass spectra. Most ion fragmentations in the low-energy collision regime have been found to be charge-directed, involving the mobility of added protons also known as “mobile protons”. The

mobile protons are firstly located on the most basic sites in the peptide/protein ions which are the N-terminus, and the side chains of basic residues. Upon activation, these mobile protons relocate to less-basic sites in the peptide/protein via various peptide linkages, triggering the charge-induced fragmentations of the peptide/protein [141-143].

Fragmentations of amide bonds in charge-directed reactions are initiated by proton transfer to amide nitrogen from a previously protonated site. This protonation weakens the amide bond and facilitates nucleophilic attack of either a carboxyl double bond (the oxazolone pathway, Scheme 1.1A) or by an amide nitrogen (the diketopiperazine pathway, Scheme 1.1B) to produce **b** and **y** ions [84]. The ‘mobile’ protons can also migrate to other protonation sites, resulting in the formation of immonium, internal fragments, and the loss of water or ammonia. However, if the energies required for these proton transfers exceed the energies for charge-remote pathways, for instance due to proton sequestration by Arg/Lys residues, the charge-remote reactions may occur competitively [143].

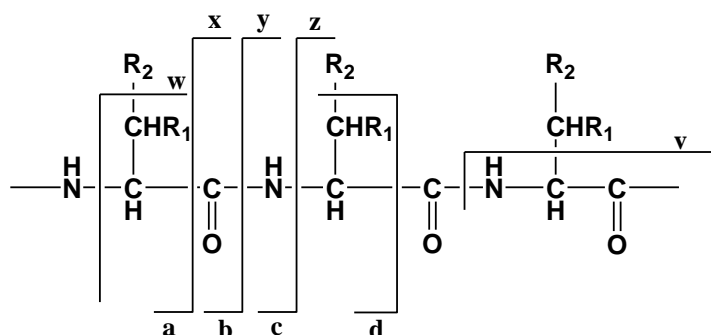


Scheme 1.1. Proposed mechanisms of **b** and **y** fragmentations of protonated ions of peptides in positive ion MS by **A** oxazolone pathway, **B** diketopiperazine pathway [143].

1.8.2 Positive ion fragmentations for peptide sequencing

Amide bond cleavage produces a **b** ion if the charge locates on the amino-terminal fragment, or a **y** ion if the carboxy-terminal fragment retains the charge (Scheme 1.1). Thus, while the **b** fragmentations allow sequencing of the peptide/protein from the N- terminus, the **y** fragmentations provide the sequence of the peptide/protein from the C-terminal end (Scheme 1.2).

Apart from the **b/y** ions, other less prevalent ion types are also utilised in sequence interpretation. These include **a/x** and **c/z** ions corresponding to the peptide backbone cleavages at CH-CO and NH-CH respectively [140, 143-144]. The side-chain cleavage ions of **d**, **v** and **w** used to distinguish between isomeric or isobaric ions (e.g., Ile from Leu) are observed in high-energy CID but not in low-energy CID.



Scheme 1.2. Schematic illustration of **a/x**, **b/y**, **c/z** peptide backbone cleavages and **d**, **v**, **w** side-chain cleavages for protonated ions of peptides.

In addition, immonium ions with the general structure of $[\text{RCH}=\text{NH}_2]^+$ are produced as a secondary fragmentation (a combination of a **y** and **a** type cleavage) of the amide bond during low energy CID. These ions are considered as diagnostic ions indicating the presence of particular amino acids in the peptide sequence [145-146].

The appearance of a peptide spectrum or the abundance of different ion types detected in a positive MS/MS or MSⁿ experiment may vary with many factors. These include the peptide structure, the instrument's observation time frame, instrument discrimination and the way energy is imparted to the system. For instance, in ion-traps, product ions with m/z being less than 30% of that of the precursor ion are not observed. Consequently, immonium ions and low m/z ions may be absent in ion-trap spectra. More information on default ion types for corresponding instrument configurations and restrictions on the ion types based on

fragmentation spectra acquired from different instruments is provided by MASCOT (Table 1.2) [8, 81].

Table 1.2. Default ion types for corresponding instrument configurations and restrictions on the ion types based on fragmentation spectra acquired from different instruments provided by MASCOT.

	Default	ESI Q-TOF	MALD I TOF- PSD	ESI Trap	ESI QQQ	ESI FTICR	MALD I TOF- TOF	FTMS ECD	MALD I Q- TOF
1+ fragments	x	x	x	x	x	x	x	x	x
2+ fragment if precursor 2+ or higher	x	x		x	x	x		x	x
2+ fragment if precursor 3+ or higher									
Immonium ions			x				x		x
a series ions	x		x				x		
a-NH ₃ if fragment includes RKNQ	x		x				x		
a-H ₂ O if fragment includes STED			x				x		
b series ions	x	x	x	x	x	x	x		x
b-NH ₃ if fragment includes RNKQ	x	x	x	x	x	x	x		x
b-H ₂ O if fragment includes STED		x	x	x	x	x	x		x
c series ions									
x series ions									
y series ions	x	x	x	x	x	x	x	x	x
y-NH ₃ if fragment includes RKNQ	x	x		x	x	x	x		x
y-H ₂ O if fragment includes STED		x		x	x	x	x		x
z series ions									
z + H series ions								x	
Internal y _b < 700 Da							x		x
Internal y _a < 700 Da							x		x

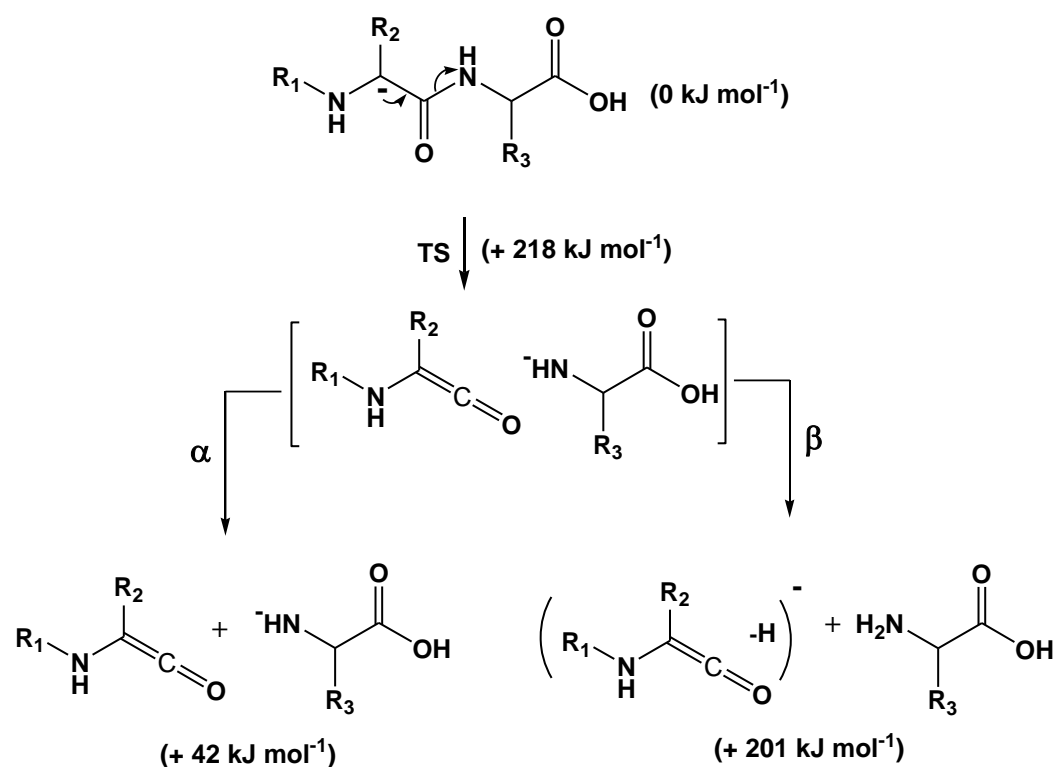
1.9 Negative ion mass spectrometry

While positive ion MS has developed to a robust state in characterisation of peptides/proteins, research on deprotonated ions of peptides and proteins has been limited primarily to a small number of research groups. Detailed information regarding the fragmentation of peptides/proteins using negative ion MS is currently not comparable to that of positive ion MS.

Bowie and co-workers have used negative ion MS to investigate a range of the $(M-H)^-$ anions of underivatised peptides, from the simplest anions of di, tripeptides to large peptides of more than twenty amino acids. Based on this work, the characteristic fragmentations of the deprotonated anions of peptides and proteins have been deduced including (i) amide backbone cleavages, (ii) backbone fragmentations initiated from some particular side chains and (iii) characteristic side-chain fragmentations.

1.9.1 Amide backbone cleavages

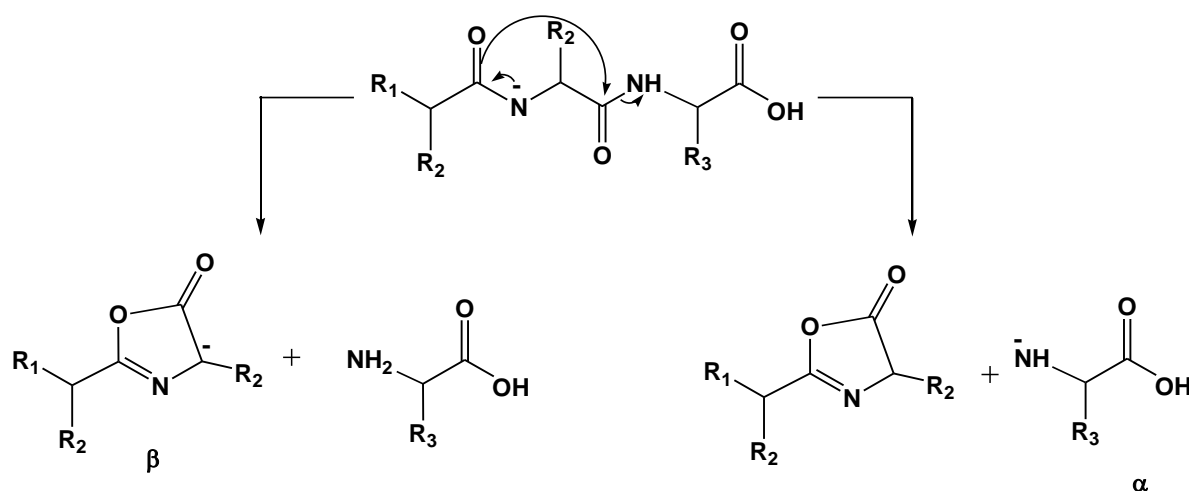
The first pattern of peptide backbone cleavages is amide backbone cleavage, known as α and β cleavages. The α fragmentation produces an amide anion, and the loss of a proton from the corresponding ketene corresponds to the β fragmentation. Both cleavages are proposed to be initiated by an enolate anion on the peptide backbone which can be produced from the initial deprotonation step or by proton transfer to a carboxylate or carboxylamine moiety (Scheme 1.3) [147-149].



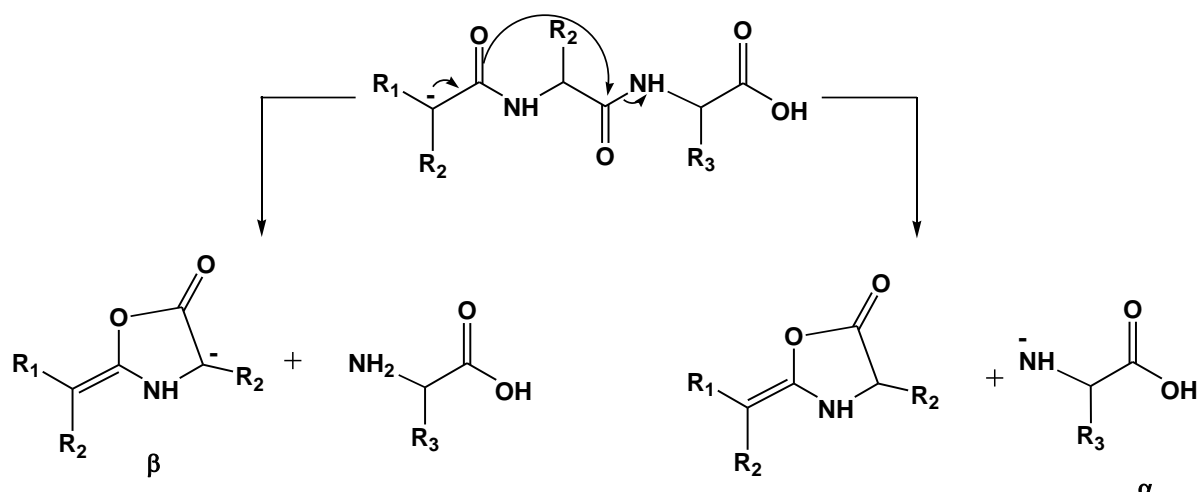
Scheme 1.3. Mechanisms for the formation of α and β ions from the deprotonated ions of peptides. Calculations at the HF/6-31G(d)//AM1 level of theory; R_1 , R_2 and R_3 are CH_3 , H and H, respectively [147-149].

The mechanisms of α and β peptide backbone cleavages have been supported by theoretical calculations using a model system at HF/6-31G(d)//AM1 level of theory. The α and β processes are endothermic by 42 kJ mol^{-1} and 201 kJ mol^{-1} respectively, indicating that the α fragmentation is energetically more favourable than the β fragmentation [150].

Two alternative mechanisms for amide backbone fragmentations have also been suggested by the Harrison group involving the formation of a β cyclic fragment. While one of these pathways is initiated by an amide anion (Scheme 1.4), the other proposes the cleavage of amide backbone by the cyclisation from an enolate anion (Scheme 1.5) [151-154].



Scheme 1.4. Formation of α and β fragments induced by an amide anion from the deprotonated ions of peptides; R_1 , R_2 and R_3 are amino-acid side chains [151, 154].

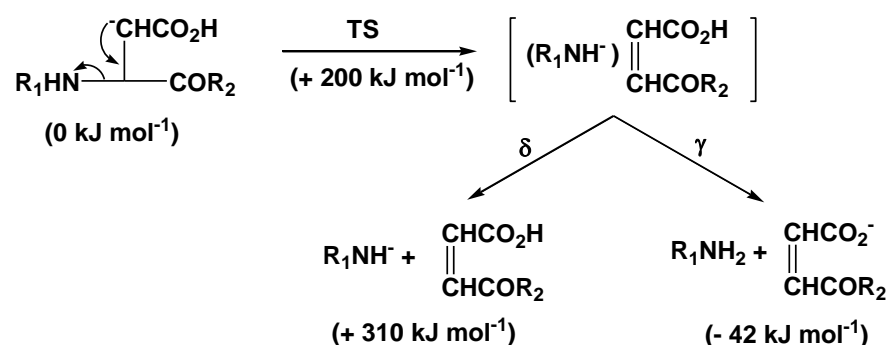


Scheme 1.5. Formation of α and β fragments induced by an enolate anion from the deprotonated ions of peptides; R_1 , R_2 and R_3 are amino-acid side chains [154].

1.9.2 Side-chain induced backbone cleavages

The second type of peptide backbone cleavage involves NH-CH bond cleavage which is initiated by particular side-chains. The production of amide anions is known as δ fragmentation, while deprotonation of the corresponding C-terminal portion will yield γ anions. This type of backbone dissociation is generally observed in peptides containing amino-acid side chains that can form stabilised anions RCH^- such as Asp, Asn, Glu, Gln,

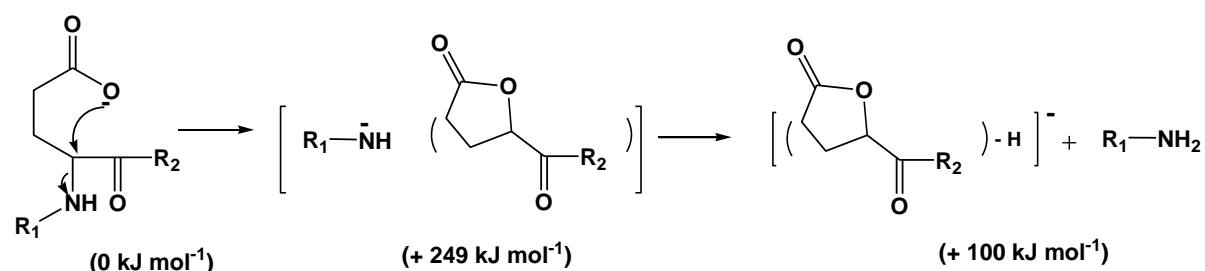
Phe, Tyr, His and Trp containing peptides [149]. The cleavages (e.g. for Asp) are most likely to be initiated by a side-chain enolate anion as illustrated in Scheme 1.6 [155-156].



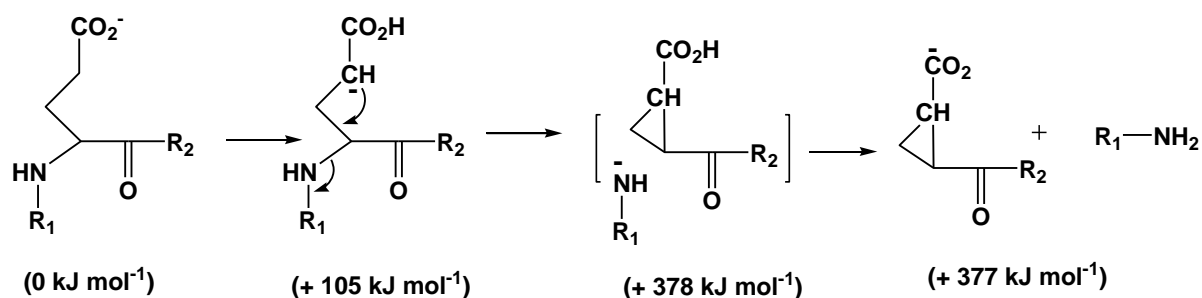
Scheme 1.6. Proposed mechanisms for the formation of γ and δ ions from the deprotonated ions of peptides containing Asp. Calculations at the HF/6-31G(d)//AM1 level of theory; R_1 and R_2 are CH_3CO and NHCH_3 , respectively [155-156].

Theoretical calculations for γ and δ fragmentations were performed at the HF/6-31G(d)//AM1 level of theory on a model system containing Asp. They showed that the γ process is significantly the more favourable by -42 kJ mol^{-1} while the δ ion formation is unfavourable ($+310 \text{ kJ mol}^{-1}$). Consequently, the γ peak is usually more intense than the corresponding δ peak in negative ion spectra.

Two other mechanisms for γ and δ cleavages of Glu and Gln containing ions are also proposed. These involve the cyclisation reactions initiated by (i) a carboxylate anion on Glu side chain (Scheme 1.7) or (ii) an enolate anion (Scheme 1.8).



Scheme 1.7. The mechanism of γ fragmentation initiated by the carboxylate anion in the deprotonated ions of peptides containing Glu. Calculations at the HF/6-31G(d)//AM1 level of theory; R_1 and R_2 are CH_3 [156-157].

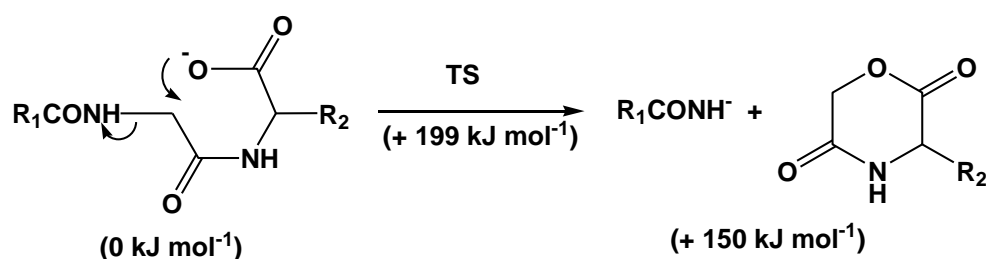


Scheme 1.8. The mechanism of γ fragmentation initiated by the enolate anion in the deprotonated ions of peptides containing Glu. Calculations at the HF/6-31G(d)//AM1 level of theory; R_1 and R_2 are CH_3 [156-157].

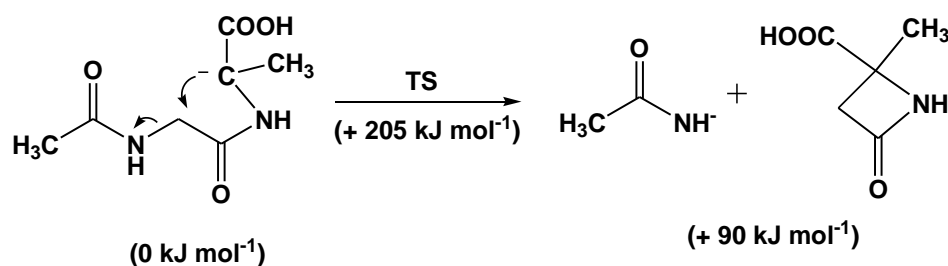
Theoretical calculations for a model system containing Glu revealed that the formation of γ ion via the carboxylate nucleophilic substitution is energetically more favourable than the three-member-ring cyclisation reaction induced by the side-chain enolate anion. This is because the first process is unfavourable by 100 kJ mol^{-1} , whereas the second requires $+377 \text{ kJ mol}^{-1}$. Formation of the γ ion is always followed by the loss of H_2O in the cases of acidic side chains (Asp and Glu) or by the loss of NH_3 in the cases of amide side chains (Asn and Gln) [155].

1.9.3 β' (beta prime) fragmentation

The backbone NH-CH cleavages can also be observed occasionally at amino acid residues which cannot initiate γ and δ fragmentations. This fragmentation, named β' (beta prime), is a cyclisation/cleavage process involving either a carboxylate cyclisation cleavage (Scheme 1.9) or backbone enolate cyclization (Scheme 1.10) [158].



Scheme 1.9. The mechanism of β' fragmentation initiated by the carboxylate anion in the deprotonated ions of peptides. Calculation at the CAM-B3LYP/6-311++g(d,p) level of theory; R_1 and R_2 are CH_3 [158].



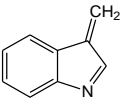
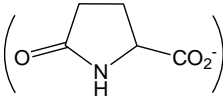
Scheme 1.10. The mechanism of β' fragmentation initiated by the enolate anion in the deprotonated ions of peptides. Calculation at the CAM-B3LYP/6-311++g(d,p) level of theory [158].

1.9.4 Characteristic side-chain fragmentations

The presence of some amino acids in a peptide sequence can be recognised from their characteristic side-chain fragmentations in negative ion MS [149]. Characteristic fragments are produced by the loss of alkyl radicals such as Me^\bullet , Pr^\bullet , Bu^\bullet from Ala, Val, Leu or Ile respectively, or by the loss of a particular molecular mass, for instance, the loss of 106 from Tyr or the loss of H_2O from Glu and Asp etc. [159-160]. The characteristic negative ion fragmentations within side-chains of amino acid residues from the $(\text{M-H})^-$ ions in small peptides are summarised in Table 1.3.

For some listed amino acids in Table 1.3, this feature is suppressed with an increase in peptide size, while the production of characteristic side-chain fragmentations of some amino acids (including the loss of H_2O from Asp, Glu, the loss of NH_3 from Asn, Gln and the losses of $\text{CH}_2\text{O}/\text{MeCHO}$ from Ser/Thr) are not dependent upon peptide size and sometimes are more pronounced than α , β , γ and δ backbone cleavage anions [149].

Table 1.3. Characteristic side-chain fragmentations in negative ion MS.

Amino acid	Loss (or formation)	Mass (m/z)
Ala	Me [•]	15
Val	Pr [•]	43
Leu (Ile)	Bu [•]	57
Phe	(PhCH ₂ ⁻)	91
	(<i>p</i> -CH ₂ -C ₆ H ₄ -CH ₂ ⁻)	107
Tyr	O= C ₆ H ₄ =CH ₂	106
Trp		129
Ser	CH ₂ O	30
Thr	CH ₃ CHO	44
Cys	H ₂ S	34
Met	CH ₃ SH	48
Asp/Glu	H ₂ O	18
Glu		128
Asn/Gln	NH ₃	17
Arg	HN=C=NH	42

1.10 Post-translational modification

Post translational modifications (PTMs) are chemical alterations to protein structures resulting from addition of modifying functional groups or proteolytic cleavage [161], which result in an improvement in the complexity of gene products and a change in properties of the modified protein. As many as 300 PTMs are currently known including a wide range of functionalities such as phosphorylation, sulfation, ubiquitination and disulfide formation. Some common PTMs are displayed in Table 1.4. Each of them adds a particular mass to the original protein, plays a different role in cellular processes, and possesses different stability (reversible or irreversible PTMs) [162-163]. MS analysis of PTMs is used not only to

determine the amino acid sequences of post-translationally modified proteins, but also the type and site of the modifications. Due to such multiple tasks, identification of PTMs in a protein by MS is more complicated than that of an unmodified protein.

Table 1.4. Some common and important post-translational modifications [161]. Stability: + labile, ++ moderately stable, +++ stable in tandem MS.

PTM type	Δ Mass (Da)	Stability	Functions and notes
Phosphorylation			Reversible, activation/inactivation of enzyme activity, modulation of molecular interaction, signalling
pTyr	+80	+++	
pSer/Thr	+80	+ / +++	
Acetylation	+42	+++	Protein stability, protection of N-terminus. Regulation of protein-DNA interactions (histones)
Methylation	+14	+++	Regulation of gene expression
Glycosylation			Excreted proteins, cell-cell recognition/signalling
N-linked	>800	+ / +++	<i>O</i> -GlcNAc, reversible regulatory functions
O-linked	203, >800	+ / +++	
Sulfation (sTyr)	+80	+	Modulator of protein-protein and receptor-ligand interactions
Disulfide bond formation	-2	++	Intra- and intermolecular crosslink, protein stability
Deamidation	+1	+++	Possible regulator of protein-ligand and protein-protein interactions, also a common chemical artifact
Pyroglutamic acid	-17	+++	Protein stability, blocked N-terminus
Ubiquitination	>1,000	+ / +++	Destruction signal. After tryptic digestion, ubiquitination site is modified with the Gly-Gly dipeptide
GPI anchor	>1,000	++	Glycosulphosphatidylinositol (GPI) anchor. Membrane tethering of enzymes and receptors, mainly to outer leaflet of plasma membrane
Hydroxyproline	+16	+++	Protein stability and protein-ligand interactions

In a general mass spectrometric strategy for mapping PTMs, a modified protein is firstly purified and enriched by several methods such as chromatographic purifications [164-165] or antibody affinity [166-169]. The purified protein is then enzymatically digested into a collection of peptides that are more readily characterised than the intact protein. The peptides can be further fractionated and/or subjected to MS experiments (MS/MS or MSⁿ). Even though multiple endoproteases are commonly used to achieve the highest sequence coverage possible, it is unavoidable that some peptide fragments (including the fragments containing PTMs) may be missed during the mapping process due to the instrumental detection limit or the size and ionisability of peptides [9]. In addition, the MS analysis of modifications such as phosphorylation, sulfation, glycosylation and disulfide bonds frequently encounter difficulties of low stoichiometry, low ionisability and unusual fragmentation behaviour of the modifying groups in the positive ion mode [163].

Each modification has its own characteristic fragmentation which may be an advantage or a disadvantage to their detection and localization using positive ion MS. For instance, some modifications are quite stable and remain attached to the modified residues during the mapping process. Examples are acetylation (+ 42 Da), which occurs on the N termini or on Lys residues [170], and arginine methylation (+ 14 Da) [171]. The fragmentation patterns of the peptides containing these groups will thus reveal their locations. In contrast, some modifications are labile and lost during ionisation or during collision activation, for examples, sulfation of Tyr/Ser/Thr (+ 80 Da) [172] and O-linked N-acetylglucosamine (GlcNAc: + 203 Da) [173]. For the peptides containing these modifications, the loss of these groups can be used as reporters to detect them. The presence of low-mass characteristic ions in mass spectra or the loss of a particular mass from the parent ions (see 2.1.1 for a detailed description of precursor ion and neutral loss scanning method) is normally used for identification of PTMs in peptides. In such cases, the modifications are identified but not their locations. Difficulties associated with PTMs detection and localisation make identification of modified peptides challenging either via manual or computer-assisted interpretation.

The CID cleavages at side-chain groups normally precede backbone fragmentations in positive ion mode because of the high lability of modifying groups. In order to alleviate this problem, some other activation methods have been introduced. The two popular alternatives to dissociation of post-translational modified peptides are electron capture dissociation

(ECD) and electron transfer dissociation (ETD). In brief, the multiply-charged peptides interact with near-thermal (< 0.2 eV) electron (ECD) or radical anions (ETD) to form peptide radicals which fragment preferentially along the peptide backbone, thus reducing cleavage of modifying groups (see section 2.1 for detail of ECD and ETD [37, 174]).

On the other hand, negative ion MS has been found to be more sensitive than positive ion mode for detecting particular PTMs owing to their nucleophilic nature. For examples, PO_3^- (79 Da) and H_2PO_4^- (97 Da) are commonly observed and used as diagnostic ions to detect phosphorylated peptides. However, negative ion CID fragmentation of post-translationally modified peptides have not been studied extensively, and so far, only play the role of the detector for some common modifications such as phosphorylation, sulfation, cysteine bond formation and nitrosylation. Therefore, more work needs to be done to shed light on the reaction mechanisms of deprotonated ions of modified peptides/proteins.

In order to gain more insight into the fragmentation mechanisms of the $(\text{M-H})^-$ anions of modified peptides/proteins and to examine the efficiency of negative ion MS as an analytical tool in characterisation of PTMs, the research described in this thesis investigates the identification of some common PTMs including phosphorylation, sulfation and disulfide using negative ion MS via an array of synthetic and natural peptides and proteins. An additional application of this research is to identify peptides secreted from the frog *Litoria rubella* in some areas in Australia. The interaction of these peptides with biomimetic lipid bilayers is investigated to ascertain whether membrane binding is the event preceding the addition of these peptides in order to act on membrane receptors.

CHAPTER 2

INVESTIGATION OF PHOSPHORYLATED PEPTIDES BY NEGATIVE ION MASS SPECTROMETRY

2.1 Introduction to phosphoproteome analysis by mass spectrometry

Phosphorylation is one of the most important and intensively studied post-translational modifications, which is controlled by two classes of enzymes, namely protein kinases and phosphatases [175-176]. It specifically occurs on Ser, Thr, Tyr and sometimes on His residues in eukaryotic proteins (Figure 2.1) [177-179]. Reversible phosphorylation regulates many cellular processes such as cell-cycle progression, cellular differentiation, intercellular communication, apoptosis, cytoskeleton arrangement, and neuronal and immunological functions [180-181]. It is also estimated that at least 30% of all proteins in a cell are phosphorylated at any given time [182]. A variety of biochemical and analytical chemical approaches have been developed to enrich and examine phosphorylated proteins and peptides. Among these, MS has emerged as a core technology for identification of phosphoproteins and phosphopeptides, determination of phosphorylation sites and quantitation of phosphorylation [183-184].

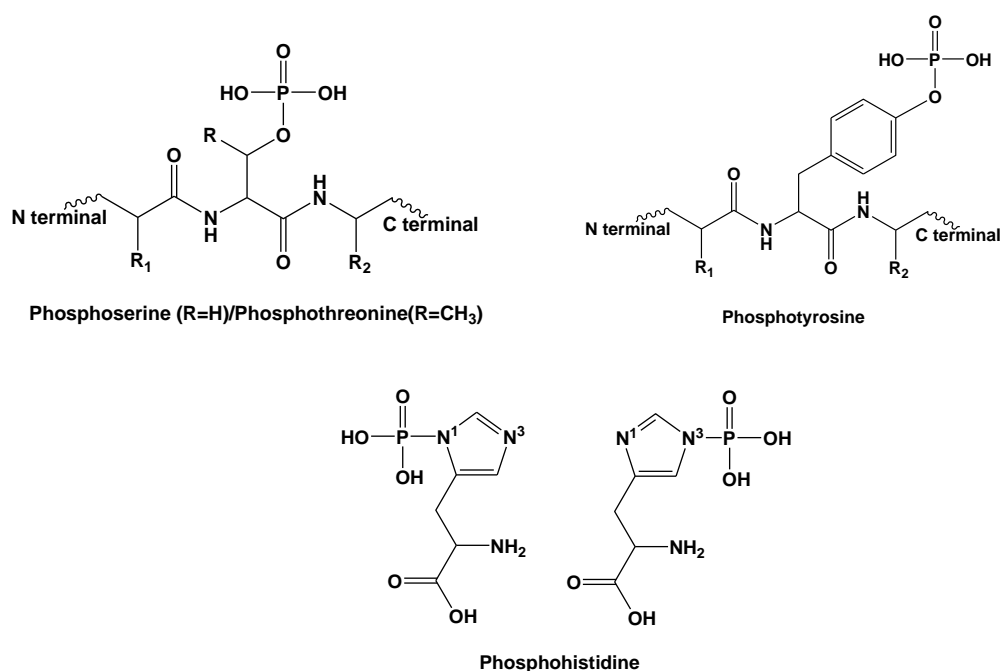


Figure 2.1. Structures of phosphorylated Ser, Thr, Tyr and His.

2.2 Tandem mass spectrometry and dissociation techniques for phosphoproteome analysis

2.2.1 Phosphopeptide detection

Studies of phosphorylated proteins have frequently encountered the challenge of detecting phosphopeptides in the pool of peptides created by proteolytic digestion of the protein of interest [185-186]. Phosphopeptides are typically present in lower abundance than other digest peptides, and hence their mass spectrometric response is suppressed by the presence of other peptides and also the unphosphorylated counterparts [187-188]. In order to improve the MS signal of phosphorylated peptides, a number of enrichment strategies have been implemented. These include separation by HPLC [189], selective binding of the phosphate moiety to metal ions by immobilised affinity chromatography (IMAC) [190], strong cation exchange (SCX) [191], barium or calcium precipitation [192-193], immuno-precipitation of targeted peptides by antibodies [194], chemical tagging of phosphorylation sites [195-196], or some combination of the independent techniques.

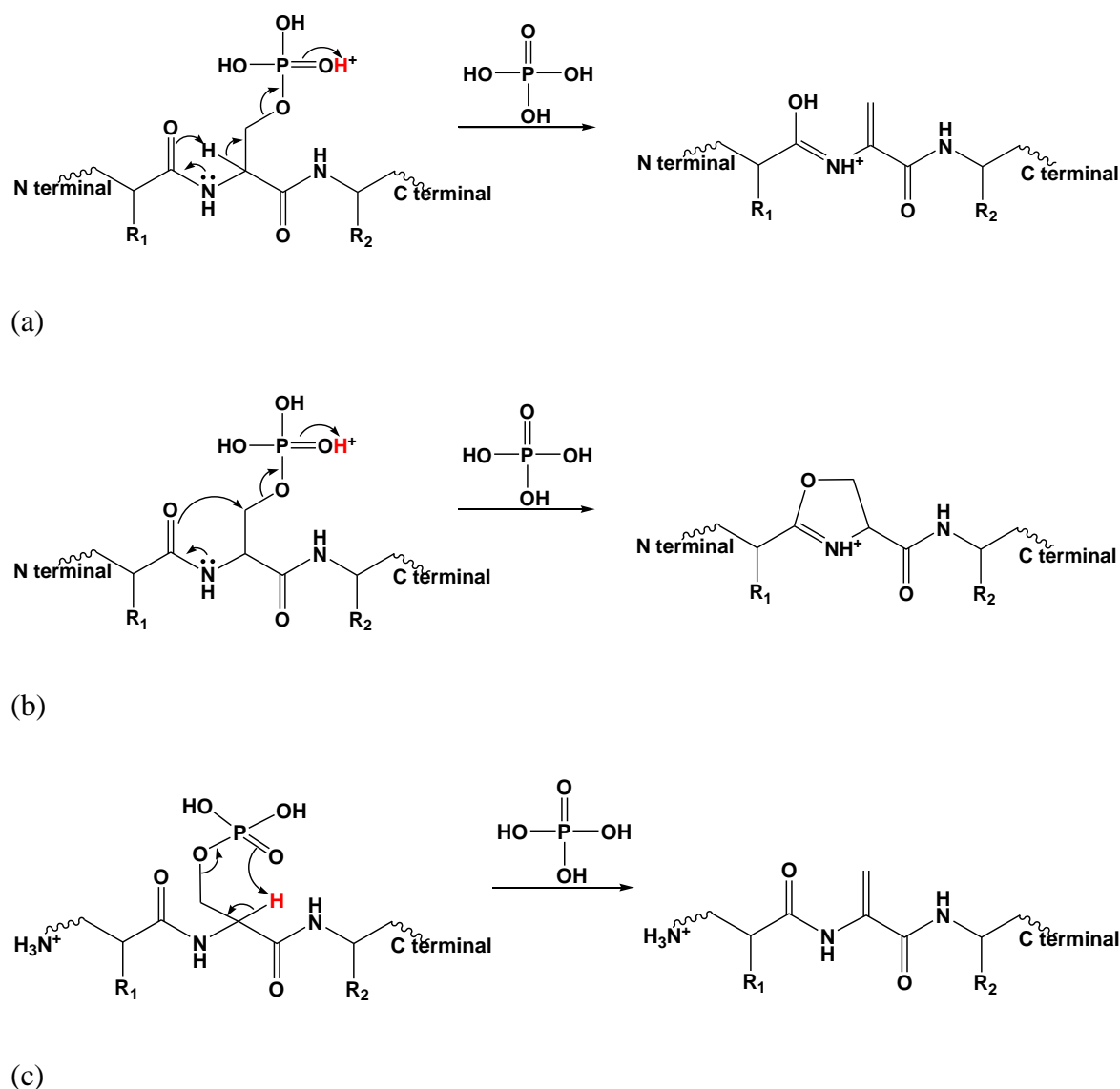
Recognition of phosphopeptides by MS generally relies on the lability of the phosphate group in CID in combination with phosphatase treatment of the interested protein. In tandem MS, precursor ion scanning and neutral loss scanning are two common mass spectrometric approaches to detect phosphate side chains in protonated peptides/proteins [183, 197]. These are implemented most effectively on triple quadrupole (Q-Q-Q) or quadrupole linear ion trap (Q-Q-LIT) [8] and recently on Q-TOF instruments via software programming [198-199].

Precursor ion scanning is a mass spectrometric detection method which generates spectra of parent ions instead of fragment ions (as normal acquired data mode). In this scan mode, the first mass analyser is the mass scanner and the second mass analyser is the mass filter. The second mass analyser (located after the collision cell) is set to allow the passage and thus detection of one particular ion, while the first mass analyser scans and detects all parent ions which produce that particular fragment ion [18]. The phosphotyrosine immonium ion ($^+\text{NH}_2=\text{CH}-\text{CH}_2-\text{C}_6\text{H}_4-\text{O}-\text{PO}_3\text{H}_2$) (m/z 216.043) is formed exclusively from phosphate Tyr residues and thus is used for selective detection of Tyr phosphorylated peptides by precursor ion scanning [197, 200-203].

In neutral scanning mode, both mass analysers are scanned in a linked fashion so that a constant neutral loss is maintained [18, 204]. The losses of HPO_3 (80 mass units) and H_3PO_4 (98 mass units) are observed predominantly in spectra of phosphorylated peptides. Therefore, detection of phosphate residues can be facilitated by neutral loss scanning of these losses [184, 205-206].

Phosphate recognition by these two scanning modes was first described using triple quadrupole mass spectrometers [207]. However, there has been a general replacement of this type of instrument by higher resolution mass spectrometers such as Q-TOFs to provide more accurate detection of phosphate moieties [197, 200-203]. In addition, phosphatase treatment followed by mass analysis can be performed to confirm the presence of phosphate groups in these peptides [208-209].

The loss of H_3PO_4 was found to be the most abundant fragmentation in positive ion mass spectra of phosphoserine (pSer) and phosphothreonine (pThr) containing peptides, and decreases from pSer to pThr. Several charge-directed mechanisms were suggested for this loss including a charge-directed E2-elimination reaction and an $\text{S}_{\text{N}}2$ neighbouring group participation (Scheme 2.1a and b) [210-211]. A charge-remote pathway (β -elimination) was also proposed to explain the prevalence of this neutral loss in partial or non-mobile conditions of ionising protons (Scheme 2.1c) [212-213]. The H transfers and elimination in charge-directed and charge-remote pathways are different. The phosphate group is cleaved with the mobile proton in charge-directed pathways whereas the charge-remote pathway abstracts a hydrogen atom from C- α of the phosphorylated residue (Scheme 2.1a-c). H/D exchange studies suggest that these reactions occur competitively but that charged-directed pathways are more dominant [210-211].



Scheme 2.1. Pathways of H_3PO_4 loss from the MH^+ ion of a pSer/pThr. (a): E2-elimination, (b) intramolecular $\text{S}_{\text{N}}2$ mechanism, (c): charge-remote β -elimination. The hydrogen involved with the loss of phosphoric acid is coloured in red.

In contrast with pSer/pThr peptides, CID MS/MS of protonated ions of pTyr show a more prevalent loss of HPO_3 than H_3PO_4 . In the case of pTyr, H_3PO_4 cannot be eliminated by any of mechanisms (a), (b) or (c). Several alternatives have been suggested to explain this phenomenon. For instance, the loss of phosphoric acid could come from concomitant losses of HPO_3 and H_2O from different residues of pTyr-peptides. Alternatively, HPO_3 could be transferred to an Asp residue or unmodified Ser or Thr facilitating the cleavage of H_3PO_4 [213-215].

There are several factors that determine the extent of neutral losses within phosphopeptides, namely (i) the chemical structure of the phosphorylated amino acid residue (pTyr, pSer or pThr), (ii) the amino acid sequence, (iii) the precursor ion polarity and charge state, (iv) ion mobility, (v) the input collision-energy and (vi) the timescale for CID. Increasing the charge on the studied peptides was reported to cause a decrease in neutral losses due to more “mobile protons” being available for charge-directed backbone cleavage which is in competition with neutral-loss pathways [211]. Phosphate losses in an ion trap were found to be more prevalent than in a tandem mass spectrometer such as a triple quadrupole or Q-TOF mass spectrometer [205-206], since the low-energy dissociation pathways of neutral losses are favoured by ion-trap instruments where the energy is deposited at a lower level and a slower rate compared to that of tandem in space mass spectrometers [183, 216].

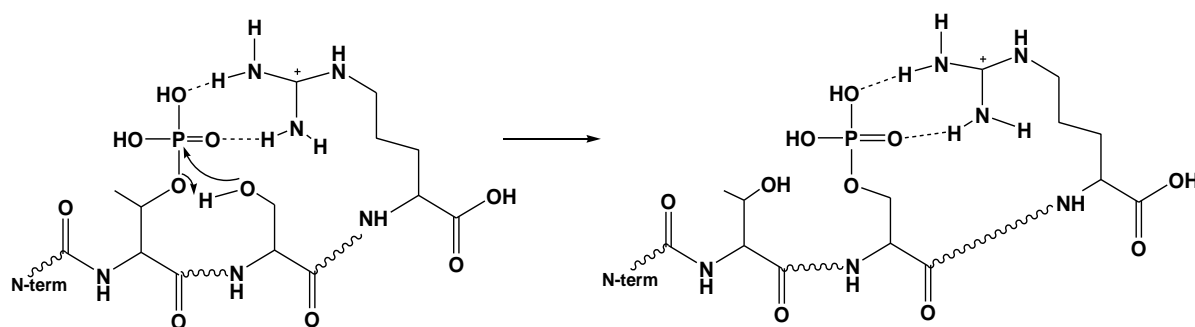
2.2.2 Phosphorylation site localisation and peptide sequencing by positive ion mass spectrometry

Although the facile losses of HPO_3 and H_3PO_4 facilitate the detection of the phosphate group, they hinder the formation of phosphorylated fragments required for peptide sequencing and phosphorylation-site localisation. Optimisation of mass spectrometric conditions based on the knowledge of the gas-phase chemistry responsible for phosphate losses (as mentioned above) could partially improve phosphate retainment but not completely eliminate phosphate losses. Therefore, determination of a phosphate position within peptides/proteins frequently has to be managed in phosphate-loss condition.

Several acquisition methods have been developed to obtain the structural information of phosphate containing peptides. Of these, multistage CID MS3 [217-221] and “pseudo-MS3” [222] are frequently used. CID MS3 method involves isolation and further fragmentation of the phosphate-loss fragment. On the other hand, “pseudo-MS3” activates the precursor ion and the resultant 98 Da neutral loss simultaneously. The “pseudo-MS3” method produces a composite spectrum of fragments originating from both the parent ion and the neutral loss species with the loss of backbone fragments due to the ion-isolation step being reduced. The sites of phosphorylation are preliminarily indicated by the presence of backbone fragments with the loss of 18 Da from Ser or Thr (due to loss of H_3PO_4 as in Figure 2.1) [211]. However, the loss of water (also 18 Da) from an unmodified residue may confuse the identification of a phosphorylation site, and hence a fragment containing an attached phosphate group is required to unequivocally determine the site of phosphorylation.

In addition, software tools and scoring programs (such as delta score, Ascore [223], MSQuant [217, 224]) have also been developed to auto-localise phosphate sites. These programs calculate the probability of phosphorylation sites based on the fragmentation spectra of the investigated phosphopeptide. The site of phosphorylation is then assigned corresponding to the localisation with the highest score. Mismatching or erroneous determination of phospho-sites may occur as peptides contain multiple Ser, Thr or Tyr residues next to each other and/or peptide backbone fragments are produced.

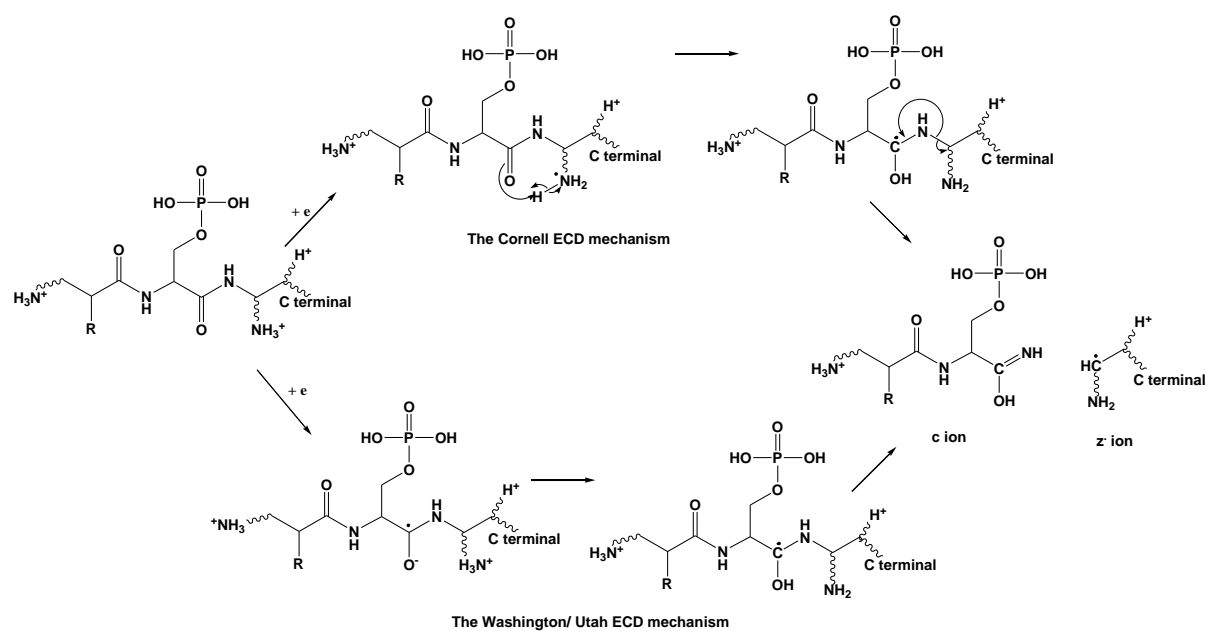
Phospho-site localisation using positive ion MS has sometimes been hampered by the rearrangement of the phosphate group in the gas phase. Beside the rearrangement of a pTyr phosphate group to Asp, (which was proposed to explain the formation of phosphoric acid from protonated ions containing pTyr), it is evident that the phosphate group may be transferred to another hydroxyl-containing amino acid mediated by hydrogen bonding interactions between the phosphate group and basic residues (e.g. see Scheme 2.2) [216, 225]. This phenomenon was found exclusively in ion-trap instruments where the activation time is in the millisecond range, while there have been no such reports of phosphate rearrangements in other types of mass spectrometers as the collision time is much shorter. These gas phase rearrangements are more prevalent for phosphopeptides with low charge states [211].



Scheme 2.2. Proposed mechanism for the gas-phase phosphate group rearrangement from pThr to pSer mediated by hydrogen bonding interactions between the phosphate group and basic residues.

The use of electron-based fragmentation methods such as electron capture dissociation (ECD) and electron transfer dissociation (ETD) have been reported to alleviate the problem of neutral losses and rearrangements, improve backbone fragmentations, and thus provide more accurate phosphate identification and sequence information [226-229]. These

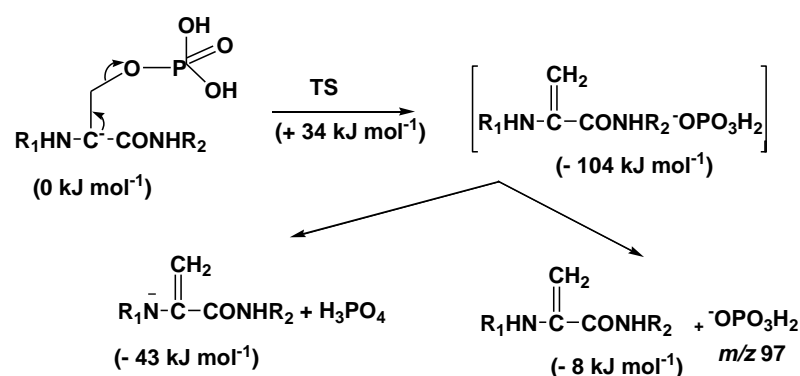
activation techniques are well suited for analysis of highly charged peptides (typically more than 3+) [230-233]. A general mechanism for these dissociations was proposed [234]. A near-thermal electron (< 0.2 eV) is attached to protonation sites of peptides such as a Lys ϵ -ammonium group, an Arg guanidinium group, a His imidazolium ring, or an N-terminal ammonium group. This attachment induces the transfer of a hydrogen atom from the protonation sites to the nearby carbonyl oxygen on the backbone. The newly formed aminoketyl intermediate dissociates to yield **c** and **z** ions (Scheme 2.3). An alternative mechanism, namely the Utah-Washington (UW) mechanism, was also provided to explain the dissociations of N-C α bonds that for steric reasons may not be able to receive a hydrogen atom from the protonation sites of the precursor ions in their initial conformation(s). It involves electron capture of the π bond (of the amide C=O group) to form a ketyl radical anion, which then abstracts a proton from a charge carrying group to form an aminoketyl. This is followed by the dissociation of the N-C α to generate **c** and **z** ions (Scheme 2.3).



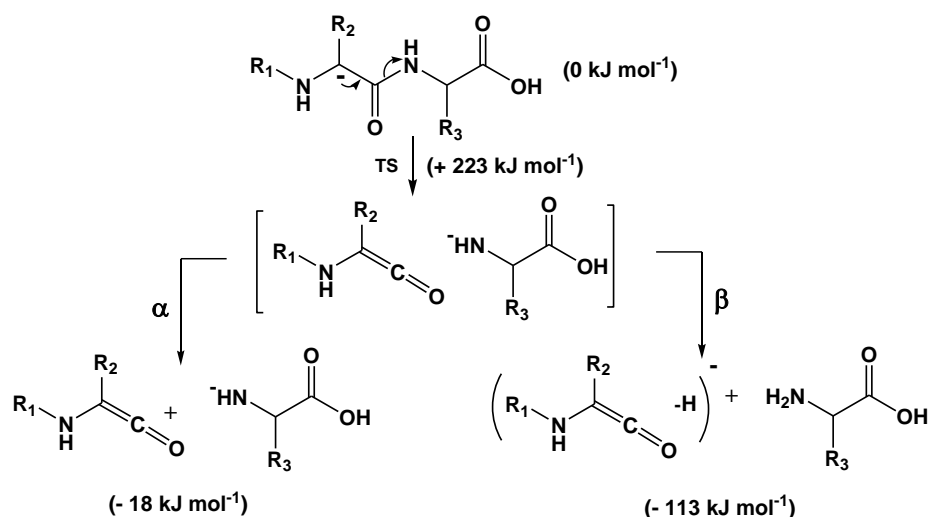
Scheme 2.3. Proposed ECD/ETD fragmentation mechanisms of phosphorylated peptides. R groups are neutral side-chain groups.

2.2.3 Peptide/protein phosphorylation under investigation of negative CID mass spectrometry

While studies of phosphorylated peptides and proteins using positive ion MS has shown significant progress, fewer investigations in this area have utilised negative ion MS. The characteristic formation of m/z 97 (H_2PO_4^-), and loss of 98 (H_3PO_4) from the $(\text{M}-\text{H})^-$ and multi-charged $(\text{M}-n\text{H})^{n-}$ ions of pSer/pThr peptides have been reported [212, 235-238] (Scheme 2.4). Calculations (at the MP2/6-31++G(d,p)//HF/6-31++G(d,p) level of theory) indicated that the two processes are exothermic [238] and the ΔG values for the formation of H_2PO_4^- and the loss of H_3PO_4 are -8 kJ mol^{-1} and -43 kJ mol^{-1} , respectively [239]. These two fragmentations are kinetically more favourable than the standard α and β negative ion backbone cleavages of peptide $(\text{M}-\text{H})^-$ ions (Scheme 2.5), since the energy barrier for the phosphate related processes is much lower [238-239].

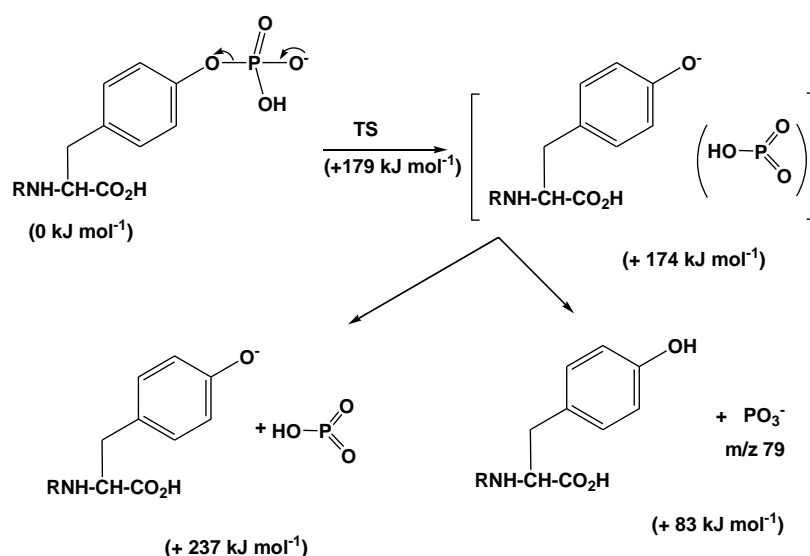


Scheme 2.4. Proposed mechanisms for the loss of H_3PO_4 and formation of H_2PO_4^- from the $(\text{M}-\text{H})^-$ anion of a model system containing pSer. Calculations at the MP2/6-31++G(d,p)//HF/6-31++G(d,p) level of theory; R_1 and R_2 are CH_3CO and NHCH_3 , respectively [238-239].



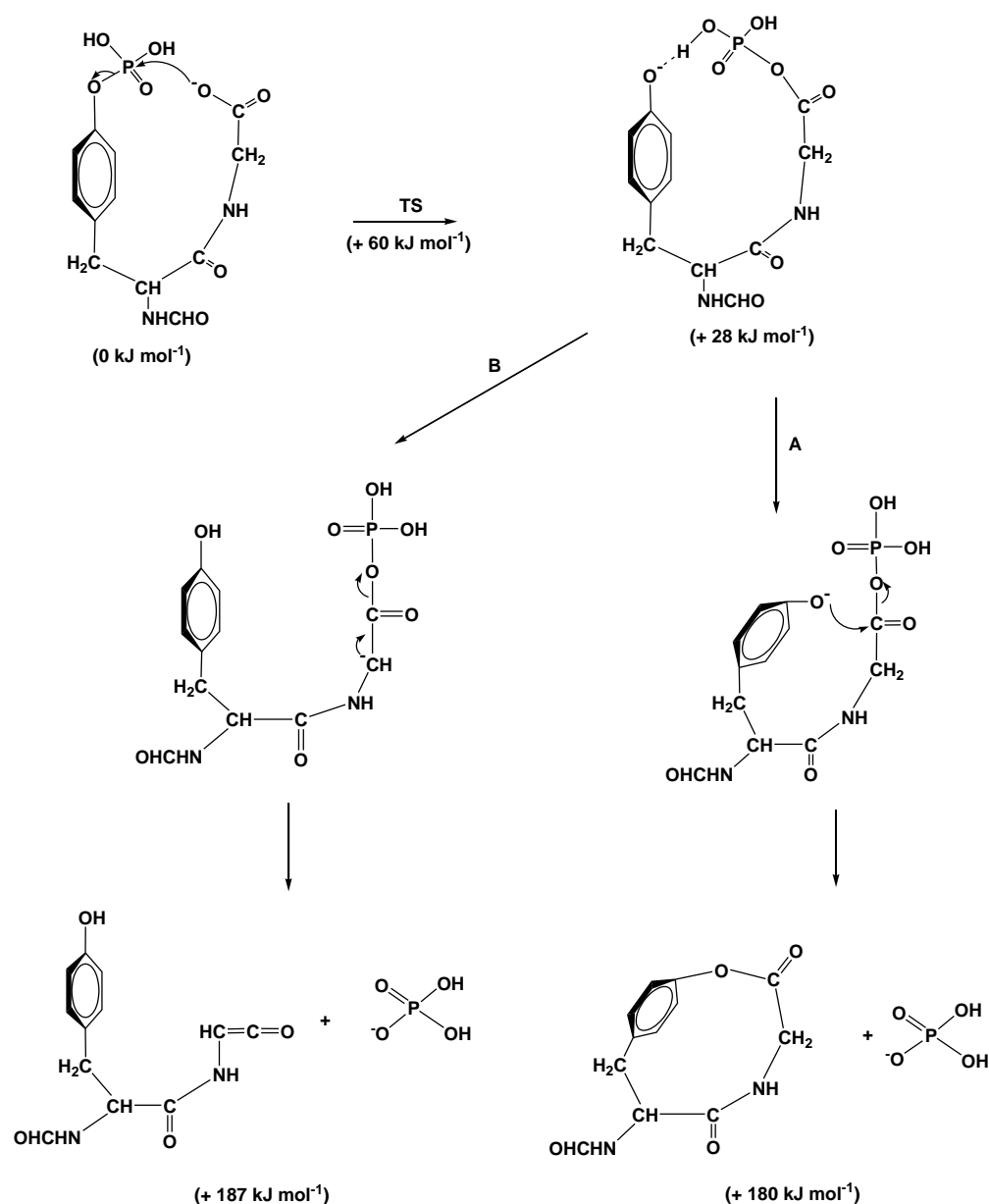
Scheme 2.5. Calculations for the formation of α and β ions from the deprotonated ions of peptides in negative ion MS, at the HF/6-31G(d)//AM1 level of theory by Dr. Tianfang Wang; R_1 , R_2 and R_3 are CH_3 , H and H, respectively. Gibbs energies (ΔG) were provided.

In contrast, the characteristic fragmentations of pTyr are different, namely, $[(M-H)^- - \text{HPO}_3]$ and $(M-H)^- \rightarrow \text{PO}_3^-$. The processes are energetically less favourable than the fragmentations of pSer and pThr shown in Scheme 2.4. Calculations at the modest HF/6-31++G(d,p)//AM1 level of theory showed that the formation of PO_3^- ($m/z = 79$) and the loss of HPO_3 from pTyr have ΔG values of $+83 \text{ kJ mol}^{-1}$ and $+237 \text{ kJ mol}^{-1}$, respectively (Scheme 2.6) [238-239].



Scheme 2.6. Proposed mechanisms for the loss of HPO_3 and formation of PO_3^- from the $(M-H)^-$ anion of a model system containing pTyr. Calculations at the HF/6-31++G(d,p)//AM1 level of theory; R is CH_3CO [238-239].

Formation of H_2PO_4^- and $[(\text{M}-\text{H}) - \text{H}_3\text{PO}_4]^-$ ions (the two diagnostic cleavages of pSer and pThr) were also identified in the negative ion spectra of monophosphorylated Tyr containing peptides [240-241]. It was suggested that the formation of these ions were initiated by nucleophilic attack of the carboxylate end group on the phosphorus of the phosphate, effecting transfer of PO_3H_2 from Tyr to the C-terminal carboxylate group. This rearranged species can then liberate H_2PO_4^- and also form $[(\text{M}-\text{H}) - \text{H}_3\text{PO}_4]^-$ following pathway A or B (Scheme 2.7) [241].



Scheme 2.7. Proposed mechanisms for the loss of H_3PO_4 and formation of H_2PO_4^- from the $(\text{M}-\text{H})^-$ anion of a model system containing pTyr. Calculations at the HF/6-31++G(d,p)//AM1 level of theory [241].

Even though phosphate transfers from pTyr (and to a lesser extent from pSer/Thr) to the carboxyl group, side-chain hydroxyl groups and the amide functionality have been reported [240], details of these phosphate rearrangements and subsequent fragmentations have not been studied in detail. For instance, how does phosphate rearranges from Tyr to carboxylate containing moieties, or to Ser/Thr (and vice versa), and do these rearrangements take place to the same extent? In addition, do the phosphate rearrangements initiate any subsequent fragmentations? The present study investigates:

1. Whether pTyr, pSer and pThr transfer phosphate to C-terminal carboxylate anions and to the carboxyl anion side chains of Asp and Glu. Are there any characteristic cleavage reactions accompanying these rearrangements?
2. Whether there is any change in the propensity of phosphate group transfers if the location of the phosphorylated residue is altered; for instance, when the phosphate group is moved further away from the C-terminal carboxylate end of the peptide or the distance between the phosphorylated residues and non-phosphorylated residues are varied.
3. Whether the phosphate group can be transferred between Tyr, Ser and Thr and if such a rearrangement is followed by a characteristic fragmentation reaction.
4. Whether the phosphate groups in di- and tri-phosphorylated serine containing peptides interact with each other or aggregate.
5. Finally, the mechanisms for phosphate rearrangement and cognate cleavage reactions are considered by experimental observation with the assistance of theoretical calculations (carried out by Dr. Tianfang Wang, the University of Adelaide).

2.3 Results and discussion

2.3.1 pTyr containing peptides: phosphate rearrangement to the C-terminal carboxylate anion followed by cyclisation/cleavage reactions of the resultant (M-H)⁻ anions

One of the aims of this study was to investigate whether the phosphate rearrangement (illustrated in Scheme 2.7) still occurs when the pTyr residue is moved further away from the C-terminal carboxylate anion. Thus, a series of monophosphorylated peptides was examined containing pTyr residues at positions 3, 4, 5 and 9 amino acid residues away from the C-terminus. These peptides were prepared deliberately to contain amino acids with

neutral side chains so that only the reactive carboxylate end group can approach and interact with the phosphate side chain. Studied peptides are listed in Table 2.1.

Table 2.1. Studied pTyr peptides.

Peptide	Sequence
1	GApYGL(OH)
2	GApYGLG(OH)
3	GApYGLGL(OH)
4	GApYGLGLGL(OH)

The Q-TOF 2 negative ion spectra of **1** and **3** are summarised in Table 2.2, whereas the spectra of **2** and **4** are recorded in Figure 2.2 and 2.3, respectively.

Table 2.2. Negative ion mass spectra of **1, 3**

1 GApYGL(OH), (M-H)⁻ m/z 558.

CID MS/MS of m/z 558 [Q-TOF 2, m/z (loss or formation) relative abundance (%)]:

558 (M-H)⁻ 28; 540 (H₂O) 16; 478 (HPO₃) 8; 460 (H₃PO₄) 15; 307 [GAY(NH⁻)] 24; 97 (H₂PO₄⁻) 100; 79 (97-H₂O) 32.

m/z 307 CID MS/MS/MS (Orbitrap mass spectrometer)

α ions, m/z 250, 179 [GAY(NH₂)]; β ions, m/z 127; δY_3 , m/z 144; γY_3 , m/z 162

m/z 307 - C₇H₆O → m/z 201 [GAG(NH⁻)]

Sequence of m/z 307: GAY(NH⁻)

3 GApYGLGL(OH), (M-H)⁻ m/z 728.

CID MS/MS of m/z 728 [Q-TOF 2, m/z (loss or formation) relative abundance (%)]:

728 (M-H)⁻ 14; 710 (H₂O) 18; 648 (HPO₃) 22; 630 (H₃PO₄) 43; 597 (β1) 6; 540 (β2) 5; 477 [GAYGL(NH⁻)] 100, 460 (477-NH₃) 16; 420 (477-G) 8; 349 (477-GA) 6; 307 [477-LG(β')] 42; 97 (H₂PO₄⁻) 43; 79 (PO₃⁻) 19.

GAYGL(NH₂) (M-H)⁻ *m/z* 477.

CID MS/MS of *m/z* 477 listed in nominal masses of α and β cleavages.

α cleavages; *m/z* 420, 349, 186. β cleavages; *m/z* 127. Sequence GAYGL(NH₂)

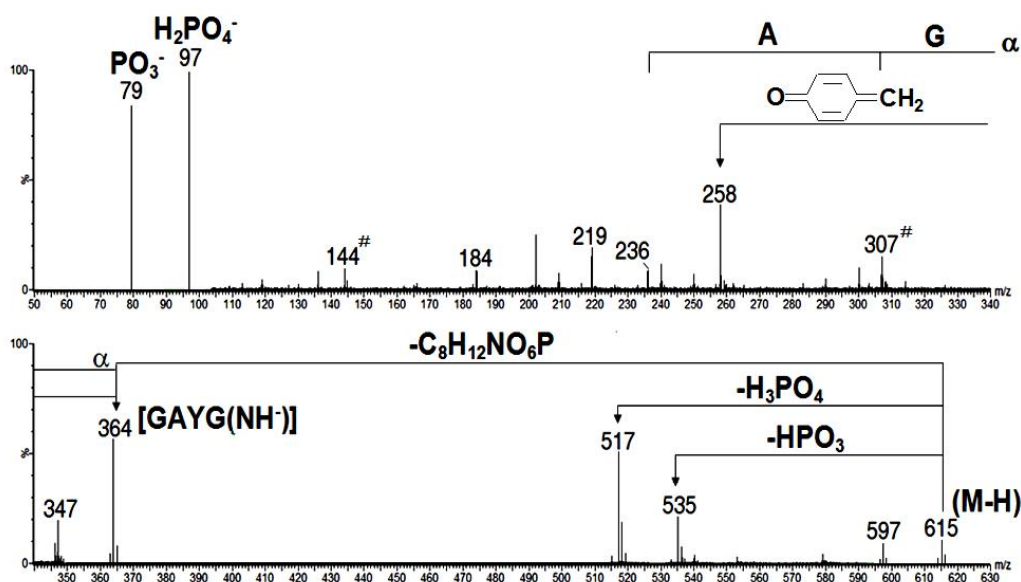


Figure 2.2. CID MS/MS of the parent (M-H)⁻ anion of **2** [GApYGLG(OH)]. Multiplication ranges as follows: *m/z* 100-350 (x10). Q-TOF 2 mass spectrometer. The CID high resolution MS/MS/MS data (Orbitrap) for the [(M-H) - HPO₃]⁻ show β cleavage anions at *m/z* 460, 347, 290 and 127 indicating a sequence GAYLG(OH).

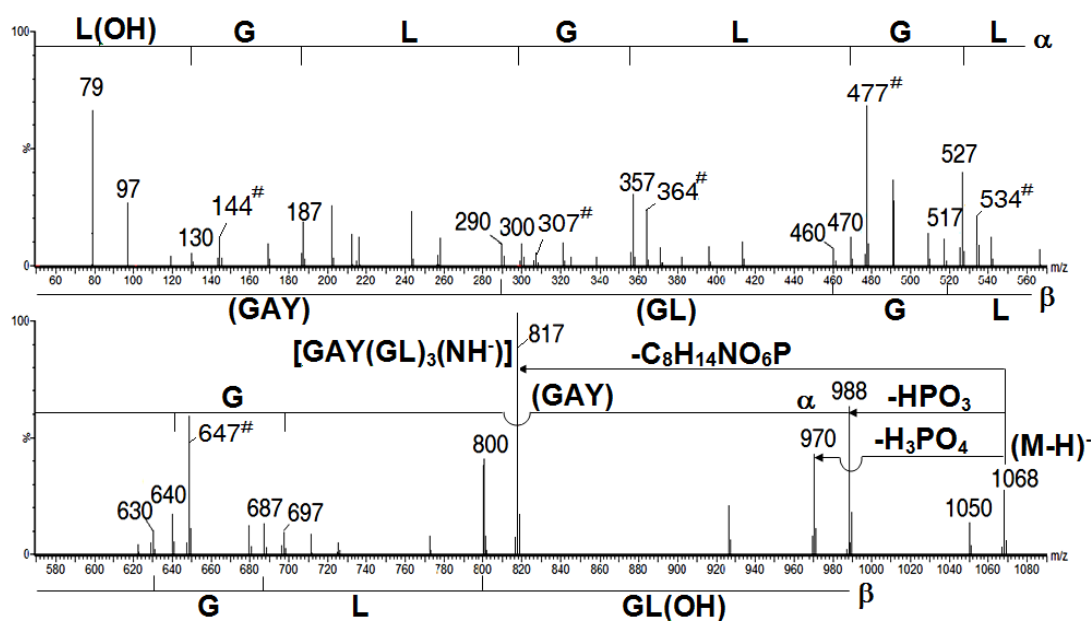


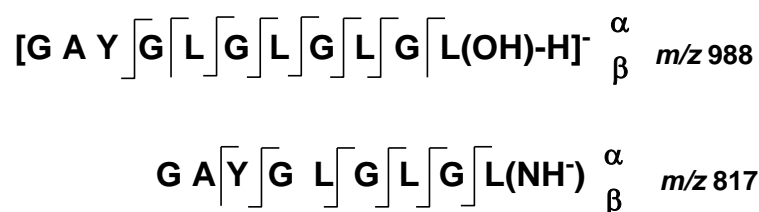
Figure 2.3. CID MS/MS data for the $(M-H)^-$ anion of **4** [GApYGLGLGLGL(OH)]. Multiplication ranges as follows: m/z 51-100 (x4), 102-295 (x36), 296-805 (x6). Q-TOF 2 mass spectrometer.

All spectra of the peptides **1-4** show peaks at m/z 97 ($H_2PO_4^-$) and peaks corresponding to loss of H_3PO_4 from $(M-H)^-$ anions. The data suggest that the phosphate group migrates from pTyr to the terminal carboxylate anion, even in the peptide that has seven amino acid residues between pTyr and the carboxylate terminus. The full sequencing information of each peptide is achieved from the fragmentation of the corresponding anion $[(M-H) - HPO_3]^-$. In addition, four major fragment ions (three of them are the most abundant fragments) in the spectra of the peptides **1-4** namely m/z 307, 364, 407, 817 respectively have one thing in common, they are all amide anions formed by cleavage of the $[(M-H) - HPO_3]^-$ anions at the centre carbons of the penultimate amino acid residues, as shown in Table 2.3.

Table 2.3.

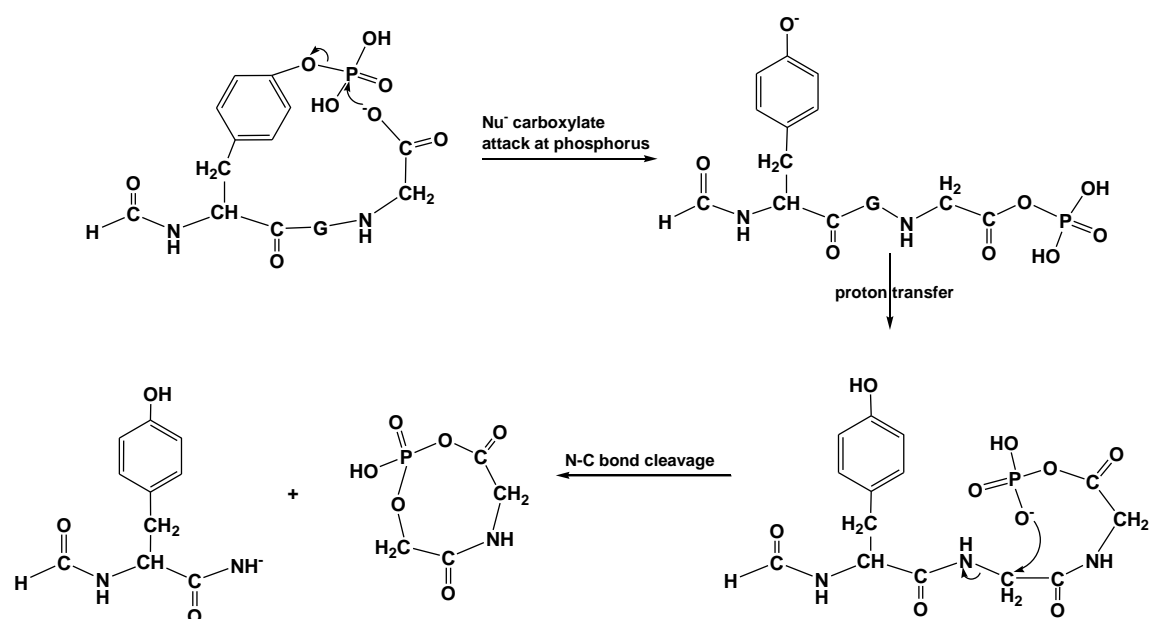
m/z 558 \rightarrow m/z 307	$[GApYGL(OH) - H]^- \rightarrow [GAY(NH_2) - H]^-$	5
m/z 615 \rightarrow m/z 364	$[GApYGLG(OH) - H]^- \rightarrow [GAYG(NH_2) - H]^-$	6
m/z 728 \rightarrow m/z 477	$[GApYGLGL(OH) - H]^- \rightarrow [GAYGL(NH_2) - H]^-$	7
m/z 1068 \rightarrow m/z 817	$[GApYGLGLGLGL(OH) - H]^- \rightarrow [GAYGLGLGL(NH_2) - H]^-$	8

The structures of the fragment anions **5-7** were confirmed by MS/MS/MS high resolution data obtained with an Orbitrap mass spectrometer. Negative ion MS/MS measurements of the (M-H)⁻ anion **4** (*m/z* 1068) and the energised source formed ions *m/z* 988 [(M-H) - HPO₃]⁻ and *m/z* 817 were carried out (data not presented here) which provide the sequencing data of the fragment ions as illustrated in Scheme 2.8 and Figure 2.3.



Scheme 2.8. Schematic representation of backbone cleavages of the energised source formed ions *m/z* 988 [(M-H) - HPO₃]⁻ and *m/z* 817.

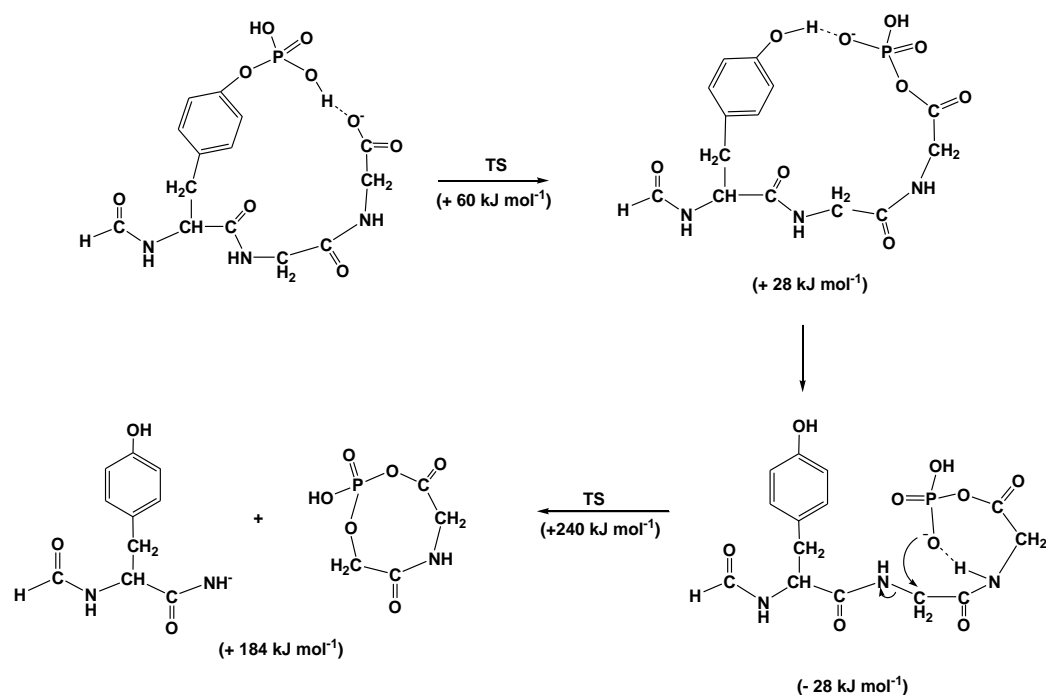
Despite having the same structures as δ anions (see section 1.9.2 in Chapter 1), the anions **5-8** cannot be formed by the classical δ backbone cleavage because a δ peptide backbone cleavage does not occur for Gly or Leu residues. Thus, this diagnostic fragmentation must involve a phosphate involved reaction as shown in Scheme 2.9. The C-terminal-carboxylate phosphate rearrangement is followed by H transfer (to the Tyr residue) to generate a phosphate anion. The phosphate anion then attacks the electrophilic carbon centre of the penultimate amino acid residue in an S_Ni reaction. N-C bond cleavage is the last step to produce the product anion and a cyclic phosphate containing moiety. The formation of H₂PO₄⁻ and the amide anion (*m/z* 817) from peptide **4** [with pTyr at 7 amino acids away from the last residue Le(OH)] indicates that the parent anion has a flexible conformation such that the C-terminal carboxylate anion can approach and interact with the phosphate to allow the phosphate transfer. It can be concluded that phosphate rearrangement takes place irrespective of the position of the pTyr residue in the studied peptide sequence.



Scheme 2.9. Proposed mechanism for the S_Ni cyclisation/cleavage reaction at the penultimate amino acid residue of a pTyr containing peptide to produce an amide anion.

Careful investigation of negative ion MS/MS data for **1-8** reveals that the phosphate S_Ni /cleavage reaction above may occur with certain amino acid residues further along the backbone toward the N-terminal end of the peptide but to a lesser extent than the sequence shown in Scheme 2.9. This is best demonstrated by the spectrum of peptide **4** (Figure 2.3) with the formation of a series of low abundant amide anions at m/z 647 [GAYGLGL(NH^-)], 534 [GAYGLG(NH^-)], 477 [GAYGL(NH^-)], 364 [GAYG(NH^-)], 307 [GAY(NH^-)] and 144 [GA(NH^-)]. Similar fragmentation behaviour is also observed in the negative ion spectra of peptides **1-3**.

The mechanism illustrated in Scheme 2.9 is supported by theoretical calculations at the modest HF/6-31+g(d)//AM1 level of theory for a simple model shown in Scheme 2.10. Following the C-terminal-carboxylate phosphate rearrangement, the cyclisation process is mediated by the formation of the H-bonded intermediate (-28 kJ mol^{-1}), in which the phosphate anion is locked in a convenient position so that it can interact with the central carbon of the penultimate amino acid residue. Although the phosphate rearrangement to C-terminal carboxylate is quite favourable energetically, the subsequent cleavage reaction occurs via a surprisingly high transition state of $+240 \text{ kJ mol}^{-1}$. The overall reaction sequence is calculated to have $\Delta G_{\text{reaction}}$ of $+184 \text{ kJ mol}^{-1}$.



Scheme 2.10. The S_{Ni} cyclisation/cleavage process of the rearranged C-terminal phosphate anion. Calculations at the HF/6-31+g(d)//AM1 level of theory by Dr. Tianfang Wang.

2.3.2 pTyr rearrangement to an internal carboxylate anion of Asp or Glu

The pTyr/C-terminal $-\text{CO}_2^-$ rearrangement was observed for all pTyr containing peptides investigated. The next question is whether this phosphate transfer can occur for another carboxylate site such as Asp or Glu side-chain carboxylate. In order to answer this question, a series of peptides **9-12** were prepared and their negative ion spectra were examined (Table 2.4).

Table 2.4. Peptides containing pTyr and Asp/Glu studied.

Peptide	Sequence
9	GLGpYDVG(V)(OH)
10	GLGpYEVGV(OH)
11	GLpYGV(D)GV(OH)
12	GLpYGV(E)GV(OH)

The spectra of **9** and **11** are displayed in Figure 2.4 and 2.5, whereas the CID MS/MS tandem data for the (M-H)⁻ parent ions of **10** and **12** are provided in Table 2.5, respectively.

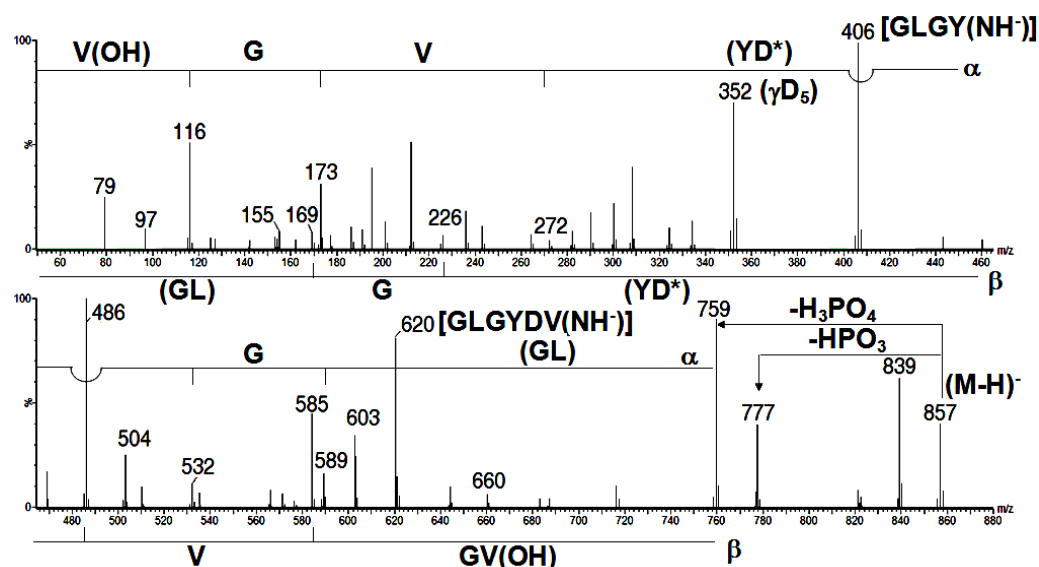


Figure 2.4. CID MS/MS data for the (M-H)⁻ anion of **9** [GLGpYDVG(V)(OH)]. Multiplication ranges as follows: m/z 100-690 (x16), 780-845 (x10). D* is NHCH(-CH=CO)-CO. Q-TOF 2 mass spectrometer.

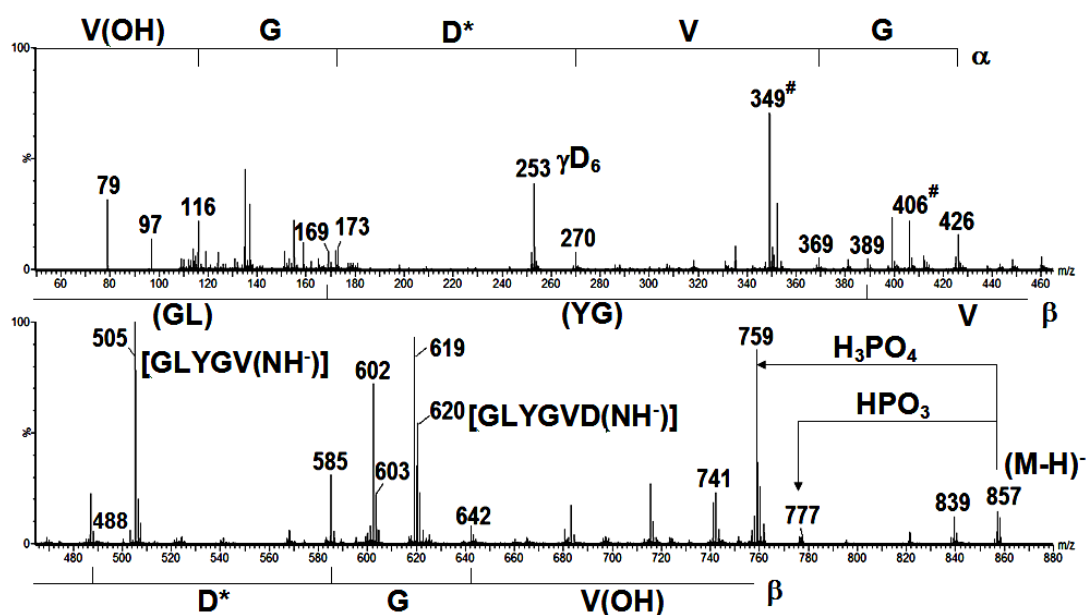


Figure 2.5. CID MS/MS data for the (M-H)⁻ anion of **11** [GLpYGV(D*)D(V)(OH)]. Multiplication ranges as follows: m/z 100-250 (x24), 260-500 (x6), 510-735 (x4). D* is NHCH(-CH=CO)CO. Q-TOF 2 mass spectrometer.

Table 2.5. Negative ion CID MS/MS data from the (M-H)⁻ anions and fragment anions derived from **10** and **12**. (Q-TOF 2 mass spectrometer).

10 GLGpYEVGV(OH) (M-H)⁻, m/z 871

[(M-H) - HPO₃]⁻, m/z 791 (identification of pY4)

α ions; m/z 734, 621, 401, 272, 173, 116

β ions; m/z 674, 226

E5: m/z 406 (δ); 384 (γ)

m/z 564(α 5) - C₇H₆O → m/z 440

Sequence [GLGYEVGV(OH)]

There are three possible (M-H)⁻ anions (m/z 871) and the presence of the appropriate backbone cleavages identify them as follows:

(a) [GLGpYEVGV(OH) - H]⁻, (m/z 871)

α ions; m/z 814, 701, 401, 173, 116 [GL(GpY)(EV)GV(OH)]

β ions; m/z 697

γ E5; m/z 384

Sequence [GL(GpY)EVGV(OH)]

(b) [GLGYEVGV(OPO₃H₂) - H]⁻, (m/z 871)

[(M-H) - H₃PO₄]⁻, m/z 773 and H₂PO₄⁻, m/z 97

α ions; m/z 814, 701 [GL-]

β ions; m/z 674, 617, 226 [(GL)(YE)VG_V(OPO₃H₂)]

Sequence [(GL)(YE)VG_V(OPO₃H₂)]

m/z 634; S_Ni/cleavage ion from [GLGYE_VVG_V(OPO₃H₂) - H]⁻, (m/z 871)

α ions; m/z 464, 407, 244, 115 [(GL)GYEV(NH₂)]

β ions; m/z 169, 389, 518 [(GL)(GY)EV(NH₂)]

E5: m/z 406 (δ); 227 (γ)

Sequence [(GL)GYEG_V(NH₂)⁻]

(c) [GLGYE(PO₃H)VG_V(OH) - H]⁻, m/z 871

α ions; m/z 814, 701, 644, 272, 173, 116 {GLG[YE(PO₃H)]VG_V(OH)}

β ions; m/z 697, 389, 226, 169 {(GL)GY[E(PO₃H)V]G_V(OH)}

Sequence [GLGYE(PO₃H)VG_V(OH)]

12 GL_pYGV_EGV(OH) (M-H)⁻, m/z 871

Rearranged phosphate [GLYG_VVEGV(OPO₃H₂) - H]⁻ produces the cleavage ions

GLYG_VE(NH₂)⁻ [m/z 634 (base peak)] with GLYG_V(NH₂)⁻ [m/z 505] and GLY(NH₂)⁻ [m/z 349] of small abundance ($\leq 10\%$).

[(M-H) - H₃PO₄]⁻ anion, m/z 773. [GLYG_VVEG*_V - H]⁻ [*_V is NHC(C₃H₇)=C=O]:

α ions, m/z 716, 603, 440, 383, 284 [(GL)YGV(EG*_V)]

β ions, m/z 674, 488, 332 [(GL)(Y_G)E(G*_V)]

δ , γ ions, m/z 186 (δ Y₃). 267 (γ E₆), 505 (δ E₆)

Sequence GLYGVE(G*V)

Rearranged phosphate [GLYGVE(PO₃H)GV(OH)] gives the cyclisation product m/z 505 [GLYGV(NH⁻)].

[(M-H) - H₃PO₄]⁻, m/z 773, [GLYGV*EGV(OH) - H]⁻ [*E is NHC(CH₂CH=C=O)CO]:

α ions, m/z 603, 440, 383, 284, 173, 116 [(GL)YGV*EGV(OH)]

β ions, m/z 559, 488, 332. {332(GV)*E[GV(OH)]}

Sequence [(GL)YGV*EGV(OH)]

The major peaks m/z 620 (from **9** and **11** in Figure 2.4 and 2.5) and m/z 634 (from **10** and **12**, Table 2.5) corresponding to the S_Ni cyclisations/cleavages at the centre carbons of the penultimate amino acid residues of these peptides (cf Scheme 2.10) are still observed in the spectra of the (M-H)⁻ anions of **9-12**. The formation of H₂PO₄⁻ (m/z = 97) and the [(M-H) - H₃PO₄]⁻ anions indicating the phosphate Tyr/C-terminal carboxylate transfer are also noted.

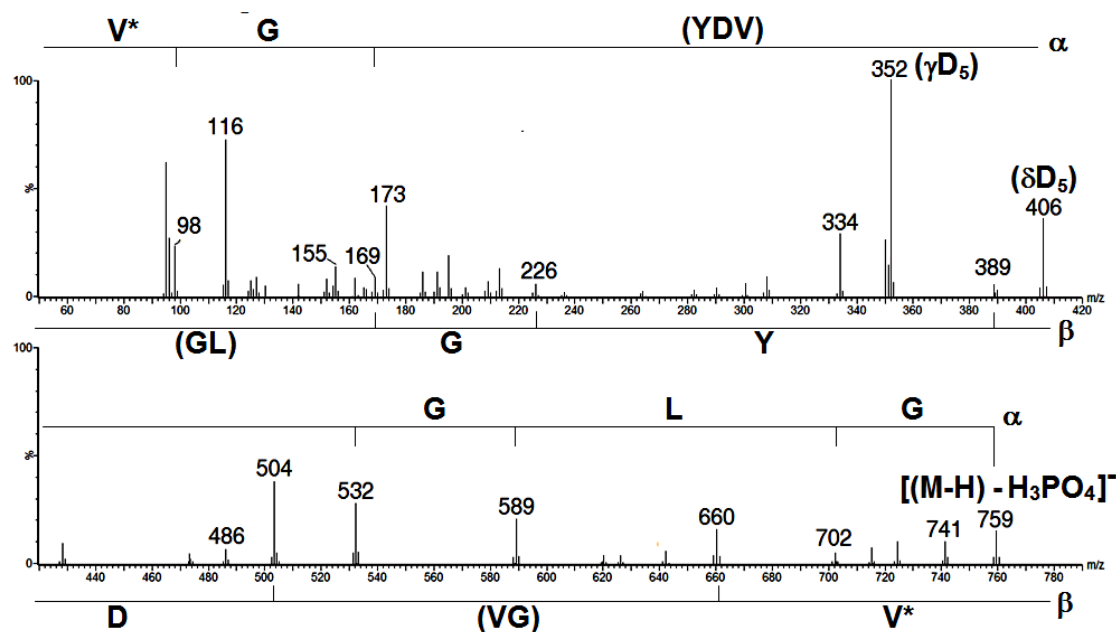
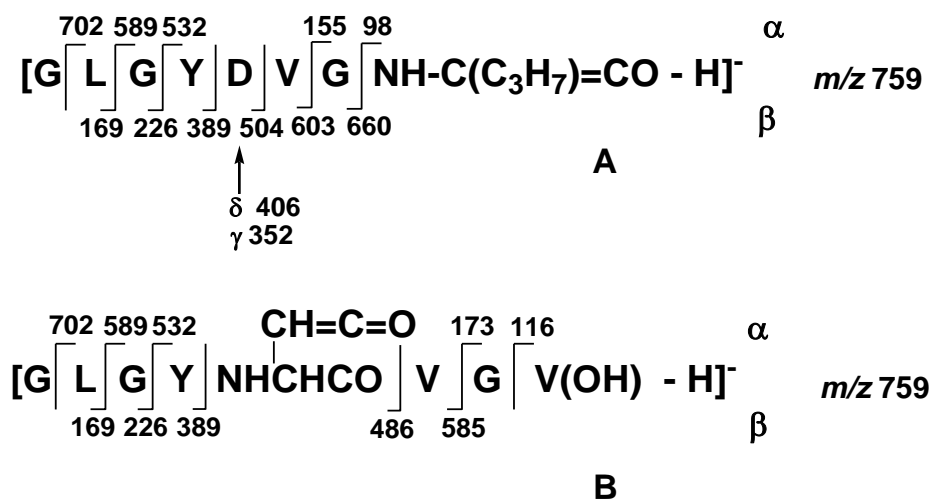


Figure 2.6. CID MS/MS data for the [(M-H) - H₃PO₄]⁻ anions of **9** [GLGpYDVGv(OH)].

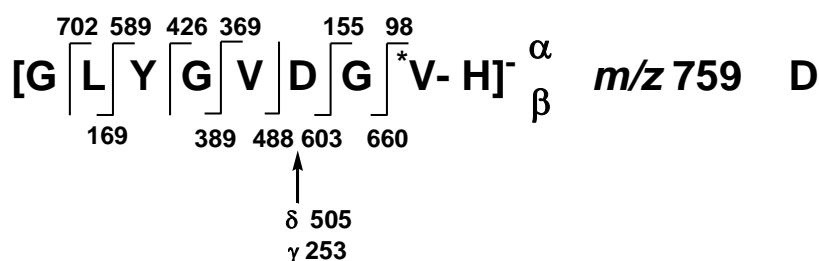
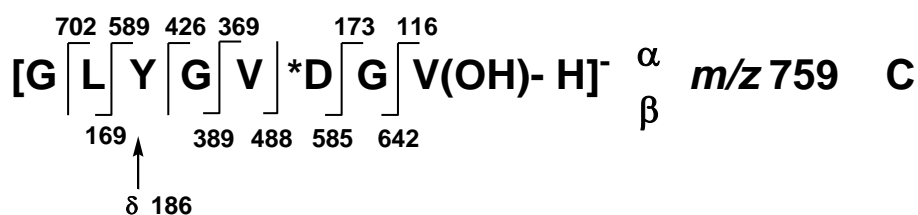
Multiplication ranges as follows: m/z 50-230 (x6), 330-436 (x16). V* is NHC(C₃H₇)=C=O. Q-TOF 2 mass spectrometer.

The CID MS/MS tandem mass spectrum of m/z 759 (loss of H_3PO_4 from the deprotonated ion of **9**) is recorded in Figure 2.6. Scheme 2.11 displays two possible structures of this species including **A** formed by the loss of H_3PO_4 from a rearranged C-terminal phosphate anion and **B** formed by the loss of H_3PO_4 from a rearranged phosphate Asp analogue.



Scheme 2.11. Schematic representation of backbone cleavages of **A** formed by the loss of H_3PO_4 from a rearranged C-terminal phosphate anion and **B** formed by the loss of H_3PO_4 from a rearranged phosphate Asp analogue of peptide **9**.

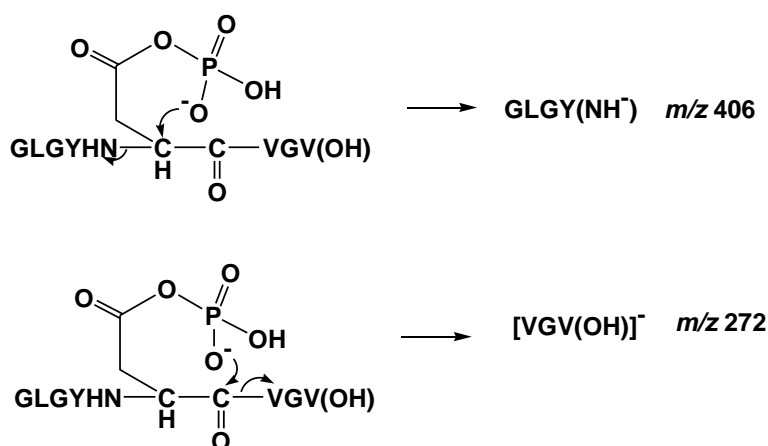
The spectrum of the $[(\text{M-H}) - \text{H}_3\text{PO}_4]^-$ ion of **9** (Figure 2.6) shows the fragment anions depicted in Scheme 2.11 indicating that some of the anions m/z 759 have the structure **A** and some have the structure **B**. In other words, the phosphate group of the precursor ion m/z 857 may migrate to either carboxylate site before loss of H_3PO_4 to form **A** and **B**. The key fragmentations of **B** are noted in Figure 2.6 and Scheme 2.11. A similar scenario is observed for the $(\text{M-H})^-$ ion of peptide **11** where Asp is moved further away from the pTyr residue (Scheme 2.12). It is interesting that there is no evidence for pTyr/Glu side-chain carboxylate rearrangement in the spectrum of $[(\text{M-H}) - \text{H}_3\text{PO}_4]^-$ of **10**. Instead there is dominant pTyr/C-terminal carboxylate transfer. In conclusion, in the cases of the $(\text{M-H})^-$ anions of **9** and **10**, the phosphate group of pTyr undergoes competitive rearrangement to the C-terminal and Asp carboxylate groups.



*D is $\text{NHCH}(\text{CH}=\text{CO})\text{CO}$, *V is $\text{NHC}(\text{C}_3\text{H}_7)=\text{C}=\text{O}$

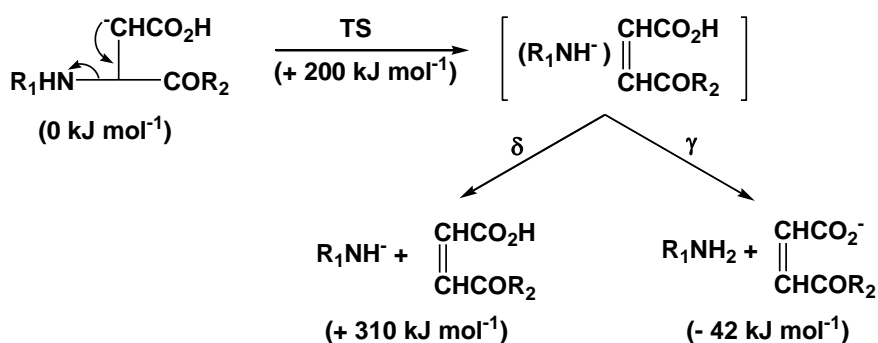
Scheme 2.12. Schematic representation of backbone cleavages of **C** formed by the loss of H_3PO_4 from a rearranged C-terminal phosphate anion and **D** formed by the loss of H_3PO_4 from a rearranged phosphate Asp analogue of peptide **11**.

The phosphate rearrangement to a side-chain Asp-carboxylate is now confirmed. Perhaps, the rearranged pAsp anion may undergo a similar cyclisation/cleavage reaction as that displayed in Scheme 2.9. According to this scenario, the phosphate rearranged anion should attack the central carbon of the amino acid located two amino acids before the Asp residue. The spectrum of the $(\text{M}-\text{H})^-$ anion of **9** [GLGpYDVG $\text{V}(\text{OH})$] (Figure 2.4) shows that there is no major product ion of [GLG(NH $^-$)] (m/z 243) corresponding to that process. There are, however, two other possibilities for further reaction of the rearranged Asp anion involving six and seven-centred cyclisations as shown in Scheme 2.13. The product anion m/z 272 has the same structure as the α_5 anion (originating from the $(\text{M}-\text{H})^-$ ion of peptide **9**), while the product anion m/z 406 has the same structure as the δ_5 anion. Thus, although there is the presence of the peak m/z 406 in the spectrum of the $(\text{M}-\text{H})^-$ anion of **9**, it is impossible to confirm experimentally from this data whether this peak comes from the δ peptide backbone cleavage or from the cyclisation reaction depicted in Scheme 2.13.

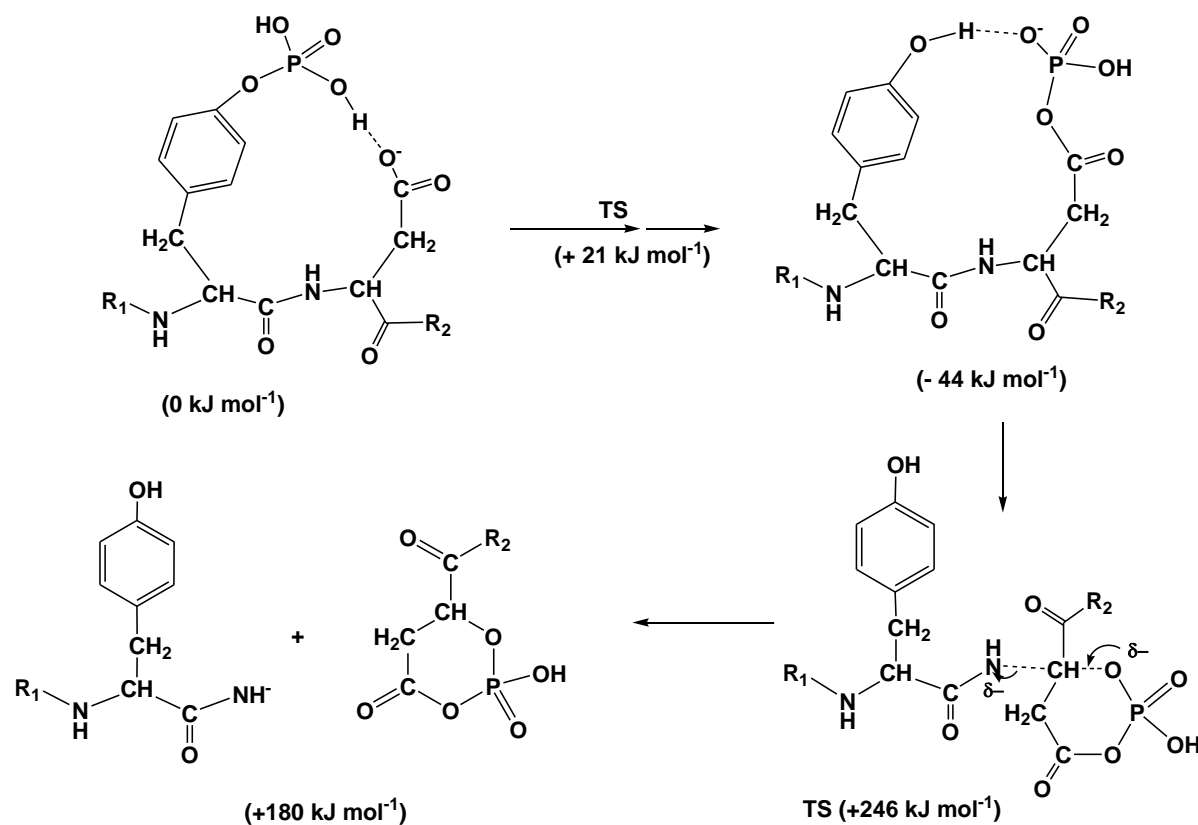


Scheme 2.13. Two possible cyclisation/cleavage processes of the rearranged phospho-Asp anion of **9**.

In this case, it turns out that theoretical calculations can assist with determination of the origin of the fragment m/z 406. At the modest HF/6-31G(d)//AM1 level of theory, a simple model basically containing only the Asp residue shows an unfavourable δ fragmentation with the $\Delta G_{\text{reaction}}$ barrier of 200 kJ mol^{-1} and an overall $\Delta G_{\text{reaction}}$ of $+310 \text{ kJ mol}^{-1}$ (Scheme 2.14). In comparison, a model consisting of pTyr located next to the Asp residue is calculated to undergo a six-centred cyclisation sequence through several intermediates as shown in Scheme 2.15. The process commences with the favourable Tyr/Asp phosphate rearrangement ($\Delta G_{\text{reaction}}$ of -44 kJ mol^{-1}). The following $S_{\text{Ni}}(\text{P})$ cyclisation/cleavage is endothermic by $+180 \text{ kJ mol}^{-1}$ which proceeds over a barrier of $+246 \text{ kJ mol}^{-1}$ (Scheme 2.15). The theoretical study therefore suggests that the rearrangement/cyclisation is more energetically favourable than the δ fragmentation process.



Scheme 2.14. Calculations for the formation of γ and δ ions from the deprotonated ions of peptides containing Asp at the HF/6-31G(d)//AM1 level of theory by Dr. Tianfang Wang. R_1 and R_2 are CH_3CO and NHCH_3 , respectively.



Scheme 2.15. The rearrangement of an $(M-H)^-$ ion of pTyr/Asp to an $(M-H)^-$ ion Tyr/pAsp followed by the cyclisation/cleavage of the pAsp species $[R_1\text{-Tyr-NHCH}(\text{CH}_2\text{CO}_2\text{PO}_3^-)\text{COR}_2]$ to form $R_1\text{-Tyr}(\text{NH}^-)$. R_1 is CHO and R_2 is OCH₃. Calculations at the HF/6-31G(d)//AM1 level of theory by Dr. Tianfang Wang.

2.3.3 Phosphate rearrangement from pSer/Thr to carboxylate anion centres

It has already been shown that pTyr may transfer the phosphate group to both C-terminal and internal carboxylate anions. The next question is whether the same processes may occur for pSer/pThr. In order to investigate these scenarios, a series of $(M-H)^-$ ions from synthesised peptides (listed in Table 2.6) were subjected to CID MS/MS. The CID mass spectrum of the $(M-H)^-$ ion of **14** is displayed in Figure 2.7 while CID MS/MS data for **13** and **15** are summarised in Table 2.7. The $(M-H)^-$ anion of **14** undergoes two series of α and β fragmentations corresponding to both the non-rearranged $[\text{GLpTGVA}(\text{OH}) - \text{H}]^-$ and the rearranged species $[\text{GLTGVA}(\text{OPO}_3\text{H}_2) - \text{H}]^-$. The first series is displayed schematically on Figure 2.7, indicating the sequence $\text{GL}^*\text{TGVA}(\text{OH})$ [$*\text{T}$ is $\text{NHCH}(\text{=CHCH}_3)\text{CO}$] (the loss of phosphoric acid from the unrearranged deprotonated ion of **14**). On the other hand, the phosphate rearrangement to C-terminal carboxylate is evidenced by the presence of α and β

fragments originating from GLTGV*A [*A is NHCH(CH₃)CO₂PO₃H₂]. These fragmentations are shown in the formula drawn on Figure 2.7. Similar fragmentations of the deprotonated ions of **13** and **15** are summarised in Table 2.7. Thus phosphate migration to a C-terminal carboxylate anion may occur from pTyr, pSer and pThr.

Finally, observation of the product ion GLTG(NH⁻) (*m/z* 344) and the loss of CH₃CHO from this ion (see Figure 2.7) suggests that phosphate rearrangement and subsequent S_Ni(P) cyclisation/cleavage occurs in the same fashion as observed for pTyr (cf Scheme 2.15)

Table 2.6. Peptides containing pSer and Asp/Glu studied.

Peptide	Sequence	Peptide	Sequence
13	GLpSGVA(OH)	21	GAYpSGL(OH)
14	GLpTGVA(OH)	22	GApYTGL(OH)
15	GLpSGVGVA(OH)	23	GAYpTGL(OH)
16	GLpSDVG(OH)	24	GLpSGSGV(OH)
17	GLpSEVG(OH)	25	GLSGpSGV(OH)
18	GLpTDVG(OH)	26	GLpSGLGLSGV(OH)
19	GLpSVGDGV(OH)	27	GLSGLGLpSGV(OH)
20	GApYSGL(OH)		

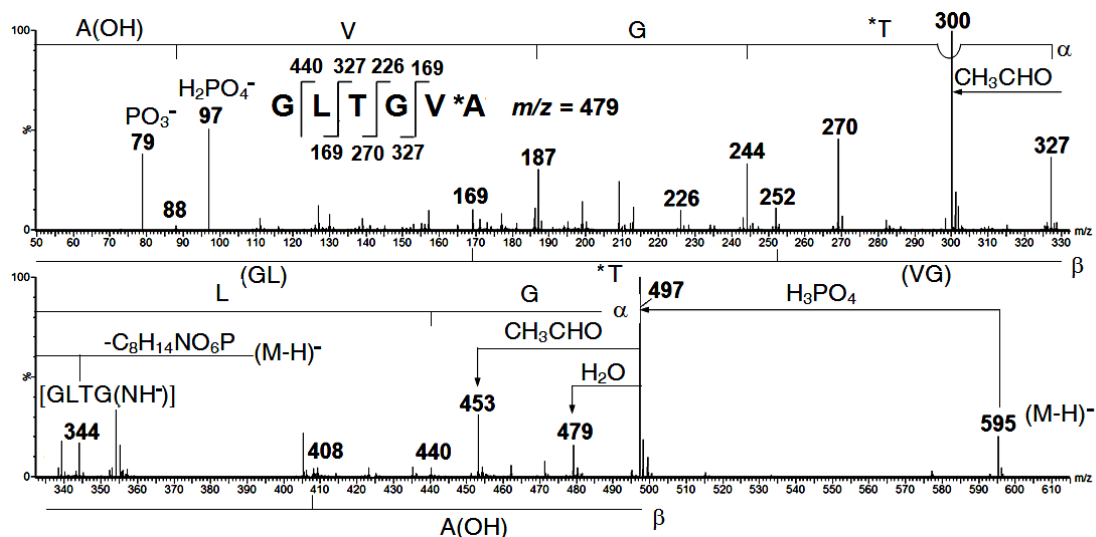


Figure 2.7. CID MS/MS of the $(M-H)^-$ precursor anion of **14** GLpTGVA(OH). *A is $NHC(CH_3)=C=O$. Multiplication ranges:- m/z 100-246 (x20), 247-495 (x6). Q-TOF 2 mass spectrometer.

Table 2.7. Negative ion data for $(M-H)^-$ and some fragment anions from **13** and **15**. [*S is $NHC(=CH_2)CO$; *A is $NHC(CH_3)=C=O$].

13 GLpSGVA(OH) $(M-H)^-$, m/z 581; $[(M-H) - H_3PO_4]^-$, m/z 483, base peak.

m/z 483 (unrearranged), α ions, m/z 426, 313, 244, 187 [GL*SG(VA(OH))]

β ions, m/z 394, 238, 169 [(GL)*S(GV)A(OH)]

Sequence GL*SGVA(OH)

$[GLSGVA(OPO_3H_2) - H]^-$, m/z 581 \rightarrow $GLSG(NH)^-$, m/z 330

m/z 483 (rearranged), α ions, m/z 426, 313, 226, 169 [GLSG(V*A)]

β ions, m/z 313, 169 [(GL)(SG)(V*A)]

15 GLpSGVGVA(OH) $(M-H)^-$, m/z 737; $[(M-H) - H_3PO_4]^-$, m/z 639, base peak.

m/z 639 (unrearranged), α ions, m/z 582, 469, 400, 343, 244, 187, 88 [GL*SGVGVA(OH)].

β ions, m/z 550, 394, 169 [(GL)(*SGV)(GV)A(OH)]

Sequence GL*SGVGVA(OH)

[GLSGVGVA(OPO₃H₂) - H]⁻, m/z 737 → GLSGVG(NH⁻), m/z 486; GLS(NH⁻), m/z 273.

m/z 639 (rearranged), α ions, m/z 582, 469, 382, 325 [GLSG(VGV*A)]

β ions, m/z 469, 412, 313 [(GLSG)VG(V*A)]

Sequence GLSGVG(V*A)

The CID mass spectrum of the (M-H)⁻ anions of **18** (Figure 2.8) is examined to determine whether the phosphate group can migrate from pThr to the side-chain carboxylate moiety of Asp. The α and β backbone cleavages of the two [(M-H) - H₃PO₄]⁻ species [GLTDV*G - H]⁻ (*G is NHCH=C=O) and [GL*TDVG(OH) - H]⁻ (*T is NHC(=CHCH₃)CO) observed in Figure 2.8 are shown in Scheme 2.16. These data indicate the co-occurrence of two phosphate migration processes, namely (i) to the C-terminal carboxylate and (ii) to side-chain carboxylate anion of Asp. Diagnostic S_{Ni}(P) cyclisation/cleavages also occur, with the formation of [GLTD(NH⁻)] (m/z 402) from [GLTDVG(OPO₃H₂) - H]⁻ and [GLT(NH⁻)] (m/z 287) from [GLTD(PO₃H⁻)VG(OH)]. Both m/z 402 and 287 lose CH₃CHO to give m/z 358 and 243, respectively. The relative abundances of the fragments originating from non-rearranged (schematically displayed on Figure 2.8) and rearranged anions infer that these processes are comparable.

Similar phosphate rearrangements are observed for (M-H)⁻ anions of pSer peptides **16**, **17** and **19** (listed in Table 2.8) regardless of distance between pSer and Asp residues. It can therefore be concluded that the phosphate groups of pSer and pThr undergo the same rearrangement processes to C-terminal carboxylate and side-chain carboxylate moieties which is followed by similar cyclisation/fragmentations to that of pTyr.

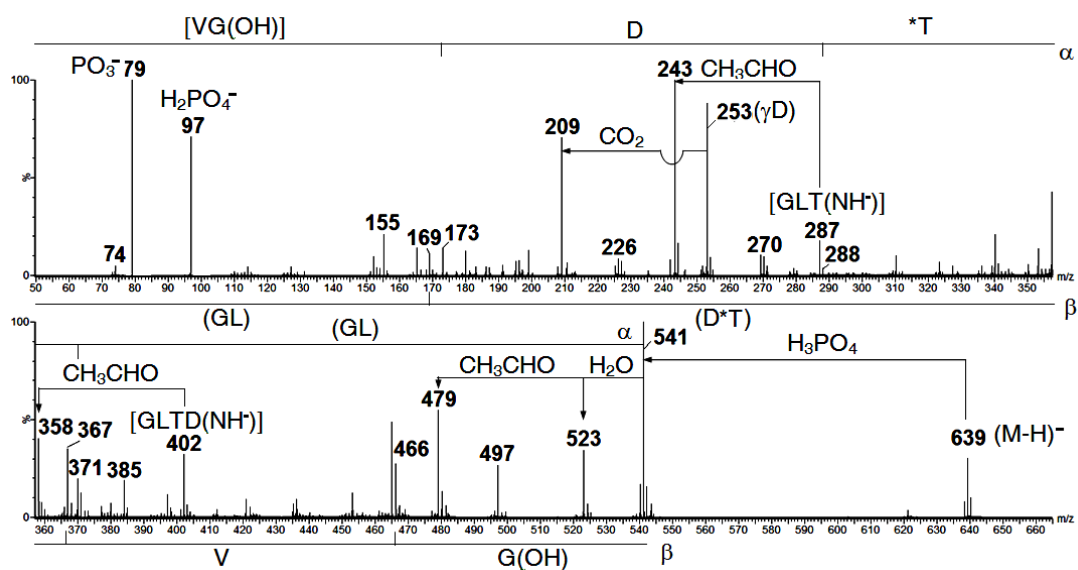
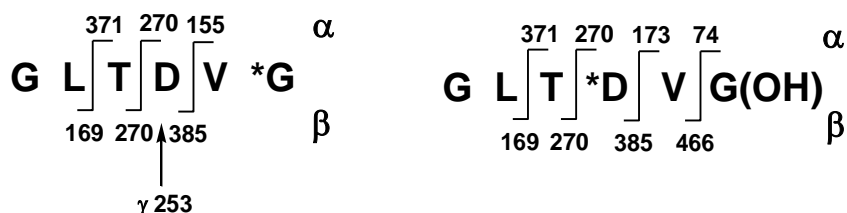


Figure 2.8. CID MS/MS of the $[M-H]^-$ precursor anion of **18** GLpTDVG(OH). *T is $NHC(=CHCH_3)CO$. Multiplication ranges: m/z 60-250 (x10), 290-490 (x15). Q-TOF 2 mass spectrometer.



m/z 541 [$*G$ is $NHCH=C=O$; $*D$ is $NHCH(CH=C=O)CO$]

Scheme 2.16. Schematic representation of backbone cleavages of the two $[(M-H) - H_3PO_4]^-$ species originated from **18**.

Table 2.8. Negative ion data for (M-H)⁻ and selected fragment anions from **16**, **17** and **19**.

*S is NHC(=CH₂)CO, *A is NHC(CH₃)=C=O], *G is NHCH=C=O, *D is NHCH(CH=C=O)CO and *E is NHCH(CH₂CH=C=O)CO.

16 GLpSDVG(OH) (M-H)⁻, *m/z* 625; [(M-H) - H₃PO₄]⁻, *m/z* 527 (base peak).

m/z 527 (unrearranged), α ions, *m/z* 357, 288, 173, 74 [(GL)*SDVG(OH)]

β ions, *m/z* 452, 353, 238, 238, 169 [(GL)*SDVG(OH)]

δD4, *m/z* 255; γD4, *m/z* 271

Sequence (GL)*SDVG(OH).

[GLSDVG(OPO₃H₂ - H)]⁻ → GLSD(NH⁻), *m/z* 388; GL(NH⁻), *m/z* 186.

m/z 527(C-term rearranged), α ions, *m/z* 357, 270, 155 [(GL)SD(V*G)]

β ions, *m/z* 256, 169 [(GL)S(DV*G)]

δD4, *m/z* 273; γD4, *m/z* 253

Sequence (GL)SD(V*G)

[GLSD(PO₃H⁻)VG(OH)] → GLS(NH⁻), *m/z* 273.

m/z 527 (D rearrangement), α ions, *m/z* 357, 270, 173, 74 [(GL)S*DVG(OH)]

β ions, *m/z* 452, 353, 169 [(GL)(S*D)VG(OH)]

Sequence (GL)S*DVG(OH)

17 GLpSEVG(OH) (M-H)⁻, *m/z* 639; [(M-H) - H₃PO₄]⁻, *m/z* 541.

m/z 541 (unrearranged). α ions, *m/z* 484, 371, 302, 173, 74 [GL*SEVG(OH)]

β ions, *m/z* 466, 238 [(GL*S)(EV)G(OH)]

Sequence [(GL*SEVG(OH)

[GLSEVG(OPO₃H₂ - H)]⁻, *m/z* 639 → GLSE(NH⁻), *m/z* 402, GL(NH⁻), *m/z* 186.

m/z 541 (C-term. rearranged), α ions, *m/z* 484, 371, 284 [GLS(EV*G)]

β ions, *m/z* 484, 256; γ E4, *m/z* 267 [(GLS)EV*G]

Sequence GLSEV*G

GLSE(PO₃H⁻)VG(OH), *m/z* 639

m/z 541 (E rearrangement), α ions, *m/z* 484, 371, 284, 173, 74 [GLS*EVG(OH)]

β ions, *m/z* 466, 256 [(GLS)(*EV)G(OH)]

Sequence GLS*EVG(OH)

19 GLpSVGDVG(OH) (M-H)⁻, *m/z* 781; [(M-H) - H₃PO₄]⁻, *m/z* 683, base peak.

m/z 683 (unrearranged), α ions, *m/z* 513, 444, 345, 288, 173 [(GL)*SVGD(VG(OH))]

β ions, *m/z* 608, 509, 337, 169 [(GL)(*SV)(GD)VG(OH)]

γD6 ion, *m/z* 411

Sequence [(GL)*SVGD(VG(OH))]

[GLSVGDVG(OPO₃H₂) - H]⁻, *m/z* 781 → GLSVGD(NH⁻), *m/z* 544

m/z 683 (C-term. rearranged), α ions, *m/z* 513, 426, 327, 270, 155 [(GL)SVGD(V*G)]

β ions, *m/z* 527, 412, 169 [(GL)(SVG)DV*G]

γD6, *m/z* 429; γD6, *m/z* 253

Sequence [(GL)SVGDV*G]

[GLSVGD(PO₃H⁻)VG(OH), m/z 781 → GLSVG(NH⁻), m/z 429

m/z 683 (D rearrangement), α ions, m/z 513, 426, 327, 270, 173 [(GL)SVG*D(VG(OH))]

β ions, m/z 608, 509, 412, 169 [(GL)(SVG)*DVG(OH)]

Sequence [(GL)SVG*DVG(OH)]

2.3.4 Phosphate migration between modified and unmodified amino acid residues of Tyr, Ser and Thr in monophospho-peptides (M-H)⁻ anions

The next problem to be addressed is whether a phosphate group can migrate from monophosphorylated Tyr to unphosphorylated residues of Ser and Thr (and vice versa). The pTyr/Ser to Tyr/pSer (and vice versa) rearrangements were studied by examination of the spectra of (M-H)⁻ anions of the peptide GApYSGL(OH) **20** (Figure 2.9) and GAYpSGL(OH) **21** (Figure 2.10). Both display similar fragmentation patterns with the most abundant peaks being [(M-H) - H₃PO₄]⁻ and H₂PO₄⁻. Considering the spectrum of the deprotonated ion of **20**, the formation of these anions is partially attributed to the rearrangement of the phosphate group to the C-terminal carboxylate anion, confirmed (i) by the fragmentations of the [(M-H) - H₃PO₄]⁻ anion of sequence GAYSG*L (m/z 547) [*L is NHC(C₄H₉)=C=O] and (ii) by the presence of the characteristic S_Ni(P) cyclisation/cleavage fragment GAYS(NH⁻) (m/z 394). There is also apparent phosphate transfer from pTyr to Ser to form [GAYpSGL(OH) - H]⁻. This transfer is evident from the observation of α and β backbone cleavages from the [(M-H) - H₃PO₄]⁻ species GAY*SGL (m/z 547) (shown schematically in Figure 2.9). On the other hand, in the CID mass spectrum of the (M-H)⁻ ion of **21** (Figure 2.10), the peak at [(M-H)⁻ - HPO₃] (the diagnostic fragment of pTyr) is low in abundance (0.3%) indicating that the pSer to Tyr process is at best a minor one.

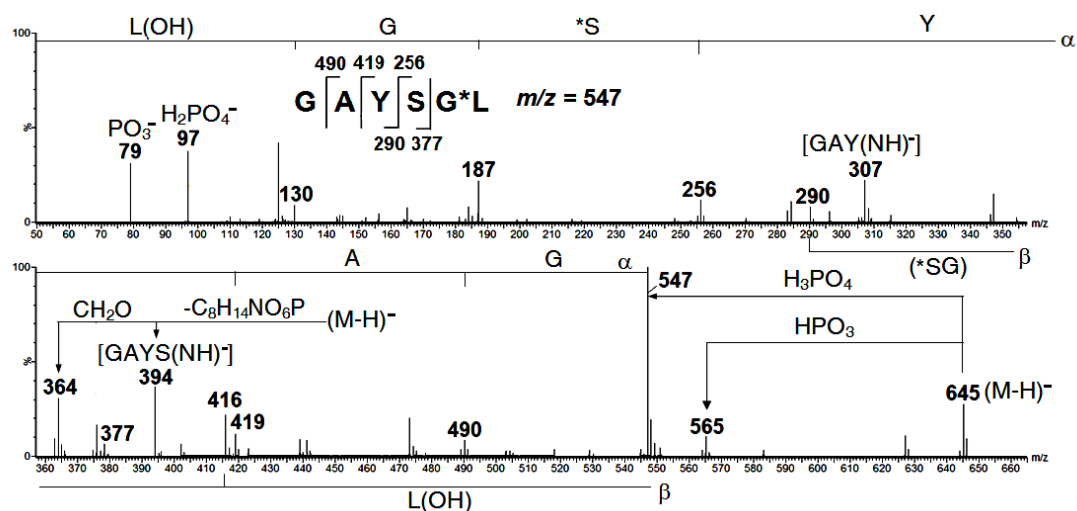


Figure 2.9. CID MS/MS data of the $(M-H)^-$ precursor anion of GApYSGL(OH). *L is $NHC(C_4H_9)=C=O$. *S is $NHC(=CH_2)CO$. Multiplication ranges: m/z 100-200 (x6), 300-547 (x4), 550-640 (x4). Q-TOF 2 mass spectrometer.

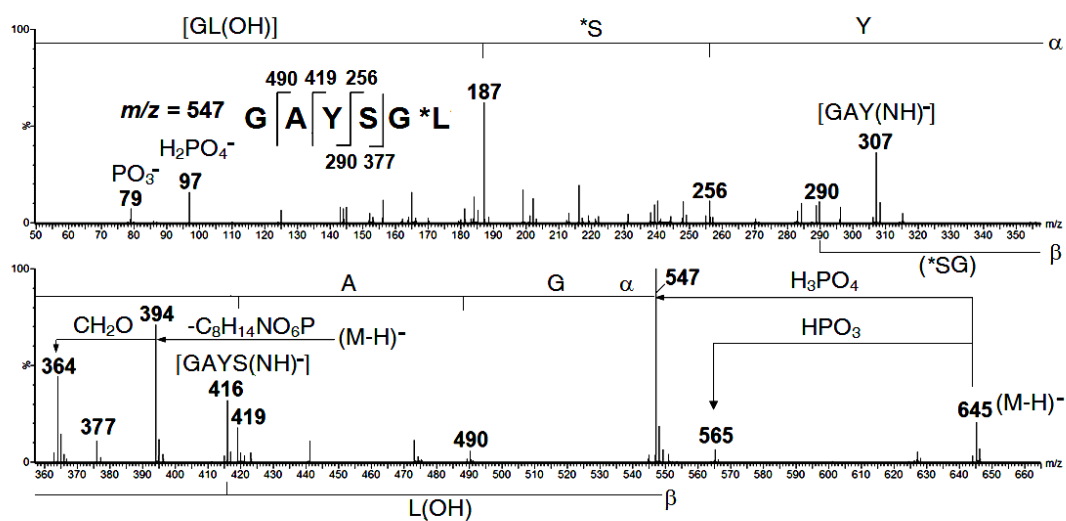


Figure 2.10. CID MS/MS data of the $(M-H)^-$ precursor anion of GAYpSGL(OH). *L is $NHC(C_4H_9)=C=O$. *S is $NHC(=CH_2)CO$. Multiplication ranges: m/z 100-250 (x16), 260-547 (x10), 550-640 (x4). Q-TOF 2 mass spectrometer.

The negative ion MS data of two other phosphopeptides, GApYTGL(OH) **22** and GAYpTGL(OH) **23** (Table 2.9), were also examined to ascertain whether the negative ion chemistry of pThr is similar to that of pSer. The phosphate rearrangement between pTyr and Thr is generally comparable with those of their Ser analogues. The pTyr/Thr to Tyr/pThr

rearrangement is a predominant one while the reverse reaction (pThr/Tyr to Thr/pTyr) is not observed.

Table 2.9. Negative ion data for (M-H)⁻ and selected fragment anions of **22** and **23**.

*T is NHC(=CHCH₃)CO; *L is NHC(C₄H₉)=C=O.

22 GApYTGL(OH) (M-H)⁻, *m/z* 659; [(M-H) - H₃PO₄]⁻, *m/z* 561.

[GAYpTGL(OH) - H]⁻, *m/z* 659 → GAY(NH⁻), *m/z* 307

m/z 561 (T rearrangement), α ions, *m/z* 504, 433, 270, 187, 130 [GAY*TGL(OH)]

β ions, *m/z* 430, 290, 127 [(GA)Y(*TG)L(OH)]

Sequence GAY*TGL(OH)

[GAYTGL(OPO₃H₂) - H]⁻, *m/z* 659 → GAYT(NH⁻), *m/z* 408; GA(NH⁻), *m/z* 144.

m/z 561 (C-terminal rearranged), α ions, *m/z* 504, 433, 270, 169 [GAYT(G*L)]

β ions, *m/z* 391, 290, 127 [(GA)YT(G*L)]

Sequence GAYTG*L

23 GAYpTGL(OH) (M-H)⁻, *m/z* 659; [(M-H) - H₃PO₄]⁻, *m/z* 561.

[GAYpTGL(OH) (unrearranged) → GAY(NH⁻), *m/z* 307.

m/z 561 (unrearranged), α ions, *m/z* 504, 433, 270, 187, 130 [GAY*TGL(OH)]

β ions, *m/z* 430, 290, 127 [(GA)Y(*TG)L(OH)]

Sequence GAY*TGL(OH)

[GAYTGL(OPO₃H₂) - H]⁻, *m/z* 659 → GAYT(NH⁻), *m/z* 408, GA(NH⁻), *m/z* 144

m/z 561 (C-terminal rearranged), α ions, m/z 504, 433, 270, 169 [GAYT(G*L)]

β ions, m/z 391, 290, 127 [(GA)YT(G*L)]

Sequence GAYT(G*L)

2.3.5 Phosphate rearrangement between two serine residues in the (M-H)⁻ of monophosphorylated peptides

It has been shown above that phosphate translocation from pTyr to Ser/Thr is more feasible than that from pSer/pThr to Tyr. The next question is that, if the peptide contains two Ser residues with only one phosphorylated, will phosphate transfer between the two sites still occur? In addition, does the phosphate rearrangement still occur if these two Ser residues are moved further away from each other? These questions were investigated using the four peptides **24-27** (Table 2.6). The first pair has two Ser residues at three amino acid residues apart while the last pair has them at six residues apart.

The CID MS/MS spectrum of **27** is presented in Figure 2.11 while the fragmentation data of the deprotonated ions of **24-26** are recorded in Table 2.10. There are several observations necessary to point out from mass analysis of these four peptides. Each pair of peptides (**24-25** or **26-27**) produces very similar CID MS/MS spectra, indicating that each pair undergoes the same rearrangements to create the same mixture of precursor ions. The mass spectrum of each of the four peptides shows phosphate transfer from one Ser to the other and to the C-terminal carboxylate moiety, with the fragments originating from the pSer to Ser rearranged species of lower abundance compared to those from the un-rearranged species and C-terminal carboxylate rearranged counterparts. The pSer to Ser rearrangement still occurs when they are located six amino acids away from each other, indicating that in gas phase the deprotonated ion (e.g. of **27**) has to adopt a random conformation so that phosphate group on Ser8 can approach and interact with Ser3.

More details of the pSer to Ser rearrangement can be elucidated by looking at Figure 2.11. This spectrum presents three sets of α and β fragmentations corresponding to three structures of precursor (M-H)⁻ anions, namely the unrearranged species, the pSer/C-carboxylate anion

and pSer/Ser rearranged species. The sequence track of the non-rearranged $[(M-H) - H_3PO_4]^-$ is shown in schematic form, whereas the fragmentations of pSer to Ser rearranged are displayed on the formula in Figure 2.11. In addition, following the C-terminal carboxylate phosphate transfer, characteristic cyclisation/cleavage reactions also occur which are evident by the presence of the diagnostic products of m/z 700 $[GLSGLGLS(NH^-)]$, m/z 443 $[GLSGL(NH^-)]$, m/z 330 $[GLSG(NH^-)]$ and m/z 186 $[GL(NH^-)]$. These anions (except m/z 186) undergo intensive loss of CH_2O from a Ser side chain. The backbone cleavages of the $[(M-H) - H_3PO_4]^-$ ion derived from $[GLSGLGLSV(OPO_3H_2) - H]^-$ are listed in the caption to Figure 2.11. Among the three rearrangement processes, the C-terminal carboxylate phosphate rearrangement is the predominant one as most of the peaks corresponding to this migration are pronounced, or subsequently fragment further to produce pronounced peaks.

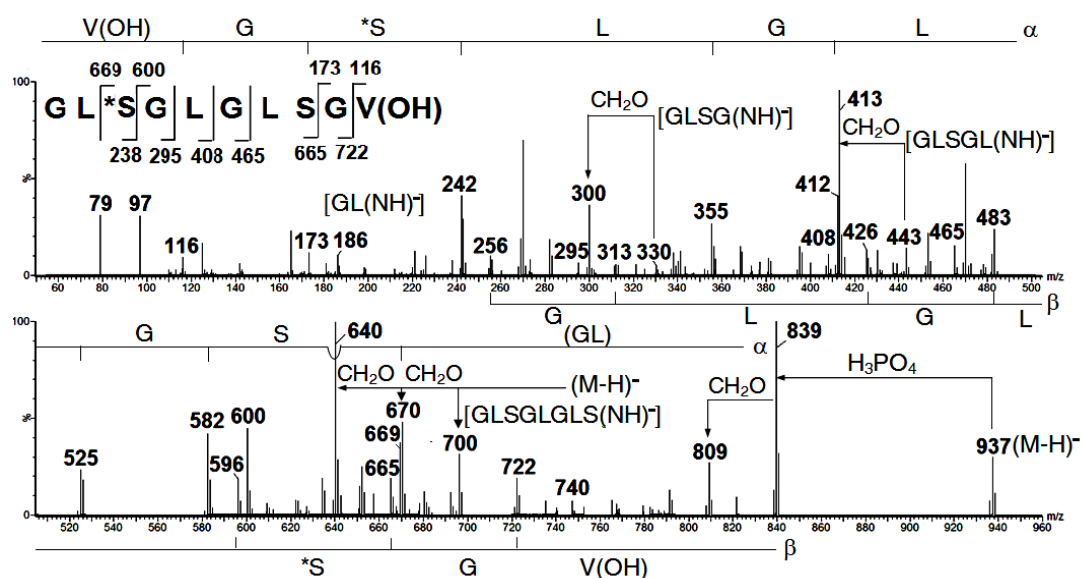


Figure 2.11. CID MS/MS of the $(M-H)^-$ precursor anion of **27** GLSGLGLpSGV(OH). *S is $NHC(=CH_2)CO$. *V is $NHC(C_3H_7)=C=O$. Multiplication ranges: m/z 60-835 (x15). Fragmentations of the C-terminal $[(M-H) - H_3PO_4]^-$ rearrangement anion GLSGLGLS*V (m/z 839) are as follows: α ions, m/z 582, 525, 412, 355, 242 $[(GLS)GLGL(SG*V)]$. β ions, m/z 740, 596, 483, 426, 313, 256 $[(GLS)GLGL(SG)*V]$. Q-TOF 2 mass spectrometer.

In conclusion, the phosphate rearrangements from pSer/Thr to unmodified Tyr, internal acidic side-chain and C-terminal carboxylate moieties are observed. Of these processes, the internal acidic side-chain and C-terminal carboxylate rearrangements are more prevalent compared to the phosphate transfers between Tyr, Ser and Thr residues. The propensity for phosphate migration from Tyr to Ser/Thr is higher than that from Ser/Thr to Tyr.

Table 2.10. Negative ion data for $(M-H)^-$ and fragment anions of **24-26**. *S is $NHC(=CH_2)CO$, *V is $NHC(C_3H_7)=C=O$.

24 GLpSGSGV(OH) $(M-H)^-$, m/z 654; $[(M-H) - H_3PO_4]^-$, m/z 556

m/z 556 (unrearranged), α ions, m/z 499, 386, 317, 260, 173, 116 [GL*SGSGV(OH)]

β ions, m/z 439, 382, 295, 238, 169 [(GL)*SGSGV(OH)]

Sequence GL*SGSGV(OH)]

m/z 556 (S rearranged), α ions, m/z 499, 386, 299, 242, 173, 116 [GLSG*SGV(OH)]

β ions, m/z 439, 382, 313, 256, 169 [(GL)SG*SGV(OH)]

Sequence GLSG*SGV(OH)]

$[GLSGSGV(OPO_3H_2) - H]^-$, m/z 654 \rightarrow $GLSGS(NH^-)$, m/z 417, $GL(NH^-)$, m/z 186

m/z 556 (C-terminal rearranged), α ions, m/z 499, 386, 299, 242, 155 [GLSGS(G*V(OH))]

β ions, m/z 457, 400, 313, 256 [(GLS)GSG*V]

Sequence GLSGSG*V

25 GLSGpSGV(OH), $(M-H)^-$, m/z 654; $[(M-H) - H_3PO_4]^-$, m/z 556

m/z 556 (unrearranged), α ions, m/z 499, 386, 299, 242, 173, 116 [GLSG*SGV(OH)]

β ions, m/z 439, 382, 313, 256 [(GLS)G*S(GV(OH))]

Sequence GLSG*SGV(OH)

m/z 556 (S rearranged), α ions, m/z 499, 386, 317, 173, 116 [GL*S(GS)GV(OH)]

β ions, m/z 439, 382 [382 (GV(OH))]

Sequence GL*S(GS)GV(OH)

[GLSGSGV(OPO₃H₂) - H]⁻, m/z 654 → GLSGS(NH⁻), m/z 417; GL(NH⁻), m/z 186

m/z 556 (C-terminal rearranged), α ions, m/z 499, 386, 299, 242, 155 [GLSGS(G*V)]

β ions, m/z 457, 400, 313, 256 [(GLS)GSG*V]

Sequence GLDGSG*V

26 GLpSGLGLSGV(OH) (M-H)⁻, m/z 937; [(M-H) - H₃PO₄]⁻, m/z 839

m/z 839 (unrearranged), α ions, m/z 782, 669, 600, 543, 430, 373, 260, 173, 116

[GL*SGLGLSGV(OH)]

β ions, m/z 722, 665, 578, 465, 408, 295, 238 [(GL*S)GLGLSGV(OH)]

Sequence GL*SGLGLSGV(OH)

m/z 839 (S rearrangement), α ions, m/z 782, 669, 582, 525, 412, 355, 242, 173

[GLSGLGL*S(GV(OH))]

β ions, m/z 722, 665, 596, 483, 426, 313, 256 [(GLS)GLGL*SGV(OH)]

Sequence GLSGLGL*SGV(OH)

[GLSGLGLSGV(OPO₃H₂) - H]⁻, m/z 937 → GLSGLGLS(NH⁻), m/z 700; GLSGL(NH⁻), m/z

443; GL(NH⁻), m/z 186

m/z 839 (C-terminal rearranged), α ions, m/z 782, 669, 582, 525, 412, 355, 242 [GLSGLGLS(G*V)]

β ions, m/z 596, 483, 426, 313, 256 [(GLS)GLGL(SG*V)]

Sequence GLSGLGLS(G*V)

2.3.6 Migration behaviour of the phosphate group in di- and tri-phosphorylated serine containing peptides

The aggregation of phosphate groups in di-phosphorylated peptides containing Ser, Thr and Tyr to form characteristic di-phosphate anions has been reported [242]. The fragment anions m/z 177 ($\text{H}_3\text{P}_2\text{O}_7^-$), 159 (HP_2O_6^-), and sometimes $[(\text{M}-\text{H}) - \text{H}_4\text{P}_2\text{O}_7]^-$ are usually found in the spectra of these peptides. The formation of m/z 177 ($\text{H}_3\text{P}_2\text{O}_7^-$) is initiated by an intramolecular nucleophilic attack of the oxygen next to CH_2 of one pSer with the phosphorus of the second pSer residue. The P-O bond cleavage with concomitant proton transfer is the last step to produce **X** (m/z 177) (Scheme 2.17). The overall process is thermodynamically favourable with ΔG of -299 kJ mol^{-1} (and a barrier of 112 kJ mol^{-1}) [242]. The loss of H_2O from **X** to generate **Y** or **Z** (m/z 159) (Scheme 2.18) takes place subsequently since **X** is formed with such significant excess energy.

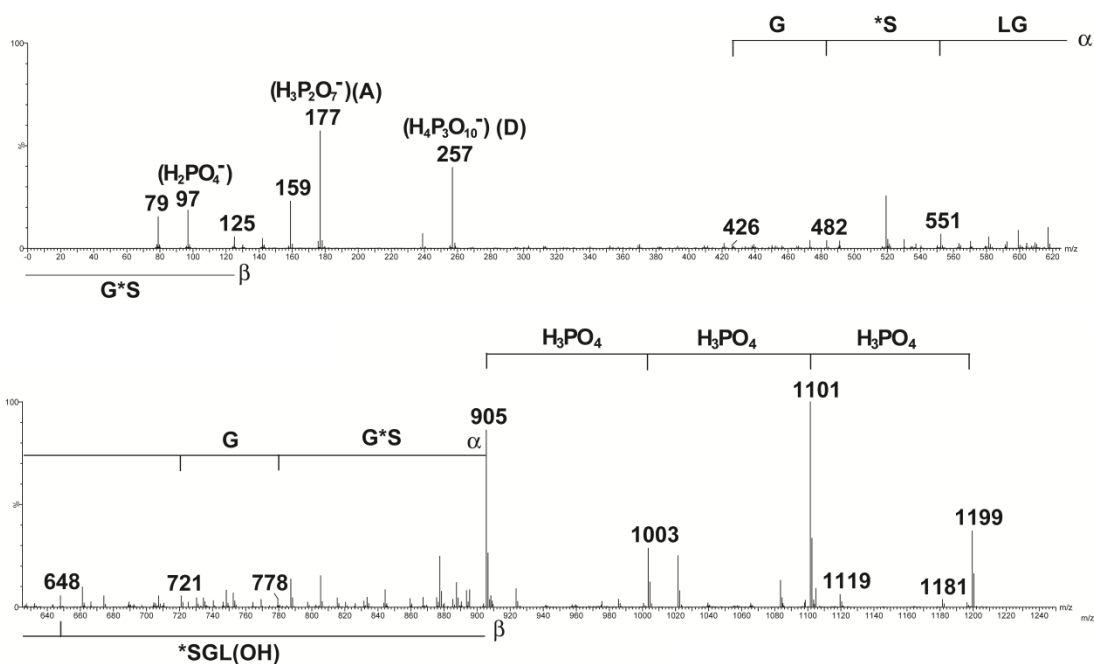


Figure 2.12. CID MS/MS data for the $(M-H)^-$ anion of GpSGLGpSGLGpSGL(OH). Multiplication ranges: m/z 1-150 (x186), 151-260 (x10), 261-910 (x25). Q-TOF 2 mass spectrometer.

The CID MS/MS spectrum shows the peak m/z 905 corresponding to the loss of three phosphoric acid molecules from the parent ion. A negative ion MS/MS measurement of the source formed $[(M-H) - 3H_3PO_4]^-$ anion was carried out to provide the sequencing data of this species as illustrated in Figure 2.12 and Scheme 2.19.

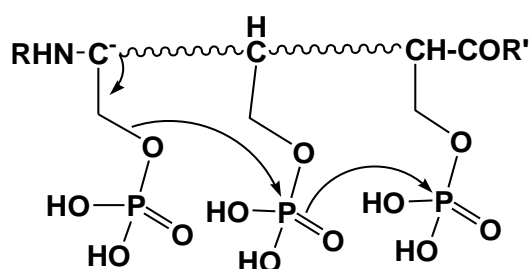


Scheme 2.19. Schematic representation of backbone cleavages of the source formed $[(M-H) - 3H_3PO_4]^-$ anion of peptide GpSGLGpSGLGpSGL(OH).

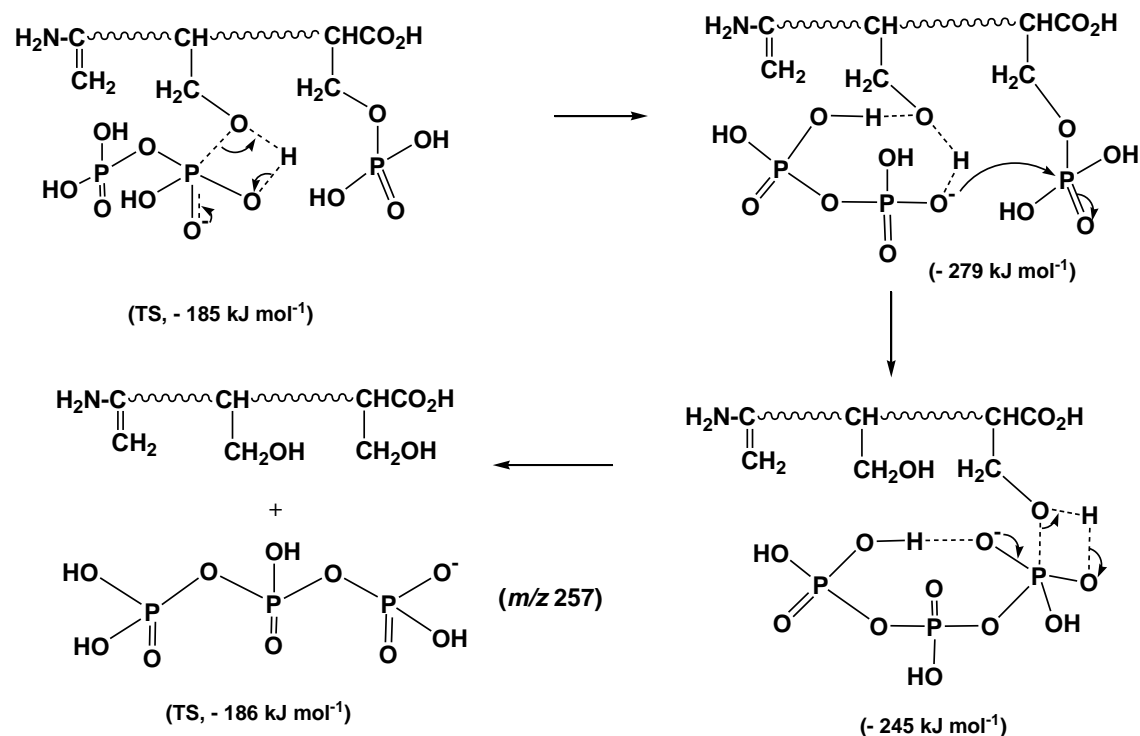
It can be seen in Figure 2.12, apart from anions of m/z 97 ($H_2PO_4^-$) and m/z 177 ($H_3P_2O_7^-$), there is a peak corresponding to m/z 257 ($H_4P_3O_{10}^-$). This indicates the aggregation of three phosphate groups to form this species. MS/MS/MS measurements on m/z 1101, 1003 and 905 were implemented using an LTQ Orbitrap XL ETD hybrid mass spectrometer, with mass resolution of 30,000. Data (not provided here) confirm atomic compositions of major

fragment anions. CID MS/MS of the doubly charged $(M-2H)^{2-}$ anion of this tri-phosphorylated peptide also produces the same fragment anions of m/z 177, 159 and 259, but not the doubly charged counterparts.

Two possible mechanisms for the formation of the tri-phosphate anion have been investigated. The first involves simultaneous migration of the two phosphate moieties to the third (Scheme 2.20). The second mechanism is an extended version of the mechanism shown in Figure 2.12, in which the phosphate groups attach to each other in a stepwise manner (Scheme 2.21).



Scheme 2.20.



Scheme 2.21. The cyclisation of three phosphorylated Ser residues to form m/z 257 ($H_4P_3O_{10}^-$). Calculations at the HF/6-31+G(d)//AM1 level of theory by Dr. Tianfang Wang.

Theoretical calculations at the HF/6-31+G(d)//AM1 level of theory have been carried out on both mechanisms to determine which one is more likely. The transition state for the first mechanism could not be found, whereas the second mechanism occurs based on the same principle shown in Figure 2.12; namely internal nucleophilic substitutions [$S_{Ni}(P)$] with concomitant proton transfer. Energies for transition states and products are displayed on Scheme 2.21.

2.4. Summary and conclusions

The phosphate group in mono-pTyr, Ser and Thr containing peptides may migrate to the C-terminal carboxylate anion, which then initiates a characteristic S_{Ni} cyclisation/cleavage reaction at the central carbon of the penultimate amino acid residue.

A similar phosphate rearrangement from pTyr to side-chain carboxylate sites also occurs. The rearranged species may undergo the S_{Ni} cyclisation/cleavage reaction as above to produce a fragment amide anion or may proceed via six or seven centred cyclisations.

pTyr may transfer phosphate to the side chains of Ser and Thr. The reverse reaction, namely transfer of a phosphate group from pSer/pThr to Tyr is at best, only a minor process.

pSer can transfer phosphate to non-phosphorylated Ser. In general, the unrearranged (M-H)⁻ species provides more abundant fragment anion peaks than does its rearranged pSer counterpart.

The triphosphoSer peptide GpSGLGpSGLGpSGL(OH) produces the singly-charged cyclised anions m/z 177 ($H_3P_2O_7^-$) and m/z 257 ($H_4P_3O_{10}^-$) from both (M-H)⁻ and (M-2H)²⁻ anions. The formations of these multi-phosphate anions are energetically favourable, with overall ΔG of - 299 kJ mol⁻¹ (see Scheme 2.17) and - 245 kJ mol⁻¹ (see Scheme 2.21) respectively at the HF/6-31+G(d)//AM1 level of theory.

In conclusion, fragmentations of energised precursor anions should not be used to determine the positions of phosphorylated residues in phospho-peptides in the following circumstance. If a phospho-peptide containing any or all of Ser, Thr and Tyr is not completely phosphorylated, negative ion cleavages will determine the number of phosphate groups, normally the positions of Ser, Thr and Tyr, but not which residues are phosphorylated. This

is a consequence of the various processes (outlined above) which involve migration of a phosphate group following formation of the initial $(M-H)^-$ species.

2.5 Experimental

2.5.1 Peptide synthesis

All pTyr containing peptides used in this study were synthesized by Hongkong GenicBio Biotech Co., Ltd (Shanghai, China). Purities were > 80% as evidenced by HPLC and MS (Shimadzu LCMS-2010) data. No attempt was made to further purify the phosphopeptides because of the possibility of hydrolysis.

The tri-phosphorylated GpSGLGpSGLGpSGL(OH) was prepared in house by Dr. Denis Scanlon, using Fmoc solid phase peptide synthesis. All listed chemicals were purchased from Sigma-Aldrich, St. Louis, MO, USA, 63178.

2.5.2 Mass spectra

Electrospray tandem mass spectra were obtained using a Micromass Q-TOF 2 hybrid orthogonal acceleration TOF mass spectrometer (Waters/Micromass, Manchester, UK) with a mass range to m/z 10,000. The Q-TOF 2 is fitted with an ESI source in an orthogonal configuration with a Z-spray interface. Samples (25 μ g) were dissolved in acetonitrile/water (1:1 v/v) and infused into the electrospray source at a flow rate of 8 μ l min^{-1} . Experimental conditions were as follows: capillary voltage 2.9 kV, source temperature 80 °C, desolvation temperature 150 °C, and cone voltage 45 V. The argon collision gas energy was 35 eV. All masses for anions shown either in Figures or in Tables are nominal masses (i.e. the sum of the integral masses of the amino acid residues).

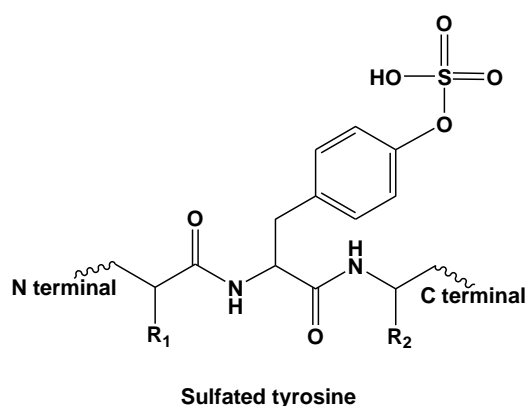
High resolution mass data were obtained with an LTQ Orbitrap XL ETD hybrid mass spectrometer (Thermo Fisher Scientific, MA, USA) equipped with an ESI source. Samples were infused at 5 μ l min^{-1} delivered by a built-in-syringe pump and a spraying voltage of 3.2 kV. A mass resolution of 30,000 (at m/z 400) was used. Tandem MSⁿ (n=2 or 3) experiments were performed using collision energy dissociation set to 25%.

CHAPTER 3

INVESTIGATION OF SULFATED PEPTIDES BY NEGATIVE ION MASS SPECTROMETRY

3.1 Introduction to sulfoproteome

Sulfation has been estimated to be the most abundant post-translational modification of Tyr (Figure 3.1a) with about 1% of the Tyr residues in the eukaryotic proteome being sulfated [243-244]. Protein Tyr sulfation was first observed by Bettelheim in bovine fibrinopeptide B in 1954 [245] and later found in many species of animals and plants including secretory proteins [246-247], plasma membrane proteins [247], adhesion molecules [248-249], coagulation factors [250], plasma proteins [251], immune components [252], G-protein-coupled receptors [253] and the neuropeptide cholecystokinin [254]. The sulfation of tyrosine residues takes place in the trans-Golgi network and is mediated by two tyrosylprotein sulfotransferases, namely TPST-1 and TPST-2 [255-256]. Tyrosine sulfation has been found to be the key modulator of protein-protein interactions of secreted proteins and membrane-bound proteins [257-258]. It is involved in a variety of pathophysiological processes such as the mediation of inflammation, leukocyte adhesion, chemokine receptor signalling and the blood coagulation cascade [255, 258-262]. Sulfation of Ser and Thr have also recently been reported to occur in several eukaryotic proteins (Figures 3.1b and 3.1c) [263]. The ongoing increase in the number of sulfated peptides and proteins discovered implies that sulfation is more ubiquitous than currently perceived.



(a)

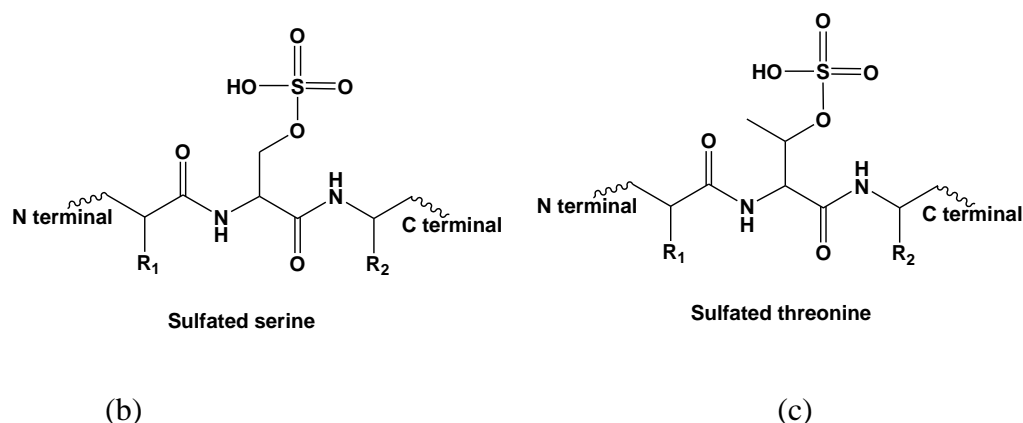


Figure 3.1. Structures of (a) sulfated Tyr, (b) sulfated Ser and (c) sulfated Thr.

Although sulfation and phosphorylation are both monoester modifications of their respective acids resulting in an increase of a nominal mass of 80 Da, they possess different chemical stabilities which lead to differences in their analysis and characterisation. While phosphate peptides/proteins are quite stable, sulfated compounds are highly sensitive to conditions used in peptide/protein preparations and analysis such as low pH, high temperature and high energy deposition [257, 264]. The ease of acidic hydrolysis of sulfate-ester moieties limits the number of biochemical methods which have been utilised for sulfoproteome analysis [265]. For instance, traditional Edman sequencing cannot be used due to the involvement of TFA in the cleavage of the anilinothialione derivatives of the amino acids. Several biochemical approaches have still been considered to be useful in detection of sulfation in peptides/proteins such as radioactive labelling of ^{35}S or amino acid analysis with ^3H -labelled Tyr/Ser/Thr [266]. However, each of these methods has its own short-comings which sometimes result in ambiguous determination of the presence and the position of sulfation in peptides and proteins [266].

3.2 Mass spectrometry based methods for analysis of sulfation

On the other hand, a multitude of studies of sulfated peptides/proteins using MS have been carried out in the last decades. Identification of sulfated moieties within a protein normally requires proteolytic digests to produce peptide fragments which are more readily characterised by MS. Apart from trypsin and chymotrypsin normally used in proteomics, Asp-N and/or Glu-C have been highly recommended for enzymatic digests of sulfated proteins since Asp and Glu are two residues most prevalently found in close proximity to sulfoTyr residues of proteins [267-269]. Proteolytic cleavages using carboxypeptidase Y

and/or aminopeptidase M may be needed to differentiate between adjacent sulfoTyr residues [267]. In addition, the proteolysis of sulfoTyr containing proteins with chymotrypsin and/or carboxypeptidase Y may be reduced or even precluded if sulfoTyr residues are close to the cleavage sites [270].

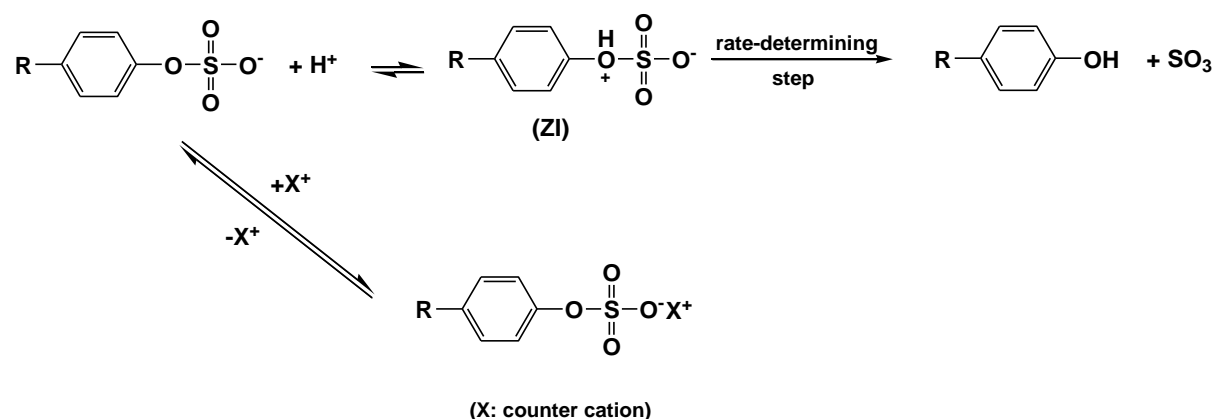
The fragment peptides resulting from enzymatic digests of a sulfated protein can be enriched before being subjected to MS. In contrast with a multitude of well-developed strategies for phosphorylation enrichment, there is a lack of reagents for enrichment of sulfated peptides/proteins. So far, only one anti-sulfoTyr monoclonal antibody which selectively enriches sulfoTyr-containing peptides/proteins has been identified by Hoffhinen's group [271]. In addition, only a small number of techniques including RP-HPLC [272], capillary electrophoresis [273] and ion exchange methods [272, 274] are employed prevalently in separation and enrichment of sulfated peptides. However, care must be taken with the solvent used in order to avoid acidic hydrolysis of the sulfate group. For example, the buffer solution in RP-HPLC, 0.1% TFA solution, is replaced by ammonium acetate at a pH near neutral in the separation of sulfated peptides [272].

3.2.1 Detection of sulfation in sulfated peptides/proteins

In positive MS mode, suppression of ionisation by the negatively-charged sulfate esters and the high lability of the sulfate group have been reported to be two major obstacles for detection of sulfated peptides/proteins. Sulfate residues are easily lost in the ion source region even during 'soft' ionisation [264]. Complete losses of sulfate moieties in matrix assisted laser desorption/ionisation (MALDI) and to a slightly lesser extent in electrospray ionisation (ESI) are observed when standard ionisation conditions are used [275-276]. Sulfate moieties are therefore prone to be identified falsely as unsulfated residues. Some non-standard ionisation conditions have been suggested to mitigate this phenomenon such as by decreasing source potentials for electrospray, or careful regulation of laser power for MALDI TOF MS [199, 264, 268, 275]. An alternative strategy for determination of the site and stoichiometry of Tyr O-sulfation in proteins makes use of chemical labelling and the lability of sulfate groups in positive mode. The peptides/proteins of interest are acetylated by reacting with S-NHSAc (sulfosuccinimidyl acetate) using imidazole as a catalyst. This only modifies tyrosyl hydroxyl and primary amino groups, leaving the sulfated Tyr moieties unmodified. During MS analysis in the positive ion mode, the sulfuryl groups of

sulfotyrosine residues are lost but the acetylTyr is stable. The detection of unblocked Tyr(s) thus indicates the site of sulfation [277].

Regardless of the ionisation method used, the extent of sulfate loss in negative mode has been reported to be less than that in positive mode [257, 264, 278-279]. This observation indicates that the loss of SO_3 is likely to be a proton-induced process, thus when the sulfated ester is deprotonated in negative mode, the loss of sulfate is diminished [278]. The rationale is suggested based on the mechanism proposed for the cleavage of SO_3 from a sulfoTyr in an acidic environment. According to this mechanism, the rate-determining step is the dissociation of a zwitterionic intermediate (ZI) or the attack of a proton to phenyl oxygen causing the elimination of SO_3 (Scheme 3.1) [280]. The decisive role of the proton in the sulfated Tyr dissociation is further evidenced by increased stability of the sulfated Tyr containing peptide $[\text{Na}]^+$ adducts compared that of their protonated counterparts [267]. The sulfoester groups can also be stabilised by intramolecular salt bridge formation with basic residues such as Arg and His, or by complexation with an external peptide containing multiple Arg residues [281].



Scheme 3.1. Proposed mechanism for the cleavage of SO_3 from a sulfoTyr in an acidic environment.

3.2.2 Differentiation of sulfation and phosphorylation modifications

Another challenge in sulfation analysis by MS is distinguishing the sulfated side chains from the isobaric phosphorylated moieties because they have the same nominal mass of 80 Da. The monoisotopic mass of the sulfate group is 79.9568 Da whereas phosphate addition is 79.9663 Da. These modifications can be in principle differentiated by high mass accuracy

measurements using a FTICR mass spectrometer (or some other high resolution instruments) due to their 9.5 mDa mass difference. However, this method encounters the challenges of, for example, the use of expensive FIICR instruments and interfering chemical noise [282].

For other MS instruments, phosphorylation can be differentiated from sulfation owing to the differences in their stabilities and fragmentation patterns [263, 283-288]. For instance, while sulfated Tyr containing peptides display intensive loss of sulfate moieties, phosphorylated Tyr peptides shows no loss of phosphate groups in positive mode MALDI-TOF mass spectra [285, 289-291]. Thus, this has been used as a means to differentiate these two modifications. In addition, the loss of H₃PO₄ (98 Da) is principally observed for deprotonated ions of pSer/pThr and to lesser extent for pTyr [292] whereas peaks corresponding to the loss of sulfuric acid (MW is also 98 Da) are hardly found in the spectra of sulfated peptides due to the high acidity of this acid [293-294]. However, discrimination between sulfate and phosphate peptides/proteins in this way depends heavily on the type of instrument used, the length of the modified peptides, their charge states and amino acid compositions [281, 295]. For example, the sulfate lability measured by MALDI mass spectrometers can be altered if the peptides contain multiple sulfate moieties or multiple basic residues [295].

Finally, the presence of sulfate residues can be verified by specific chemical or enzymatic removal of sulfate groups followed by MS analysis. Desulfation is normally carried out by acid or sulfatase treatment and the shift of 80 mass units in the mass spectra of the peptides before and after desulfation confirms the presence of sulfate groups [296].

3.2.3 Localization of sulfation sites by mass spectrometry

To date, identification of sulfation sites in peptides and proteins has still remained a challenge for mass spectrometric analysis due to the high lability of sulfate groups as mentioned above. It should be noted that the loss of SO₃ from sulfate residues occurs at the O-S bond not at the C-O bond, resulting in unmodified Tyr/Ser/Thr residues, leaving no trace of the location of sulfated moieties. Therefore, the requisite requirement for determination of sulfation sites is the retention of sulfate groups on their original sites by manipulating ionisation conditions (see section 3.2.1) and dissociation methods.

Some electron-radical based dissociation methods such as electron capture dissociation (ECD) and electron transfer dissociation (ETD) (for details see Chapter 2 section 2.2.2) have

been reported to enhance peptide sequencing and site determination of post-translational modifications [34, 297]. They cleave the peptide backbone randomly, not at the weakest bonds first. Thus, more structural information and less loss of labile sulfate groups have been achieved by these techniques compared to CID [298-299]. However, they are only applicable to sulfonated peptides containing at least one basic amino acid and multiple charges [300]. Charge enrichment by the formation of a divalent metal cation-peptide complex or Na^+ peptide complex may improve ionisation efficiency and modification retainment of sulfate groups in ECD [300-301].

In order to take advantage of the highly efficient ionisation of acidic sulfated peptides in the negative mode, several new dissociation methods have been introduced to characterise this class of peptide; for example electron detachment dissociation (EDD) [302], negative ETD (NETD) [303], negative ion ECD (niECD) [304] and metastable atom-activated dissociation (MACD) [279] to characterise this class of peptide. However, these techniques usually require costly FTICR instruments and not much information is available about the efficiency of these dissociation methods in sulfoproteome analysis to date [279].

A variety of phosphate rearrangement processes within deprotonated $(\text{M-H})^-$ anions of phosphopeptides has been described [41, 239, 241-242, 292, 305]. This may preclude the site determination of this type of post translational modification by negative ion MS. In addition, both sulfate and phosphate residues possess high electron affinities and labilities under negative ion ESI CID conditions. Do sulfate groups behave similarly to phosphate groups in negative mode in terms of rearrangement reactions, and can negative ion ESI CID be used to determine sulfate sites in peptides/proteins? In order to answer these questions, this study considers the negative ion fragmentations of $(\text{M-H})^-$ anions of a number of synthetic sulfated peptides to determine (i) the characteristic fragmentations of sulfate moieties, and (ii) whether sulfate anions can undergo rearrangement analogous to those reported for phosphate anions. The mechanisms for characteristic fragmentations of sulfated peptides observed experimentally are proposed with the assistance of theoretical calculation at the CAM-B3LYP/6-311++g(d,p) level of theory. All theoretical calculations in this study were carried out by Dr. Tianfang Wang.

3.3 Results and discussion

3.3.1 Formation of deprotonated ions of sulfated peptides

A problem with peptide negative ion fragmentations is knowing which deprotonated species is the precursor anion of a particular process, and whether that precursor is formed directly by ESI process, or by collision-induced dissociation of another more stable deprotonated anion following ESI. In this study, several precursor anions may be involved including: sulfate ($-\text{OSO}_3^-$), carboxylate ($-\text{COO}^-$), amide ($-\text{CON}^- \text{-R}$), enolate (either backbone or side chain) and methoxyl ($-\text{CH}_2\text{O}^-$). Deprotonation of the sulfate moiety to form a sulfate anion is the most energetically feasible and thus normalised to be 0 kJ mol^{-1} . The formation of other anions relative to the deprotonation of the sulfate anion requires some 100, 120-160, 200-225, 300 kJ mol^{-1} respectively (calculations at the CAM B3LYP/6-311++g(d,p) level of theory). There are three possible scenarios for the formation/origination of these ions, namely (i) the exclusive formation of sulfate anion due to the energetic favourability of this process compared to others, CID of the sulfate anions can then effect proton transfers to form other anions, (ii) all anions (or most of the anions mentioned) are generated simultaneously in the ionisation source; and (iii) some combination of (i) and (ii) may constitute the collection of precursor ions of sulfated peptides.

A. Sulfated Tyr fragmentations

The synthetic peptides containing Tyr(SO_3H) investigated in this study are listed in Table 3.1. All peptides contain Tyr sulfate in position 3, except for the third peptide (Tyr sulfate in position 4). Peptides **(1)** and **(2)** have sequences with the only difference being the C-terminal carboxylate for peptide **(1)** and C-terminal CO-NH_2 for peptide **(2)**. Peptide **(4)** was synthesized to test the sulfate rearrangement between Tyr and Ser, and thus contains Ser in position 5.

Table 3.1. Sulfated Tyr containing peptides investigated.

Peptide	Sequence
(1)	GLY(SO ₃ H)GVA(OH)
(2)	GLY(SO ₃ H)GVA(NH ₂)
(3)	GLGY(SO ₃ H)VA(OH)
(4)	GLY(SO ₃ H)GSA(OH)

3.3.2 Loss of SO₃ from sulfated Tyr

The negative ion CID MS/MS data for the deprotonated ion of peptides (1) and (3) are shown in Figures 3.2 and 3.3 respectively, while the fragmentation data of the (M-H)⁻ anions of peptide (2) is summarised in Table 3.2. The fragmentation patterns of peptide (1) and (2) are comparable, with the exception that the peaks corresponding to certain fragment ions are 1 mass unit different in the two spectra due to the different masses of the C-terminal CO₂H and CONH₂ termini.

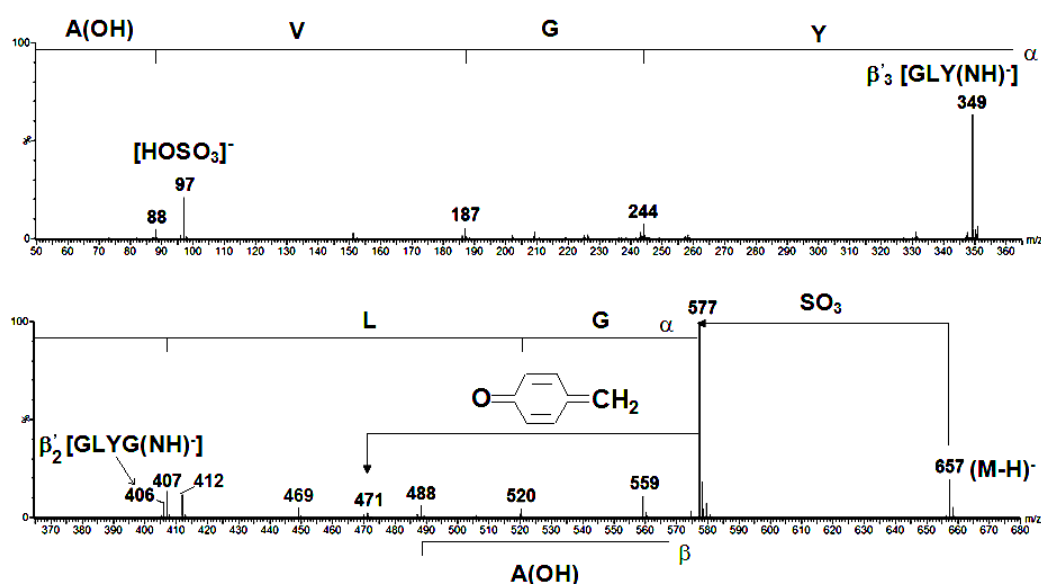


Figure 3.2. CID MS/MS of [GLY(SO₃H)GVA(OH) - H]⁻. Multiplication ranges m/z 60-570 (x70). Q-TOF 2 mass spectrometer.

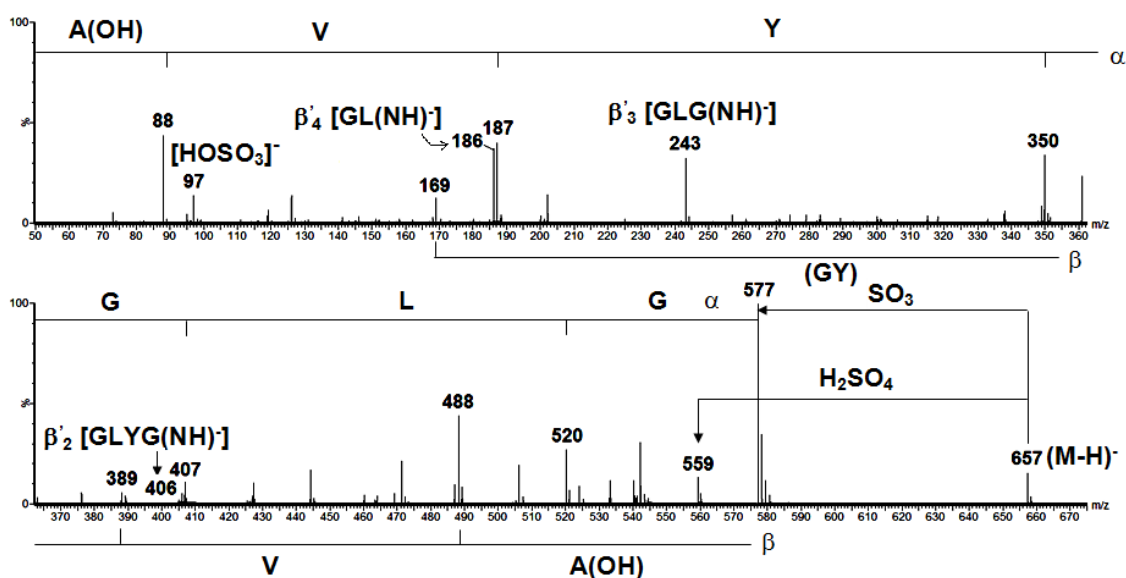


Figure 3.3. CID MS/MS of $[\text{GLGY}(\text{SO}_3\text{H})\text{VA}(\text{OH}) - \text{H}]^-$. Multiplication ranges m/z 60-565 (x24). Q-TOF 2 mass spectrometer.

Table 3.2. CID MS/MS of $(\text{M}-\text{H})^-$ ion of (2) Mass (loss or formation) relative abundance (%).

$\text{GLY}(\text{SO}_3\text{H})\text{GVA}(\text{NH}_2)$, $(\text{M}-\text{H})^-$, m/z 656.

656 $(\text{M}-\text{H})^-$ 16: fragmentations from the $(\text{M}-\text{H})^-$ anion as follows: 576 (SO_3) 32; 470 ($\text{SO}_3 + \text{C}_7\text{H}_6\text{O}$) 58; 469 (β_2) 12; 412 (β_3) 5; 406 ($\beta'_4[\text{GLYG}(\text{NH})^-]$) 60; 349 ($\beta'_5[\text{GLY}(\text{NH})^-]$) 0; 300 ($\beta'_4 - \text{C}_7\text{H}_6\text{O}$) 100; 243 ($[\beta'_5 - \text{C}_7\text{H}_6\text{O}]$ or α_3) 85; 186 ($[\text{GL}(\text{NH})^-]$ or α_7) 53; 169 (β_4) 20; 97(HOSO_3^-) 20; 73 $[\text{G}(\text{NH})^-]$ 17.

$[\text{GLY}(\text{SO}_3\text{H})\text{GVA}(\text{NH}_2) - \text{SO}_3]^-$, m/z 576.

α ions: m/z 519 (α_1) 7; 406 (α_2) 47; 243 (α_3) 77; 186 (α_4) 48; 87 (α_5) 2.

β ions: m/z 169 (β_4) 14.

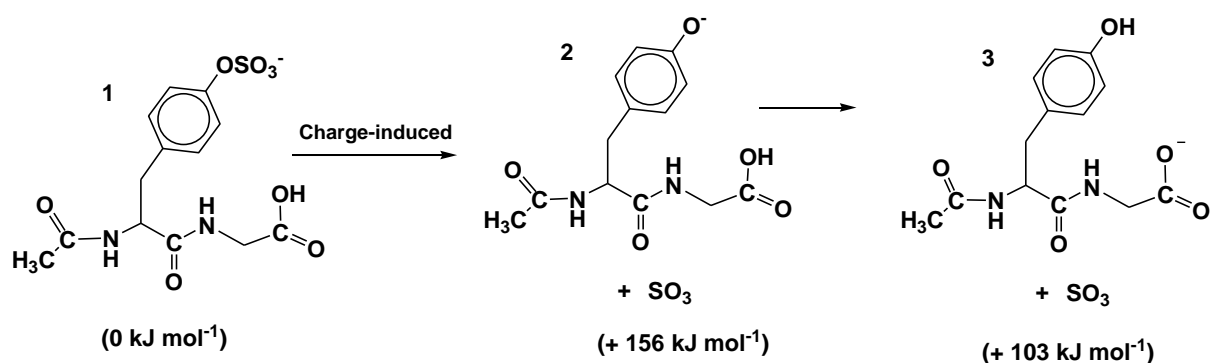
m/z 413 ($\alpha_1 - \text{C}_7\text{H}_6\text{O}$) 18; 300 ($\alpha_2 - \text{C}_7\text{H}_6\text{O}$) 100; 226 ($\beta_3 - \text{C}_7\text{H}_6\text{O}$) 15.

Sequence $[\text{GLYGVA}(\text{NH}_2)]$

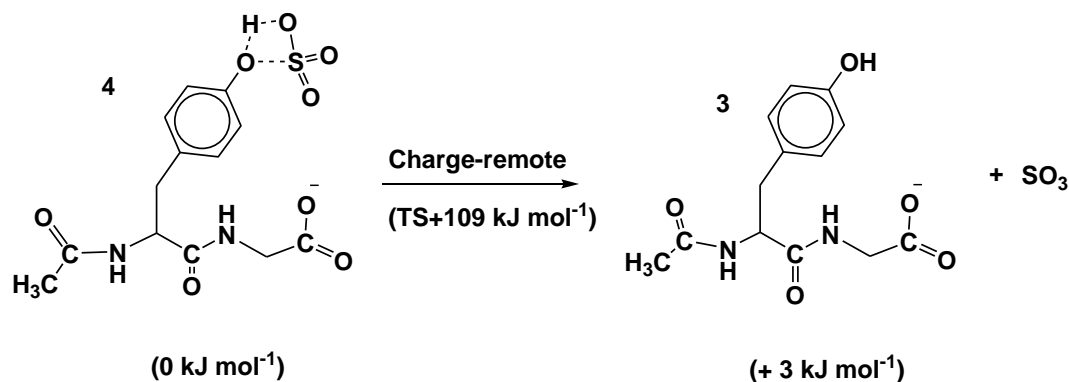
The most abundant peaks in the negative CID MS/MS spectra of peptides **(1)**-**(3)** correspond to the $[(M-H) - SO_3]^-$ species. Due to the fact that several deprotonated precursor ions can in principle be formed upon deprotonation of the peptides (see section 3.3.1), there may be several mechanistic pathways for the loss of SO_3 from these precursor ions. In principle, sulfur trioxide can be eliminated from a sulfate side chain by a charge-directed/charge-induced mechanism or a charge-remote mechanism. The charge-induced reaction requires the negative charge to be located on the sulfate group in order to initiate the cleavage reaction, while a charge-remote reaction occurs remote from and uninfluenced by the anionic site(s) of the $(M-H)^-$ species.

The charge-directed mechanism for the elimination of SO_3 from $(M-H)^-$ ion is shown in Scheme 3.2, whereas the charge-remote counterpart is displayed in Scheme 3.3. Direct loss of SO_3 from sulfate anion **1** to form Tyr-phenoxy anion **2** has a $\Delta G_{\text{reaction}}$ of + 156 kJ mol⁻¹. The Tyr-phenoxy anion may undergo internal proton transfer to give the more stable carboxylate anion **3**. The overall reaction sequence from **1** to **3** is endothermic by + 103 kJ mol⁻¹. On the other hand, the charge-remote reaction is the four-centre neutral reaction initiated from carboxylate anion **4**. In this case, the negative charge is sequestered on C-terminal carboxylate anion and thus does not interact with the active sulfate site. This reaction is endothermic by only + 3 kJ mol⁻¹ and has a transition state of + 109 kJ mol⁻¹.

From the energy profiles of Scheme 3.2 and 3.3, the charge-remote reaction for the elimination of SO_3 seems to be more energetically favourable than the charge-directed counterpart. However, it should be noted that they start with different precursor anions. While the sulfate anion is the initial anion in the charge-induced reaction, the charge-remote mechanism commences with a carboxylate anion, and hence requires an extra energy of about 100 kJ mol⁻¹ to convert the sulfate to the carboxylate if the later is not formed directly during ESI. Thus, if these two reactions start with the same sulfate anion, the energy profile of the charge-remote reaction would be 100 kJ mol⁻¹ more than those shown in Scheme 3.3. In other words, the sulfate cleavage reaction is likely to be charge-directed, if the $(M-H)^-$ anions correspond principally to the sulfate anion **1**. In contrast, if carboxylate anions are formed directly by the electrospray deprotonation process, the charge-remote mechanism is more energetically feasible.

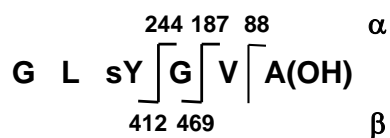


Scheme 3.2. Charge-directed mechanism for the elimination of SO₃ from (M-H)⁻ species. Calculation at the CAM-B3LYP/6-311++g(d,p) level of theory by Dr. Tianfang Wang.



Scheme 3.3. Charge-remote mechanism for the elimination of SO₃ from (M-H)⁻ carboxylate anion. Calculation at the CAM-B3LYP/6-311++g(d,p) level of theory by Dr. Tianfang Wang.

Even though [(M-H) - SO₃]⁻ fragment anions dominate the negative ion spectra of sulfated-Tyr peptides, fragment anions of low abundance containing the intact sulfated-Tyr residue were still observed at low abundance. Particularly, fragmentation of peptide (1) gives cleavage anions containing the Tyr-sulfate moiety at *m/z* 412 and 469 (Figure 3.2). The fragmentation of the (M-H)⁻ anion of peptide (1) is illustrated in Scheme 3.4.



Scheme 3.4.

The CID source-formed MS/MS data for the $[(M-H) - SO_3]^-$ fragment of peptide (**3**) is reproduced in Figure 3.4. The standard peptide backbone α and β' fragmentations are shown schematically on the spectrum which allows sequencing of the $[(M-H) - SO_3]^-$ species. The characteristic loss of $CH_2=C_6H_4=O$ (106 Da) from the Tyr side chain of the $[(M-H) - SO_3]^-$ fragment anion is also observed.

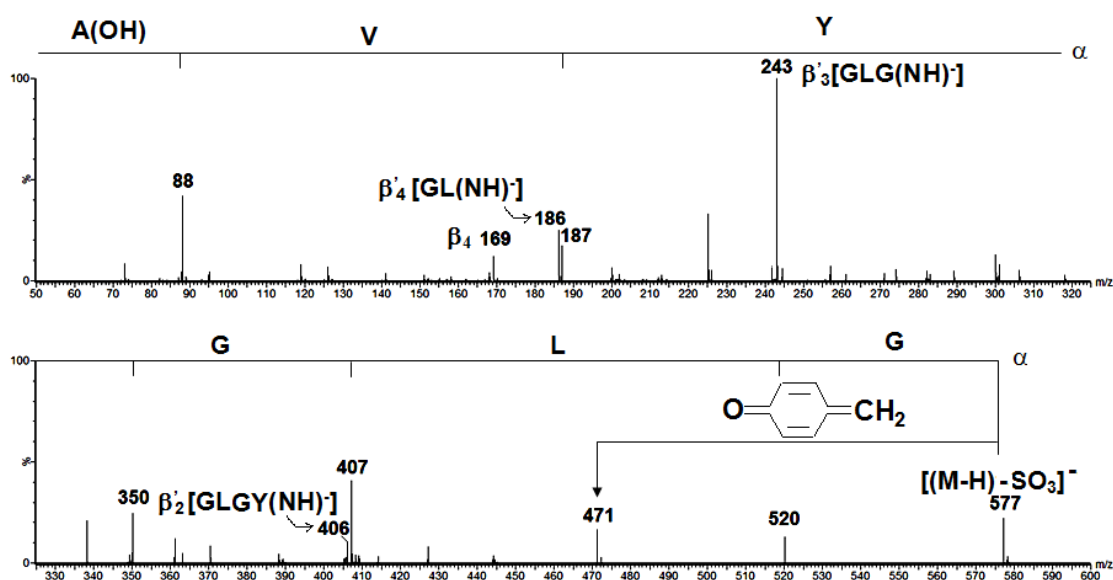


Figure 3.4. CID MS/MS of source-formed $\{[GLGY(SO_3H)VA(OH) - H] - SO_3\}^-$. Multiplication ranges: m/z 250-570 (x4). Q-TOF 2 mass spectrometer.

3.3.3 Sulfate rearrangement from sulfate Tyr (sTyr) to a C-terminal carboxylate anion

The formation of $HOSO_3^-$ (m/z 97) and $[(M-H) - H_2SO_4]^-$ from the deprotonated ions of peptide (**1**) and (**3**) can be seen in Figures 3.2 and 3.3. Examination of the MS/MS data for peptide (**3**) (Figure 3.3) and CID source-formed MS/MS data for the corresponding $[(M-H) - SO_3]^-$ fragment of peptide (**3**) (Figure 3.4) infers that anion m/z 559 in Figure 3.3 is formed exclusively by the loss of sulfuric acid from the deprotonated ion of peptide (**3**). The two fragment anions $HOSO_3^-$ (m/z 97) and $[(M-H) - H_2SO_4]^-$ are of minor abundance, which is in marked contrast to major rearrangement peaks in the cognate negative ion spectra of peptides containing Tyr phosphate (see Chapter 2 section 2.2).

Each of these two fragment anions can only be formed directly from a sTyr side chain if the system is energised enough to break the aromatic C-O bond of Tyr; calculations at the CAM-

B3LYP/6-311++g(d,p) level of theory showed that this requires some + 350 kJ mol⁻¹. The formation of these cleavage anions is therefore not energetically feasible, and the sulfate group must be transferred to another site (the carboxylate terminal anion in this case) to effect these cleavages. In addition, the CID MS/MS data for source formed *m/z* 559 shown in Figure 3.5 is consistent with an anionic structure produced by the loss of H₂SO₄ from a sulfate-rearranged C-terminal group, suggesting that the sulfate group has migrated to the C-terminal carboxylate site preceding the elimination of sulfuric acid.

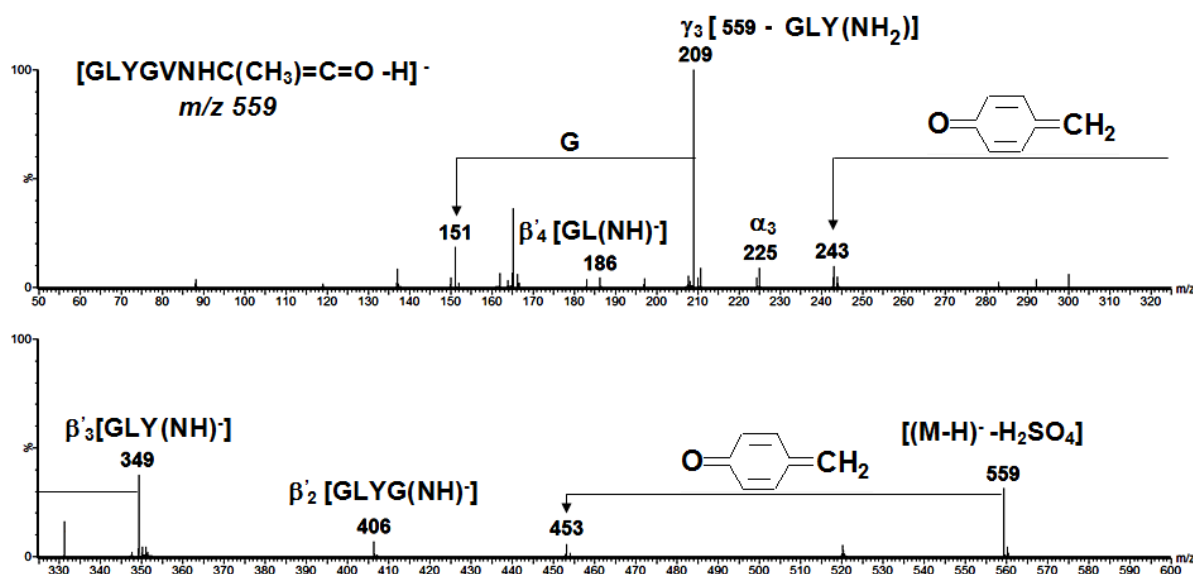
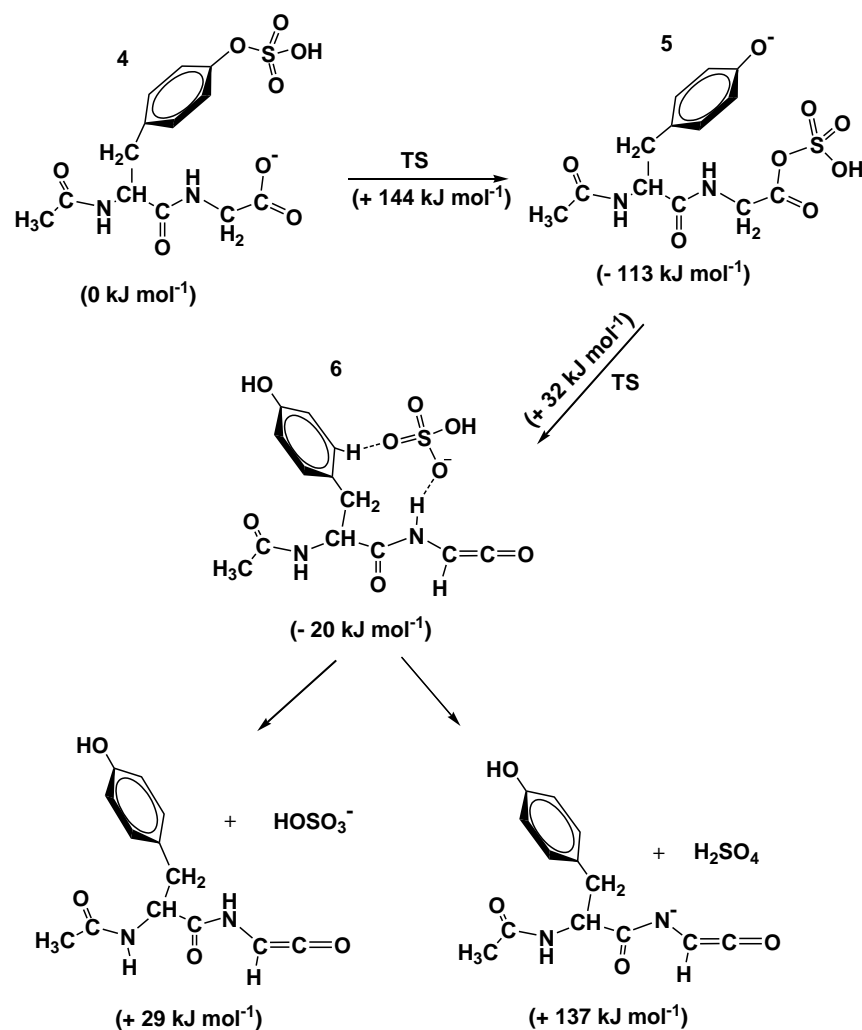


Figure 3.5. CID MS/MS of source-formed $\{[\text{GLY}(\text{SO}_3\text{H})\text{GVA}(\text{OH}) - \text{H}] - \text{H}_2\text{SO}_4\}^-$ (*m/z* 559). Q-TOF 2 mass spectrometer.

Possible mechanisms for the formation of HOSO₃⁻ (*m/z* 97) and the loss of sulfuric acid from (M-H)⁻ of sulfated peptides are shown in Scheme 3.5. The overall process commences with an S_{Ni}(S) reaction which converts the initial carboxylate anion **4** to the sulfate modified C-terminal carboxylate anion **5**. This species rearranges further into the key intermediate **6**, which then fragments to form HOSO₃⁻ (*m/z* 97) and/or [(M-H) - H₂SO₄]⁻. Both fragmentations are endothermic by 29 and 137 kJ mol⁻¹ respectively, with the highest energy barrier being + 144 kJ mol⁻¹ for the sulfate migration step. If the reaction commences with a sulfate anion instead of a carboxylate anion, it requires some 100 kJ mol⁻¹ to reach the transition state for the proton transfer reaction. The overall process is therefore more energetically unfavourable compared to the reaction shown in Scheme 3.5.



Scheme 3.5. Proposed mechanism for the rearrangement of the sulfate of tyrosine to the carboxylate anion of the model system $[RY(SO_3H)G(OH) - H]^-$ ($R=CH_3CO$). Calculation at the CAM-B3LYP/6-311++g(d,p) level of theory by Dr. Tianfang Wang. Relative energies in kJ mol⁻¹ from **4** (depicted as a nominal 0 kJ mol⁻¹).

3.3.4 Sulfate rearrangement from sTyr to Ser

It has been reported from studies of negative ion fragmentations of peptides containing Tyr phosphate that the phosphate readily migrates from Tyr to Ser. Does a similar reaction occur for Tyr sulfate? In order to answer this question, the CID MS/MS data for the $(M-H)^-$ ion of peptide (**4**) $[GLY(SO_3H)GSA(OH)]$ and the corresponding $[(M-H) - H_2SO_4]^-$ anion were investigated. The spectra are displayed in Figures 3.6 and 3.7, respectively. The elimination of SO₃ and the characteristic loss of CH₂O from the Ser residue are observed, with the former constituting the base peak of the spectrum of peptide (**4**). Peptide sequencing is possible from both $[(M-H) - SO_3]^-$ and $[(M-H) - (SO_3 + CH_2O)]^-$ as illustrated in Figure 3.6.

Peaks corresponding to sulfate rearrangements are also found with the abundance of the HOSO_3^- (m/z 97) and $[(M-H) - \text{H}_2\text{SO}_4]^-$ (m/z 547) anion being 10% and 2%, respectively.

The negative ion mass spectrum of m/z 547 (Figure 3.7) is complex and clearly shows peaks resulting from sulfate migration from the Tyr to the Ser side chain. This is evidenced by the presence of the modified Ser residue $[\text{NHC}(=\text{CH}_2)\text{CO}]$ in various α , β and β' [158, 306-307] cleavage anions originating from m/z 547. Even though there is no unambiguous evidence for the competitive sulfate rearrangement to a C-terminal carboxylate anion, this possibility cannot be excluded. It may contribute, at least in part, to the formation of HOSO_3^- (m/z 97) and $[(M-H) - \text{H}_2\text{SO}_4]^-$ in this system.

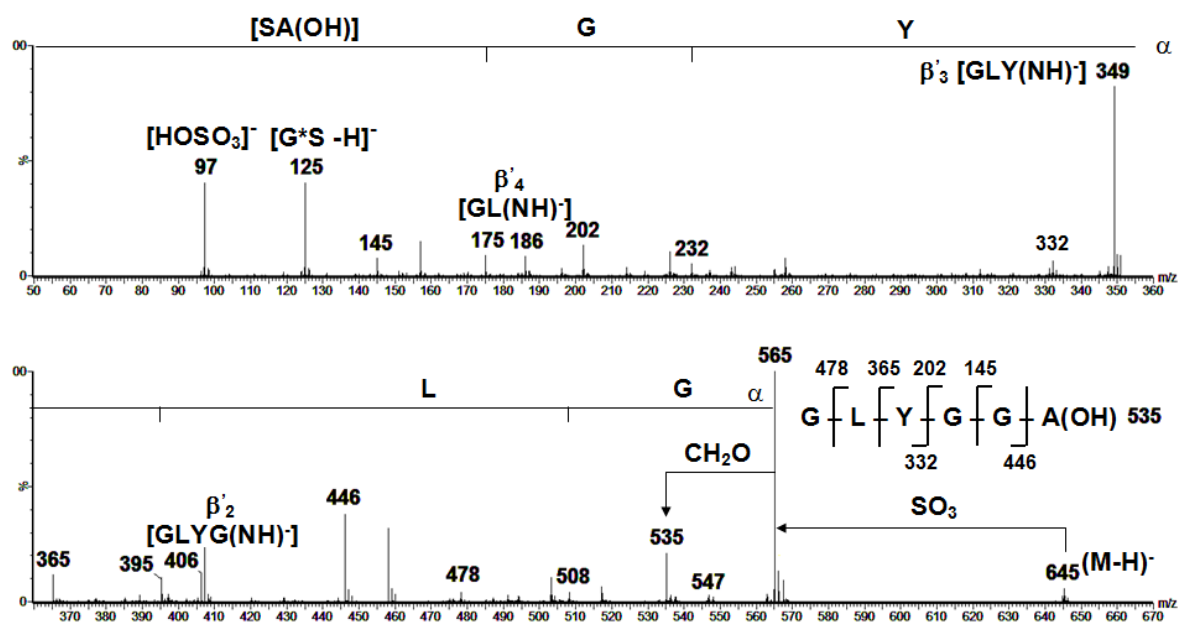


Figure 3.6. Negative ion electrospray CID MS/MS of $[\text{GLY}(\text{SO}_3\text{H})\text{GSA}(\text{OH}) - \text{H}]^-$. *S is $-\text{NHC}(=\text{CH}_2)\text{CO}-$. Multiplication ranges m/z 50-120 (x5), 121-530 (x34). Q-TOF 2 mass spectrometer.

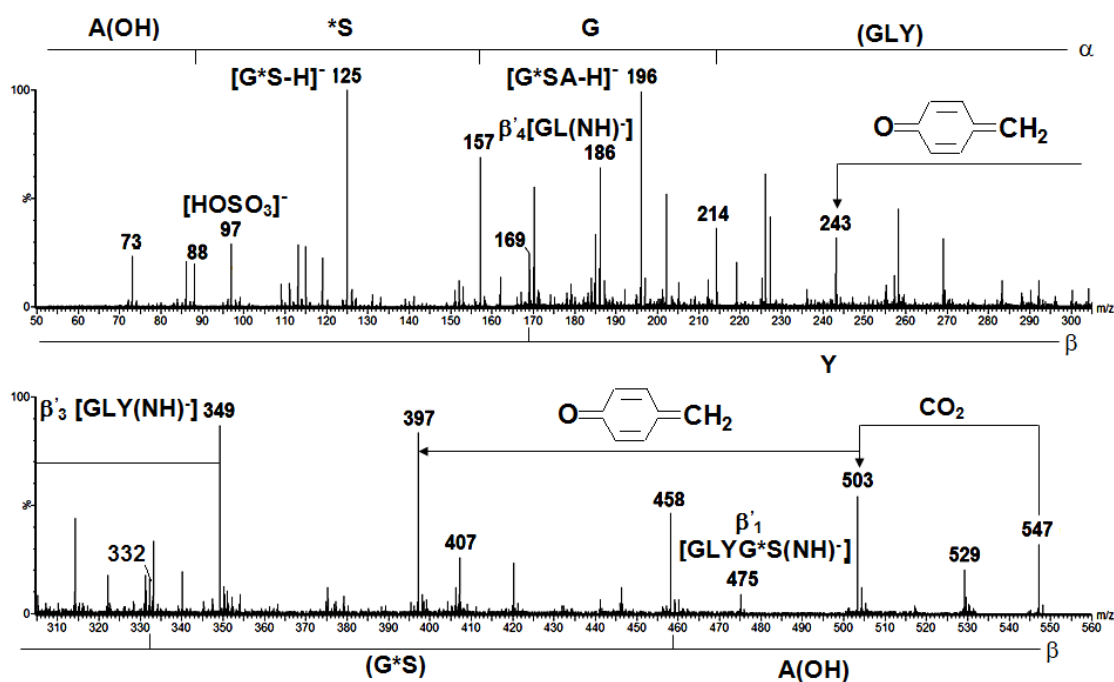


Figure 3.7. CID MS/MS of source-formed $\{[GLY(SO_3H)GSA(OH) - H] - H_2SO_4\}^-$ $[GLYG^*SA(OH)-H]^-$, (m/z 547). *S is $NHC(=CH_2)CO$. Q-TOF 2 mass spectrometer.

B. Sulfated Ser fragmentations

The Ser sulfate containing peptides chosen for study are listed in Table 3.3. Two of the peptides contain Ser sulfate in the C-terminal amino acid position, and two related peptides have C-terminal CO_2CH_3 (instead of CO_2H) groups. The remaining six-residue peptides have Ser sulfate in position 3 with Val, Asp or Ser sulfate in positions 5.

Table 3.3. Sulfated serine containing peptide investigated.

Peptide	Sequence	Peptide	Sequence
(5)	GS(SO ₃ H)(OH)	(7)	GLS(SO ₃ H)GVA(OH)
(6)	GAVS(SO ₃ H)(OH)	(8)	GLS(SO ₃ H)GDA(OH)
(5a)	GS(SO ₃ H)(OCH ₃)	(9)	GLS(SO ₃ H)GS(SO ₃ H)A(OH)
(6a)	GAVS(SO ₃ H)(OCH ₃)		

3.3.5 Fragmentations of (M-H)⁻ ions of peptides with Ser(SO₃H) in the C-terminal position. Formation of HOSO₃⁻ and [(M-H) - H₂SO₄]⁻

The negative ion spectra of energized (M-H)⁻ ions of **(5)**, **(5a)** and **(6a)** are summarised in Table 3.4, while those of the (M-H)⁻ and [(M-H) - SO₃]⁻ ions of GAVS(SO₃H)(OH) **(6)** are shown in Figures 3.8 and 3.9 respectively.

Table 3.4. CID MS/MS of (M-H)⁻ ions from (5), (5a) and (6a). Mass (loss or formation) relative abundance (%).

(5). GS(SO₃H)(OH), (M-H)⁻, *m/z* 241.

241(M-H)⁻16: fragmentations from the (M-H)⁻ anion as follows:- 223 (H₂O) 2; 179 (H₂O+CO₂) 5; 161 (SO₃) 56; 131 (SO₃+CH₂O) 10; 97 (HOSO₃⁻) 100; 74 (SO₃+H₂O+G)1.

(5a). GS(SO₃H)(OCH₃), (M-H)⁻, *m/z* 255.

255 (M-H)⁻ 12; 97 (HOSO₃⁻) 100.

(6a). GAVS(SO₃H)(OCH₃), (M-H)⁻, *m/z* 425.

425 (M-H)⁻ 15; 97 (HOSO₃⁻) 100.

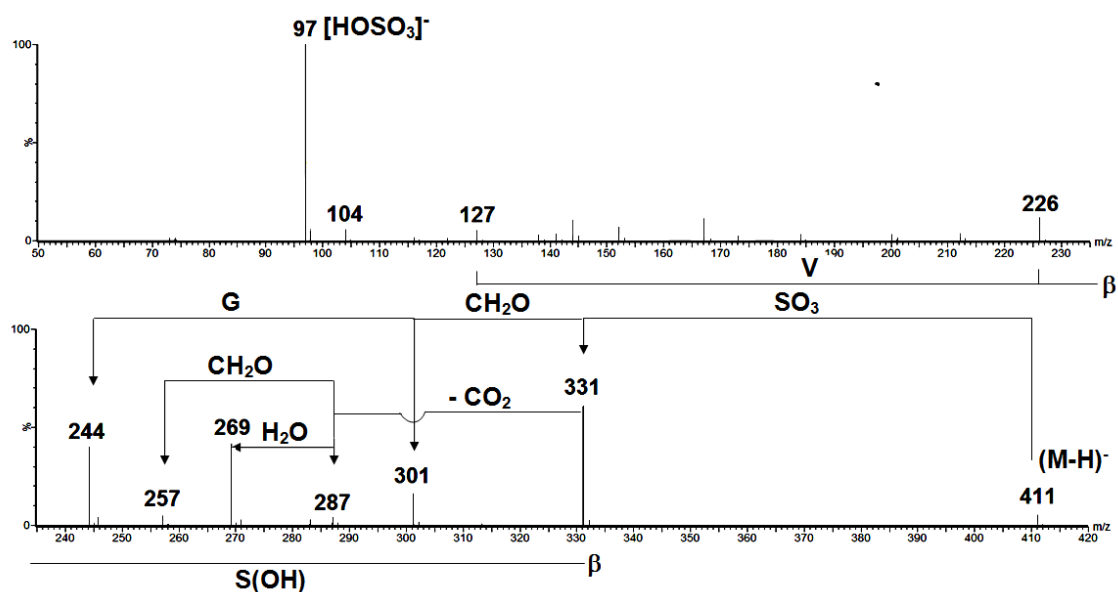


Figure 3.8. CID MS/MS of $(M-H)^-$ of GAVS(SO₃H)(OH) (**6**). Multiplication ranges: m/z 420-300 (x10) and 295-100(x10). Q-TOF 2 mass spectrometer.

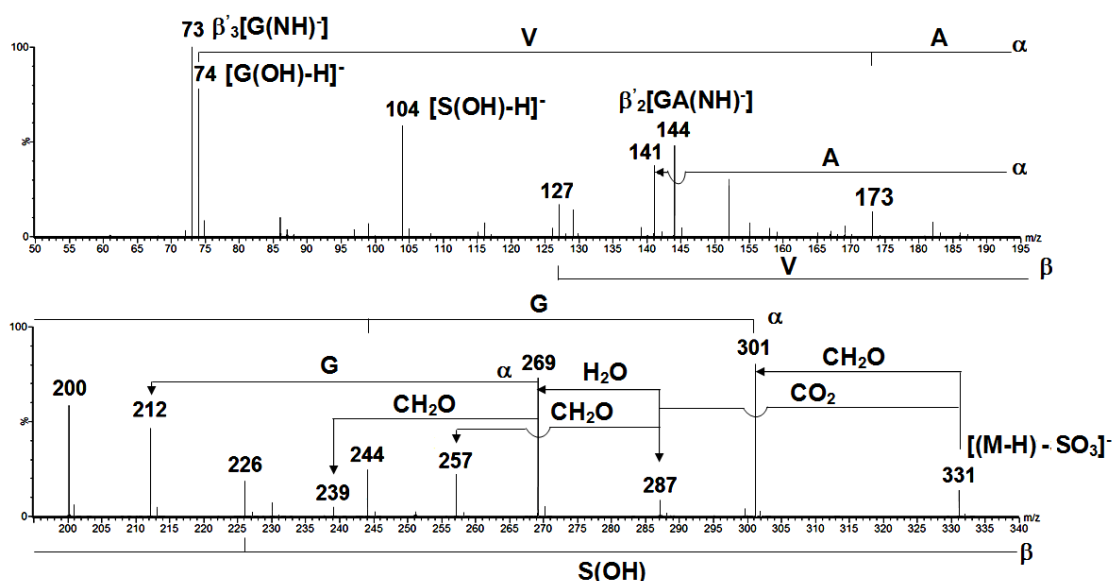


Figure 3.9. CID MS/MS of source formed $[(M-H)-SO_3]^-$ of GAVS(SO₃H)(OH) (**6**). Q-TOF 2 mass spectrometer.

The negative ion CID MS/MS spectra of two Ser sulfate containing peptides (**5**) and (**6**) show a base peak at m/z 97 ($HOSO_3^-$) and pronounced peaks corresponding to $[(M-H) - SO_3]^-$ anions. Most other fragment peaks in the spectra occur from an $[(M-H) - SO_3]^-$ anion

including the characteristic loss of CH₂O from Ser along with the α , β and β' backbone cleavage ions. However, no peak corresponding to [(M-H) - H₂SO₄]⁻ fragments are observed in these spectra. This is in marked contrast to negative ion fragmentations of peptides containing Ser phosphate, where formation of H₂PO₄⁻ is always accompanied by loss of phosphoric acid from (M-H)⁻ ions.

The lack of an [(M-H) -H₂SO₄]⁻ anion in the negative ion spectra of the sulfated peptides is likely due to the low basicity of HOSO₃⁻ in the gas phase. The deprotonation processes of phosphoric acid and sulfuric acid show corresponding ΔG_{acid} values being 1351 and 1261 kJ mol⁻¹, respectively. Obviously, HSO₄⁻ is a poorer gas-phase base than H₂PO₄⁻ and therefore it shows less protonation efficiency in gas phase. In addition, the ΔG_{acid} value for deprotonation of the carboxyl centres on, for example, Gly is 1406 kJ mol⁻¹ or Ser is 1363 kJ mol⁻¹ [308-309], and is much higher than the ΔG_{acid} of HSO₄⁻. Thus, HOSO₃⁻ can deprotonate these residues only if particular systems containing either of these amino acids are significantly energised.



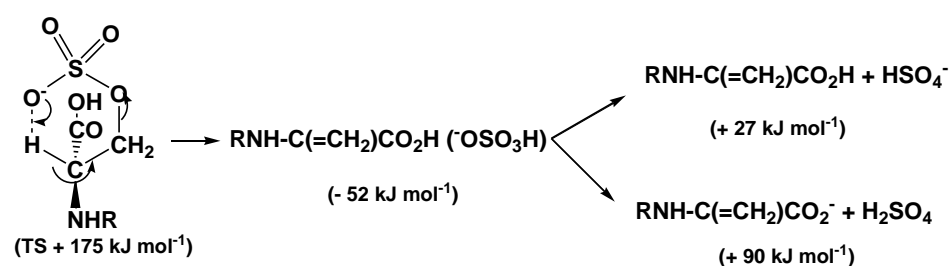
The major concern of studies of negative ion fragmentations of sulfated peptides is whether the sulfate group remains on modified amino acid residues (Tyr/Ser) or it undergoes various rearrangement processes like phosphorylated peptides. Can negative ion mass spectrometry be used to determine sulfate sites in peptides and proteins? The ultimate aim of this study is therefore to determine whether the major fragmentations [(M-H) - SO₃]⁻ and HOSO₃⁻ of Ser sulfate originate directly from an intact Ser sulfate, or whether the sulfate group migrates to anion sites within the peptide such as the C-terminal carboxylate, a side-chain carboxylate group of Asp or another Ser to effect these fragmentations.

The first scenario examined is the formation of HOSO₃⁻ and [(M-H) - SO₃]⁻ following sulfate rearrangement to the C-terminal carboxylate anion. In order to give such rearrangement the best chance to succeed, the Ser sulfate is placed in the C-terminal position. Experimentally, ¹⁸O-labelled on the C-terminal CO₂H (or on Ser side chain) could be used to track the genesis of HOSO₃⁻. If the HOSO₃⁻ ion is formed after C-terminal rearrangement of the sulfate group, it has *m/z* 99 instead of 97. However, this method might not be efficient due to

sulfate hydrolysis during the long procedure of ^{18}O -labelled attachment. In addition, the labelling technique cannot clarify the origin of the $[(\text{M}-\text{H}) - \text{SO}_3]^-$ fragment anion. An alternative approach that was chosen in this study was to block any sulfate transfer to the C-terminal carboxylate, by esterifying the C-terminal carboxylic group so that it cannot interact in an S_{Ni} (S) reaction with the Ser sulfate group.

Consider the CID MS/MS data of the carbomethoxy derivatives (**5a**) and (**6a**) recorded in Table 3.4. Sulfate transfer to the C-terminal carboxylate group in these two peptides is blocked because the C-terminal CO_2H has been converted to CO_2CH_3 . The two peptides give simple negative ion mass spectra with the base peak corresponding to the HOSO_3^- (m/z 97) anion and other peaks are less than 1% intensity of the base peak. The presence of HOSO_3^- in the spectra of (**5a**) and (**6a**) suggests that this anion is formed directly from the intact Ser sulfate. Surprisingly, no loss of SO_3 is observed in these mass spectra. Therefore, it is proposed that the formation of $[(\text{M}-\text{H}) - \text{SO}_3]^-$ anions must require the presence of an adjacent C-terminal CO_2H group.

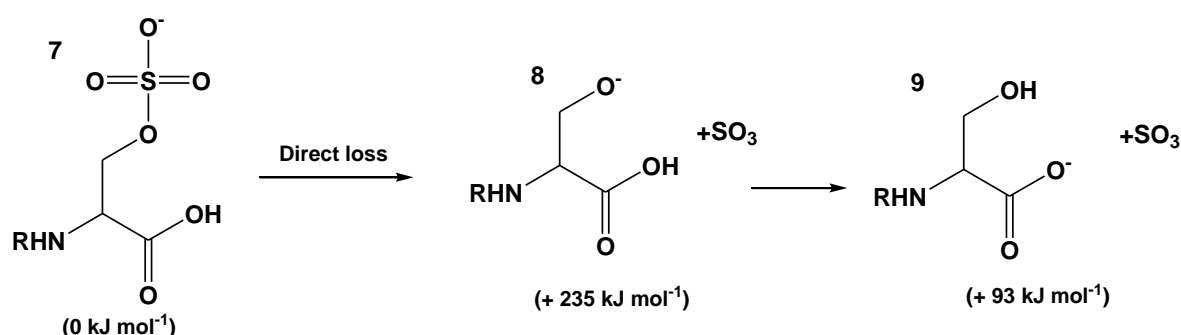
The direct formation of HOSO_3^- from a C-terminal Ser(SO_3H) is also supported by theoretical calculations at the CAM-B3LYP/6-311++g(d,p) level of theory for a simple model $\text{RNHCH}(\text{CH}_2\text{OSO}_3^-)\text{CO}_2\text{H}$ ($\text{R}=\text{COCH}_3$). Among several mechanistic pathways proposed for this fragmentation, the lowest-energy process is displayed in Scheme 3.6, involving proton transfer through an enolate anion. On the other hand, the formation of HOSO_3^- following Ser sulfate to C-terminal carboxylate migration is much more energy demanding and thus an unlikely possibility (data is not presented here).



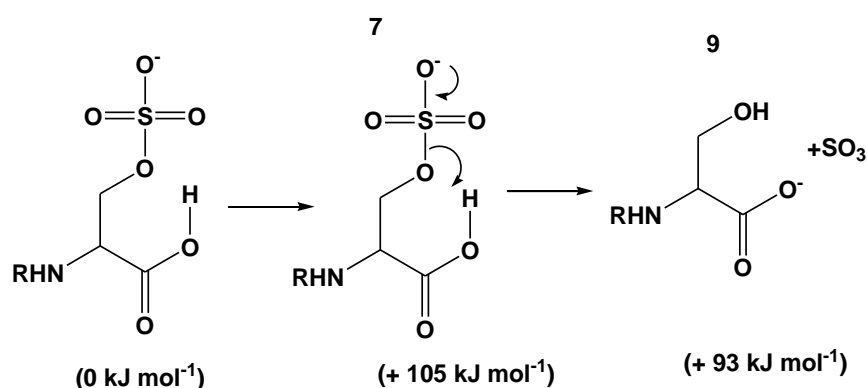
Scheme 3.6. Mechanism for direct formation of HOSO_3^- and the loss of H_2SO_4 from a C-terminal Ser(SO_3H) via a six-centred transition state involving proton transfer of an enolate hydrogen ($\text{R}=\text{COCH}_3$). Calculation at the CAM-B3LYP/6-311++g(d,p) level of theory by Dr. Tianfang Wang.

3.3.6 Fragmentations of (M-H)⁻ ions of peptides with Ser(SO₃H) in the C-terminal position. The formation of [(M-H) - SO₃]⁻

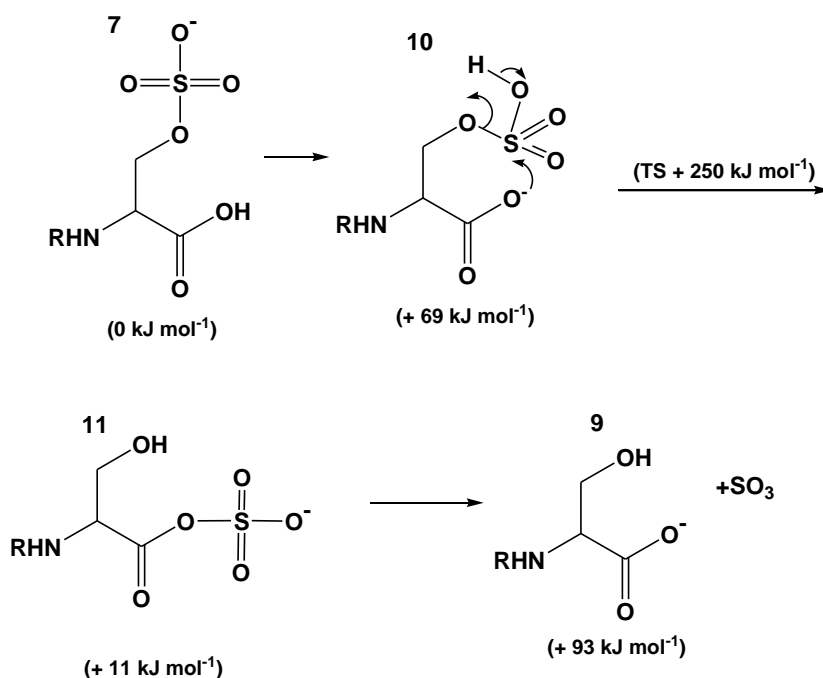
At this stage of the investigation, the mechanisms for the loss of SO₃ from the (M-H)⁻ anions of sulfated Ser containing peptides and the reason for its absence when the C-terminal carboxylate is blocked needs to be explored using theoretical calculations. Several mechanistic pathways for [(M-H) - SO₃]⁻ formation were proposed and calculated at the CAM-B3LYP/6-311++g(d,p) level of theory. Two possible mechanisms for direct loss of SO₃ from Ser sulfate are shown in Scheme 3.7 and 3.8, while Scheme 3.9 displays the formation of [(M-H) - SO₃]⁻ anion mediated by C-terminal sulfate rearrangement.



Scheme 3.7. Mechanism for the direct cleavage of SO₃ from RNHCH(CH₂OSO₃⁻)CO₂H (R=COCH₃). Calculation at the CAM-B3LYP/6-311++g(d,p) level of theory by Dr. Tianfang Wang.



Scheme 3.8. Mechanism for the cleavage of SO₃ accompanied by proton transfer from the carboxyl group of RNHCH(CH₂OSO₃⁻)CO₂H (R=COCH₃). Calculation at the CAM-B3LYP/6-311++g(d,p) level of theory by Dr. Tianfang Wang.



Scheme 3.9. Mechanism for the cleavage of SO_3 from $\text{RNHCH}(\text{CH}_2\text{OH})\text{C}(=\text{O})\text{OSO}_3^-$ ($\text{R}=\text{COCH}_3$) **11**, following sulfate transfer from $\text{RNHCH}(\text{CH}_2\text{OSO}_3^-)\text{CO}_2\text{H}$ **7** to **11**. Calculation at the CAM-B3LYP/6-311++g(d,p) level of theory by Dr Tianfang Wang.

In Scheme 3.6, the Ser sulfate anion **7** directly dissociates to yield the Ser alkoxide anion **8** in an endothermic process of $+ 235 \text{ kJ mol}^{-1}$. The Ser alkoxide anion may be converted to a more stable carboxylate anion **9** by proton transfers. This pathway of fragmentation is highly energy demanding and occurs independent of the nature of the C-terminal group.

The process shown in Scheme 3.8 requires the presence of a C-terminal carboxylic group. Loss of SO_3 in this case is mediated by proton transfer via a six-centred transition state involving the C-terminal CO_2H . This reaction is more energetically favourable than that displayed in Scheme 3.6 with a transition state of only $+ 105 \text{ kJ mol}^{-1}$, and has a $\Delta G_{\text{reaction}}$ of $+ 93 \text{ kJ mol}^{-1}$. It is also consistent with the absence of an $[(\text{M}-\text{H}) - \text{SO}_3]^-$ fragment from peptides containing C-terminal CO_2CH_3 groups (Table 3.4).

The loss of SO_3 facilitated by rearrangement of the sulfate from Ser to the C-terminal CO_2^- is explored in Scheme 3.9. The sulfate anion **7** is first converted to the carboxylate anion **10** ($+ 69 \text{ kJ mol}^{-1}$), which then attacks the sulphur atom of the sulfate group in an $\text{S}_{\text{Ni}}(\text{S})$ reaction to effect the transfer of this group to form the C-terminal sulfate anion **11**. The sulfate anion decomposes further to the products **9** and SO_3 . The overall reaction sequence

has a high transition state of + 250 kJ mol⁻¹; and as a result, this is not an energetically feasible process compared with that shown in Scheme 3.8.

3.3.7 The formation of [(M-H) - SO₃]⁻ from a non-C-terminal Ser(SO₃H)

Peptides (7)-(9) have been studied in order to examine the fragmentation behaviour of a Ser sulfate located at a non-C-terminal position. The negative ion mass spectra of these peptides show peaks due to HOSO₃⁻ and [(M-H) - SO₃]⁻ with the later normally being the base peak. The spectrum of the (M-H)⁻ anion of (7) (Figure 3.10), for example, shows the base peak at *m/z* 501 (loss of SO₃) and series of α and β fragment ions originating from this peak. The characteristic loss of CH₂O from Ser together with β' fragmentations are also observed.

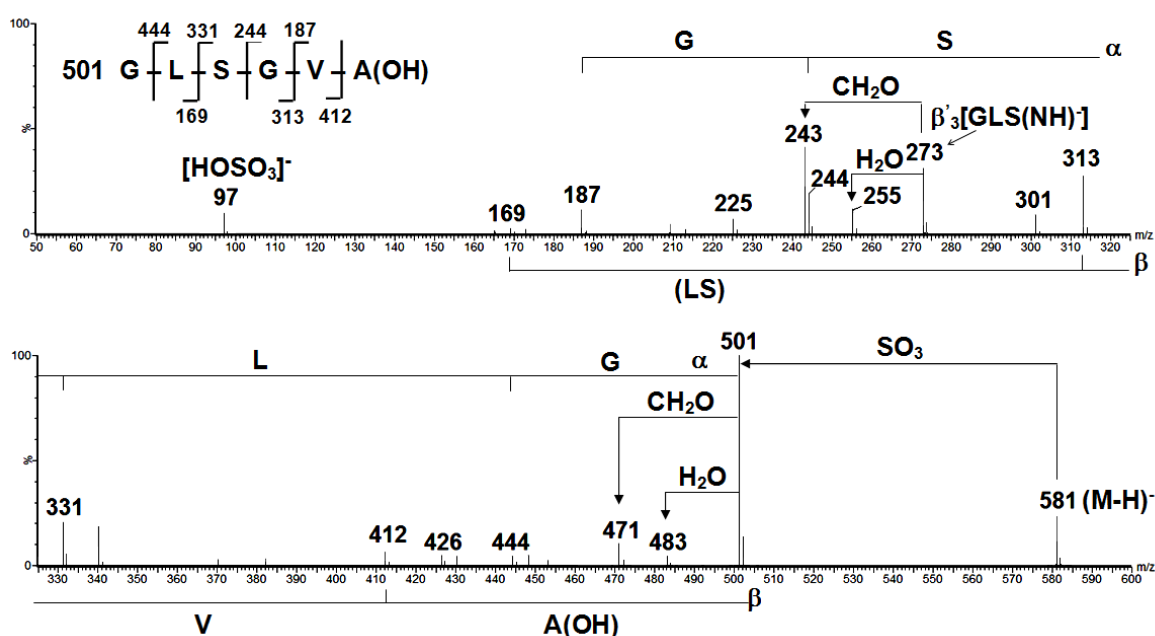
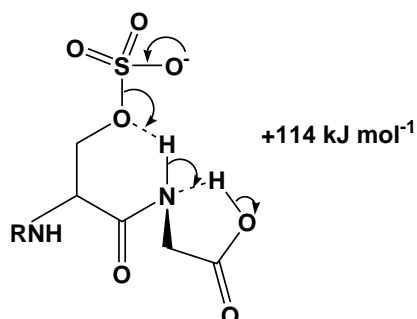


Figure 3.10. CID MS/MS of (M-H)⁻ of GLS(SO₃H)GVA(OH) (7). Multiplication ranges, *m/z* 100-465(x50). Q-TOF 2 mass spectrometer.

As has been seen in section 3.3.6, the most energetically feasible mechanism for the loss of SO₃ from a C-terminal Ser(SO₃H) is the process involving proton transfer from the carboxylic acid group (Scheme 3.8). If the Ser sulfate is not located at the C-terminal position, the mechanism has been found to be more complex. SO₃ dissociation is now mediated by two concomitant proton transfers from and to the adjacent backbone amide nitrogen (Scheme 3.10). The loss of SO₃ by this mechanism therefore requires the backbone of the peptide to be flexible to allow approach of the adjacent amide nitrogen and the C-

terminal carboxyl group. The energy barrier for this process is + 114 kJ mol⁻¹ and this value increases with increasing distance between the sulfate group and the C-terminal carboxylic group.



Scheme 3.10. Transition state for SO₃ cleavage from a RNHCH(CH₂OSO₃⁻)COOH (R is COCH₃). Calculation at the CAM-B3LYP/6-311++g(d,p) level of theory by Dr. Tianfang Wang.

3.3.8 Fragmentation of a sulfated Ser peptide also containing Asp

Previous calculations indicated that sulfate transfer is unlikely to occur from Ser(SO₃H) to a C-terminal carboxylate anion (see section 3.3.6). Similarly, sulfate transfer from a Ser sulfate to a side-chain carboxylate anion, for example to an Asp carboxylate, also seems unlikely. The possibility of sulfate transfer from a Ser sulfate to a side chain carboxylate has been investigated by examining the negative ion CID MS/MS of the (M-H)⁻ of the Asp-containing peptide GLS(SO₃H)GDA(OH) (**8**) (Figure 3.11). The spectrum shows the domination of the classical Asp cleavages which occur even more prevalently than the standard **α** and **β** backbone cleavages (not many of the **α** and **β** fragment ions are observed). The characteristic **δ** (*m/z* 330), **γ** (*m/z* 186) cleavage ions of Asp are formed principally from *m/z* 517. In addition, the CID MS/MS/MS data for *m/z* 517 and 499 (from Orbitrap mass spectrometer, see Experimental section for details) show that *m/z* 499 is formed by the characteristic loss of H₂O from the Asp side chain. Sulfate transfer from Ser(SO₃H) to the side-chain carboxylate of the Asp residue to facilitate the loss of H₂SO₄ from the (M-H)⁻ of (**8**) is therefore unlikely.

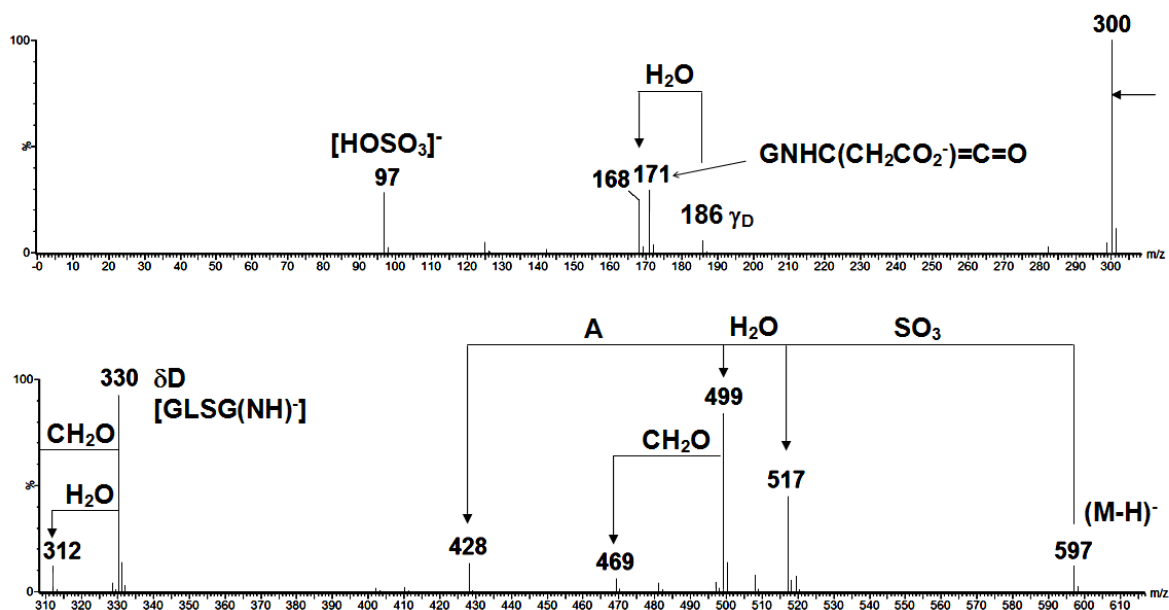
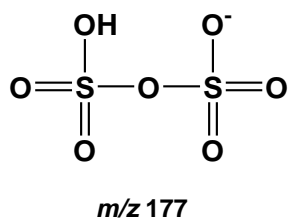


Figure 3.11. Negative ion electrospray CID MS/MS of $(M-H)^-$ of $GLS(SO_3H)GDA(OH)$ (8). Q-TOF 2 mass spectrometer.

3.3.9 Fragmentation of a disulfate containing peptide

The aggregation of phosphate residues in $(M-H)^-$ anions of di- and tri-phosphate peptides to produce $H_3P_2O_7^-$ (m/z 177) and $H_4P_3O_{10}^-$ (m/z 257) anions have been reported [239, 242, 292]. In order to test whether an analogous reaction can occur for a disulfate containing peptide to form the disulfate anion at m/z 177 (Scheme 3.11), the CID MS/MS data of the disulfate peptide $GLS(SO_3H)GS(SO_3H)A(OH)$ (9) was examined (Figure 3.12). The spectrum is dominated by peaks due to $HOSO_3^-$, $[(M-H)^- - SO_3]$ and $[(M-H)^- - 2SO_3]$. No peak at m/z 177 ($HO_7S_2^-$) is present, indicating that the aggregation of sulfate moieties in multiple sulfate containing peptides is unlikely.



Scheme 3.11.

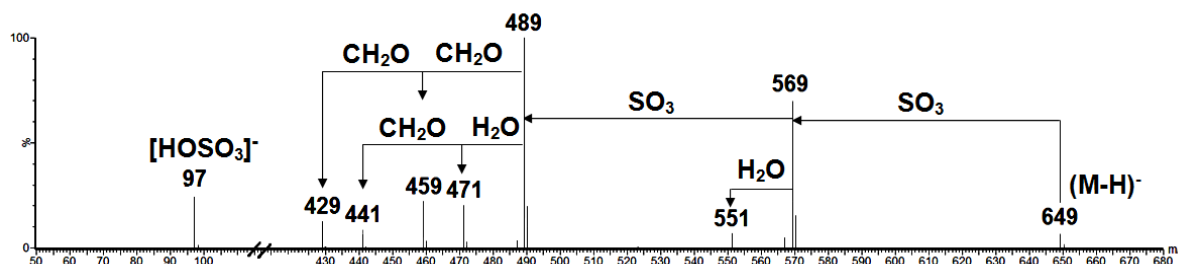


Figure 3.12. Negative ion electrospray CID MS/MS of $(M-H)^-$ of GLS(SO₃H)GS(SO₃H)A(OH) (**9**). Waters Q-TOF 2 mass spectrometer.

3.4. Summary and conclusion

The major fragmentations occurring from energised $(M-H)^-$ ions of sTyr is $[(M-H) - SO_3]^-$, while those of Ser sulfate containing peptides are $[(M-H) - SO_3]^-$ and $(M-H)^- \rightarrow HOSO_3^-$

Rearrangements involving sulfate migrations to C-terminal carboxylate, side chain carboxylate sites and to Ser are minor for Tyr sulfate containing peptides, and are not observed in mass spectra of sulfated Ser peptides

Sequencing information can normally be obtained using CID MS/MS data of source formed of $[(M-H) - SO_3]^-$ ions of the peptides studied, with the exception of the peptide containing Asp, where the diagnostic fragmentations of Asp are more facile than those of the Ser sulfate group. This restricts the formation of most α and β fragment ions from the $[(M-H) - SO_3]^-$ anion.

The negative ion spectra of di- and triphosphate serine containing peptides contain peaks corresponding to anions formed following cyclisation of the phosphate groups. In comparison, corresponding peaks are not detected in the spectra of energised $(M-H)^-$ ions of Ser disulfate containing peptides.

In contrast with the various rearrangements of phosphate groups within deprotonated anions of phosphopeptides (see Chapter 2), rearrangement reactions of sulfate groups are found to be insignificant as outlined above. In addition, the extent of sulfate loss in the negative ion mode is less than that in the positive MS mode. Sulfate detection and site determination using fragmentation of the deprotonated anions are therefore more feasible than that of the positive ion counterparts. However, care should be taken as sulfate migrations following

formation of the initial $(M-H)^-$ anions still occur to a certain extent, which may result in false-negative identification of this modification.

3.5 Experimental

3.5.1 Peptides

All Ser containing peptides used in this study were synthesised by Hongkong GenicBio Biotech Co., Ltd (Shanghai, China). Purities were generally better than 80% as evidenced by HPLC and MS (Shimadzu LCMS-2010) data provided by the manufacturer. These Ser containing peptides were converted into their Ser sulphates by treatment with chlorosulfonic acid using the standard method of Burlingame et al [301]. No attempt was made to purify the Ser sulfate containing peptides further because of the problem of possible hydrolysis of the sulfate containing residues. Experimental studies utilised (i) MS/MS data from $(M-H)^-$ anions, (ii) MS/MS/MS data from $[(M-H) - SO_3]^-$ fragment anions (or MS/MS data from CID activated source formed $[(M-H) - SO_3]^-$ fragment anions), and (iii), when appropriate, MS/MS data from CID activated source formed $[(M-H) - H_2SO_4]^-$ fragment anions.

3.5.2 Mass spectra

Electrospray ionisation mass spectra were obtained using a Q-TOF2 hybrid orthogonal acceleration time-of-flight mass spectrometer (Waters/Micromass, Manchester, UK) with a mass range to m/z 10,000. Samples (25 μ g) were dissolved in acetonitrile/water (1:1 v/v) and infused into the electrospray source at a flow rate of 8 μ l min^{-1} . Experimental conditions were as follows: capillary voltage 2.9 kV, source temperature 80 °C, desolvation temperature 150 °C, and cone voltage 50V. MS/MS data were acquired using argon as the collision gas and the collision energy was set to 50 eV. All masses for anions shown either in Figures or a Table are nominal masses (i.e. the sum of the integral masses of the amino acid residues).

High resolution MS/MS and MS/MS/MS data were measured with an LTQ Orbitrap XL ETD hybrid mass spectrometer (Thermo Fisher Scientific, MA, USA) equipped with an electrospray ion source. Samples were infused at 5 μ l min^{-1} delivered by a built-in-syringe pump and a spraying voltage of 2.3 kV. A mass resolution of 30,000 (at m/z 400) was used. Multistage mass spectrometry MS^n ($n=2$ or 3) experiments were performed using CID with normalised collision energy set between 8 and 11%.

High resolution MS/MS data for (M-H)⁻ ions and MS/MS/MS data for [(M-H) - SO₃]⁻ (and [(M-H) - (H₂O + SO₃)]⁻ ions when appropriate) were obtained for peptides GAVS(SO₃H)(OH), GLS(SO₃H)GVA(OH) and GLS(SO₃H)GDA(OH). Atomic compositions are consistent with those of anions described in this thesis (all mass measurements were correct to the third decimal place). High resolution data are not presented here.

CHAPTER 4

IDENTIFICATION OF DISULFIDE BONDS IN RICIN BY NEGATIVE ION MASS SPECTROMETRY

4.1 Disulfide linkage in peptides and proteins

A disulfide bond is a covalent bond between two Cys side chains of peptides/proteins occurring intra- or intermolecularly, and is the most common crosslink between amino acids in proteins aside from the peptide bond itself. It is formed mainly in the endoplasmic reticulum during peptide/protein folding owing to the action of some enzymes such as ero1 [312-313], peroxiredoxin IV [314-315], vitamin K epoxide reductase [316], and glutathione peroxidase [317]. However, disulfide formation has also recently been found to occur in the extracellular environment (in the Golgi apparatus or in extracellular fluids) under catalysis of quiescin sulfhydryl oxidase [318]. Disulfide bonds are observed in secreted proteins, antibodies, key growth factors and a wide range of polypeptide toxins. This post-translational modification limits the number of accessible conformational states of a protein, contributes to the thermodynamic stability of proteins, enhances resistance of proteins to proteases, and is involved in the regulation of protein activity [319-321]. Identification of the positions of disulfide bonds is therefore vital to gain a comprehensive understanding of the three-dimensional structures of disulfide containing proteins.

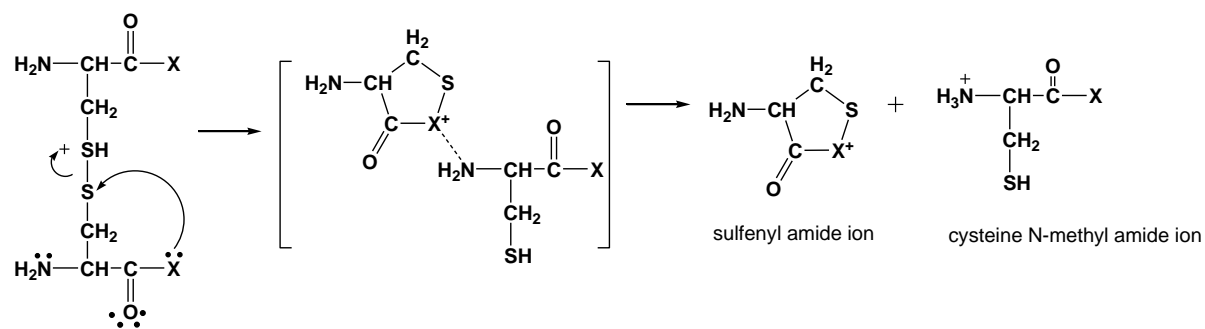
4.2 Positive ion mass spectrometry of disulfide linkages

Positive ion MS has historically been among the most important of the analytical techniques used for disulfide connectivity assignments in peptides/proteins. The general strategy involves the identification of disulfide peptides in the digests of proteins and the characterisation of these disulfide containing fragments directly or indirectly. The direct approach is based on the occasional fragmentations of the disulfide moieties at the C^β-S bond or S-S bond.

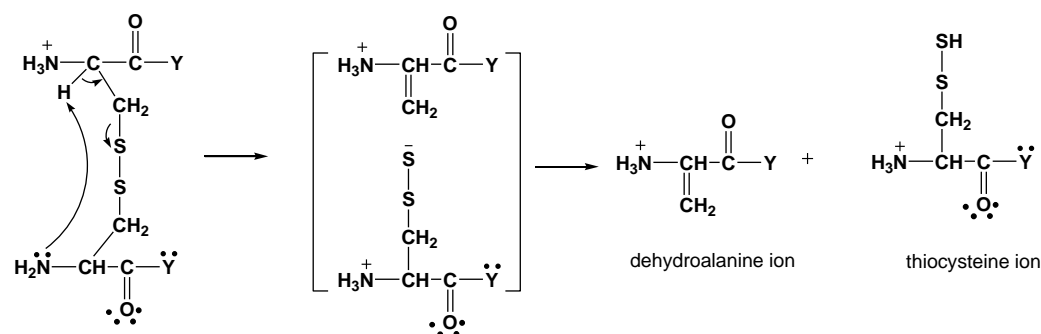
Various mechanisms have been proposed and investigated to provide insight into fragmentation processes of disulfide containing peptides/proteins under positive ion CID conditions. O'Hair's research group has identified three low-energy pathways of C^β-S and S-

S bond cleavages using a joint experimental and theoretical study (calculations performed on protonated (CysNHMe)₂) at the MP2/6-311 + G(2d,p)// B3LYP/ 3-21G(d) level of theory [322]. According to this study, the most energetically preferable pathway for breaking an S-S bond is a charge directed neighbouring group process, involving the C-terminal amide N to produce either a protonated cysteine N-methyl amide or protonated sulfenyl amide ion (Scheme 4.1a). C^β-S bond cleavage process is dominated via a salt bridge mechanism, which involves abstraction of the α-hydrogen by the N-terminal amino group to form either a protonated dehydroalanine or protonated thiocysteine ion (Scheme 4.1b). A less energetically favourable pathway of C^β-S cleavage is via a Grob-like process. This involves nucleophilic attack of the N-terminal amino N to form dithiazolidine product ion and eliminating methylacrylamide and NH₃ (Scheme 4.1c). Two mechanisms for fragmentation of disulfide linkages at the C^β-S and S-S bonds have also been proposed by Balaram's group, with protonated dehydroalanine, cysteinpersulfide, cystein and cysteinthioaldehydes being the four characteristic fragment ions produced (Scheme 4.1d) [323-328]. These mechanisms are simplified versions of the fragmentation pathways introduced by O'Hair's group.

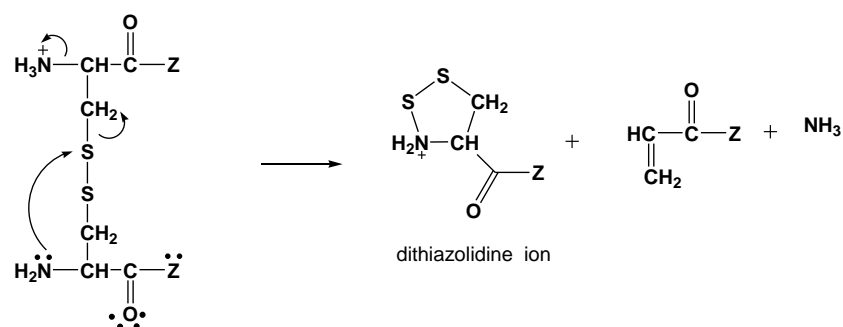
In comparison to the energetics of simple amide bond cleavage, the S-S and C^β-S bond cleavage reactions are higher in energy, and therefore bond cleavage processes involving the disulfide bond are rarely observed for low-energy CID of disulfide containing peptides with mobile proton(s). However, the absence of a mobile proton appears to promote disulfide bond cleavage reactions owing to the salt bridge mechanism [322], and thus, the application of non-mobile proton conditions has been suggested to improve the extent of disulfide fragmentations. Disulfide connectivity assignments using the characteristic fragmentations of disulfide moieties (shown in Scheme 4.1) have been found to be challenging due to the complexity of Cys fragmentations, internal loss and the low abundance of these cleavages as discussed above [323-328].



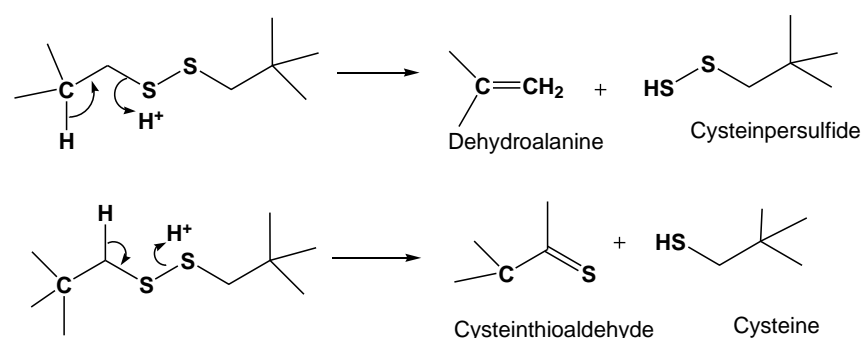
a. S-S cleavage by a charge directed neighbouring group process, X= NHCH₃



b. C^β-S salt bridge cleavage reaction, Y= OH, OCH₃, NHCH₃, Gly,



c. C^β-S Grob like cleavage reaction, Z= OH, OCH₃, NHCH₃, Gly,



d. Simplified S-S, C^β-S fragmentation mechanisms

Scheme 4.1. Fragmentation pathways of the MH⁺ ion from disulfide containing peptides under CID conditions.

On the other hand, the indirect approach of sulfated peptide/protein characterisation in the positive ion mode is applied more often, and is initiated by some derivatisation or reduction of the disulfide unit prior to mass spectroscopic sequencing [329]. One such method involves comparison of the non-reduced and reduced (using dithiothreitol in ammonium bicarbonate buffer) aliquots of a proteolytic digest of a peptide/protein. For example, the solvent containing 50% H₂¹⁸O is used to incorporate ¹⁸O into terminal carboxylates to assist with the interpretation of MSⁿ positive ion mass spectra [330]. In another approach, the disulfide bond is reduced by reductive agents such as tris(2-carboxyethyl)phosphine (TCEP) in pH 3.0 citrate buffer, followed by cyanylation with 1-cyano-4-(dimethylamino)pyridinium tetrafluoroborate (CADP) [331], or by alkylation with iodoacetamide, acrylamide and 4-vinylpyridine [332-333]. The reduced products are subsequently investigated by MS. In general, positive ion MS based methods of disulfide characterisation are not straightforward and require much care in sequestering and paring of half-cyanylnyl sequences to establish disulfide connectivity patterns [328-329, 334-335].

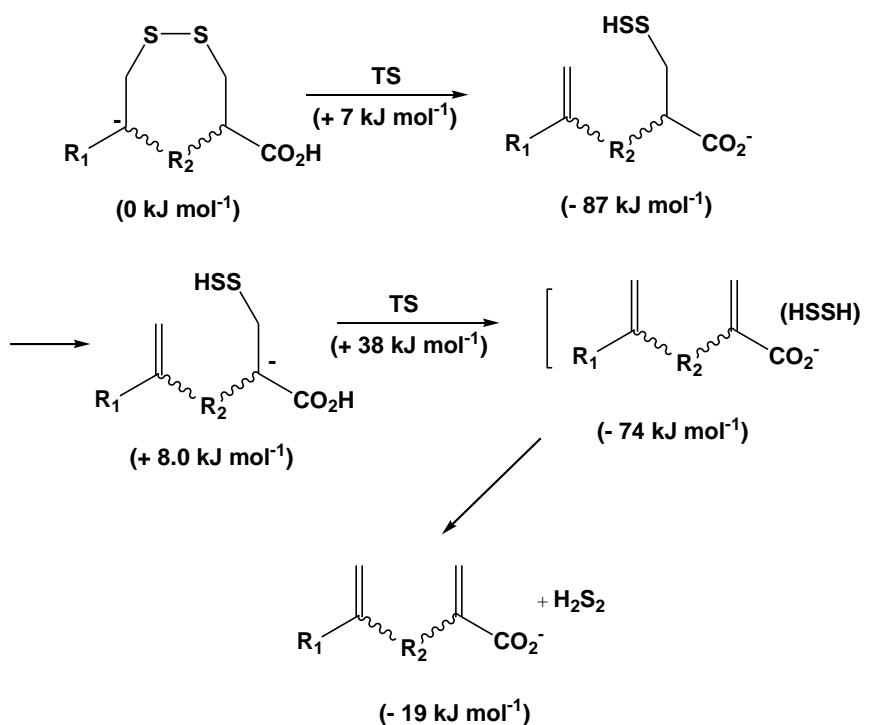
4.3. Negative ion mass spectrometry of disulfide linkages

Disulfide containing peptides/proteins are prone to fragment at the disulfide residues leaving the backbone intact under negative ion CID conditions. Investigations into fragmentation pathways of underivatised disulfide-containing peptides/proteins in the negative mode show that fragmentation of disulfide moieties result in groups of signature cleavage ions (see sections 4.3.1 and 4.3.2) [326, 336-337]. This provides a reliable means to identify the presence and position of both intramolecular and intermolecular disulfide residues in peptides/proteins.

In the negative ion mode, fragmentation patterns produced by tandem in space mass spectrometers are found to be more reliable for determination of disulfide linkages than that by tandem in time mass spectrometers [336]. In tandem in time mass spectrometers, such as in a Fourier transform mass spectrometer, dissociation of disulfide bonds and losses of side chains are commonly accompanied by backbone fragmentations. This complicates the fragmentation pattern of a disulfide containing peptide anion, reduces the abundance of disulfide fragments, and therefore prevents the unambiguous identification of disulfide bonds in the precursor ion by using this type of instrument.

4.3.1 Intramolecular disulfide linkages

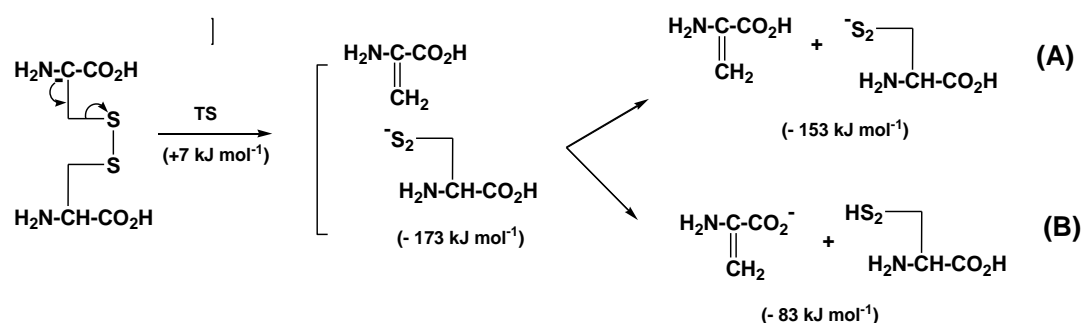
The key negative ion fragmentation of an intramolecular disulfide is the facile loss of the elements of H_2S_2 to form a fragment anion $[(\text{M}-\text{H}) - \text{H}_2\text{S}_2]^-$ which then undergoes backbone cleavages to provide a partial or full sequence of the peptide. A mechanism for the loss of H_2S_2 is shown in Scheme 4.2. The process is favourable by 19 kJ mol^{-1} with the highest barrier of 38 kJ mol^{-1} at the HF/6-31 G(d)//AM1 level of theory [338].



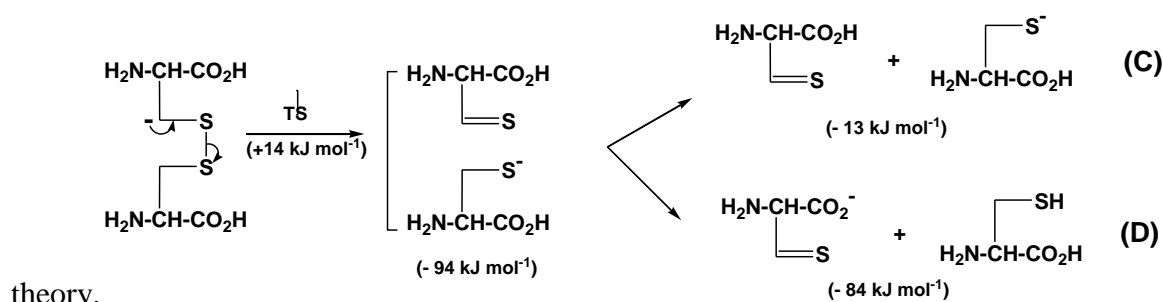
Scheme 4.2. Proposed mechanisms for the loss of H_2S_2 from an intramolecular disulfide moiety [338]. $\text{R}_1 = \text{HCONH}$, $\text{R}_2 = \text{CONHCH}_2\text{CHNH}$. Calculations at the HF/6-31 G(d)//AM1 level of theory.

4.3.2 Intermolecular disulfides

The (M-H)⁻ parent anions of intermolecular disulfide containing peptides cleave through the disulfide moiety in some of the most favourable of negative-ion peptide fragmentations. For a symmetrical intermolecular disulfide system, four possible fragmentations are observed (Scheme 4.3 and 4.4) as the fragmentations can occur at the S-S bond, or at C-S bonds on either side of the disulfide linkage. If the intermolecular disulfide is unsymmetrical then there are eight possible disulfide cleavage products. Calculation at the HF/6-31 G(d)//AM1 level of theory of a simple peptide containing a symmetrical intermolecular disulfide unit shows that the cleavages for intermolecular disulfides are highly exothermic with small energy barriers to transition states (+7 and +14 kJ mol⁻¹ for the process in Schemes 4.3 and 4.4, respectively) [339].



Scheme 4.3. Proposed mechanism for the fragmentation occurring at a C-S bond of an intermolecular disulfide residue [339]. Calculations at the HF/6-31 G(d)//AM1 level of



theory.

Scheme 4.4. Proposed mechanism for the fragmentation occurring at an S-S bond of an intermolecular disulfide residue [339]. Calculations at the HF/6-31 G(d)//AM1 level of theory.

Negative ion MS has been successfully applied to characterise some small disulfide containing proteins such as insulin and lysosome. This identifies the positions of all disulfide

units and much of the sequences of the proteins [336, 340]. The question now is whether this method can be used for disulfide detection and positioning in large proteins. This chapter reports the identification of disulfide bonds in ricin using proteolytic cleavage followed by negative ion nanospray MS of peptide fragments. Partial sequencing data of ricin are also determined and presented.

4.4 Ricin: structure and bioactivity

4.4.1 Biosynthesis of ricin

Ricin is a toxic protein isolated from the seeds of the castor bean plant. It is synthesized in the endosperm of *Ricinus* seeds as preproricin, the polypeptide precursor of ricin, which consists of 576 amino acids. The primary sequence of preproricin (Figure 4.1) was first determined by chemical degradation following proteolysis and genomic cloning, and was later confirmed by MS and NMR. The first 35 amino acids of preproricin constitutes the signal sequence [341], followed by chain A of 267 amino acids [342-343]. Chain B of 262 amino acids [344-345] is connected to the A chain by a 12-amino-acid linking peptide [341, 346].

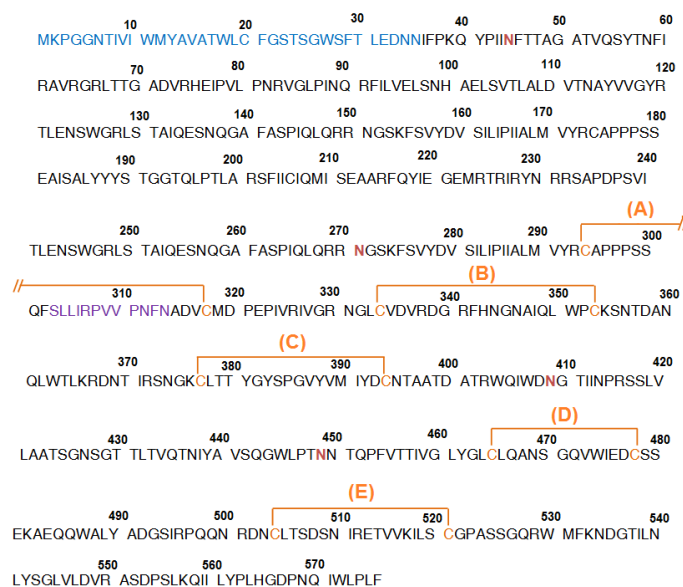
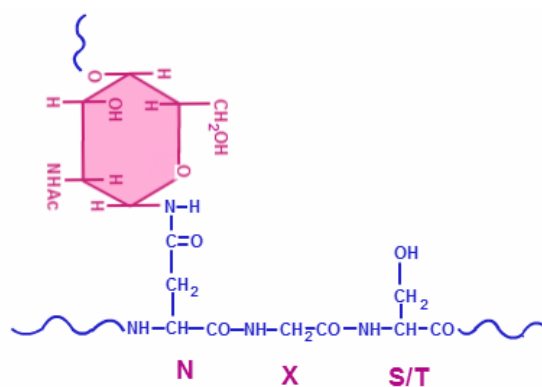


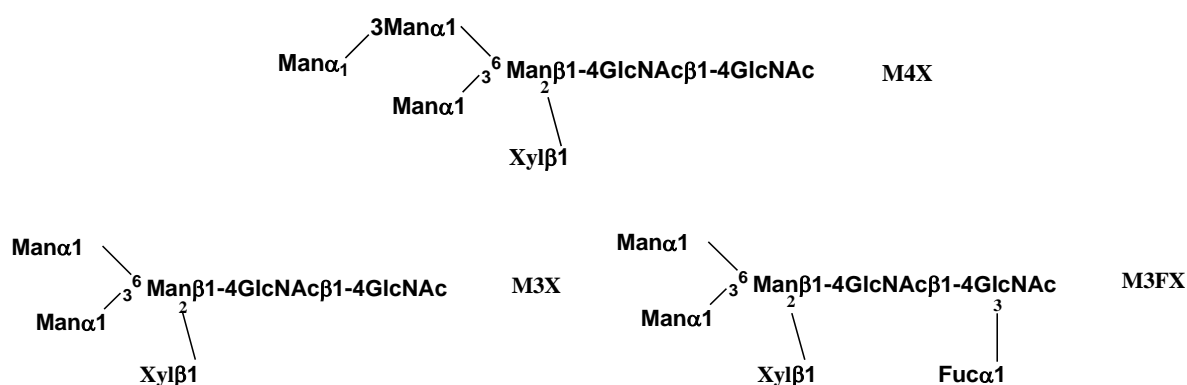
Figure 4.1. Primary structure of preproricin (also known as preproricin D, see more details in section 4.4.4) according to the Swiss-Prot database. Amino acid 1-35: signal peptide, 303- 314: linker peptide, 36-302: A chain protein, 316-576: B chain protein, C-C: disulfide links, N: potential glycosylation sites.

After its synthesis, the N-terminal signal sequence directs the nascent preproricin to the endoplasmic reticulum (ER) lumen, where the first 22 amino acids of the signal sequence is cleaved [347]. Within the ER lumen, the preproricin is glycosylated at the three N-glycosylation sites Asn45, 409 and 449 (see Figure 4.2a for structure of an N-linked glycosylated Asn). Asn409 is commonly found to link to oligomannose type sugar chains ($\text{Man}_{6-7}\text{GlcNAc}_2$), Asn449 to ($\text{Man}_{5-7}\text{GlcNAc}_2$) or M4X, and, Asn45 to M3FX or M3X (see Figure 4.2b for structures of M3X, M3FX and M4X) [348]. Glycosylation of Asn271 by M3FX is sometimes found [349]. However, the sugar content of ricin may change during the biosynthetic pathway of ricin, and thus, ricin extract commonly exhibits a high level of structural heterogeneity mainly due to the presence of many glycoforms [350].

At this stage, five disulfide bridges, one connecting the A-chain and the B-chain and four located in the B-chain, are formed under the catalytic action of protein disulfide isomerases. The resulting proricin is transported to and stored in the protein bodies via the Golgi complex. This transport is accompanied by (i) the enzymatic modification of the glycosylation side chains of proricin and (ii) the elimination of the 12-residue linker [351] and the small remaining N-terminal signal peptide [352] (from amino acid 23-35), generating the native/mature ricin also known as ricin D which is the major form of ricin (see more details in section 4.4.4). This is also the structure of ricin being dealt with throughout this chapter.



a.



b.

Figure 4.2. a. Structure of N-linked glycosylation which only occurs on the nitrogen atom of an Asn residue (glycosylation site) in the sequence Asn-X-Ser or Asn-X-Thr with X being any amino acid except for Pro. **b.** Structures of M3X, M3FX and M4X ligands attached to Asn residues in ricin, with Man being D-mannose (MW: 162); Xyl being D-xylose (MW: 132); Fuc being L-fructose (MW: 146); GlcNAc: N-Acetyl glucosamine (MW: 203.195). Subscripts stand for the carbon positions of sugar units being connected.

4.4.2 Three dimensional structure of ricin

The detailed structure of ricin has been solved by X-ray crystallography [353-360] and refined to 2.5 Å resolution. The A-chain is globular shaped with a pronounced binding site cleft, consisting of eight alpha helices and eight strands of beta sheet [353, 357]. The B-chain is an elongated dumbbell with galactose binding sites at both ends [355-356] (Figure 4.3).

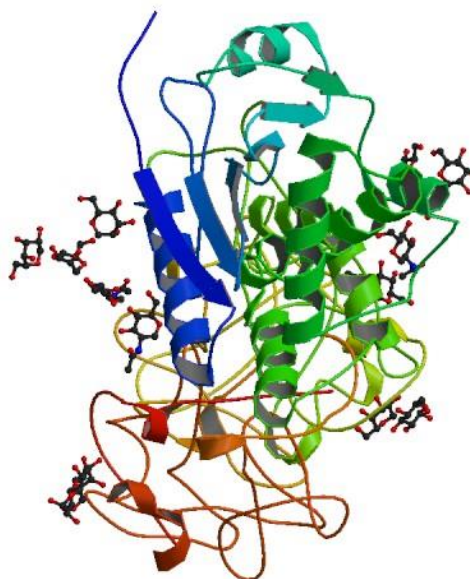


Figure 4.3. Crystallographic structure of ricin D. The structure has been obtained from the PDB protein data bank (code 2AAI).

4.4.3 Ricin activity

Ricin is known as one of the type two ribosome inactivation proteins (RIPs) due to its toxicity to mammalian cells. The entry of ricin into mammalian cells is facilitated by the binding of the B chain to beta-D-galactopyranoside sites on the cell surface glycoproteins and glycolipids. Once inside the cells, the A chain acts as a glycosidase that removes a specific adenine residue from an exposed loop of the 28S rRNA (A4324 in mammals). The toxin itself does not break the RNA but makes it susceptible to hydrolysis, leading to rRNA breakage [361]. The damaged ribosomes no longer function or take part in the protein synthesis process and thus the cell is terminated. Mutation studies showed that the residues Glu212 and Arg215 are essential for the activity of the ricin A-chain [359].

Due to the toxicity of ricin to mammalian cells, it is categorised as a restricted substance in Schedule 1 of the Chemical Weapons Convention [362]. The median lethal dose (LD₅₀) of ricin is around 20 micrograms per kilogram of body weight for humans (1.8 mg for an average adult) if exposure is from injection or inhalation [363-364].

4.4.4 Ricin detection and identification

The ease of production of toxins from castor bean seeds and the accessibility of this plant makes ricin a potential chemical used in terrorist activities. The first documented case was the assassination of the Ukrainian journalist, Georgi Markov, in 1978 managed by injection of ricin via an umbrella tip. Recently, two threatening letters containing ricin-suspected chemicals were sent to the U.S. President B. Obama in 2013. This led to a high demand for methods of rapid and accurate identification of ricin (and other type II RIPs). So far, the most common methods used for ricin detection are immunoaffinity based assays. These assays involve interaction between ricin and an antigen that is specific for ricin. In many cases, fluorescence is used to detect the bound ricin [365-367]. Even though these methods are very sensitive, they are time consuming and false positives can occur due to cross reactivity of other molecules with the same binding motifs. Ricin can also be recognized using bioassays which take advantage of its ribonuclease activity [368-370]. However, these methods are not specific as other ribosome-inactivating proteins can produce the same results, or false negatives may occur by loss of enzymatic activities due to ricin denaturation.

MS has been commonly used to confirm the presence of ricin. Attempts have been made to detect and characterise ricin using both MALDI and ESI positive ion MS. Detection of intact ricin by measuring the molecular mass of the target protein has been reported [371-372]. However, the detection sensitivity is very poor, and accurate molecular mass is difficult to determine due to the presence of many monoisotopic peaks which come from post-translationally modified analogues of ricin. The detergent Tween 80 is recommended as an additive to improve the detection limit of ricin and reduce interference from the castor bean seed storage proteins, but the problem of low mass accuracy still has not been solved [373]. In order to improve the detection sensitivity, the target protein is normally purified, commonly by immuno affinity purification which makes use of the binding ability of the ricin B-chain to sugar chains such as β -D-galactopyranoside and β -D-N-acetylgalactosamine [374-375]. Another mass spectrometric approach involves structural analysis of peptides obtained from enzymatic digest of ricin. This method identifies much of the sequence of ricin, but the precise positions of disulfide bonds are not determined directly and unambiguously by positive ion MS/MS [373-377].

Two basic isoforms of ricin are ricin D and ricin E, with ricin D being the major and higher potency form of ricin. Ricin E comprises of an identical A-chain and a B-chain differing by 15% to that of ricin D [378]. In addition, there are several type II RIPs and proteins that are co-synthesized with ricin D in the castor bean plant; these have high sequence similarity to that of ricin [379]. For instance, ricinus communis agglutinin (RCA) is a heterodimeric type II RIP consisting of two ricin-like heterodimers. The amino acid sequence homology between RCA and ricin D is 93% for the A-chain and 84% for the B chain [380-381]. However, while ricin D is a cellular toxin, RCA is only weakly toxic to intact cells. Furthermore, ricin activity depends critically on the disulfide connectivity between the A-chain and B-chain. Therefore, sequence determination of the digested peptides from ricin and the identification of disulfide links within ricin are necessary in order to avoid false-positive identification of ricin homologues.

4.5 Results and discussion

4.5.1 Sequencing data obtained from proteolytic digest of ricin

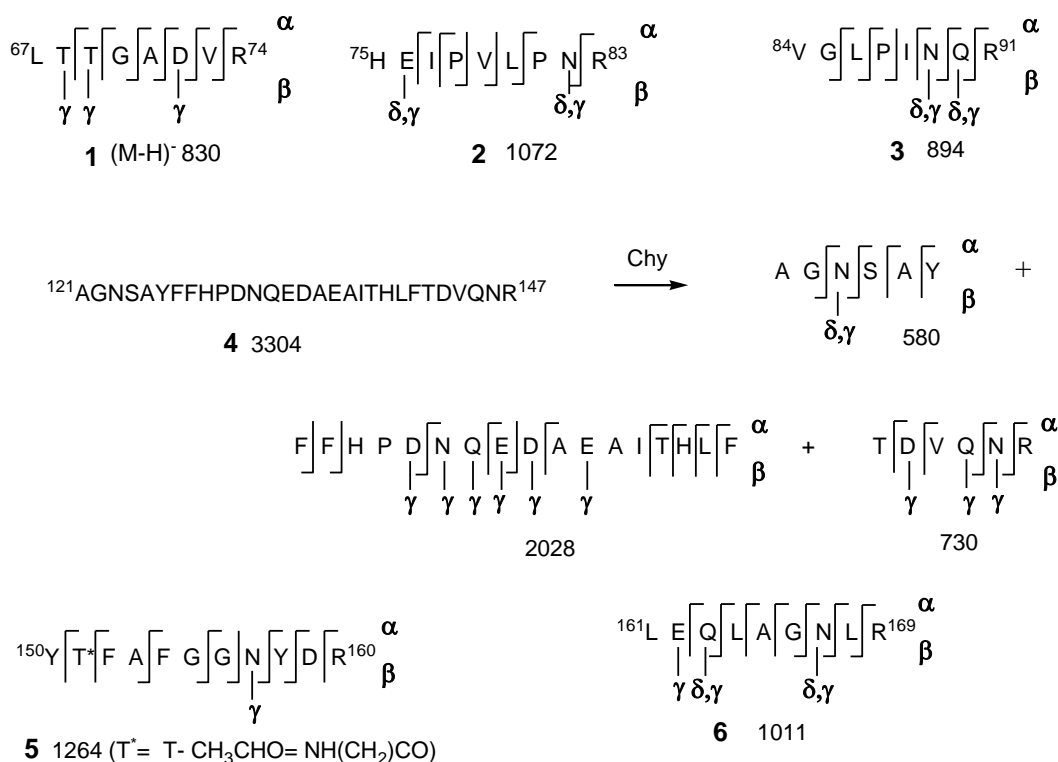
Expected fragment peptides from tryptic digestion of ricin are shown in Table 4.1. The peptides containing potential sites for glycosylation are denoted by a hash sign (#).

Table 4.1. Expected fragment peptides from tryptic digest of ricin. Those detected by negative ion MS are indicated in red.

Position	Sequence	Nominal m/z (M-H) ⁻	Observed nominal m/z (M-nH) ⁿ⁻
36-39	IFPK		
40-61 (#)	QYPIINFTTAGATVQSYTNFIR		
62-64	AVR		
65-66	GR		
67-74	LTTGADVR	830	830 ⁻
75-83	HEIPVLPNR	1072	1072 ⁻
84-91	VGLPINQR	894	894 ⁻
92-120	FILVELSNHAELSVTLALDVTNAYVVGYR		
121-149	AGNSAYFFHPDNQEDAEAIHLFTDVQNR	3304	1102 ⁽³⁻⁾
150-160	YTFAFGGNYDR	1308	1308 ⁻
161-169	LEQLAGNLR	1011	1011 ⁻
170-201	ENIELGNGLPEEAISALYYSTGGTQLPTLAR	3437	1718 ⁽²⁻⁾
202-215	SFIICIQMISEAAR	1579	1579 ⁻
216-224	FQYIEGEMR	1170	1170 ⁻
225-226	TR		
227-228	IR		
229-231	YNR		
232	R		
233-248	SAPDPSVITLENSWGR	1726	1726 ⁻ /863 ⁽²⁻⁾
249-269	LSTAIQESNQGAFASPIQLQR	2256	2256 ⁻ /1128 ⁽²⁻⁾
270	R		
271-274(#)	NGSK		
275-293	FSVYDVSILIPIIALMVYR	2209	2209 ⁻ /1104 ⁽²⁻⁾
294-302 and 315-326	<u>C</u> APPSSQF <u>ADV</u> CMDEPIVR	2272	1136 ⁽²⁻⁾
327-330	IVGR		
331-338 and 341-354	NGL <u>CVDVR</u> <u>FHNGNAIQLWPCK</u>	2397	1198 ⁽²⁻⁾
339-341	DGR		
355-367	SNTDANQLWTLK	1388	1388 ⁻
367	R		
368-372	DNTIR		
373-376	SNGK		
377-403	<u>CL</u> TTYGYSPGVYVMIYDCNTAATDATR	2944	1471.5 ⁽²⁻⁾
404-416(#)	WQJWDNGTIINPR		
417-482(#)	SSLVLAATSGNSGTTLTVQTNIAVSQGWLPTNNTQPFVT TIVGLY <u>GLCLQANSQVWIEDCSSEK</u>	2162	1081 ⁽²⁻⁾
483-501 and 502-512 and 518-529	AEQQWALYADGSIRPQQNR <u>DN</u> CLTSDSNIR <u>IL</u> SCGPASSGQR	2228 2407	2228 ⁻ /1114 ⁽²⁻⁾ 1203 ⁽²⁻⁾
513-517	ETVVK		
530-533	WMFK	609	609 ⁻
534-550	NDGTILNLYSGLVLDVR	1859	1859 ⁻
530-550	WMFK NDGTILNLYSGLVLDVR	2451	1225 ⁽²⁻⁾
551-557	ASDPSLK		
558-576	QIILYPLHGDPNQIWLPLF	2274	2274 ⁻ /1136.5 ⁽²⁻⁾

In order to keep all disulfide links in ricin intact, ricin was subjected to tryptic digestion without a prior reduction step. Subsequent HPLC separation of the resulting products gave 23 peptides detected by negative ion nanospray ionisation MS (coloured in red in Table 4.1). Five of them are disulfide containing peptides. Some of the larger of non-disulfide containing peptides gave complex negative ion spectra which did not provide satisfactory sequence information; these peptides were treated further with chymotrypsin to give smaller peptides. Most of these peptides appeared in singly charged form; some larger peptides were observed as doubly and triply charged anions as shown in Table 4.1 and discussed in section 4.5.3.

The amino acid sequence coverage of ricin A and B chains by negative ion MS are 72% and 70%, respectively. A number of peptides from both the A- and B-chains were not observed. This may be because they were not retained (e.g. too small or too large peptides) by the C18 stationary phase with the elution condition being used, or they could not compete for the negative charges (low ionisability) and/or were outside the m/z range monitored, or the tryptic cleavage sites were hindered in the compact structure of ricin such that trypsin could not reach these sites. None of glycosylated fragments was detected by negative ion MS. The primary structures of all peptides together with data obtained by backbone cleavages are summarised in Figure 4.4.



produced by tryptic/chymotrypsin (1:1) digest of ricin. For simplicity, all masses displayed are of singly-charged anions and are nominal masses, obtained by the summation of the integral masses of all the amino acid residues.

4.5.2 Identification of disulfide containing peptides from proteolytic digestion of ricin

Tryptic digestion of ricin produced four (out of five) disulfide containing peptides of ricin including three intermolecular disulfides **13**, **14** and **19** and one intramolecular disulfide **16** (Figure 4.4). The final intramolecular peptide **17** (see Figure 4.4) was prepared and identified using digestion with trypsin and chymotrypsin (1:1 molar ratio). For comparison purposes, both positive and negative ion mass spectrometric measurements of the disulfide containing fragments were implemented. The five disulfide containing peptides were synthesized and spectra of these synthetic peptides were shown to be identical to those of the fragment peptides obtained from proteolytic digestions.

Positive and negative-ion electrospray ionisation MS/MS data for the MH^+ and $(M-2H)^{2-}$ ions of disulfide **13** are displayed in Figures 4.5 and 4.6, respectively. Although Figure 4.5 is the most informative of all of the positive ion disulfide spectra measured, its fragmentation pattern only provides side chain sequencing information, not the location of the disulfide bond. The side chain sequences were identified using standard **b** and **y** backbone cleavages [140, 143, 382] as shown in Figure 4.5.

The intermolecular disulfide peptides 13, 14 and 19

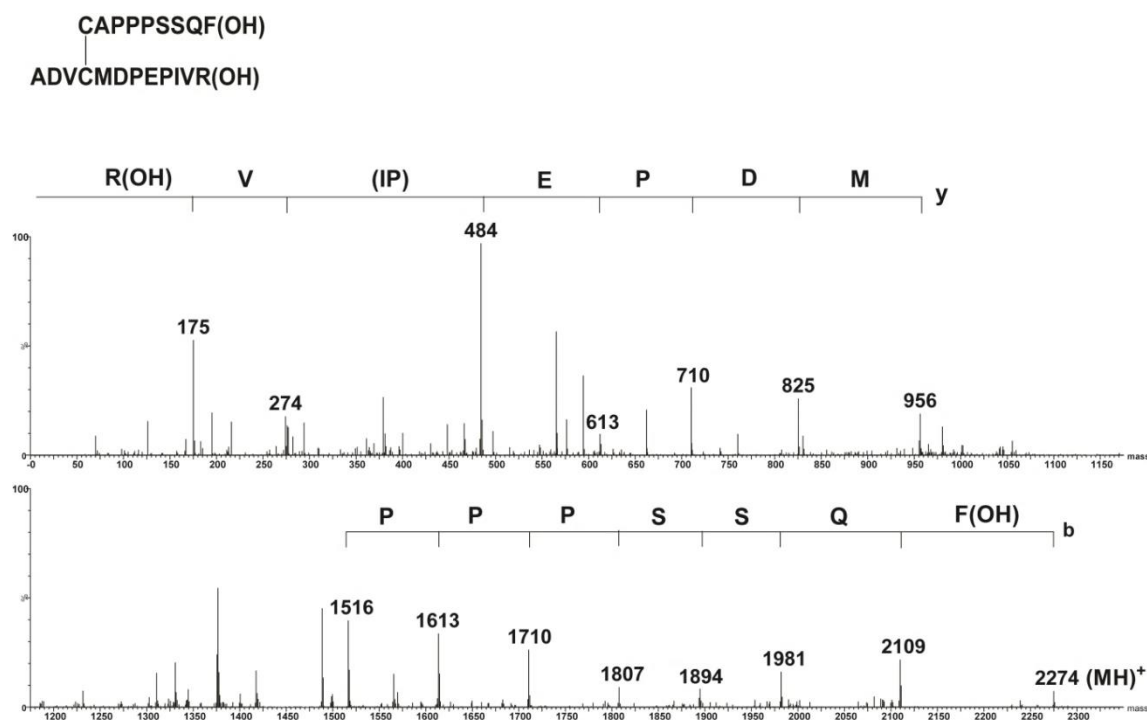


Figure 4.5. Collision-induced positive ion MS/MS spectrum of the MH⁺ parent cation of **13**. Q-TOF 2 mass spectrometer.

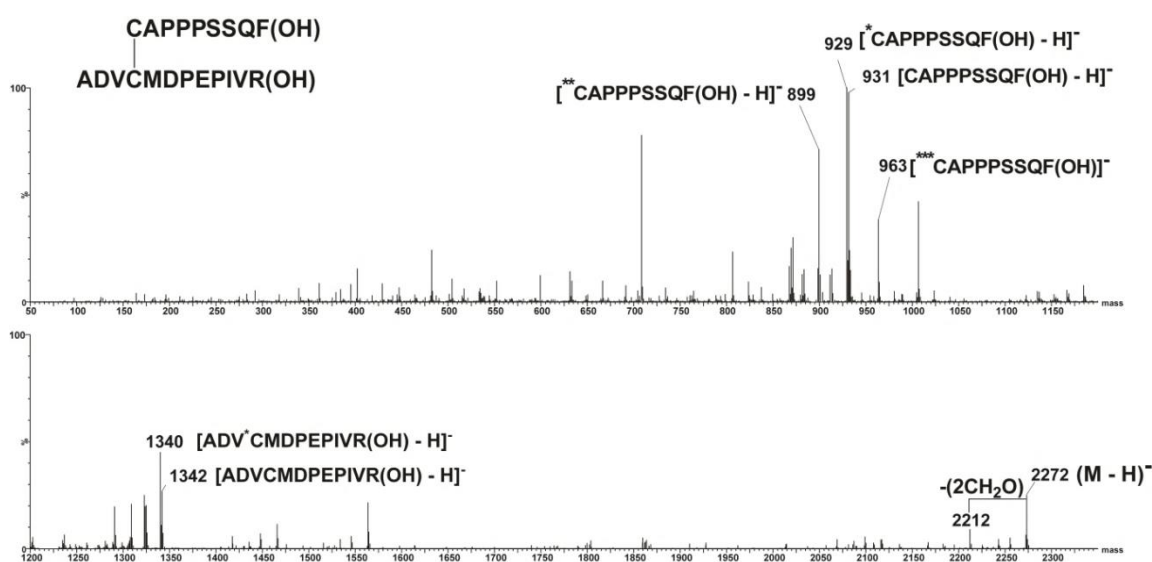
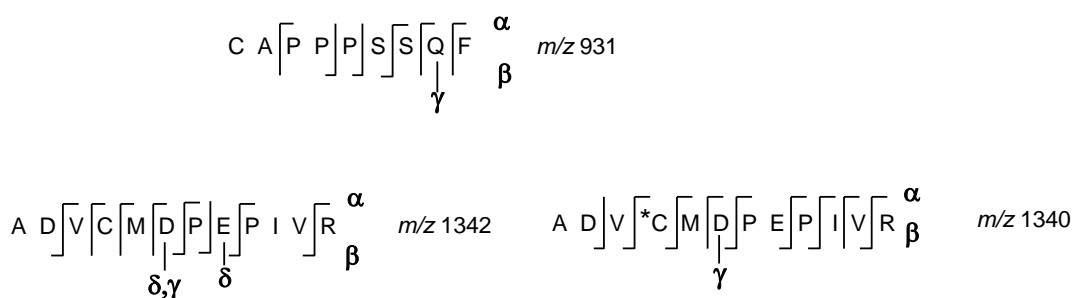


Figure 4.6. Collision-induced negative ion MS/MS spectrum of the (M-2H)²⁻ parent anion of **13**, converted to a ‘singly-charged’ spectrum using MassLynx software (see Experimental sections for details). Q-TOF 2 mass spectrometer.

In contrast with the positive ion MS/MS data, the negative ion data are in accord with the standard negative ion cleavages shown for the simplest disulfide model system in Schemes 4.3 and 4.4. This enables the determination of disulfide connectivities in these peptides. The four basic negative ion cleavages of an intermolecular disulfide shown in Scheme 4.3 and 4.4 are for a symmetrical model system. Peptide **13** is unsymmetrical, so, in principle, there could be eight fragment anions originating from cleavage of the disulfide linkage. However, the spectrum in Figure 4.6 only shows six characteristic cleavage ions, namely two type **C** cleavages [CAPPPSSQF(OH)-H]⁻ (*m/z* 931) and [ADV^{*}CMDPEPIVR(OH)-H]⁻ (*m/z* 1342), together with two type **D** cleavages [^{*}CAPPPSSQF(OH)-H]⁻ (*m/z* 929) [^{*}C is NHCH(CH₂S⁻)CO] and [ADV^{*}CMDPEPIVR(OH) - H]⁻ (*m/z* 1340). One type **A** anion [^{***}CAPPPSSGF(OH) - H]⁻ (*m/z* 963) [^{***}C is NHCH(CH₂S₂⁻)CO] and one type **B** anion [^{**}CAPPPSSQF(OH) - H]⁻ (*m/z* 899) [^{**}C is NHC(=CH₂)CO] are also formed. Source-formed collision induced negative ion nano-electrospray ionisation spectra of any of the six disulfide cleavage anions provide sequencing information (see e.g. for *m/z* 931, 1340 and 1342 as shown in pictorial form in Scheme 4.5). Numerical details of cleavage anions *m/z* 931, 1340 and 1342 are recorded in Table 4.2.



Scheme 4.5. Schematic representation of backbone cleavages of three selected disulfide fragments from peptide **13**, [^{*}C = NHCH(CH₂S)CO].

Table 4.2. Negative ion mass spectrometric data for the (M-2H)²⁻ anions of **13**, **14** and **19**.

13 (M-2H)²⁻ *m/z* 1135. Disulfide cleavage gives a number of singly-charged fragment ions including *m/z* 931, 1340 and 1342.

(i) *m/z* 931, α ions, *m/z* 757, 379, 292, 164 [(CA) (378)SQF(OH)]. β ions, *m/z* 367, 464, 551 [(368)PS(380)]. (**931- 2CH₂O - H₂S**), *m/z* **837**, α ions, *m/z* 768, 697, 406, 349, 292, 164 [^{**}CAP(P)^{*}S^{*}SQF(OH)]. β ions, *m/z* 139, 236, 333, 430, 487, 544, 672

[(*CA)PPP*S*SQF(OH)]. (**C = C - H₂S = NHC(CH₂)CO, *S = S - CH₂O = NHCH₂CO). Overall sequence [CAPPPSSQF(OH)].

(ii) m/z 1340, α ions, m/z 1055, 954, 823, 708, 482, 385, 272, 173, [(285)*CMD(PE)PIVR(OH)]. β ions, m/z 185, 284, 385, 631, 857, 954, 1166 [(AD)V*C (MD)(PE)P(IV)R(OH)]. γ ions, m/z 806 (γ D6). [*C = NHCH(CH₂)CO]. Sequence [(AD)V*C MD(PE)PIVR(OH)]

(iii) m/z 1342, α ions, m/z 1156, 1057, 954, 823, 708, 482, 173 [(AD)VCMD(PE)(309)R(OH)]. β ions, m/z 185, 633, 730, 859, 1168 [(AD)(448)PE(309)R(OH)]. δ and γ ions m/z 535 (δ D6), 747 (δ E8), 806 (γ D6). Sequence [(AD)VCMDPE(309)R(OH)]. Overall sequence obtained from the negative ion CID MS/MS of m/z 1340 and m/z 1342 [(AD)VCMDPEPIVR(OH)].

CAPPPSSQF(OH)

Overall sequence of **13**: **(AD)VCMDPEPIVR(OH)**

14 (M-2H)²⁻ m/z 1198. Disulfide cleavage gives a number of singly-charged fragment ions including m/z 873 and 1525.

(i) m/z 873, α ions, m/z 759, 702, 589, 387, 272, 173 [NGL(CV)DVR(OH)]. β ions, m/z 113, 283, 600, 699 [N(GL)(317)VR(OH)]. δ and γ ions, m/z 300 (δ C4), 370 (γ D6), 502 (δ D6), 572 (γ C4). Sequence [NGL(CV)DVR(OH)].

(ii) m/z 1525. α ions, m/z 1241, 1127, 1070, 956, 885, 772, 345 [(FH)NGNAI(427)(346)]. δ and γ ions, m/z 231 (γ C12), 300 (δ N3), 471 (δ N5), 755 (γ Q8), 769 (δ Q8), 1053 (γ N5), 1224 (γ N3). Sequence [(FH)NGNAIQ(LW)PCK(OH)].

NGL (CV)DVR(OH)

Overall sequence of **14**: **(FH)NGNAIQ(LW)PCK(OH)**

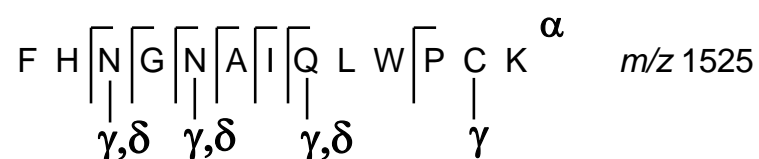
19 (M-2H)²⁻ m/z 1203. Disulfide cleavage gives a number of singly-charged fragment ions including m/z 1173 and 1235.

(i) m/z 1173, α ions, m/z 1060, 947, 860, 757, 700, 603, 532, 445, 358, 301, 173 [ILSCGPASSGQR(OH)]. β ions, m/z 225, 312, 415, 472, 640, 727 [(IL)SCG(PA)S(446)]. γ ions, m/z 843 (C4), 515 (S8), 428 (S9), 284 (Q11). Sequence [ILSCGPASSGQR(OH)].

(ii) m/z 1235, α ions, m/z 1006, 689, 487, 286, 173 [(DN)(317)(SD)(SN)IR(OH)]. β ions, m/z 114, 444, 632, 747, 834 [D(330)(TS)DS(401)]. γ ions, m/z , 383 (N9), 585 (D7), 989 (C3), 1103 (N2). Sequence [DNCLTSDSNIR(OH)].



The CID MS/MS data of the $(M-2H)^{2-}$ parent ion of **14**, modified by MassLynx software is reproduced in Figure 4.7. Five disulfide fragment ions originating from the cleavage of the disulfide moiety are observed and CID of these provides sequencing information. Cleavages of [FHNGNAIQLWPCK(OH)-H]⁻ (m/z 1525 from **14**) are summarised in Scheme 4.6, while the negative ion CID source-formed MS/MS data for [NGLCVDVR(OH)-H]⁻ (m/z 873) is shown in Figure 4.8. The latter spectrum is shown to illustrate how the simple α and β backbone cleavages compete with δ and γ cleavages (particularly of Asp and Cys). Details of the negative ion spectra of the two source formed anions m/z 1525 and m/z 873 from **14** are summarised in Table 4.2.



Scheme 4.6. Schematic representation of backbone cleavages of a selected disulfide fragment from peptide **14**.

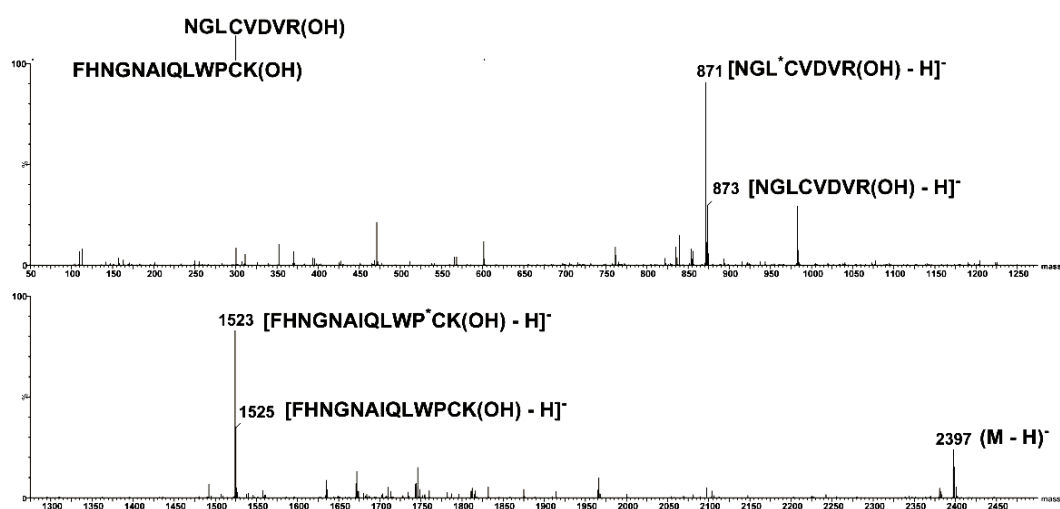


Figure 4.7. Collision-induced negative ion MS/MS of the $(M-2H)^{2-}$ parent anion of **14**, converted to a ‘singly-charged’ spectrum using MassLynx software (see Experimental section for details). Q-TOF 2 mass spectrometer.

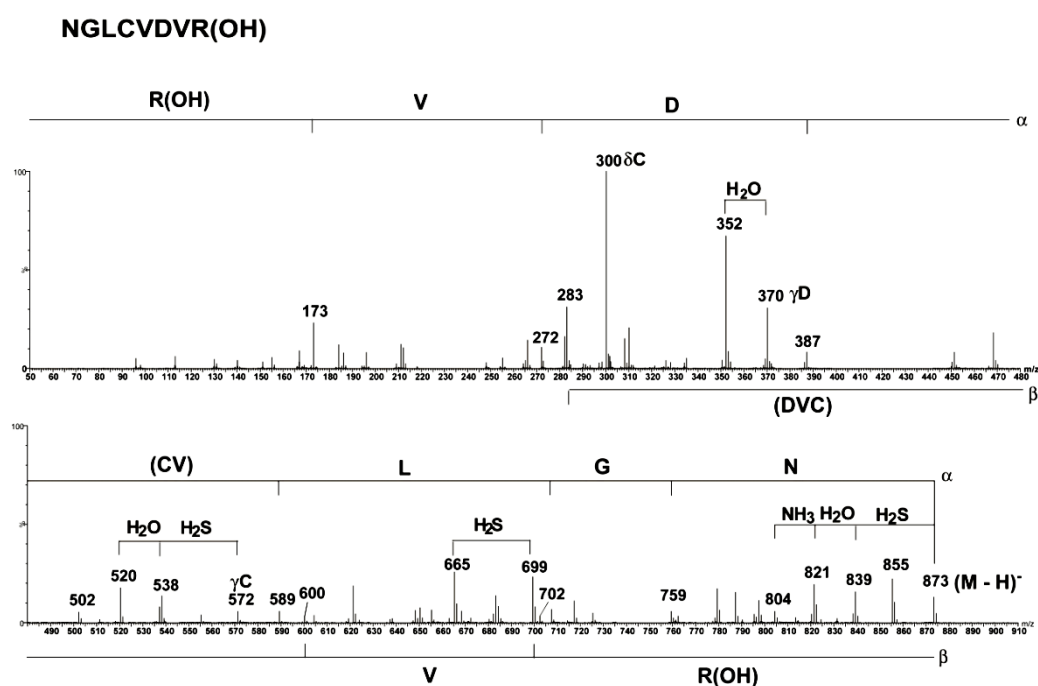
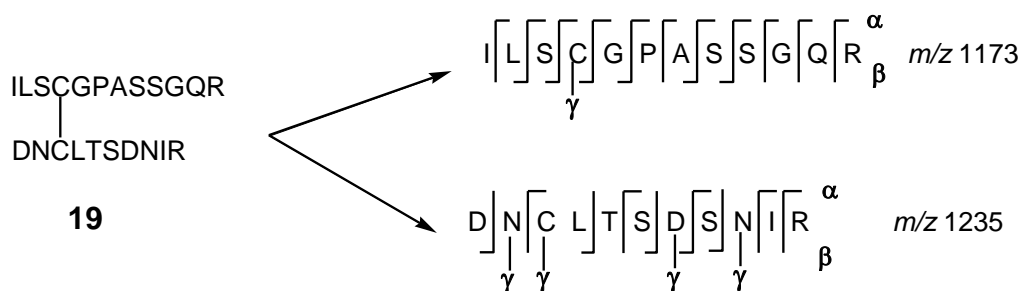


Figure 4.8. Collision-induced negative ion MS/MS of the source formed fragment anion $[NGLCVDVR(OH)-H]^-$ (m/z 873). Q-TOF 2 mass spectrometer.

Fragmentation of the final intermolecular disulfide **19** $(M-2H)^{2-}$ (m/z 1203) is similar to that of peptides **13** and **14**, in defining the position of the disulfide bridge. The negative ion cleavages of the fragment anions shown in Scheme 4.7 (and detailed in Table 4.2) provide sequencing data for disulfide **19**.



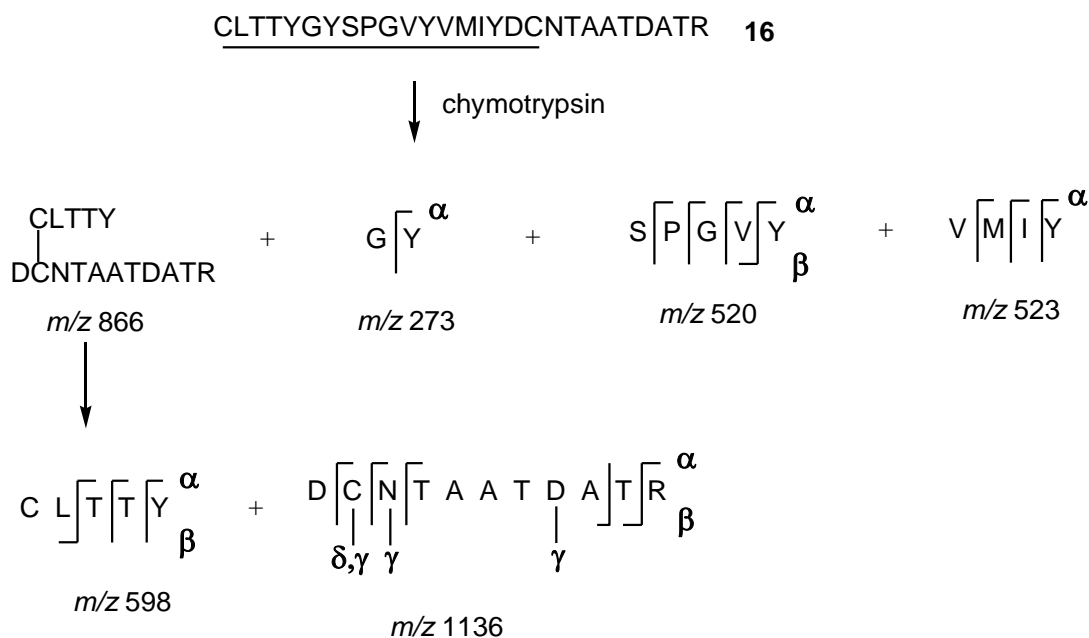
Scheme 4.7. Schematic representation of backbone cleavages of two selected disulfide fragments from peptide **19** (M-2H)²⁻ m/z 1203.

The intramolecular disulfides 16 and 17

In previous studies of the negative ion cleavages of peptides containing an intramolecular disulfide moiety, it was shown that such a disulfide unit could be identified by characteristic loss of H₂S₂ from the (M-H)⁻ anion [338, 340, 383]. The loss of H₂S₂ results in two NHC(=CH₂)CO moieties within the peptide backbone, and thus, backbone fragmentations of the [(M-H) - H₂S₂]⁻ fragment ion facilitate the identification of both the position of the disulfide and the sequence of the peptide. Unfortunately, this is not as straightforward for the parent anions of **16** and **17**. This is due to the presence of certain amino-acid residues in these peptide (M-2H)²⁻ anions whose side chain fragmentations compete with H₂S₂ loss. For example, **16** has five Thr (facile side chain loss of CH₃CHO from each Thr [156]) and Asp (γ cleavage [156]), and these fragmentations mask the normal backbone cleavages. In the case of the (M-2H)²⁻ anion of **17** there are three Ser (facile loss of CH₂O from each Ser [156, 383]) together with Asp, Glu and Gln (γ cleavages) [156, 383]. Therefore, a different strategy needs to be employed to deal with the intramolecular disulfide containing peptides from ricin.

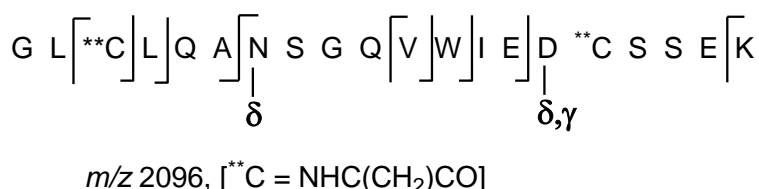
Since intermolecular disulfide cleavages (Schemes 4.3 and 4.4) are among the most energetically favoured of all negative ion peptide cleavages and the identification of three disulfides from ricin are experimentally straightforward, the intramolecular disulfide peptides were therefore converted to intermolecular disulfides by proteolysis. These peptides were cleaved at the backbone within the intramolecular disulfide ring but keeping the disulfide residue intact. Different digestion methods were used for **16** and **17**.

Peptide **16** was subjected to chymotryptic digestion to cleave at Tyr 5,7, 12 and 16, yielding four peptides. Backbone cleavages of these four peptides are shown in Scheme 4.8. In particular, the intermolecular disulfide doubly charged anion m/z 866 fragments as shown to provide a partial sequence for this species.



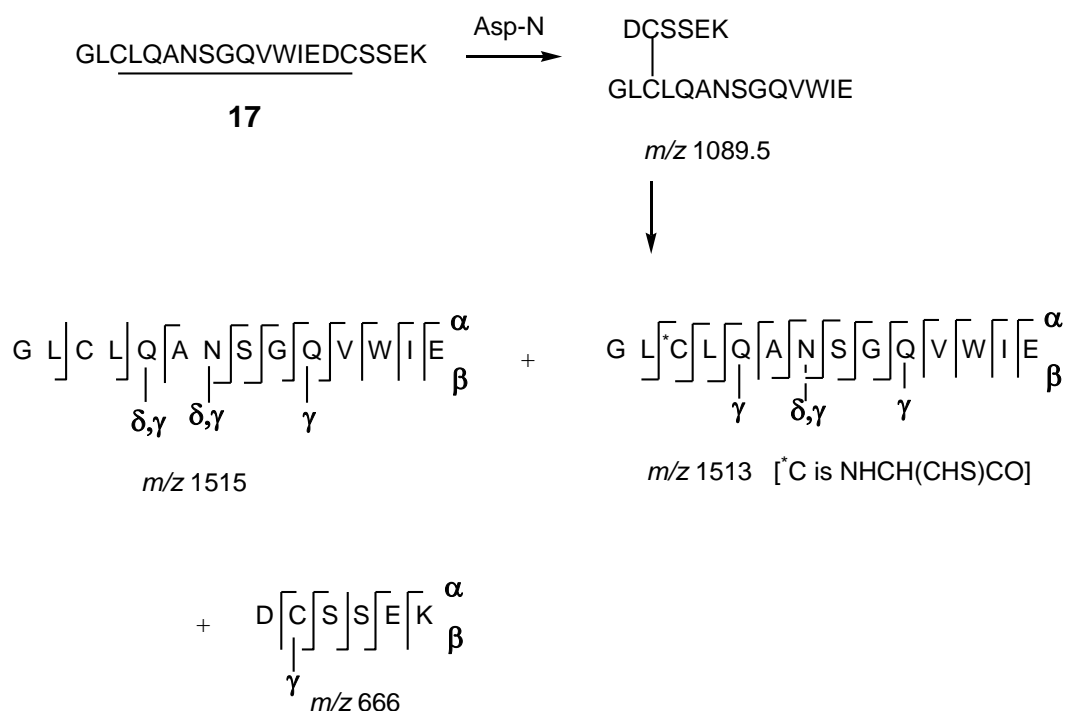
Scheme 4.8. Schematic representation of chymotryptic digest of peptide **16** and negative ion backbone cleavages of disulfide fragments derived from peptide **16**.

The fifth peptide containing the last of the disulfide links derived from tryptic digest of ricin D is not detected by either positive or negative ion MS. This could be due to the low ionisation efficiency and/or high mass of this tryptic peptide resulted from the glycosylation of Asn449. In order to reduce the size of the peptide and to trim off the Asn449 residue, ricin was digested with a 1:1 mixture of trypsin and chymotrypsin, to yield the disulfide containing peptide **17** (see Figure 4.4). The negative ion spectrum of the $(M-2H)^{2-}$ parent ion of **17** shows a peak (m/z 2096) corresponding to the loss of H_2S_2 from the parent ion. The backbone cleavages occurring from this anion are displayed in Scheme 4.9. However, this provides only a partial sequence of peptide **17**.



Scheme 4.9. Schematic representation of backbone cleavages from the anion of peptide **17** after losing H_2S_2 .

Peptide **17** has no residue within the disulfide ring which will be hydrolysed by chymotrypsin. Thus, Asp-N was used instead of chymotrypsin to convert peptide **17** to an intermolecular disulfide containing peptide. The intermolecular disulfide formed from **17** produces an $(\text{M}-2\text{H})^{2-}$ anion (m/z 1089.5) which fragments through the disulfide link to yield seven singly-charged cleavage anions (Figure 4.9), three of which (m/z 666, 1515 and 1513) fragment as shown in Scheme 4.10. The collision induced negative ion spectra of both m/z 1515 and 1513 are needed in order to identify the position of the second Cys. All numerical details of the negative ion spectra of peptide **16** and **17** are provided in Table 4.3.



Scheme 4.10. Schematic representation of Asp-N digest of peptide **17** and negative ion CID cleavages of the disulfide fragments derived from peptide **17**.

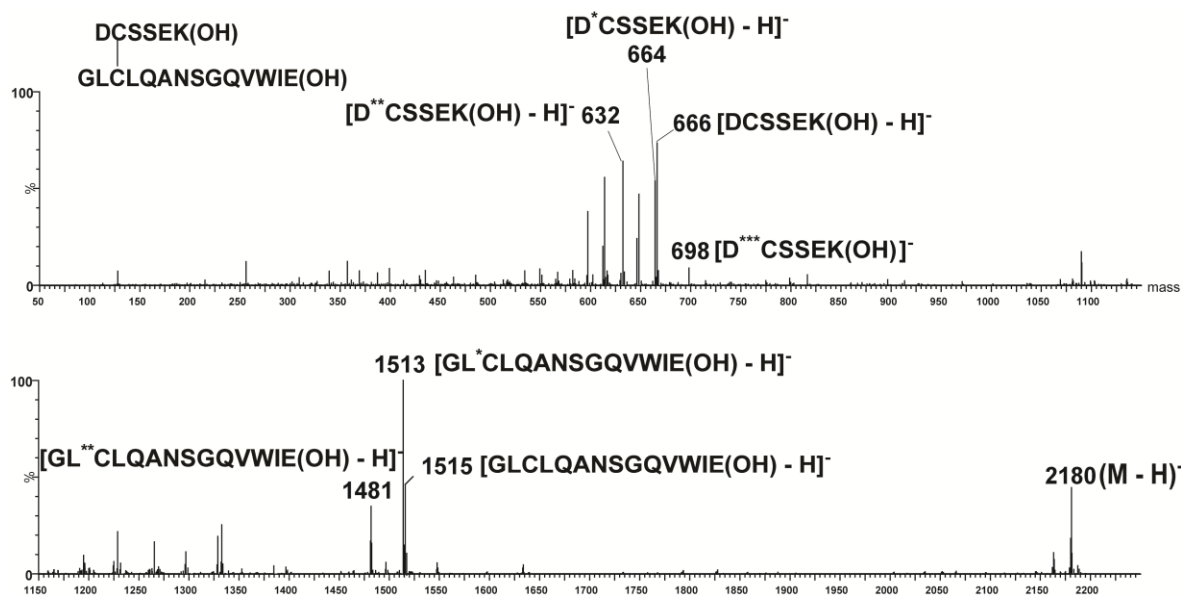


Figure 4.9. Collision induced MS/MS of the $(M-2H)^{2-}$ anion (m/z 1089.5) derived from Asp-N proteolytic cleavage of peptide **17**, converted to a ‘singly-charged’ spectrum using MassLynx software (see Experimental section for details). [$^*C = NHCH(CH_2S_2^-)CO$], [$^{**}C = NHC(=CH_2)CO$] and [$^{***}C = NHCH(CH_2S_2^-)CO$]. Q-TOF 2 mass spectrometer.

Table 4.3. Negative ion mass spectral data for the singly-charged fragments from $(M-2H)^{2-}$ anions of **16** and **17**.

16 $(M-2H)^{2-}$ m/z 1471.5. Chymotrypsin digestion of **16** gives four fragment peptides m/z 237, 520, 523 and 866 (intermolecular peptide).

(i) m/z 237. α ions, m/z 180. Sequence [GY(OH)].

(ii) m/z 520. α ions, m/z 433, 336, 279, 180 [SPGVY(OH)]. β ions, m/z 339 [(340)Y(OH)]. Sequence [SPGVY(OH)].

(iii) m/z 523, α ions, m/z 424, 293, 180. Sequence [VMIY(OH)].

(iv) Disulfide cleavage of the $(M-2H)^{2-}$ parent anion m/z 866 gives two singly-charged fragment anions including (a) m/z 598 and (b) 1136.

(a) m/z 598, α ions, m/z 382, 281, 180 [(CL)TTY(OH)]. β ions, m/z 215 [(CL) (383)].

(b) m/z 1136. α ions, m/z 1021, 918, 804, 173 [DCN(631)R(OH)]. β ions, m/z 861 [(862)TR(OH)]. δ and γ ions, m/z 131 (δ C2), 443 (γ D8), 901 (γ N3), 1004 (γ C2) Sequence [DCN(344)DATR(OH)].

Overall sequence of **16** is $\text{(CL)TTYGVYVMIYDCN(344)DATR(OH)}$

17 (M-2H)²⁻ m/z 1080.5. **17** is an intramolecular disulfide containing peptide which gives a singly-charged fragment corresponding to loss of H₂S₂ (m/z 2096). α ions, m/z 1926, 1545, 1159, 145 [(GL)(381)(386)(1014)K(OH)]. β ions, m/z 238, 351, 550, 1035, 1221, 1463, [(239)L(QA)(485)W(IE)(633)]. δ and γ ions, m/z 567 (δ N7), 616 (γ D15), 1480 (δ D15). Sequence [GL^{**}CL(QA)N(272)VW(IE)D(372)K(OH)] [^{**}C is NHC(=CH₂)CO].

17 treated with Asp-N gives an intermolecular disulfide (M-2H)²⁻ (m/z 1089.5) which undergoes disulfide cleavage to give seven singly-charged fragments, three of which are m/z 666, 1513 and 1515.

(i) m/z 666, α ions, m/z 551, 448, 274, 145 [DC(SS)EK(OH)]. β ions, m/z 217, 304, 391 [(DC)SS(EK(OH))]. γ ions, m/z 534 (C2). Overall sequence is [DCSSEK(OH)].

(ii) m/z 1513, α ions, m/z 1343, 1242, 1124, 1001, 930, 816, 729, 672, 544, 445, 259, 146 [(GL)^{*}CLQANSGQVWIE(OH)]. β ions, m/z 169, 270, 383, 582, 696, 783, 840 [(GL)^{*}CL(QA)NSG(673)] δ and γ ions, m/z 599 (δ N7), 655 (γ Q10), 913 (γ N7), 1112 (γ Q5). Overall sequence [(GL)^{*}CLQANSGQVWIE(OH)], [^{*}C is NHCH(CH₂S)CO].

(iii) m/z 1515, α ions, m/z 1001, 816, 729, 672, 544, 445, 146 [(514)(AN)SGQVWIE(OH)]. β ions, m/z 169, 385, 698, 785, 842, 970 [(GL)(CL)(331)SGQ(544)]. δ and γ ions, m/z 402 (δ Q5), 601 (δ N7), 655 (γ Q10), 913 (γ N7), 1112 (γ Q5). Overall sequence [(GL)(CL)QANSGQVWIE(OH)]. Overall sequence obtained from the negative ion CID MS/MS of m/z 1515 and m/z 1513 is [(GL)CLQANSGQVWIE(OH)].

Overall sequence of **17** is $\text{(GL)CLQANSGQVWIEDCSSEK}$

4.5.3 Fragment peptides not containing disulfides

The full or partial sequences of eighteen peptides which do not contain disulfide residues (see Figure 4.4) were obtained using α , β , δ and γ negative ion backbone cleavages. Spectra are CID MS/MS of (M-H)⁻ anions with the exception of **22** which are CID MS/MS of (M-2H)²⁻ anions converted to ‘singly-charged’ spectra using Mass Lynx software. In some of the negative ion CID MS/MS spectra of these peptides, side-chain and δ/γ fragmentations are dominant, and thus, backbone cleavages of the parent ions after losing side chains and/or of δ/γ anions are observed to be more prevalent than those of the precursor parent anions. In most of these spectra, the first cleavage from the N-terminus is missing. Negative ion spectra of some of the larger of these peptides are complex and did not afford satisfactory sequence information (see Figure 4.4). These peptides were treated further with chymotrypsin to give smaller peptides, CID MS/MS of which provide further sequencing information.

Taking peptide **7** (ENIELGNGPLEEAISALYYYSTGGTQLPTLAR(OH), MW 3438) as an example (see Figure 4.4), this peptide contains a large number of residues whose side chains are labile or able to trigger δ/γ fragmentations (see section 1.9, Chapter 1). The sequence of this peptide could not be obtained directly from the negative ion CID MS/MS data due to the complexity of various side-chain induced cleavages. It was therefore subjected to chymotryptic digestion to give two chymotryptic fragments m/z 1929 and m/z 1199. The fragmentation pattern of m/z 1929 and m/z 1199 anions are quite different. The negative ion CID MS/MS spectrum of m/z 1929 shows all the backbone cleavages of the peptide, α and β backbone cleavages and side-chain triggered backbone (δ/γ) cleavages from Asn and Glu (Figure 4.10). Side-chain losses of these residues also occur competitively with the backbone fragmentations. In contrast, the losses of CH₃CHO from Thr side chains produce the major peaks in the CID MS/MS spectrum of m/z 1199 (Figure 4.11). Backbone fragmentations of the [(M-H) - 3CH₃CHO]⁻ anion dominate the spectrum, while only minor backbone cleavages of the parent anion are observed. As it is seen in these two examples, the competition between side-chain losses and backbone fragmentations of certain amino acid residues determines the fragmentation pattern of a peptide. In particular, side chain losses may occur competitively with backbone cleavages for residues such as Asn, Asp, Gln and Gln, Ser, Thr and Cys and thus suppress the negative ion backbone processes of the parent anion.

The primary structures of all peptides together with data obtained by backbone cleavages are summarised in Figure 4.4. Full numerical details of α , β , δ and γ negative-ion cleavages given in Figure 4.4 are presented in Table 4.4.

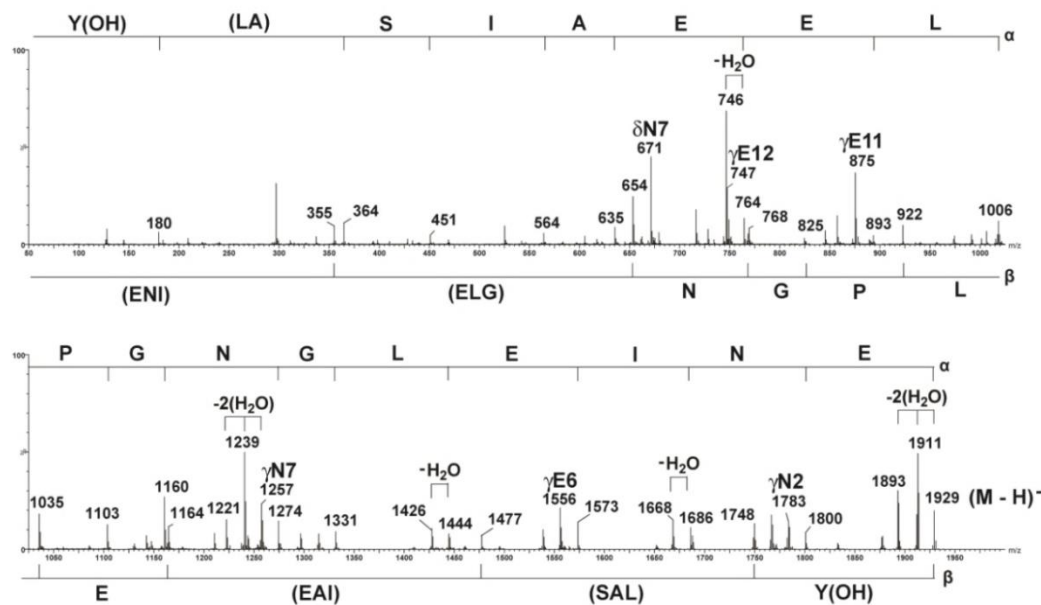


Figure 4.10. Collision-induced negative ion MS/MS of the chymotryptic fragment $[\text{ENIELGNGPLEEAI S A L Y(OH)} - \text{H}]^-$ (m/z 1929) derived from peptide 7. Multiplication ranges as follows:- m/z 1250-1850 (x4). Q-TOF 2 mass spectrometer.

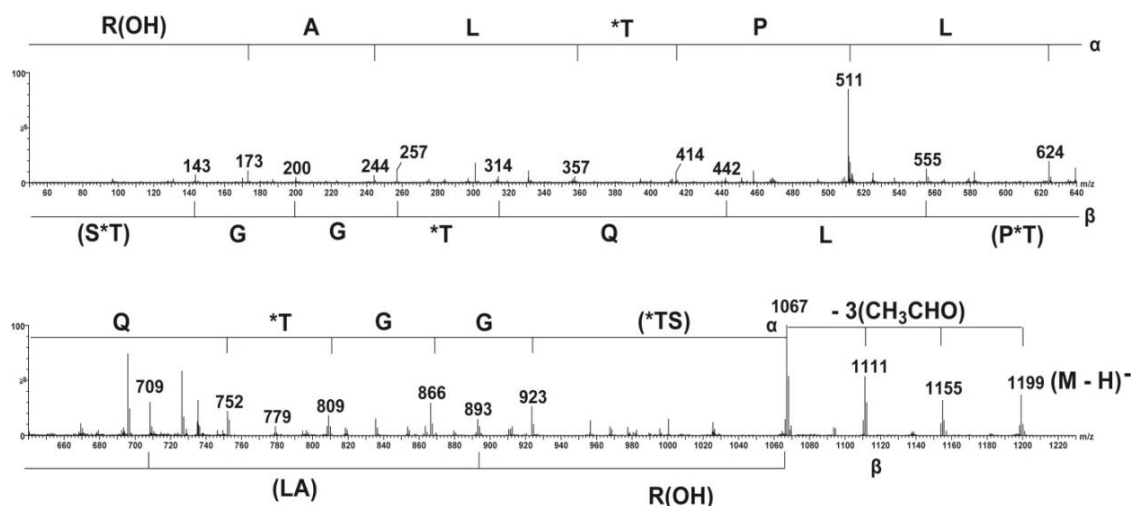


Figure 4.11. The collision-induced negative ion MS/MS of the chymotryptic fragment $[\text{STGGTQLPTLAR(OH)-H}]^-$ (m/z 1199) derived from peptide 7. Multiplication ranges as follows:- m/z 51-1000 (x8). *T = T- $\text{CH}_3\text{CHO} = \text{NHCH}_2\text{CO}$. Q-TOF 2 mass spectrometer.

Table 4.4. Negative ion mass spectral data for the (M-H)⁻ anions of 18 non-disulfide containing peptides from tryptic digest of ricin. CID MS/MS data are from (M-H)⁻ anions except for **22** which are from (M-2H)²⁻ parent anions with the resulting data modified to ‘singly charged’ spectra using Mass Lynx software. Peptides **10, 11, 12, 18** and **23** appear as both singly-charged and doubly charged anions; the originally singly-charged spectra and the converted doubly-to-singly charged spectra of these peptides are very similar in terms of fragmentation pattern, but the abundances of peaks in the two spectra may be different.

MS does not differentiate between isomeric L and I. The structure of ricin is known so the correct residue (L or I) is indicated below. Masses used are nominal masses, i.e. the sum of the integral masses of the individual amino acid residues.

1 (M-H)⁻ m/z 830. α ions, *m/z* 616, 515, 458, 387, 272, 173 [(LT)TGADV(R)(OH)]. β ions, *m/z* 371, 442, 557, 656 [(372)ADV(R)(OH)]. γ ions, 700 (T2), 599 (T3), 370 (D6). Overall sequence [LTTGADV(R)(OH)].

2 (M-H)⁻ m/z 1072. α ions, *m/z* 806, 693, 384, 173 [(HE)I(309)(PN)R(OH)]. β ions, *m/z* 475, 574, 687, 898 [(476)VL(PN)R(OH)]. δ and γ ions, *m/z* 153 (δE2), 270 (γN8), 801 (δN8), 918 (γE2). Sequence [HEIPVLPNR(OH)].

3 (M-H)⁻ m/z 894. α ions, *m/z* 738, 625, 415, 301, 173 [(VG) L(PI)NQR(OH)]. β ions, *m/z* 155, 268, 365, 592, 720 [(VG)LP(IN)QR(OH)]. δ and γ ions, *m/z* 284 (γQ7), 398 (γN6), 495 (δN6), 609 (δQ7). Sequence [(VG)LPINQR(OH)].

4 (M-3H)³⁻ 1102. Chymotrypsin digest gives (i) AGNSAY(OH), *m/z* 580; α ions, *m/z* 452, 338, 251, 180 [(AG) NSAY(OH)]. β ions, 127, 241 [(AG)N(339)]. δ and γ ions, *m/z* 144 (δN3), 435 (γN3). Sequence [(AG)NSAY(OH)]. (ii) FFHPDNQEDAEAITHLF(OH), *m/z* 2028, α ions, *m/z* 1385, 1143, 899, 628, 515, 414, 277 164 [(643)(NQ)(ED) (384)THLF(OH)]. β ions, *m/z* 146, 293, 642 [FF(349)(1386)]. γ ions, *m/z* 1483 (D5), 1368 (N6), 1254 (Q7), 1126 (E8), 997 (D9), 811 (E11). Sequence [FF(HP)DNQEDAE(AI)THLF(OH)]. (iii) TDVQNR(OH), *m/z* 730. α ions, *m/z* 629, 514, 287, 173 [TD(VQ)NR(OH)]. β ions, *m/z* 442, 556 . [(443) NR(OH)]. γ ions, *m/z* 612 (D2), 398 (Q4), 270 (N5). Sequence [TDVQNR(OH)].

5 (M-H)⁻ m/z 1308, [(M-H)⁻ -CH₃CHO] m/z 1264. α ions, *m/z* 1101, 1044, 826, 622, 451, 288, 173 [Y^{*}T(FA)(FG)(GN)YDR(OH)]. β ions, *m/z* 437, 641, 698, 812, 975 [(438)(FG)GNY(DR(OH))]. γ ions, *m/z* 550 (N8). Sequence [Y^{*}T(FA)(FG)GNYDR(OH)].

6 (M-H)⁻ m/z 1011. α ions, *m/z* 769, 641, 528, 457, 400, 286, 173 [(LE)QLAGNLR(OH)]. β ions, *m/z* 369, 610, 724, 837 [(370)(241)NLR(OH)]. δ and γ ions, *m/z* 258 (δQ3), 383 (γN7), 627 (δN7), 752 (γQ3), 881 (γE2). Sequence [LEQLAGNLR(OH)].

7 (M-2H)²⁻ 1718. Chymotryptic digest give (i) *m/z* 1929. α ions, 1800, 1686, 1573, 1444, 1331, 1274, 1160, 1103, 1006, 893, 764, 635, 564, 451, 364, 180 [ENIELGNNGPLEEAS(AL)Y(OH)]. β ions, *m/z* 355, 654, 768, 825, 922, 1035, 1164, 1477, 1748 [(356)(299)NGPLE(313)(217)Y(OH)], sequence [ENIELGNNGPLEEAS(AL)Y(OH)]. (ii) *m/z* 1199. α ions, *m/z* 1112, 668, 555, 458, 357, 244, 173 [S(444)LPTLAR(OH)]. β ions, *m/z* 244, 301, 1025 [(245)G(724)R(OH)]. γ ions, *m/z* 779 (Q6), sequence [S(TG)GTQLPTLAR(OH)]. Overall sequence ENIELGNNGPLEEAS(AL)Y(YY)S(TG)GTQLPTLAR(OH)].

8 (M-H)⁻ 1579. α ions, *m/z* 1119, 903, 775, 644, 531, 444, 315, 173 [(460)(CI)QMI(AA)R(OH)]. β ions, *m/z* 1405. δ and γ ions, *m/z* 476 (δC5), 1102 (γC5), 692 (δQ7), 886 (γQ7), 1151 (γE11). Sequence [(461)CIQMISE(AA)R(OH)].

9 (M-H)⁻ m/z 1170. α ions, *m/z* 895, 732, 619, 490, 433, 304, 173 [(FQ)YIEGEMR(OH)]. β ions, *m/z* 274, 736, 996 [(FQ)(462)(EM)R(OH)]. δ and γ ions, *m/z* 567 (δE5), 602 (γE5), 753 (δE7). Overall sequence [(FQ)YIEGEMR(OH)].

10 (M-2H)²⁻ m/z 863 and (M-H)⁻ m/z 1726. *m/z* 1276, α ions, *m/z* 1276, 1356, 859, 746, 617, 503, 172 [(370)(497)LEN(330)R(OH)]. β ions, *m/z* 553, 979, 1108, 1222, 1309, 1495, 1552 [(554)(426)ENSWGR(OH)]. δ and γ ions *m/z*, 271(δD4), 600 (γN12), 729 (γE11), 943 (γT9), 1081 (δN12), 1410 (γD4). Overall sequence [(SA)PD(PS)(VI)TLENSWGR(OH)].

11 (M-2H)²⁻ m/z 1128 and (M-H)⁻ m/z 2256, [(M-H)-CH₃CHO]⁻ m/z 2212. *m/z* 2212, α ions, *m/z* 2099, 1955, 1057, 839, 752, 592, 414, 173 [L(S^{*}T)(898)(FA)S(PI)Q(LQ)R(OH)]. β ions, *m/z* 568, 1026, 1910 [(569)(458)(884)(QR(OH))]. δ and γ ions, *m/z* 801 (δN9), 1626

(γ E7), 1686 (δ Q18), 1754 (γ Q6), 1995 (γ^* T3). Overall sequence [(LS)*TAIQESNQGA(FA)SPIQ(LQ)R(OH)] (*T is NHCHCO).

12 (M-H)⁻ m/z 2209. α ions, m/z 2062, 1713, 1598, 1499, 1412, 1299, 1186, 1073, 435, 336, 173 [F(349)DVSILI(638)VYR(OH)]. β ions, m/z 332, 1022, 1642, 1773, 1872 [(333)(690)(620)MV(YR(OH))]. δ and γ ions, m/z 163(δ S2), 512 (δ D5), 1482 (γ S7), 1696 (γ D5), 2045 (γ S2). Overall sequence [FSVYDVSILI(638)VYR(OH)].

15 (M-H)⁻ m/z 1388. α ions, m/z 1301, 1187, 971, 900, 786, 658, 545 [SN(TD)ANQL(546)]. δ and γ ions, m/z 1284 (γ N2), 1170 (γ D6), 883 (γ N6), 769 (γ Q7), 504 (δ N6). Overall sequence [SNTDANQL(546)].

18 (M-2H)²⁻ m/z 1113.5 and (M-H)⁻ m/z 2228. m/z 2228, α ions, m/z 996, 796, 640, 543, 415, 287, 173 [(1232)(SI)RPQQNR(OH)]. β ions, m/z 199, 327, 455, 641, 1059, 1940, 2054 [(AE)QQW(418)(881)NR(OH)]. δ and γ ions, m/z 398 (γ Q17), 1076 (δ D10), 1883 (γ Q3), 1957 (δ N18), 2011 (γ Q2). Overall sequence [(AE)QQWA(481)DG(SI)RPQQNR(OH)].

20 (M-H)⁻ m/z 609. α ions, m/z 423, 292, 145 [WMFK(OH)]. β ions, m/z 463. δ and γ ions, m/z 275(γ F3), 333 (δ F3). Overall sequence [WMFK(OH)].

21 (M-H)⁻ m/z 1859, α ions, m/z 1573, 1472, 1246, 1132, 1019, 856, 769, 712, 387, 272, 173 [(286)T(IL)NLYSG(325)DVR(OH)]. β ions, m/z 1002, 1358, 1471, 1586 [(1003)(356)(VL)D(VR(OH))]. δ and γ ions, m/z 130 (δ D2), 370 (γ D15), 1229 (γ N7). Overall sequence [NDGT(IL)NLYSGL(VL)DVR(OH)].

22 (M-2H)²⁻ m/z 1225. α ions, m/z 1630, 1573, 1132, 1019, 856, 769, 387, 272, 173 [(821)G(441)(LYS)(382)DVR(OH)]. β ions, m/z 820, 1204, 1681, 1738, 2271 [(822)(384)(477)G(539)R(OH)]. δ and γ ions, m/z 333 (δ F3), 370 (γ D19), 608 (δ N5), 722 (δ D6), 1229 (γ N11), 1728 (γ D6), 1842 (γ N5). Overall sequence [(WM)FKNDG(327)NLY(325)DVR(OH)]. Combine 20 and 21 sequences gives [WMFKNDGT(IL)NLYSGLVDVR(OH)].

23 (M-2H)²⁻ m/z 1136.5 and (M-H)⁻ m/z 2274. m/z 2274, α ions, m/z 2033, 1920, 1807, 1644, 1434, 1297, 1240, 914, 786, 673, 374, 164 [(QI)ILY(PL)HG(326)QI(WL)(PL)F(OH)].

β ions, m/z 127, 240, 839, 1033, 1487, 2109 [QI(599)(HG)(454)(622)F(OH)]. δ and γ ions, m/z 897 (γ Q13), 1011 (γ N12), 1050 (δ D10), 1223 (γ D10), 1262(δ N12). Overall sequence [QIILY(PL)HGDPNQI(WL)PLF(OH)]

4.6. Summary and conclusions

Proteolytic digest/negative ion nanospray MS was used to determine the five disulfide units and much of the amino acid sequence of ricin. To the best of our knowledge, it was the first time all five disulfide linkages in ricin are identified by MS.

The $(M-2H)^{2-}$ ions of intermolecular disulfides undergo facile cleavage of the disulfide bond to form singly-charged fragment anions. CID MS/MS data of these ions provide full or partial sequencing of the peptide side chains. The negative ion spectra of the two intramolecular disulfides in this study provide incomplete structural information. They are converted proteolytically into intermolecular disulfides which may be identified as outlined above.

Tryptic digest of ricin produces a number of peptides not containing Cys: sequence information of these may be obtained using negative-ion backbone cleavage data. Some of these peptides are large giving very complex negative ion spectra; these have been further digested with chymotrypsin to yield smaller peptides which produce more satisfactory negative ion spectra.

This study demonstrates that negative ion MS is more effective than positive ion MS in identification and sequencing disulfide bridged peptides. While positive ion MS only provides partial sequences of disulfide containing peptides and often does not specify the positions of disulfide residues, negative ion MS gives clear evidence for the presence and positions of disulfide linkages via characteristic fragmentations as outlined above.

The negative ion MS based methodology described here addresses both ricin detection and structural confirmation and enables ricin to be distinguished from other type II RIPs. This is highly relevant in the context of the Chemical Weapons Convention, since this MS procedure determines all disulfide linkages in ricin. One of these disulfides connects the two chains of ricin indicating the presence of the intact toxin.

4.7 Experimental

4.7.1 Materials

Ricin, trypsin, chymotrypsin and Asp-N were commercial samples and were used unpurified. Synthetic peptides were synthesised by Mimotopes (Victoria, Australia) and were of greater than 90% purity.

4.7.2 Digests

Ricin (1mg) was digested in 0.2% Rapigest in 50 mM NH_4HCO_3 buffer at 37°C for 5-10 hours. The molar ratio between ricin and trypsin was 1:1. The reaction was stopped by acidifying the mixture with formic acid and incubating at 37°C for 45 mins. The tryptic digestion was conducted by Dr. Craig Brinkworth, Defence Science and Technology Organisation, Victoria 3207, Australia. In order to produce peptide **17**, a similar procedure was applied with the only difference being the use of a mixture of trypsin and chymotrypsin (1:1 molar ratio) instead of trypsin. All experiments with ricin were carried out with appropriate safety measures. All containers containing more than a lethal dose were handled in a level 2 biosafety cabinet equipped with HEPA filters, while working solutions containing less than the lethal dose were handled in a fumecupboard.

Chymotryptic [384] and Asp-N digests [385-386] of the peptide fragments (obtained from the tryptic digest of ricin) were carried out using standard procedures. Chymotryptic and Asp-N digests were carried out in 50 mM NH_4HCO_3 buffer at 37 °C for 2-4 hours, with the ratio between peptide and chymotrypsin or Asp-N 25:1 by weight. The reaction was stopped by freezing the mixture.

4.7.3 Synthesis of disulfide containing peptides from cysteine precursors

2,2'-dithiodipyridine (Aldrithiol) was dissolved in isopropanol (solution A) and the first Cys containing peptide was dissolved in 20% acetonitrile/water (solution B). The molar ratio between 2,2'-dithiodipyridine and the Cys containing peptide used was 1:1. Solutions A and B were mixed and stirred for 30 mins. The activated product of the first Cys containing peptide (pep1-SPyr) was detected by ESI/MS and purified by HPLC. Fractions containing the pure product were pooled and lyophilised. Equimolar amounts (3 μM) of the second Cys containing peptide and the activated pep1-SPyr were dissolved in 2 ml of 0.1 mM NH_4HCO_3

and sonicated for 30 mins. Formation of the disulfide containing peptide from the two Cys precursors was confirmed by ESI/MS.

4.7.4 High performance liquid chromatography

Peptides were separated using a 2-60 % acetonitrile linear gradient on a C₁₈ column (Vydac, Cat No: 218TP54) at a flow rate of 1.0 mL/min. 30 sec fractions were collected over the elution window. UV detection at 214 nm.

4.7.5 Nanospray ionisation mass spectrometry

Nanospray MS/MS data were collected using a Micromass Q-TOF 2 orthogonal acceleration time-of-flight mass spectrometer with a mass range to 10,000 Da. Conditions were as follows: capillary voltage 1.5 kV, source temperature 80 °C, and cone voltage 50 V. Argon collision gas energies at 30-80 eV were used for collision induced MS or MS/MS experiments. Mass spectra of fragment anions were collision induced mass spectra of anions formed in the ionisation source.

Fragmentations of (M-H)⁻ not containing disulfide linkages shown in Figure 4.4 were determined from (M-H)⁻ parent anions with the exception of **22** which are doubly-charged mass spectra of (M-2H)²⁻ ions converted into ‘singly-charged’ spectra using the Mass Lynx software of the Q-TOF2 mass spectrometer [CID MS/MS spectra of (M-H)⁻ and Mass Lynx modified (M-2H)²⁻ peptide spectra give the same fragment peaks, but the abundances of peaks in the two spectra may be different (checked for peptides **10**, **11**, **12**, **18** and **23** in Table 4.4)].

CID MS/MS spectra of singly-charged (M-H)⁻ anions have been used for disulfide-containing peptides in previous studies . In this study intermolecular disulfides **13**, **14**, **19** (Figure 4.4), and intermolecular disulfides formed from **16** (Scheme 4.8) and **17** (Scheme 4.10) give more abundant (M-2H)²⁻ than (M-H)⁻ peaks, and so doubly charged (M-2H)²⁻ precursor parent peaks were used for all of these disulfides. Mass Lynx software was used to convert all of the doubly-charged spectra into ‘singly charged’ spectra (e.g. Figures 4.6, 4.7 and 4.9). However (M-2H)²⁻ parent anions fragment to produce both singly-charged and

doubly charged fragment anions. CID MS/MS data of the source-formed singly-charged fragment anions (from the $(M-2H)^{2-}$ parent anions) were used to determine sequence data for these fragments (see Figure 4.8, Schemes 4.5, 4.6, 4.7, 4.8, 4.9 and 4.10). Procedure used:- select $(M-2H)^{2-}$ ion, effect CID MS/MS using cone voltage 50 V and argon pressure 50 eV, select singly-charged source formed fragment anion to be studied, increasing cone voltage to 70 V to cause maximum fragmentation to produce CID source formed MS/MS data.

CHAPTER 5

PEPTIDES FROM THE SKIN GLANDS OF *Litoria rubella*

5.1 Peptides from amphibian skin secretions

5.1.1 Overview

Of all the vertebrates, the amphibians underwent the most profound evolution as they moved from an aquatic to a terrestrial environment at the close of the Paleozoic era [387-388]. They have been found in all continents except for Antarctica and survive in different climatic conditions from arid desert to deep freshwater lakes, and from underground to tropical forest canopy [389]. Their ability to adapt to a wide range of climate and geology has been attributed to many different physiological, biochemical and behavioural adaptations, with the flexibility in skin structure and function being a key factor for their survival [390-392].

The many functions of amphibian skin, including respiration, water regulation, anti-predator, anti-microbial and anti-fungal defence, in turn depend on the secretory mechanism of cutaneous glands located on the skin surface. The dermal layer of anuran skin basically contains two types of glands, namely the mucus glands and granular glands; a third type, the tubulosacular or alveolar glands is only found in a small group of frogs. The mucus glands are small and release a watery mixture of mucins, mucopolysaccharides and salt that help to control the skin pH, moisture balance, thermoregulation, and prevent mechanical damage to the skin [388, 393-394]. On the other hand, the granular glands are the storage sites of the toxic or noxious substances secreted by the animal in response to various environmental threats [388, 394].

The exploitation of amphibian skin in various ways as folk medicine, witchcraft and poisons has been empirically known and orally transmitted for centuries in many societies such as in Europe, Africa, America and ancient China [395-397]. However, attempts to isolate and characterise biologically active components from amphibian skin only began in the early 1960s with pioneering work by Erspamer and colleagues. It has been revealed that the anuran skin is a store of a vast array of active compounds including biogenic amines [398], steroids [399], alkaloids [400-401], peptides and proteins [402-403]. In addition, several enzymes involved in the activation of pro-peptides have also been isolated [387-388]. These

compounds are stored in highest concentration in the skin glands but some are also found in the internal organs, blood and tadpoles of some amphibian species [404].

Studies of some 500 distinct species of frogs and toads have established that the amphibian skin secretions contain a diversity of peptides, polypeptides and proteins in significant quantities, and that different species secrete a different spectrum of bioactive peptides. Peptides with similar or equivalent pharmacological activity may be found in many different amphibian species and their structures, though not necessarily identical, are highly conserved. Identified peptides have shown a vast array of antibacterial activity with the leading discovery of magainin peptides from the skin of the African clawed toad, *Xenopus laevis* [405-406]. Antifungal, antiviral, anticancer and neurotransmitter action are other additional biological functions of skin secreted peptides. In addition, the unique peptide profile of each species assists the classification, taxonomy and evolutionary studies of amphibians. The difference in size, sequences, 3-dimensional structures and bioactivity spectra of glandular peptides facilitate the assignment of anurans into species, even subspecies [407-409]. For example, analysis of peptide profiles of *L. caerulea* from different locations around Australia has revealed that this species has evolved into two subspecies, an eastern and a northern central subspecies [410-411].

Erspamer and colleagues categorized amphibian neuro- and hormonal peptides into five groups namely tachykinins, bradykinins, caeruleins, bombesins and opioid peptides [412]. Each of these peptide groups possesses similar chemical structures, receptor binding affinities and spectra of biological activities. Erspamer also predicted that every neuropeptide present in the frog skin should have a mammalian counterpart [402]. This prediction is supported by the identification of crinia-angiotensin II from *Crinia georgina* [413] and the mammalian analogue angiotensin II [413-414], and xenopsin from *Xenopus laevis* [415-416] and the mammalian analogue neurotensin [417-418]. However, this hypothesis does not hold when considering membrane-active amphibian peptides from Australian amphibians [419].

5.1.2 Peptides from Australian anurans

From several thousand anuran species worldwide, about 230 species have been found in Australia with 93% of them endemic [420]. Investigation of skin secretions in Australian amphibians was initiated in 1964 by Erspamer's research group. Hundreds of Australian amphibian species from various locations were studied in the first decade after the commencement of Erspamer's work using the extracts of dried skins [421]. The identification methods were limited to chemical/enzymatic degradation and biological screening on smooth muscle and blood pressure preparations. In addition, these studies were limited to the identification of peptides belonging to the caerulein, bombesin and tachykinin families in Australian amphibian skin secretions. Peptides with other characteristics remained to be discovered and they thus did not provide much information about evolutionary trends in these species.

Later investigations were carried out on skin secretions of anurans from the Australian *Crinia*, *Cyclorana*, *Litoria*, *Limnodynastes* and *Uperoleia* genera. Secretions were obtained using mild electrical stimulation of the frog skin and washing the resulting peptide mixture with water, followed by HPLC and ESI MS/Edman sequencing to identify individual peptides [403, 409, 422]. With this strategy, it is not unusual to be able to identify all of the major bioactive peptides using a small amount of secretion from a small number of animals. The studies on more than 35 species of Australian frogs have showed a significantly more diversity of peptide structures than shown by previous studies of the Erspamer group. Selected peptides isolated from Australian amphibian skin secretions are displayed in Table 5.1. Most of the frogs studied from these genera have a range of peptides in their skin secretions, including at least one neuropeptide (normally a smooth muscle active peptide that sometimes also possesses analgesic activity), and a broad spectrum antibiotic (antimicrobial peptides). Peptides with antiviral, anticancer, antifungal, hormone and pheromone activity, and peptides complexing with the regulatory protein calmodulin (CaM) to inhibit formation of nitric oxide (NO) have also been identified. Many of these peptides show multifaceted activity, while the activity of some others remains to be discovered [403, 409, 422].

Table 5.1. Selected peptides isolated from Australian amphibian skin secretions.

Name	Sequence	MW	Species	Activity*
Aurein 1.1	GLFDIHKKIAESI-NH ₂	1444	a	1, 2
Caeridin 1.1	GLLαDGLLGTGL-NH ₂	1140	b, c, d, e, f	
Caerin 1.1	GLLSVLGSVAKHVLPHVVPVIAEHL-NH ₂	2582	b, c, d	1, 2, 3, 4
Caerulein 1.1	pEQDY(SO ₃)TGWMDF-NH ₂	1351	h	5
Citropin 1.1	GLFDVIKKVASVIGGL-NH ₂	1613	i	1, 2, 3, 4
Dahlein 1.1	GLFDIKNIVSTL-NH ₂	1430	j	1
Dynastin 1	GLVSNLGI-OH	729	k	
Electrin 2.1	NEEEKVKWEPDVP-NH ₂	1743	o	
Fletcherin	AGPVSKLVSGIGL-OH	1197	p	
Frenatin 1	GLLDALSGILGL-NH ₂	1140	q	
Lesueurin	GLLDILKKVGKVA-NH ₂	1352	r	4
Mactulatin 1.1	GLFGVLAKVAAHVPAIAEHF-NH ₂	2145	s	1, 2, 3, 4
Rubellidin 4.1	GLGDILGLLGL-NH ₂	1039	t	
Rubellidin 4.2	AGLLDILGL-NH ₂	883	t	
Rothein 2.1	AGGLDDLLEPVLNSADNLVHGL-NH ₂	2230	u	
Rothein 3.1	ASAAGAVRAGGLDDLLEPVLNSADNLVHGL-NH ₂	2964	u	
Signiferin 1	RLC*IPYIIPC*-OH (*disulfide bridge)	1187	v	5
Splendipherin	GLVSSIGKALGGLLADVVKSKGQPA-OH	2364	b, c	4, 6
Tryptophyllin L 1.1	PWL-NH ₂	414	t	
Tryptophyllin L 2.1	IPWL-NH ₂	527	t	
Tryptophyllin L 3.1	FPWP-NH ₂	545	o, t	
Tryptophyllin L 4.1	LPWY-NH ₂	577	t	
Tryptophyllin L 5.1	pEIPWFHR-NH ₂	965	t	
Uperin 1.1	pEADPNAFYGLM-NH ₂	1208	w	5
Uperolein	pEPDPNAFYGLM-NH ₂	1232	x	5

Activity nomenclature: (1) antibiotic activity; (2) anticancer activity; (3) fungicide activity; (4) nNOS inhibitor; (5) neuropeptide, smooth muscle active; (6) aquatic sex pheromone. Species: (a) *Litoria aurea*, *Litoria raniformis* [423]; (b) *Litoria splendida* [424]; (c) *Litoria caerulea* [425]; (d) *Litoria gilleni* [426]; (e) *Litoria xanthomera* [427]; (f) *Litoria chloris* [428]; (g) *Litoria eucnemis* [429]; (h) various species of the genus *Litoria* [412]; (i) *Litoria citropa* [430]; (j) *Litoria dahlia* [431]; (k) *Limnodynastes interioris* [432]; (l) *Limnodynastes dumerilii* [432]; (m) *Limnodynastes terraereginae* [432]; (n) *Limnodynastes salmini* [433]; (o) *Litoria electrica* [434]; (p) *Limnodynastes fletcheri* [433]; (q) *Litoria infrafrenata* [435]; (r) *Litoria lesueur* [436]; (s) *Litoria genimaculata* [437]; (t) *Litoria rubella* [422, 438] and; (u) *Litoria rothii* [431]; (v) *Crinia signifera* (w) *Uperoleia inundata* [439]; (x) many species of the genus *Uperoleia* [412].

5.1.3 Production of glandular peptides

The main component of a granular gland is a syncytium which consists of a large number of densely packed secretory granules located at the central cytoplasmic area, and, nuclei, endoplasmic reticulum and Golgi complexes occupying the periphery. The secretory compartment is surrounded by myoepithelial cells which regulate the contraction of the gland [440]. Secretion of the glandular contents is generally under control of the sympathetic nervous system and occurs in response to a behavioural defence position [440-441]. The stimulation results in the release of 80-90% of the glandular contents and several days to several weeks are required to replenish the contents of the gland [440, 442-443].

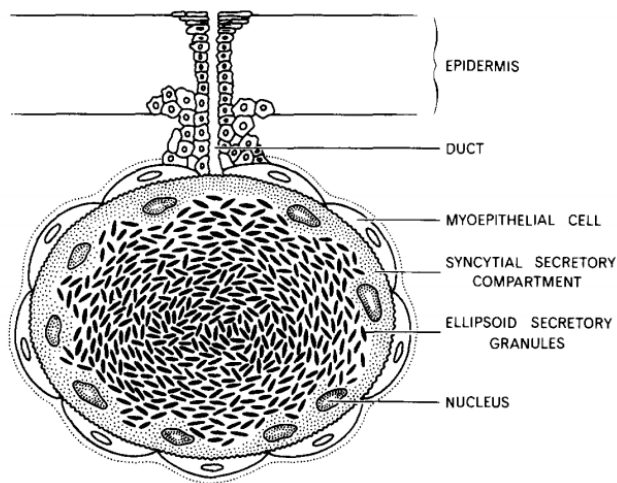


Figure 5.1. Structure of an amphibian granular gland [440].

The biologically active peptides secreted by the amphibian granular glands are only a small portion of a much larger inactive peptide, known as a prepropeptide which consists of three regions, the signal, spacer and active peptide. Once synthesized in the endocrine system, the signal peptide facilitates transportation of the prepropeptide across the cellular membrane and directs it through the endoplasmic reticulum. The signal sequence is then cleaved by enzymatic action to give the propeptide. This propeptide is destined to Golgi complexes where it is modified, packaged and sent to granules (formed by the fusion of vacuolar structures derived from Golgi complexes). The secretion (granules) is released from the gland by a holocrine mechanism, which requires disruption of the plasma membrane at the base of the gland duct to excrete the content [440].

The spacer region (pro-piece) of the peptide counteracts the activity of the mature peptide, assists peptide folding and inhibits any enzymatic degradation. The propeptide is stored as the inactive precursor and only processed to the active peptide upon release of the secretion. Upon activation of the granular gland, the spacer segment will be removed by endoproteases to yield the active peptide [442, 444]. There are many examples of the active peptide being cytotoxic to the host, especially at the concentration. There is growing evidence that the co-secreted precursors and spacer peptides also possess certain bioactivities. For instance, the primary peptides from spacer segments of the precursors of xenopsin and caerulein showed predominant lytic activity and antibacterial activity [442, 445].

5.1.4 Collecting skin secretions

In the past, the components of the skin secretions were normally obtained from the dried skin extracts of amphibians and often a large number of animals were sacrificed for a single study [421, 446]. This method required the skins to be removed, dried and extracted with organic solvent to obtain the glandular contents. This method is inappropriate chemically and environmentally, since it mostly results in inactive peptides from the glands of the animals rather than the active compounds produced in response to the environmental stimulation [403]. In addition, such a method is now unacceptable due to the significant decline of numerous frog populations noted in recent years. A non-harmful procedure to extract skin peptides is thus essential. One such alternative is injecting adrenaline or noradrenaline directly into the gland [440, 442]. Although it is non-fatal, the method has declined in use due to its invasive nature. A more common method to collect the secretions makes use of an electrical stimulation technique [447]. It involves gentle massage of a platinum electrode over the dorsal surface of the animal, causing an immediate discharge of the granular contents onto the skin surface, which can be washed from the surface and collected. The procedure is harmless to the animals and can be repeated on a monthly basis (Figure 5.2).

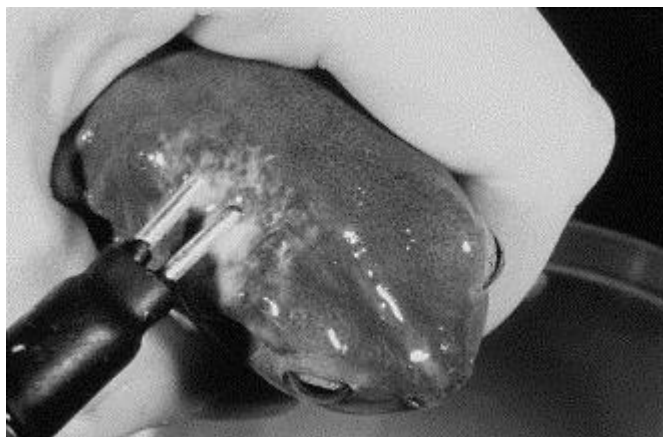


Figure 5.2. Surface electrical stimulation method for collection of amphibian skin secretion.

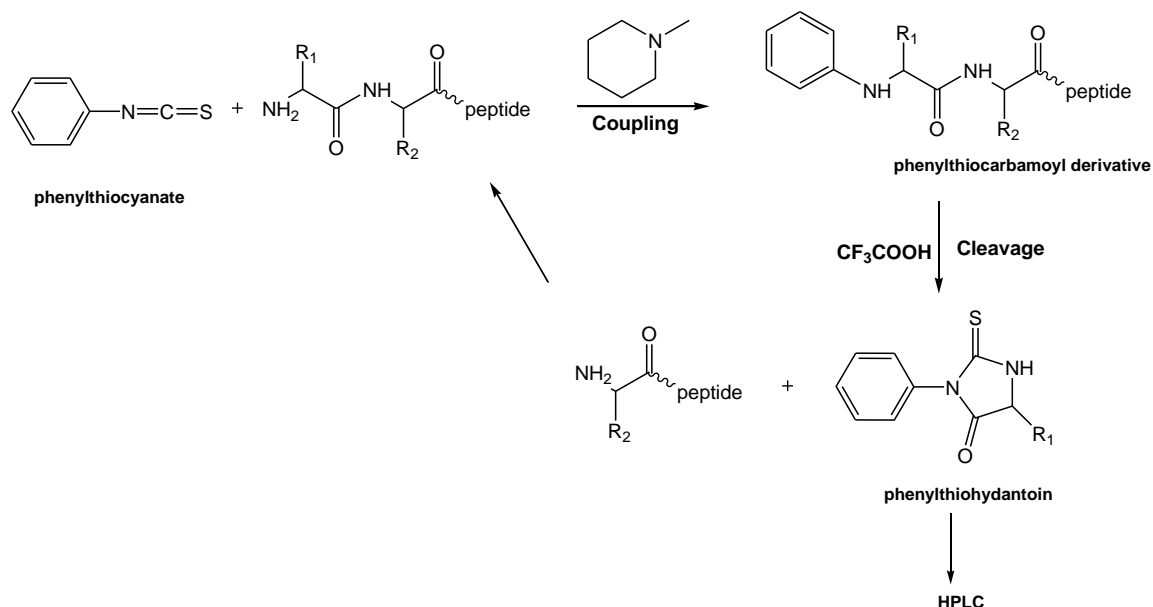
5.1.5 Peptide sequencing by mass spectrometry and Edman degradation

Currently, MS and automated Edman degradation are two techniques complementarily employed to sequence unknown peptides from Australian amphibians. The details of peptide sequencing using positive and negative ion MS were described in Chapter 1. MS is very useful to sequence underivatized and post-translational modified peptides. However, it is unable to distinguish between isomeric residues Leu and Ile (113 Da) and, to a lesser extent the isobaric residues Lys and Gln (128 Da). In some cases, incomplete fragmentation of peptide backbones of the investigated peptide also limits the application of this method to sequence identification. For these reasons, it is often coupled with complementary techniques such as Edman degradation to provide supporting sequence information.

Edman sequencing involves a cycle of chemical reactions to sequentially remove and identify amino acids from the N-terminal end of a peptide [448-450]. In this process, the C-terminal end of the peptide is attached to a solid membrane support, and in each cycle of the sequencing process, the free N-terminal amine is reacted with phenylisothiocyanate to yield a phenylthiocarbamoyl derivative. It is followed by acid hydrolysis of the amide bond to produce a phenylthiohydantoin which is subjected to HPLC analysis (Scheme 5.1). The presence of a particular amino acid in the peptide sequence is identified based on the known retention time for that amino acid. The shortened peptide with its newly exposed N-terminal group is then subjected to another Edman cycle.

Edman degradation is a very sensitive technique (picomolar range) and can be automated to allow efficient sequencing of peptides of up to 30 amino acids [451]. However, there are

several drawbacks inherent in the application of this technique to peptide sequencing [382, 452]. Firstly, it is susceptible to contamination due to incomplete additions of phenylisothiocyanate and degradation reactions. Low yield of phenylthiohydratoin derivatives with a number of amino acid such as Ser, Thr, Arg and His may sometimes prevent unambiguous sequencing. Furthermore, amino acid identification is reliant on known HPLC retention times, and thus uncommon or modified amino acids cannot be detected by this technique. Peptides with blocked N-terminal ends such as pGlu residues are not suited for Edman sequencing, as the initial phenylthiocarbamoyl derivative cannot form. Finally, as the peptide decreases in size, there is an increased risk that it can be washed from the solid support, therefore missing sequencing information. Despite these limitations, Edman sequencing is a valuable technique used in combination with MS to effectively determine the primary sequences of peptides.



Scheme 5.1. Edman sequencing reaction scheme.

5.2 *Litoria rubella*, the Red-tree frog

Litoria rubella (*L. rubella*) also known as the Red-tree frog or Desert-tree frog is a small frog measuring up to 4.5 cm in length (Figure 5.3). It occupies a large area of central and northern Australia [420]. The broad geographic distribution of *L. rubella* suggests that this frog may have evolved into different sub-species in order to adapt to a wide range of climates from the arid conditions in the centre of Australia to the humid conditions of the north-east coast. Studies of peptide profiles from the dorsal secretions of *L. rubella* from 15

locations throughout Australia support this proposal [422, 438, 453]. Peptide glandular profiles showed that there are at least five different populations of this genus (Table 5.3), and, the tryptophyllins L and the rubellidins are two major peptide families which are present in the skin secretions of the frogs (Table 5.4) [422].



Figure 5.3. Appearance of *Litoria rubella* [420].

The tryptophyllin L peptides have four to seven residues and possess a characteristic Pro-Trp sequence, while the rubellidins are five amino acid containing peptides with a Phe-Phe sequence near the C-terminal end of the peptide. In addition, two rubellidins have the longest sequences (nine and eleven amino acids) with eight amino acids identical in their sequences (see Table 5.4) [419, 422].

Bioactivity tests of the tryptophyllins L and rubellidins showed that the activities of tryptophyllins L are limited and the rubellidins display no known activity. The tryptophyllins have no antimicrobial activity but may exhibit minor smooth muscle activity and modest opioid activity (L1.2 and L3.1 at 10^{-7} M) [419, 454].

Table 5.3. Peptide profiles of the skin secretion of *Litoria rubella* as a function of geographic location, identified by the mass to charge ratios of the protonated ions of the peptides. The presence of a specific peptide is indicated by * and major peptides are indicated by X.

Location	Tryptophillins L											Rubellidins				
	414	527	545	546	561	577	672	706	724	805	965	598	626	655	883	1039
1. Derby (WA)					X				*			*	*	*		
2. Lalumuburu (WA)					X		*	*						*		*
3. Lake Argyle					X		*									
4. Jabiru (NT)							X				*		*			
5. Adelaide river (NT)							X				*					
6. Davenport Ranges (NT)					X			*							*	*
7. Simpson's Gap (NT)	*	*	*		X	*							*	*	*	*
8. Dulkaninna (SA)					X											
9. Farina (SA)					X											
10. Arkaroola (SA)					X											
11. Maryborough (Qld)					X											
12. Gracemere (Qld)					X											
13. Townsville (Qld)					*						*					
14. Ollera Creek (Qld)					*						*					
15. Mt. Carbine (Qld)					*	*					*					

Table 5.4. Sequences of glandular peptides from *Litoria rubella*.

Peptide	Sequence	MH ⁺
The tryptophyllins L		
1.1	Pro-Trp -Leu (NH ₂)	414
1.2	Phe- Pro-Trp -Leu (NH ₂)	561
1.3	pGlu-Phe- Pro-Trp -Leu (NH ₂)	672
1.4	Phe-Pro-Phe- Pro-Trp -Leu (NH ₂)	805
2.1	Ile- Pro-Trp -Leu (NH ₂)	527
3.1	Phe- Pro-Trp -Pro (NH ₂)	545
3.2	Phe- Pro-Trp -Pro (OH)	546
3.3	pGlu-Phe- Pro-Trp -Phe (NH ₂)	706
4.1	Leu- Pro-Trp -Tyr(NH ₂)	577
4.2	Phe-Leu- Pro-Trp -Tyr(NH ₂)	724
5.1	pGlu-Ile- Pro-Trp -Phe-His-Arg (NH ₂)	965
The rubellidins		
1.1	Val-Asp- Phe-Phe -Ala (OH)	598
2.1	Ile-Glu- Phe-Phe -Ala (OH)	626
3.1	Ile-Glu- Phe-Phe -Thr (NH ₂)	655
The rubellidins (caeridin type)		
4.1	Gly-Leu-Gly-Asp-Ile-Leu-Gly-Leu-Leu-Gly-Leu (NH ₂)	1039
4.2	Ala-Gly-Leu-Gly-Asp-Ile-Leu-Gly-Leu- (NH ₂)	883

From previous studies, the change in the peptide secretions of *L. rubella* has showed an evolutionary divergence of this genus over the locations investigated. Further investigation of the peptide profiles of *L. rubella* from other areas of Australia thus would provide more examples of evolutionary and/or chemically distinct populations of this frog. In order to achieve this, this chapter presents the study of glandular secretions of *L. rubella* collected from three further locations of Australia including the Flinders Ranges (700 km north of Adelaide), a region of south-western Queensland (98 km north east of Innamincka in South Australia), and Noonbah Station which is approximately 100 km south west of Longreach, Queensland (Figure 5.4). The research details the isolation, sequencing and testing of opioid

activity of selected peptides from these locations. The peptide profiles are then compared with each other and with those previously identified to examine the evolutionary trend of these populations.

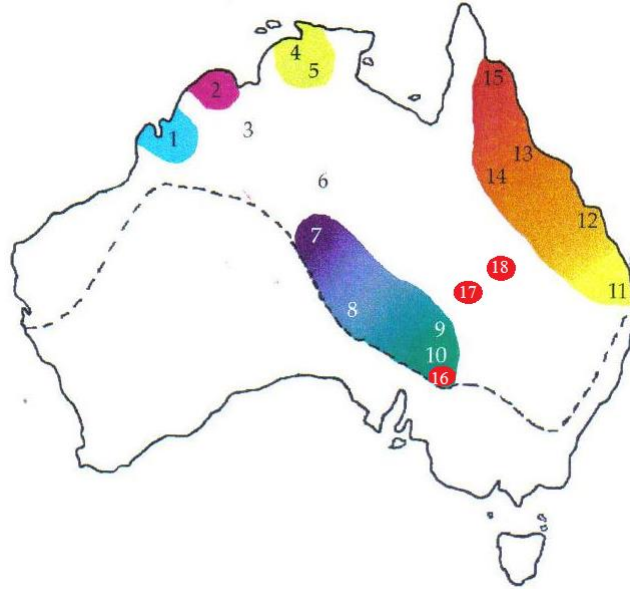


Figure 5.4. A schematic representation of the chemically distinct populations of *L. rubella* over 15 locations (see Table 5.3) and three locations of Australia currently studied, including **16** the Flinders Ranges (700 km north of Adelaide), **17** a region of south-western Queensland (98 km north east of Innamincka in South Australia), and **18** Noonbah Station which is approximately 100 km south west of Longreach, Queensland.

5.3 Results and discussion

5.3.1 HPLC separation of the skin secretions

Skin secretions were collected using the surface electrical stimulation technique for three groups of live *L. rubella* frogs (from Longreach, the south-west corner of Queensland and Flinders Ranges). The HPLC profiles of the secretions are presented in Figures 5.5-5.7 respectively and did not change during the four-month period of the experiment. The peptide containing fractions are numbered. For Longreach specimens, fraction (2) (Figure 5.5) was found to contain two peptides, and was thus submitted to further purification by HPLC. A gradient elution was used with the acetonitrile content increasing from 30- 40% solution A (1% trifluoroacetic acid/acetonitrile) in 60 minutes. However, it failed to separate these two peptides due to their consistent co-elution.

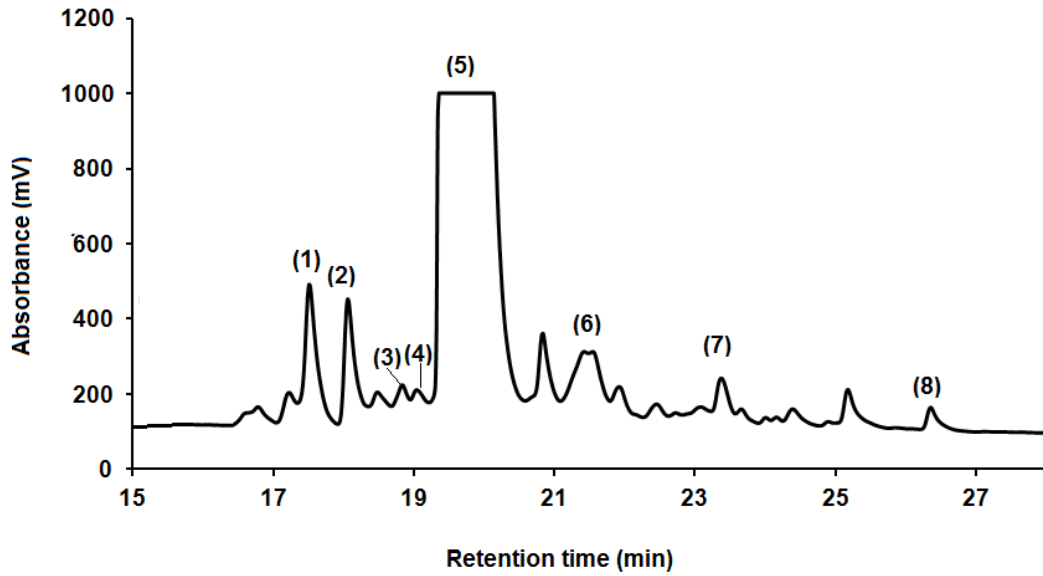


Figure 5.5. Representative HPLC trace from *L. rubella* specimen collected from Longreach.

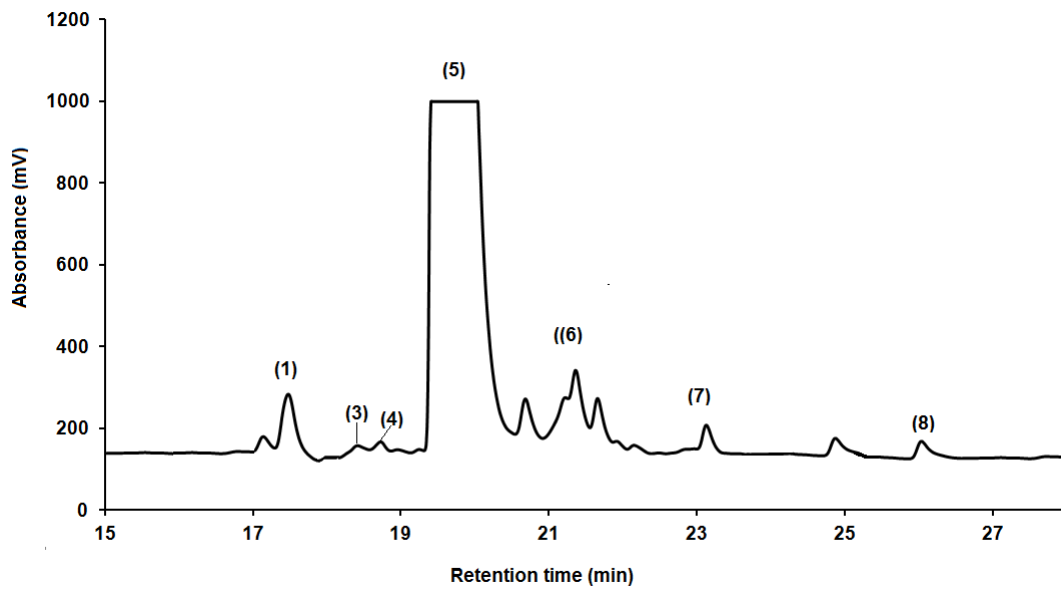


Figure 5.6. Representative HPLC trace from *L. rubella* specimen collected from the south-west corner of Queensland.

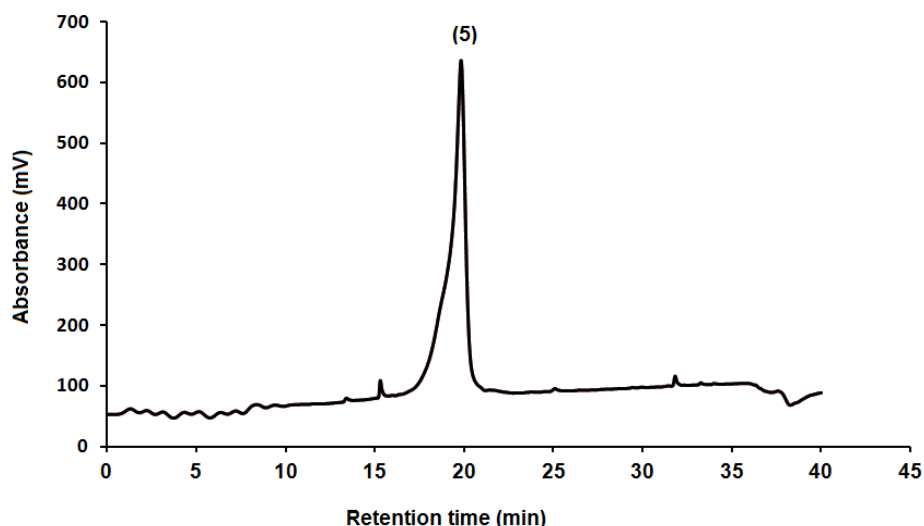


Figure 5.7. Representative HPLC trace from *L. rubella* specimen collected from Flinders Ranges.

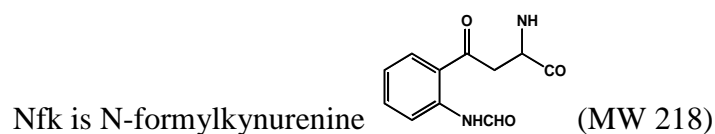
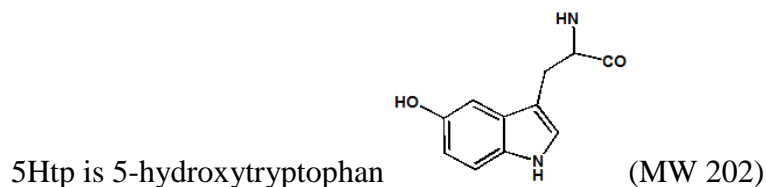
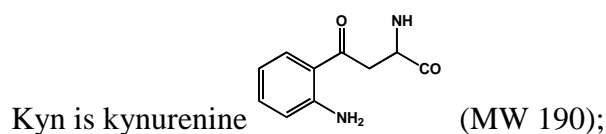
5.3.2 Peptide sequence determination

The peptides isolated by HPLC were studied using a Q-TOF 2 mass spectrometer and electrospray MS/MS data were acquired in both positive and negative mode. The characteristic **b** and **y** fragmentations were utilised to assign most of the sequences of the peptides. Additional sequencing information was obtained using negative ion CID MS/MS and high resolution MS/MS or MS/MS/MS data measured with an LTQ Orbitrap XL ETD hybrid mass spectrometer. Automated Edman degradation was used to differentiate Ileu and Leu and to confirm the primary sequences.

The sequences of nine peptides exuded from skin secretions of three *L. rubella* frog groups are listed in Table 5.5. All masses given are nominal masses, i.e. obtained by summation of the integral masses of all the amino acid residues. Three of these peptides including the tryptophyllin L1.2 (MW 560) and two caeridin rubellidins (MW 882 and 1038) were reported previously (see Table 5.4).

Table 5.5. Peptides characterised from the skin secretions of *L. rubella* at the three locations studied.

Name	Fraction	MW	Sequence
Tryptophyllin L 1.1.1	2	415	Pro-Trp -Leu(OH)
Tryptophyllin L 1.2	5	560	Phe- Pro-Trp -Leu (NH ₂)
Tryptophyllin L 1.2.1	6	561	Phe- Pro-Trp -Leu (OH)
Tryptophyllin L 1.5	1	501	Ser- Pro-Trp -Leu(OH)
Tryptophyllin L 1.6	2	564	Phe- Pro-Kyn -Leu(NH ₂)
Tryptophyllin L 1.7	4	576	Phe- Pro-5HTP -Leu(OH)
Tryptophyllin L 1.8	3	592	Phe- Pro-Nfk -Leu(OH)
Caeridin type Rubellidin 4.2	7	882	Ala-Gly-Leu-Gly-Asp-Ile-Leu-Gly-Leu- (NH ₂)
Caeridin type Rubellidin 4.1	8	1038	Gly-Leu-Gly-Asp-Ile-Leu-Gly-Leu-Leu- Gly-Leu (NH ₂)



The HPLC profiles of *L. rubella* from three locations showed the domination of fraction 5 which contained the tryptophyllin L1.2. The Flinders Ranges frogs secrete only this peptide, whereas the *L. rubella* frogs from the south-west corner of Queensland and the Noonbah Station produce a number of peptides from their dorsal surfaces. The peptide profiles from these two clusters are quite similar. The only difference is the absence of fraction 2 in the secretion of the *L. rubella* frogs from south-western Queensland.

a. Tryptophyllin metabolite containing peptides: tryptophyllin L1.6, 1.7, 1.8, 1.9

Among the isolated peptides, the tryptophyllin L1.6 (MW 564 in fraction 2) was of particular interest because it was one of the peptides isolated before from a *L. rubella* frog cluster within a 20 km radius of Alice Springs in central Australia in January 1993, but its structure was not then identified. (The spectra of the unidentified peptide obtained in 1993 and of the tryptophyllin L1.6 showed identical fragmentations).

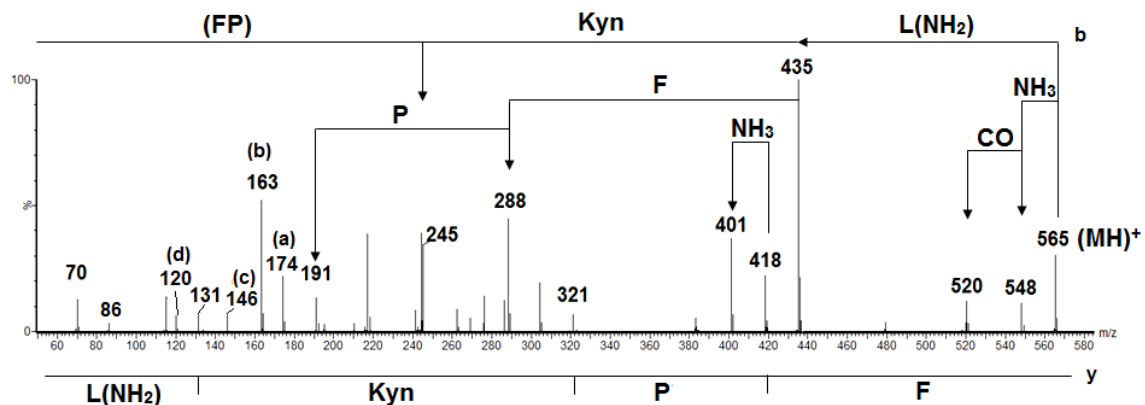


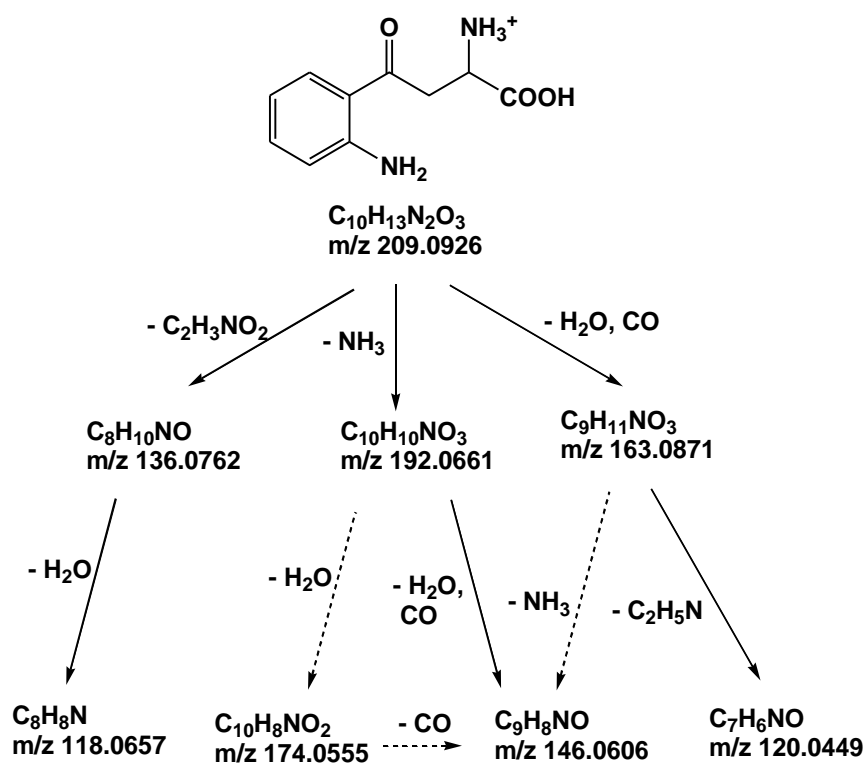
Figure 5.8. CID positive ion ESI MS/MS of the MH^+ ion of FP-Kyn-L(NH_2). Q-TOF 2 mass spectrometer. **b** and **y** backbone cleavages are shown schematically above and below the spectrum respectively.

The positive ion MS/MS spectrum of the MH^+ 565 is displayed in Figure 5.8. A combination of **b** and **y** cleavages provide a partial sequence of the peptide, with **y** cleavage ions at m/z 418 and 321 inferring the presence of Phe and Pro (Phe-Pro) from the C-terminal end, and a **b** cleavage ion at m/z 435 indicating the location of Leu or Ileu at the N-terminal end. The major **b** fragmentation ion at m/z 435 also loses Phe then Pro to form m/z 288 and 191. Automated Edman sequencing (carried out in 1993) [455] confirms this partial sequence and pointed out the presence of Leu at the N terminal. Consequently, the remaining mass is 190.

This mass does not correspond to any or a combination of any natural α amino acids, but it corresponds to one of the metabolites of tryptophan, kynurenine (Kyn).

Kyn is one of the oxidative products of tryptophan and is synthesised enzymatically by tryptophan 2,3-dioxygenase (TDO) or indoleamine 2,3-dioxygenase (IDO) [456]. It can also be formed by direct oxidation of tryptophan using various oxidative agents such as hydrogen peroxide, ozone, oxidising lipids, heat/oxygen, light/oxygen, etc. [457-458]. Kyn has been found in a number of proteins including lens crystalline [459-463], human Cu, Zn superoxide dismutase [464], bleached wool protein [465-466], milk proteins [467], oligopeptides with C-terminal Trp [468], Cu ion oxidised low density lipoproteins [469], and Cu bound protein MopE from *Methylococcus capsulatus* [470]. L-Kyn is also reported to be the sex pheromone (in the urine) of a female masu salmon [471].

The presence of Kyn in the peptide sequence of the MH⁺ 565 is firstly evident by the appearance of several characteristic Kyn cleavage ions (in Figure 5.7) including m/z 174 (a), 163 (b), 146 (c) and 120 (d), which have been reported by a number of studies of the application of positive ion MS/MS to identify Kyn in peptides and proteins [472-476]. The typical fragmentation pathways of protonated Kyn to form these ions are illustrated in Scheme 5.2 [477].



Scheme 5.2. Fragmentation pathways of protonated Kyn [477].

The high resolution MS/MS/MS spectrum of MH^+ 163 (Figure 5.9) showed the accurate masses of the ions (b), (c) and (d) are 163.0866 ($\text{C}_9\text{H}_{11}\text{N}_2\text{O}$ requires 163.0871), 146.0599 ($\text{C}_9\text{H}_8\text{NO}$ requires 146.0606) and 120.0444 ($\text{C}_7\text{H}_6\text{NO}$ requires 120.0449) respectively, proving the atomic compositions of these ions to be the same as those of the fragment ions originated from Kyn (see Scheme 5.2).

Furthermore, the positive CID MS/MS spectrum of a synthetic peptide with the sequence Phe-Pro-Kyn-Leu(OH) shows identical fragmentations to those observed in Figure 5.7. The sequence Phe-Pro-Kyn-Leu(OH) of the MH^+ 565 is confirmed.

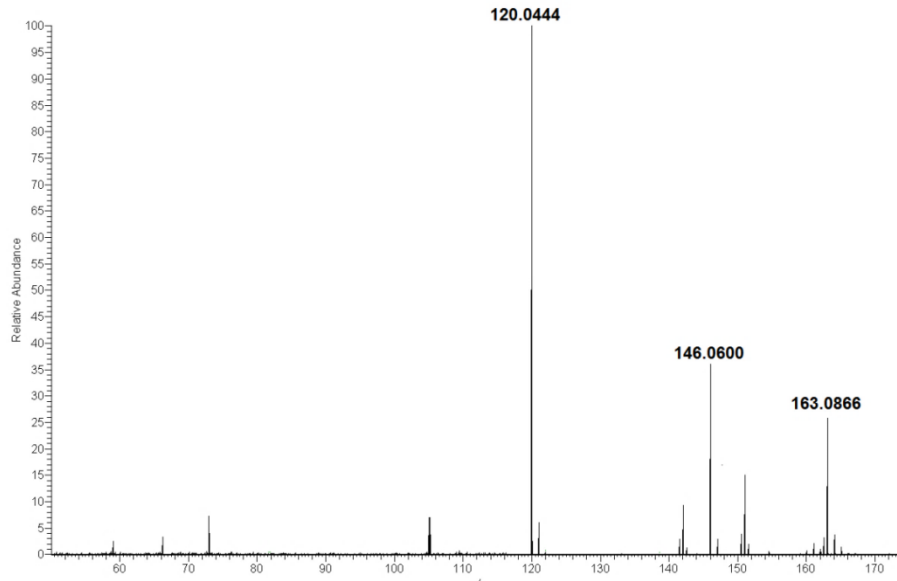


Figure 5.9. Accurate mass measurement and high resolution MS/MS/MS spectrum of MH^+ 163. LTQ Orbitrap XL ETD hybrid mass spectrometer.

The negative ion CID MS/MS spectrum of tryptophillin L1.6 reproduced in Figure 5.10 is most unusual with the cleavage from the Kyn side-chain enolate anion dominating the spectrum. The negative ion backbone fragmentations which normally provide sequencing information are not observed [156].

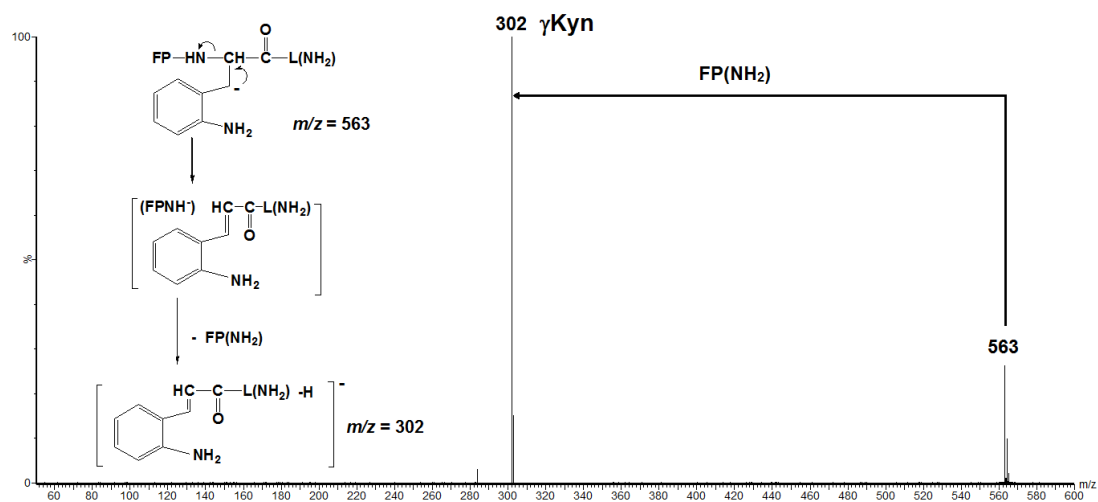


Figure 5.10. CID negative ion ESI MS/MS spectrum of the $(M-H)^-$ ion of FP-Kyn-L(NH₂). Q-TOF 2 mass spectrometer. The mechanism of the γKyn_3 cleavage is shown on the left of the spectrum.

The next tryptophyllin-metabolite containing peptides to be considered are tryptophyllin L1.7 and 1.8. The positive and negative CID MS/MS spectra of tryptophyllin L1.7 are displayed in Figure 5.11 and 5.12 respectively, and the mass spectral data for tryptophyllin L1.8 is summarised in Table 5.6.

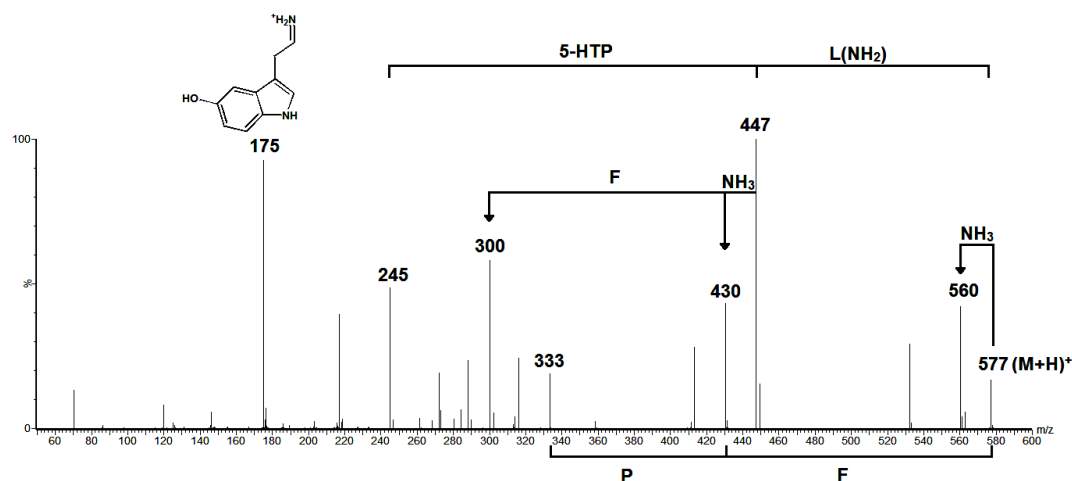


Figure 5.11. CID positive ion ESI MS/MS spectrum of the MH^+ ion of FP-5Htp-L(NH_2). Q-TOF 2 mass spectrometer. The sequence derived from the **b** cleavages is given above the spectrum while that from the **y** cleavages is displayed below.

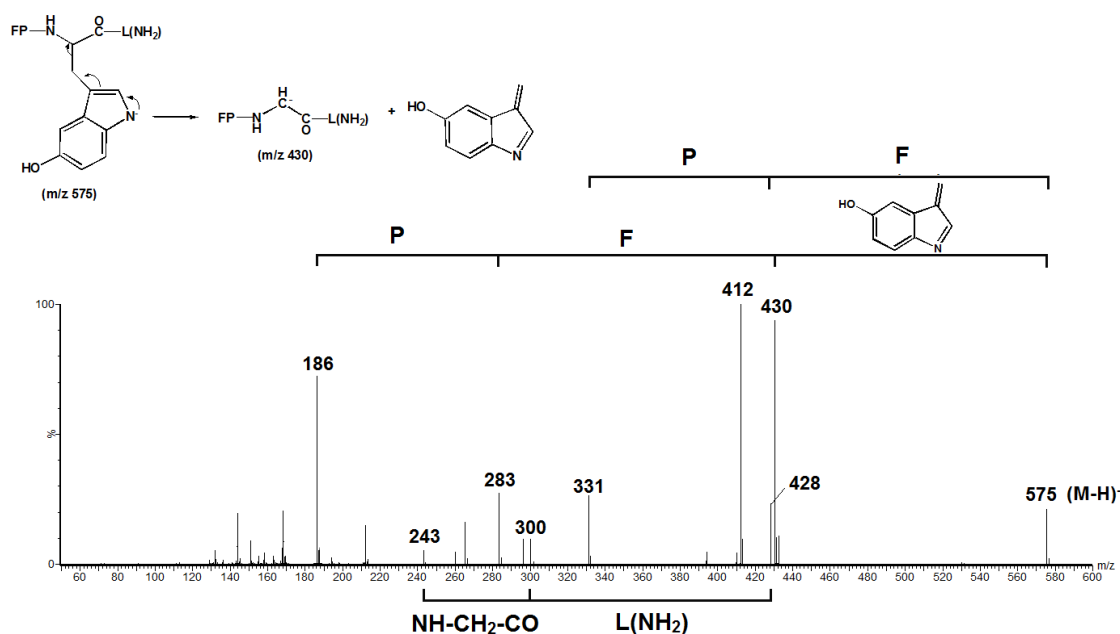


Figure 5.12. CID negative ion ESI MS/MS of the $(M-H)^-$ ion of FP-5Htp-L(NH_2). Q-TOF 2 mass spectrometer. α and β fragment ions are shown schematically above and below

the spectrum respectively. The loss of the indole ring is illustrated in the formula above the spectrum.

Table 5.6. Mass spectral data for tryptophyllin L 1.8. Format of fragment ion [m/z (fragment lost)]

(MH)⁺ m/z 593

b ions: m/z 576 (NH₃), 463 (L-NH₂), 245 (FP)

y ions: m/z 446 (F), 349 (P), 131 (NFK)

immonium ions: m/z 191 (of NFK), 120 (of F), 70 (of P)

The sequence of tryptophyllin L 1.8 is FP-NFK-L(NH₂)

The **b** and **y** cleavages, and the **α** and **β** fragmentations of tryptophyllin L1.7 are shown schematically above and below Figure 5.11 and 5.12 respectively. This peptide contains a third residue with a molecular mass of 202 in the peptide sequence. This molecular mass corresponds to two isomers of tryptophan metabolites, namely 5-hydroxytryptophan (5-HTP) and oxindolylalanine (Figure 5.13) [478-479]. The most abundant peak at m/z 175 was observed in the positive spectrum of tryptophan L1.7. The CID activated source-formed fragmentation of this ion (illustrated in Figure 5.14) showed a number of ions including m/z 158, 148, 146 and 130. These ions are the characteristic cleavage ions of the immonium ion of 5-HTP which were reported in detail in studies of 5-HTP using positive MS [480-481]. This suggests the inclusion of 5-HTP in the peptide sequence and eliminates the possibility of the isomeric oxindolylalanine (which is also formed from oxidative processes of Trp), since this isomer was reported to produce only two diagnostic fragments from its immonium ion (same m/z 175) including m/z 130 and 132 [481-482].

Furthermore, the positive and negative-ion electrospray ionisation MS/MS data for the MH⁺ and (M-H)⁻ ions of a synthetic peptide with the sequence Phe-Pro-5Htp-L(NH₂) are identical to those in Figure 5.11 and 5.12. This confirms the sequence Phe-Pro-5Htp-L(NH₂) of L1.7.

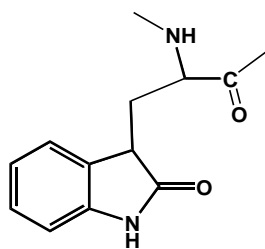


Figure 5.13. Structure of oxindolylalanine.

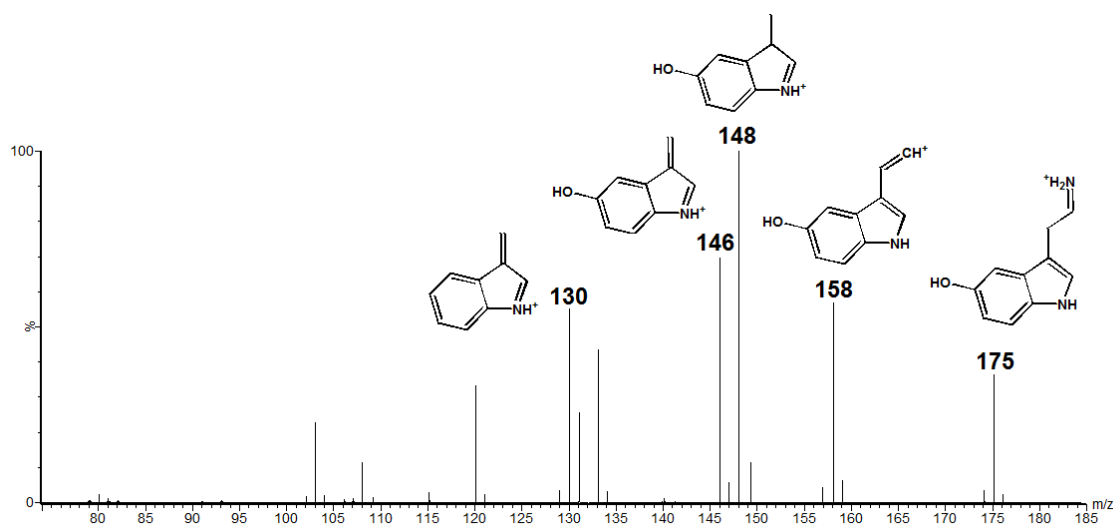


Figure 5.14. CID ESI MS/MS data for the source formed immonium ion of 5-HTP. Q-TOF 2 mass spectrometer.

Similar to tryptophyllin L1.6 and 1.7, tryptophyllin L1.8 is a derivative of tryptophyllin 1.2 with the Trp residue at the third position being oxidised to N-formylkynurenine. N-formylkynurenine, an oxidative product of Trp, has been found in a number of proteins such as cardiac mitochondrial proteins [483], bovine crystalline [484] or the CP43 subunit of photosystem II [485]. Its molecular weight is 32 mass units higher than that of Trp. The **b** and **y** cleavage ions of the protonated ion of tryptophyllin L1.8 provide the peptide sequence of tryptophyllin L1.8 as indicated in Table 5.6.

b. Tryptophyllin L1.1.1, 1.2.1 and 1.5

The mass spectral sequencing data for tryptophyllin L1.1.1, 1.2.1 and 1.5 are given in Table 5.7. Tryptophyllin L1.1.1 and L1.2.1 are carboxylic-acid terminal counterparts of tryptophyllins L1.1 and 1.2 (the major peptide). The protonated ion of tryptophyllin L1.1.1

and L1.2.1 produces the same **b** cleavage ions as those of tryptophyllin L1.1 and 1.2, respectively. However, the **y** cleavage ions of these peptides are one mass unit higher than those of their amide-terminal counterparts.

The CID MS/MS spectrum of the protonated ion of tryptophyllin L 1.5 is simple with the **b** and **y** fragment ions unambiguously assigning the peptide sequence. In addition, immonium ions of Trp, Pro and some **z** ions were also observed, contributing to the elucidation of the sequence of tryptophyllin L1.5.

Table 5.7. Mass spectral sequencing data for tryptophyllins L1.1.1, 1.2.1 and 1.5. Format of fragment ion [m/z (fragment lost)]

Tryptophyllin L1.5

(MH)⁺ m/z 502

b ions: m/z 484 (H₂O), 371 (L-OH), 185 (W)

y ions: m/z 415 (S), 318 (P), 132 (W)

Immonium ions: m/z 159 (of W), 120 (of F) 70 (of P)

The sequence of tryptophyllin L1.5 is SPWL(OH)

Tryptophyllin L1.1.1

b ions: m/z 397 (H₂O) , 284 (L(OH))

y ions: m/z 318 (P), 132 (W)

a ions: m/z 256 [PW– CO]

Immonium ions: m/z 159 (of W), 70 (of P)

The sequence of tryptophyllin L1.1.1 is PWL(OH)

Tryptophyllin L1.2.1

(MH)⁺ *m/z* 562

b ions: *m/z* 544 (H₂O), 431 (L-OH), 245 (W)

y ions: *m/z* 415 (F), 318 (P), 132 (W)

immonium ions: *m/z* 159 (of W), 120 (of F) 70 (of P)

The sequence of tryptophyllin L1.2.1 is FPWL(OH)

5.3.3 Evolutionary significance of peptides from *L. rubella*

The application of amphibian peptide secretions to identify chemical distinct populations of frogs within a species was introduced in sections 5.1. Differences in the peptide profiles of *L. rubella* suggested that different populations were located around Darwin (NT), in the Kimberley region of Western Australia, along the eastern seaboard of Queensland and in the central area of Australia (see Figure 5.4). The current investigation of the peptides secretions of *L. rubella* collected from the three locations adds more information about the evolutionary divergence of this genus.

Of three peptide profile identified, the peptide secretion from location **16** (see Figure 5.4) Flinders Ranges only shows one major peptide tryptophyllin L 1.2, which is the same as those identified from locations **8, 9** and **10**, indicating that the frogs collected from these four areas belong to the same population.

There is an obvious change in peptide content as moving north east from southern-central Australia. The peptides profiles of locations **17** and **18** are quite complex, which contain tryptophyllin L 1.2 as the major constituent, two rubellidins (caeridin type) and a number of small tryptophan metabolite containing peptides. The tryptophan metabolite containing peptides mark the difference in peptide profiles of these two populations from those obtained from the eastern seaboard of Queensland (see Table 5.3). This suggests that the frogs from these two areas may belong to a distinct sub-species.

5.3.4 Opioid activity

Of the *L. rubella* frog peptides discovered, only two major peptides tryptophyllin L1.2 and L3.1 showed low opioid activity and no other activities were detected for other tryptophyllin peptides. Therefore, tryptophyllin L1.6 (Kyn containing peptide) was synthesised to test for its opioid activity, as well as to examine the hypothesis that it may be produced from tryptophyllin 1.2 in an attempt to reduce the opioid activity of the major peptide. Tryptophyllin L 1.6 was tested for activity against electrically stimulated myenteric plexus-longitudinal muscle preparation of guinea pig ileum (GPI). The specific action of opioid agonist in GPI is to depress the firing of myenteric neurons, inhibiting the release of acetylcholine and thereby reducing the nerve-mediated cholinergic contractions of the smooth muscle contractions [486-487]. The opioid activity is thus expressed as a percentage of stimulated ileum basal contraction of the control (100%) with inhibition of contraction indicated by a decrease in % control.

This peptide exhibited a modest opioid activity commencing at a concentration of 10^{-7} M (Figure 5.13). The activity is significantly shifted in the presence of naloxone. Since naloxone shows a ten time preference for μ over κ opioid receptors [487-488], tryptophyllin 1.6 is thus likely to act via the μ opioid-receptor (δ opioid receptors are not involved in ileum [486, 489]).

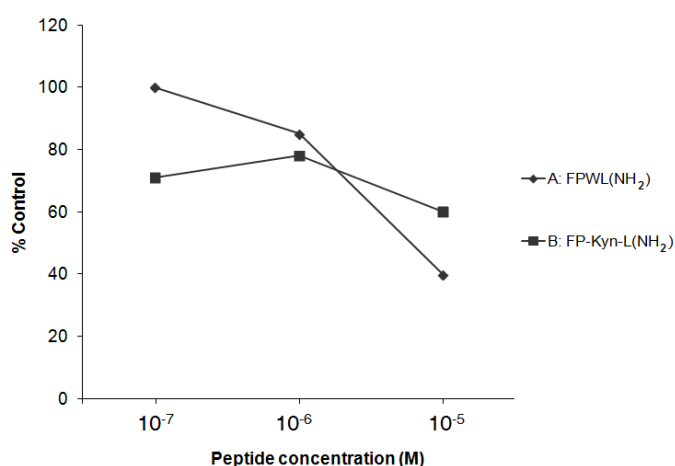


Figure 5.13. Inhibition of stimulated ileum contraction response curves for (A) FPWL(NH₂) (major peptide) and (B) FP-Kyn-L(NH₂). The activity is expressed as a percentage of stimulated ileum basal contraction of the control (100%) with inhibition of contraction indicated by a decrease in % control.

The opioid activity-test result unambiguously showed that tryptophyllin 1.6 is not converted from the major peptide tryptophyllin 1.2 in order to reduce the opioid activity of this peptide. On the other hand, it has been suggested by a number of studies that Trp metabolites may be formed in modulation of emotional behaviours or after physical efforts in mammals [490-493]. However, finding the origin of the genesis of the tryptophyllin metabolites is beyond the scope of the present study and was thus not pursued further.

5.4 Summary and conclusion

Nine peptides were isolated from live specimens of *L. rubella* from three locations; namely Flinders Ranges, a region of south-western Queensland, and Longreach Queensland. The secretion from the frogs from the Flinder Ranges (**16**) consisting of only the major peptide, tryptophyllin L1.2 indicates that this group belongs to the southern central population of *L. rubella*. The frogs from south-western Queensland (**17**) and Longreach Queensland (**18**) produce a number of tryptophyllin peptides and two rubellidins (caeridin type). The noticeable findings were the discovery of three tryptophyllin metabolite containing peptides including tryptophyllin L1.6, 1.7 and 1.8 in the two locations **17** and **18**, suggesting that the *L. rubella* frogs in the central area of Queensland may constitute a distinct sub-species of this genus.

Tryptophyllin L1.6, chosen as the representative of the three tryptophyllin metabolite containing peptides, showed a minor opioid activity from a concentration of 10^{-7} M.

5.5 Experimental

5.5.1 Peptide secretion collection

All the *L. rubella* secretions were provided through the courtesy of Associate Professor Michael Tyler from the Department of Zoology, the University of Adelaide. The specimens of interest were collected live from the three locations and kept in captivity. The secretory glands situated on the back of the frogs were electrically stimulated by gently rubbing a platinum electrode over the dorsal surface of the animal using 10 V and a pulse duration of 3 ms. The secretion was washed from the frog with deionised water (50 ml), and diluted with an equal volume of methanol, centrifuged, and filtered through a Milex HV filter unit (0.45

µm). The solution was lyophilised to a volume of about 1 ml using a Savant SC 100A Speed vac Concentrator.

5.5.2 HPLC separation of the skin secretions

Analytical HPLC profiles were obtained using a VYDAC218TP54 C₁₈ protein and peptide reverse phase column (5 µ, 300 Å⁰ particle size, 4.6 mm i.d. x250 mm; Separations Group, Hesperia, CA, USA). The column was equilibrated with 10% acetonitrile/water (ACN/H₂O) and 0.1% TFA (spectroscopic grade, Aldrich) as an ion-pairing agent. The flow rate was set at 1 ml min⁻¹. 100 µl of the crude solution was injected each time into a Rheodyne injector fitted with a 1 ml injection loop.

The separation employed a linear gradient produced by an ICI DP 800 Data Station (ICI Australia, Melbourne, Australia), typically increasing from 10-75% ACN over a period of 30 min. The eluant was monitored by ultraviolet absorbance at 214 nm using an ICI LC-1200 variable wavelength detector.

5.5.3 Mass spectra

Electrospray mass spectra were obtained using a Micromass Q-TOF 2 hybrid orthogonal acceleration time-of-flight mass spectrometer (Waters/Micromass, Manchester, UK) with a mass range to *m/z* 10,000. Samples (25 µg) were dissolved in acetonitrile/water (1:1 v/v) and infused into the ES source at a flow rate of 8 µl min⁻¹. Experimental conditions were as follows: capillary voltage 3.1 kV, source temperature 80 °C, desolvation temperature 150 °C, and cone voltage 40 V. Tandem mass spectrometry (MS/MS) data were acquired using argon as the collision gas and the collision energy was typically set at 40 eV to give maximum fragmentation.

All high resolution mass data were measured with an LTQ Orbitrap XL ETD hybrid mass spectrometer (Thermo Fisher Scientific, MA, USA) equipped with an ES ion source. Samples were infused at 5 ml min⁻¹ delivered by a built-in-syringe pump and a spraying voltage of 3.2 kV. A mass resolution of 30,000 (at *m/z* 400) was used. MS/MS tandem experiments were performed using collision energy dissociation set to 25%.

5.5.4 Solid state synthesis of FP-Kyn-L(NH₂)

Tryptophyllin 1.6 was prepared in house by Dr. Denis Scanlon using Fmoc-solid phase peptide synthesis. The synthesis was performed manually in a syringe fitted with a polypropylene sinter and stopcock on Rink resin (Merck –Novabiochem, Beeston, UK, NG9 2JR) on a scale of 0.25 mmole (0.5 g). Kynurenine was supplied as the fluorenylmethyloxycarbonyl (Fmoc) derivative with no protection on the aromatic amine side-chain (Advanced Chemtech, Louisville, KY, USA, 40228). Due to this fact Fmoc amino acids were activated with one equivalent of diisopropylcarbodiimide/hydroxybenzotriazole to form the active ester (with the exclusion of base catalyst). The coupling time was 1 hour. A four-fold excess was used in all cases except for Fmoc-Kynurenin which was coupled with a 2 fold excess. The peptide was cleaved from the resin at the end of the synthesis by treatment with 95% trifluoroacetic acid/2.5% triisopropylsilane/2.5% water (5 ml) for one hour. The peptide was precipitated from the cleavage reaction by addition of 40 ml of cold diethyl ether. The peptide was isolated by centrifugation, dissolved in 30% acetonitrile/water and lyophilised. Yields were 105 mg and 94 mg respectively for the Leu and Pro derivatives. The peptides were > 95% pure and exhibited the expected MW by ESI MS.

Other peptides were synthesized by Hongkong GenicBio Biotech Co., Ltd (Shanghai, China). Purities were > 80% as evidenced by HPLC and MS (Shimadzu LCMS-2010) data.

5.5.5 Biological testing

Opioid testing was carried out (by Dr. Ian F. Musgrave of the Pharmacology Department, the University of Adelaide) following a standard procedure [486] using myenteric plexus-longitudinal muscle preparation of guinea pig ileum stimulated at 60V, 0.1Hz, with a pulse of 2 ms duration. Agonist activity of the peptide was determined by the naloxone antagonist method [487, 489]. Activity is described as a percentage of the stimulated control contractions (basal contraction: 100% control). Dynorphin A was used as a peptide standard: stimulated contraction at 10⁻¹¹ M (IC₅₀= 7.2 x 10⁻¹¹ M), consistent with dynorphin A binding to opioid receptors [494].

CHAPTER 6

DO NEUROPEPTIDES “PARK” ON THE LIPID BILAYER OF A MEMBRANE BEFORE MOVING TO AN ADJACENT ACTIVE RECEPTOR SITE? A QCM INVESTIGATION

6.1 Introduction

6.1.1 Membrane-bound pathway of receptor binding of neuropeptides

Cell-surface receptors play a pivotal role in cellular communication by transmitting signals from outside the cell into the cell. Extracellular signalling molecules such as hormones, neurotransmitters, cytokines, growth factors or cell-recognition molecules associate with cell-surface receptors causing changes in the conformations of the receptors. This is known as receptor activation, which triggers cellular responses via secondary messengers. Even though interaction between peptide ligands and cell-surface receptors has been studied intensively for many decades, the mechanistic pathways by which peptides bind to membrane (or transmembrane) receptors to initiate biological responses still present many enigmas [495-497]. Binding of a peptide to its receptor directly from its random conformations in extracellular fluid sometimes requires high energy in order to effect reorientation and conformation changes of both the peptide and receptor during the interaction. However, regardless of the significant energy barriers associated with conformation changes, some peptides/proteins still show high potencies which implies that there are other interactions rather than only peptide-receptor interaction involved [498-500].

It was pointed out by Kaiser and Kezdy 30 years ago that many hormones and toxins shift from their extended (random) conformations in aqueous solution to amphiphilic helices in membrane-mimicking environment [501-502]. Subsequently, it was proposed that the adopted amphiphilic structures enable these peptides to anchor themselves onto the membrane surface where they were subsequently recognised by their receptors [501-502]. This proposal of Kaiser and Kezdy was developed further by Schwyzer to Membrane Compartment Theory [503-504]. This concept describes the correlation between the receptor-subtype selectivity of a number of peptides for neurokinin and opioid receptors and their membrane interaction specified by three parameters; namely hydrophobic association,

amphiphilic moment and Boltzman distribution [505-507]. According to this theory, interaction between the cell membrane and peptide ligands helps to distribute them into particular compartments such as the aqueous phase, the water-membrane interface or the hydrophobic core of the lipid bilayer. As a result, the searching probability of peptides for their receptors is improved not only by the accumulation of the peptide active sites in certain surface layers but also by the reduction of the three-dimensional diffusion of the peptides to two-dimensional movement on the membrane surface.

A thermodynamic and kinetic study of the interaction of two hormone peptides adrenocorticotropin-(1-24)-tetracosapeptide (ACTH₁₋₂₄) and dynorphin-(1-13)-tridecapeptide (dynorphin₁₋₁₃) with neutral model membranes or liposomes, together with examination of their pharmacological and binding data with corresponding receptors, led Schwyzer and co-workers to suggest a multi-stage mechanism for binding of a neuropeptide to a transmembrane receptor [496, 508-513]. Peptides with random conformations in extracellular fluid initially bind to the membrane. The cell membrane then imposes constraints on the peptide’s translation, orientation and conformation which guide the peptide to the receptor site. The ligand-receptor reaction is thus divided into several steps with favourable dissociation times and lower energy barriers for each step. A detailed mechanism for receptor binding of hormone peptides from membrane-bound states based on the studies of dynorphin₁₋₁₃ and ACTH₁₋₂₄ is depicted in Figure 6.1.

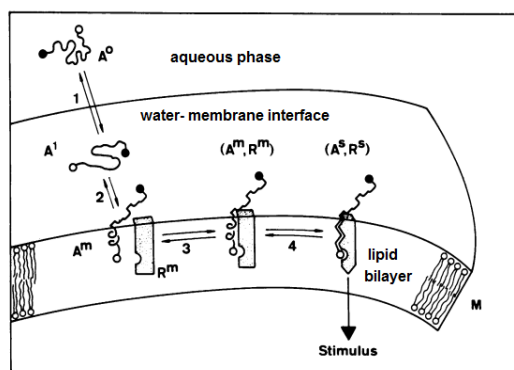


Figure 6.1. A stepwise model for binding of a peptide to a receptor with the membrane lipid phase as a catalyst. Adapted from [2]. (1) and (2): Transfer of an amphiphilic peptide from the aqueous phase to the water-membrane interface and then membrane surface due to electrostatic and hydrophobic interaction, (3) the peptide partially inserts and undergoes

conformational change to approach the receptor site, (4) the peptide binds to the receptor to exert the biological effect.

This membrane-bound pathway of receptor binding has been heavily debated and evaluated by several research groups [497]. In particular, Zerbe and colleagues have shown a correlation between pharmacological trends and the state (in-solution or lipid-bound) from which peptides are recognised by the receptors. This assumes that peptides with similar pharmacology for different receptor subtypes should display similar conformations in the state from which they are recognised [497, 514-520]. These studies involved a series of peptides of the neuropeptide Y family mainly using NMR techniques, and showed a relationship between the pharmacology and the micelle-bound conformations of the peptides. Accordingly, a mechanistic pathway of receptor binding quite similar to that of Schwyzer was proposed [515]. However, while the Schwyzer model assumed that peptides diffuse into binding pockets of the receptors directly from the membrane-associated state, Zerbe and his co-workers predicted that after moving laterally along the membrane surface toward the receptors, the peptides with membrane-adjusted conformations come off the membrane to interact with the binding pocket. Zerbe reasoned that it was unlikely for the rigid receptors [e.g. G-protein coupling receptors] to reorganise to engage with lipid-bound peptides (Figure 6.2) [497, 515].

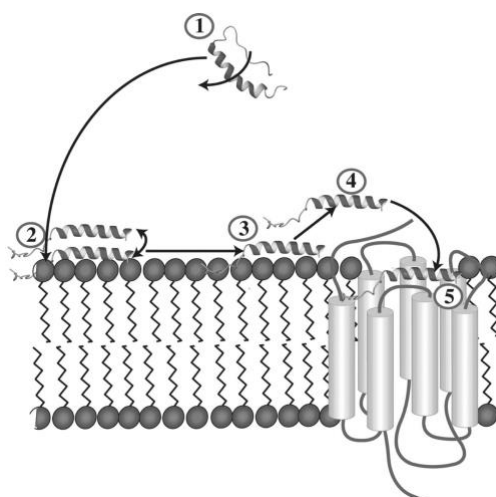


Figure 6.2. Zerbe’s version of membrane-mediated receptor binding of a neuropeptide includes: (1) ligand-membrane association, (2) lateral movement of the ligand on the membrane surface, (3) the ligand comes off the membrane surface to (4) temporarily link to a receptor’s segment and (5) attack the active site of the receptor.

Although the details of the two receptor-binding mechanisms show some differences, the peptide-membrane interaction was agreed to be the first event of the mechanism pathway. If this is true, differences in membrane interaction of peptides might alter their receptor effects. Different approaches have been used to study membrane-peptide interaction such as circular dichroism (CD) [521-522], Nuclear Magnetic Resonance (NMR) Spectroscopy [497, 514-516, 523], Fluorescence Spectroscopy, Fourier Transform Infrared Spectroscopy (FTIR) [524], and recently Atomic Force Microscopy (AFM) [525] and Surface Plasmon Resonance Spectroscopy (SPR) [526]. In the present study, the quartz crystal microbalance (QCM) technique was employed to investigate the interactions of a number of neuropeptides (extracted from frogs and toads) with model lipid bilayer membranes.

6.1.2 Peptides to be studied

The skin peptide profiles of Australia amphibian species have been found to contain a range of antimicrobial, anticancer active peptides and neuropeptides. In particular, neuropeptides have been recognised as an integral part of the host-defence system of amphibians and also play an important role in regulating dermal physiology [403, 409, 527]. These peptides often act through G-protein coupled receptors which are widely distributed in the central nervous system (CNS) or periphery systems. Neuropeptide activities are varied, depending on the tissue type affected. The sequences and bioactivity data of a large number of neuropeptides from Australian frog and toad genera have been reported. Many possess multi-faceted activities [403, 409, 527].

In this study, peptides from frogs and toads consisting of the genera *Litoria*, *Crinia* and *Uperoleia* were investigated. A summary of the biological activities of these peptides is provided in Table 6.1. Selected neuropeptides were riparin 1 from *C. riparia* [528], signiferin 1 from *C. signifera* [529]; rothein 1 from *L. rothii* and two synthetic variations [530]; uperolein from *U. rugosa* or *marmorata* [531] and the *iso*-Asp3 analogue of uperin 1.1 from *U. inundata* [532]; tryptophyllin 3.1 and kyurenine from *L. rubella* [422, 533]. Signiferin 1, riparin 1 and the rothein peptides effect either smooth muscle contraction, lymphocyte proliferation (or both) via interacting with the mammalian type II cholecystokinin receptor (CCK2R) [534-535]. Uperolein and *iso*-Asp3-uperin1.1 are potent smooth-muscle contractors, however they act on the neurokinin receptor 1 (NK1) [536-537].

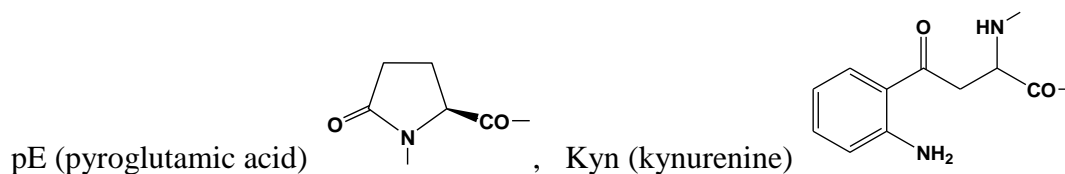
Tryptophillin 3.1 and kynurenine show modest opiate activity exerting their biological effects via the μ -opioid receptor.

There is a significant variation in the biological activities of the peptides chosen for this study. Riparin 1 does not show smooth-muscle contraction activity whereas signiferin 1 initiates this action at the low concentration of 10^{-9} M. Ala substitution of Ser 1 and 3 improve the lymphocyte and smooth muscle activities with respect to rothein 1. Finally, the smooth-muscle contracting action of *iso*-Asp3-uperin1.1 exceeds that of uperolein. The aim of this study is to determine whether these peptides actually interact with biomimetic lipid bilayers (to follow the membrane-associated receptor binding pathway) and how the difference in these peptide-membrane interactions may contribute to the difference in their biological activities.

Table 6.1.

Frog species	Peptide	Sequence	Bioactivity	Initial conc. (M)
C. riparia	Riparin 1	RLC <u>IPVIFPC</u> (OH)	a	10 ⁻⁷
			b	inactive
C. signifera	Signiferin 1	RLC <u>IPYIIPC</u> (OH)	a	10 ⁻⁶
			b	10 ⁻⁹
L. rothii	Rothein 1:	SVSNIPESIGF(OH)	a	10 ⁻⁵
			b	inactive
Synthetic variation	Rothein 1.1:	AVSNIPESIGF(OH)	b	10 ⁻⁷
			a	10 ⁻⁶
Synthetic variation	Rothein 1.2:	SVANIPESIGF(OH)	b	inactive
			a	10 ⁻⁶
U. inundata	<i>iso</i> -Asp3 uperin 1:1	pEA(<i>iso</i> D)PNAFYGLM(NH ₂)	b	10 ⁻¹⁴
U. rugosa or marmorata	Uperolein	pEPDPNAFYGLM(NH ₂)	b	10 ⁻¹³
L. rubella	Tryptophyllin 3.1	FPWP(NH ₂)	c	10 ⁻⁷
L. rubella	Kyn-tetrapeptide	FPKynL(NH ₂)	c	10 ⁻⁷

- a. Lymphocyte proliferation
- b. Smooth muscle active
- c. Opioid active



6.1.3 Biomimetic membranes

The phospholipids comprising the membrane of eukaryotic (mammalian) cells are asymmetrically distributed. The outer leaflet exclusively consists of neutral (zwitterionic) phosphatidylcholine (PC) and sphingomyelin (SM) whereas the inner leaflet is composed of negatively charged phosphatidylserine (PS). In contrast, prokaryotic (bacterial) membranes only contain negatively-charged phospholipids such as phosphatidylglycerol (PG), phosphatidylserine (PS) and cardiolipin (CL). In addition, sterols such as cholesterol and ergosterol are commonly found in eukaryotic membranes but not in prokaryotic membranes [538-539]. Thus, in studies related to cell membranes, zwitterionic lipids such as dioleoylphosphatidylcholine (DOPC), 1,2-dimyristoyl-*sn*-glycero-3-phosphocholine (DMPC) are commonly used to represent the extracellular surface of mammalian cells while a mixture of DMPC and anionic 1,2-dimyristoyl-*sn*-glycero-3-phospho-*rac*-(1-glycerol) (DMPG) has been commonly used to model bacterial membranes (Figure 6.3).

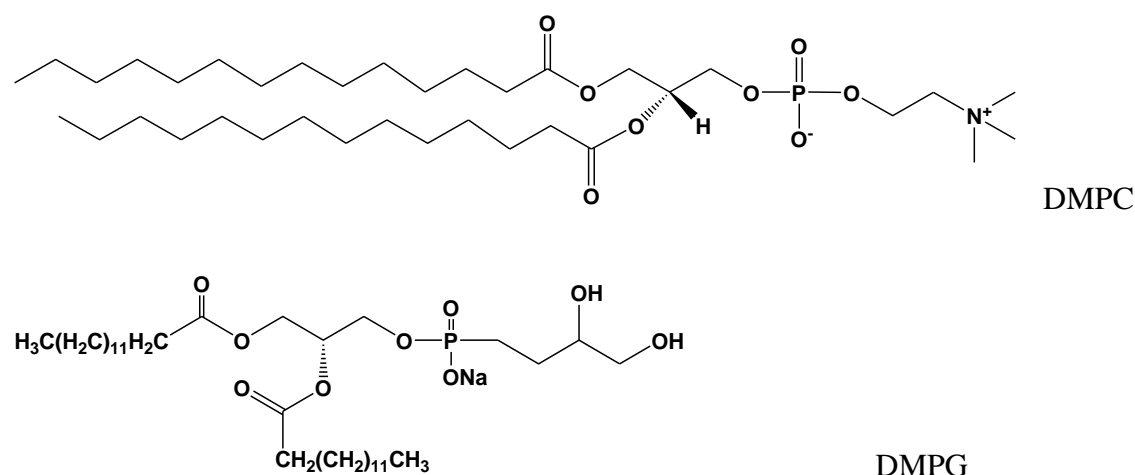


Figure 6.3. Structure of zwitterionic lipid DMPC and anionic lipid DMPG.

Solid supported membranes, lipid bilayers supported on solid substrates, have received increasing attention due to their importance as models for biological membranes which are used to study the properties and functions of membrane-bound peptides/proteins or membrane mediated processes [540-545]. Spreading of lipid vesicles (ideally unilamellar vesicles) on hydrophilic supports, followed by rupture and fusion of these vesicles to form a biomimetic lipid bilayer, was pioneered by McConnell *et al.* in the early 1980s [546]. Since then, the mechanism of supported lipid bilayer (SLB) formation and factors that control SLB formation have been studied using a multitude of surface-sensitive and optical techniques

such as quartz crystal microbalance and dissipation (QCM-D), reflection interference contrast microscopy (RICM), atomic force microscopy (AFM) and SPR [525, 547-549].

Different pathways of vesicles absorption and bilayer formation can occur depending on the interplay of vesicle-substrate, vesicle-vesicle and intra-vesicle interactions. Lipid vesicles (liposomes) may (i) not absorb on the supporting solid, (ii) absorb and remain intact, (iii) absorb and rupture immediately, (iv) absorb and rupture as a certain surface density of vesicles is reached or (v) absorb and fuse to reach a certain liposome size before rupture [549-553]. The formation of SLBs following scenarios (iii), (iv) and (v) are desirable for membrane related studies. Subsequently, the disruption of an absorbed liposome results in a bilayer patch with an exposed (hydrophobic) edge which is thermodynamically unfavourable [554-555], and thus it tends to interact with other liposomes (or other bilayer patches) in a cascade of rupture events to extend the bilayer area and to finally form a planar bilayer [549, 556-558].

Electrostatic interactions between the charged support and the lipid vesicles together with ionic strength of the buffer are the major factors that influence lipid bilayer formation [559-561]. Alternating one of the experimental parameters such as (i) the substrate's charge, (ii) the vesicle charge or (iii) the ionic composition of the buffer, may result in different bilayer formation pathways. Practically, the pH or the ionic strength of the buffer is normally adjusted as a simple way to regulate SLB formation for a given set of surface and lipid compositions [552, 560]. The hydrophilicity of supports is found to be essential for SLB preparation, thus surfaces such as gold, TiO₂ or platinum are found to be less efficient supports than mica or silicon-base materials. For liposomes formed from a mixture of lipid species, distribution of individual lipids between two SLB leaflets can affect the timescale of the rupture and fusion of the liposome. In addition, increasing temperature was reported to lower critical vesicular coverage (density) for SLB formation [551].

Among methods used to study membrane related processes, QCM-D is a well-established technique to monitor SLB preparation and SLB's interaction with biomolecules such as peptides, proteins or drugs. The advantage of QCM-D is that it examines the real time kinetics of these processes by characterizing simultaneously the mass and viscoelastic properties of adsorbed materials (for details see section 6.2) (Figure 6.4). In a QCM-D experiment, SLBs can be prepared by a spontaneous process or a controlled process.

Regulation of SLB formation is carried out by altering the chip-adhered substrates, the buffer composition or the lipid preparation (size and composition). Gold-coated quartz chips are commonly covered with silica, mica or charged self-assembled monolayers (SAMs) to improve the interaction of the surface of the chip with the hydrophilic parts of liposomes [559, 562]. Small unilamellar vesicles (SUVs) with diameters in the 15-100 nm range are recommended for SLB preparation. These are produced from large multilamellar vesicles (LMVs) by either sonication or extrusion. Each of these methods generates SUV populations with different mean sizes [563]. However, the size distribution of vesicles may evolve further by (i) spontaneous fusion of SUVs or (ii) individual phospholipid molecule exchange between liposomes. This results in a mixture of unilamellar vesicles with larger mean sizes [562, 564]. This process of changing size distribution is determined by entropic and other thermodynamic factors established at the equilibrium of a particular liposome preparation. Furthermore, it is common to adjust the concentration of a particular cation (especially a divalent cation) in the buffer mixture at a particular point of time in experimental process to control the rupture and fusion of the liposomes to form SLBs [549, 556, 561, 565-568] .

Change in frequency (Δf) and dissipation (ΔD) corresponding to the formation of a complete SLB vary depending on the nature of the supports. For instance, a change of 25 Hz and no change in dissipation indicated the formation of a lipid bilayer on silica or mica [547, 552, 557] while 13 Hz and a small change in dissipation were suggested to correspond to a single bilayer formation on a 3-mercaptopropionic acid-coated surface [562]. Achieving homogeneity in SLB formation is critical to membrane related studies. However, the SLB is commonly formed with a small percentage of defects such as the composite membrane of bilayer stacks, embedded vesicles or gap-containing bilayer. While a perfect SLB is required for some applications, low-defect SLBs are generally accepted for peptide/protein adsorption studies [552]. Experimentally, the quality of SLBs may vary slightly from time to time even though the same experimental protocol is used [562].

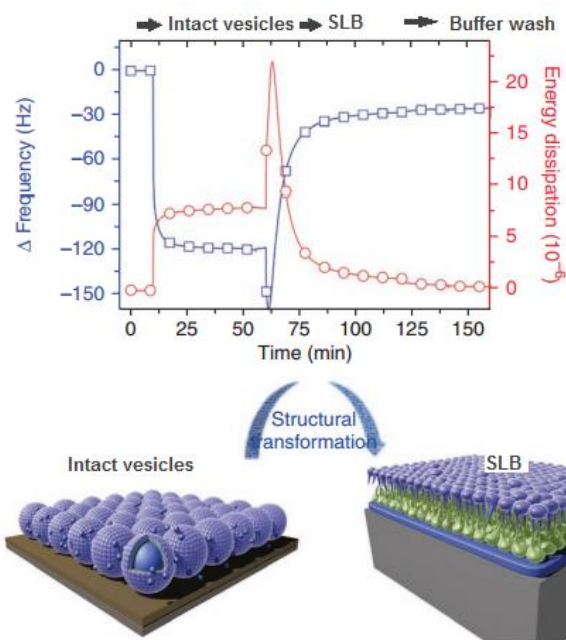


Figure 6.4. Changes in frequency and dissipation along the formation of a lipid bilayer. Adapted from [565].

6.1.4 Peptides/protein-membrane interactions

Binding of peptides/proteins to lipid membranes is a complex function involving both electrostatic and hydrophobic interactions [569-573]. Electrostatic attraction is found to contribute significantly to the membrane binding of many peripheral proteins. This is due to the interaction between the cluster of basic residues (or positively charged portions) of the peptides/proteins and the negatively charged phospholipids. The charge distribution over the peptide/protein also affects its membrane orientation and association. However, the total net charges of peptides/proteins do not precisely reflect their membrane-binding propensity since binding between neutral or negatively charged protein domains and acidic phospholipids are still observed [574-575]. This indicates that electrostatic effects are accompanied and sometimes dominated by other interactions. Indeed, although the electrostatic interaction initially acts as the long-range driving force to guide the peptide/protein toward (or away from) the membrane, at shorter distance, the peptide/protein and the membrane experience two additional interactions: namely (i) the repulsive desolvation caused by the unfavourable loss of solvent molecules around the peptides/proteins and on the lipid surface, and (ii) the hydrophobic interaction between the hydrophobic portion of the peptide/protein and the fatty acid hydrocarbon chain of the

membrane [576]. In certain cases, the hydrophobic binding is energetically significant enough to overcome the repulsion by electrostatic and desolvation interaction to bring the peptide/protein to the membrane surface. The relative significance of electrostatic, desolvation and hydrophobic interactions in the binding of peptides is dependent on the structure and composition of the peptide/protein-membrane system.

The measurement of each contribution of membrane binding energies of peptides/proteins has to date been only carried out based on computational simulations. In such methods, the electrostatic component can be determined by solving the Poisson-Boltzmann equation (I) [577-579], whereas the non-polar contribution is obtained from the equation calculating free energy-surface area relationships (II) [573, 576]. The addition of these components can be used as an approximation to the total binding energy of the peptide/protein-membrane system. However, it has experimentally been shown that the effective charge of a cationic peptide may be altered depending on the hydrophobicity of that peptide, with an increase of 12.5 kJ mol^{-1} in hydrophobic energy causing a decrease of approximate 20% of the effective charge of the peptide. This brings about a reduction in electrostatic interaction of the peptide with the membrane [573].

The PB equation: $\nabla[\varepsilon(r) \nabla\phi(r)] - \varepsilon_r \kappa(r)^2 \sinh[\phi(r)] + e^2/(\varepsilon_0 k_B T) \rho^f(r) = 0$ (I)

where $\varepsilon(r)$ is the dielectric constant, $\phi(r)$ is the electrostatic potential, $\kappa(r)$ is the Debye-Huckel parameter and $\rho^f(r)$ is the fixed charge density of the protein and lipids; these parameters are functions of space $r = (x,y,z)$. k_B is the Boltzmann constant, T is the temperature (Kelvin degree). The resultant electrostatic potentials are used to calculate the electrostatic free energy of the system.

The free energy-surface area relationship equation: $\Delta G = \gamma \Delta A$ (II)

where γ is the surface tension coefficient and ΔA is the change in solvent accessible surface area upon association.

In an attempt to thermodynamically quantify the interaction of small hydrophobic peptides with lipid membranes, White and Wimley have measured the free energy required to transfer each of 20 natural amino acids from the aqueous phase to the water-membrane interface or into the hydrophobic interior of membranes (Table 6.2) [580-581]. These data indicate that

Trp, Tyr, Phe and Leu contribute most to membrane association. This result was generally in agreement with the observation by Killian and co-workers from studies of the arrangements of transmembrane proteins within lipid membranes [582-583], which demonstrate the prevalence of Trp and Tyr (but not Phe) in regions close to the membrane-water surface. The “snorkelling behaviour” of Lys and Arg were also suggested to explain the preference of Lys and Arg for the interfacial environment, in which the hydrophobic portions of Lys and Arg contact with the hydrophobic core of the membrane while the charged ends reach the more polar part of the membrane [584]. Lys and Arg were found mainly on the cis-side (membrane interior side) of the interface while aromatic containing amino acids prefer to locate on the other side of the interface (aqueous side) [582] .

Table 6.2. The Wimley-White experiment-based interfacial hydrophobicity scale: free energies for transferring amino acids from water to 1-palmitoyl-2-oleoylphosphatidylcholine (POPC) interface (wif) and to hydrophobic environment n-octanol (woct). Adapted from [580].

Amino acid	ΔG_{wif} (kJ/mol)	ΔG_{woct} (kJ/mol)	Amino acid	ΔG_{wif} (kJ/mol)	ΔG_{woct} (kJ/mol)
Ala		+2.09	Ile	-1.30	-4.69
Arg+		+7.58	Leu	-2.34	-5.23
Asn		+3.56	Lys+	+4.14	+11.72
Asp-		+15.24	Met	-0.96	-2.80
Asp		+1.08	Phe	-4.72	-7.16
Cys		-0.08	Pro	+1.88	+0.56
Gln		+3.22	Ser	+0.54	+1.93
Glu-		+15.19	Thr	+0.59	+1.05
Glu		+0.46	Trp	-7.74	-8.75
Gly		+4.81	Tyr	-3.93	-2.97
His+		+9.75	Val	+0.29	-1.93
His		+0.46			

6.2 Theory of quartz crystal microbalance-dissipation

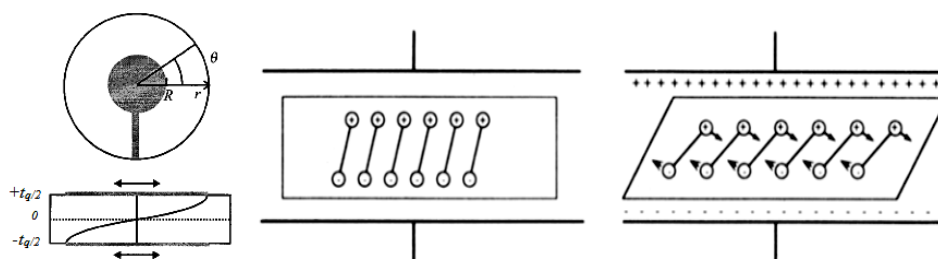
6.2.1 Quartz crystal microbalance: basic components and operation

The main component of a QCM instrument is a thickness shear mode (TSM) resonator which consists of a very thin disk of AT-cut quartz (a quartz plate cut at an angle of $35^{\circ}10'$ with respect to the optical z-axis of the quartz crystal). Two metal electrodes are deposited on each side of the disk. Due to the piezoelectric property and crystalline orientation of the quartz, application of an alternating potential difference perpendicular to the surfaces of the electrodes induces the quartz chip to vibrate in shear mode, and resonance occurs when the acoustic wavelength is an odd multiple of twice the crystal thickness (Figure 6.5a) [585]. The resonant frequency is given by equation (1).

$$f_o = v_{tr} / 2t_q = (\mu_q^{1/2} / \rho_q^{1/2}) / 2t_q \quad (1)$$

where v_{tr} is the propagation velocity of acoustic waves in quartz, μ_q is the shear modulus, ρ_q is the density of quartz and t_q is the quartz thickness.

The quartz chip can be pulsed with different voltages to resonate at higher frequencies called overtones or harmonics. The frequency of the n^{th} harmonic is n times the fundamental ($f_n = nf_o$). The chip can only be excited electrically by odd harmonics indexed by the number of nodal planes of the acoustic wave (within the quartz thickness) parallel to the crystal surfaces. This is because only odd harmonics can induce charges of opposite sign at the two crystal surfaces in order to make the quartz chip oscillate (Figure 6.5b) [586-587].



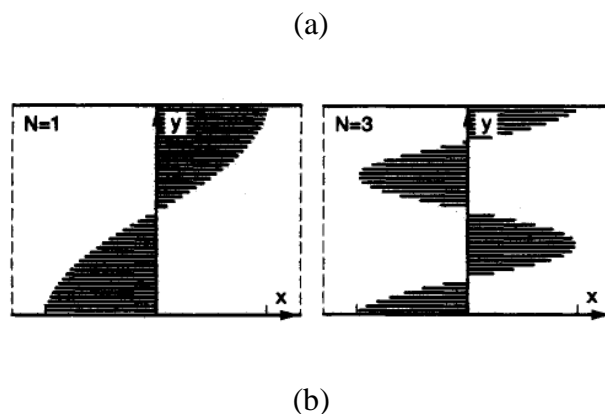


Figure 6.5. (a) The quartz chip from top view and side view. Adapted from [588]. (b) Shear displacement profiles across the QCM thickness for the fundamental and the third harmonic. Adapted from [3].

If (i) there is a uniform rigid foreign material deposited on the surface of the quartz crystal and (ii) it is assumed to have identical acoustic properties to those of quartz (known as a no-slip condition), the whole system is treated as a “composite resonator” with a new thickness. A fractional change in frequency due to the change in quartz thickness can be determined by the Sauerbrey equation (2) [589].

$$\Delta f = \frac{-2f_0^2 \Delta m}{A(\mu_q \rho_q)^{1/2}} \quad (2)$$

Where Δf is the measured frequency shift, f_0 the frequency of the quartz crystal prior to mass change, Δm is the mass change, A the piezoelectrically active area, μ_q the shear modulus and ρ_q the density of quartz.

6.2.2 Quartz crystal microbalance-dissipation in liquid phase

A frequency shift obeys the Sauerbrey equation mentioned above only when the measurement is carried out in vacuum or gas environments and there is no phase shift between the quartz and the added material. However, most QCM measurements involve quartz crystal surfaces that are either immersed in liquid and/or coated with films which have different phase properties. In 1982, Nomura and Okuhara demonstrated that quartz

resonators can oscillate in fluid media and that their resonant frequencies were affected by the density and viscosity of the media [590]. Since then, the impact of contacting liquid on a resonator’s frequency has been the subject of a multitude of studies using electromechanical models [590-593]. Most of those models are based on the assumption that the first molecular layer of the liquid is rigidly attached to an ideally smooth quartz surface allowing the shear displacement to be transferred into adjacent fluid layers. As the shear wave propagates, the kinetic energy of the oscillation is radiated gradually into the solution and the wave is then attenuated (Figure 6.6). An equation (3) describing the effect of Newtonian liquids on the frequency of TSM sensors was introduced by Kanazawa and Gordon [593].

$$\Delta f = -\sqrt{\frac{f_0^3 \eta_l \rho_l}{\pi \rho_q \mu_q}} \quad (3)$$

where μ_q is the shear modulus and ρ_q is the density of quartz, η_l is the viscosity and ρ_l is the density of the contacting liquid.

The penetrating distance of the shear wave into a bulk liquid of viscosity η_l and density ρ_l is estimated from the decay length of the acoustic wave for a Newtonian liquid and is given in equation (4). A 5 MHz quartz crystal was calculated to produce a wave with a penetrating distance (δ) of 250 nm in water which means only a small volume of the QCM cell is actually sensed [593]. According to equation (4), the penetration depth of an acoustic wave is inversely proportional to the frequency of the wave. Thus, higher frequencies probe closer to the surface of the quartz chip than lower frequencies.

$$\delta = \sqrt{\frac{\eta_l}{\pi \rho_l f}} \quad (4)$$

where f is the frequency of the resonator.

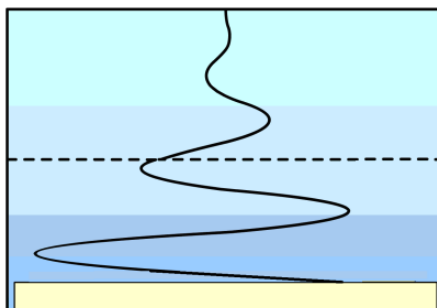


Figure 6.6. The attenuated acoustic wave in a dissipating liquid medium.

The situation becomes more complex if both mass and liquid are loading. The general configuration for a simultaneous mass and liquid loading is illustrated in Figure 6.7a. A quartz crystal with a film attached resonating in a homogeneous bulk liquid generates a shear wave which propagates through various media. The wave penetrates through the film and is reflected partly at the upper surface of the film while the damped wave continues to cross the film-liquid interface and dissipates in the liquid phase [591]. The relationship between mass change and frequency shift becomes complex because it depends on a number of factors including (i) the viscoelastic properties of the added mass and the contacting solvent [592, 594], (ii) the surface roughness [595] and (iii) the interfacial slippage (the first film layer is not tightly bound to the electrode surface) [596]. Consequently, the equation expressing the relationship between the mass change and frequency change involves a large number of parameters such as the elasticity and density of the film together with viscosity, elasticity of the solvent (etc.) [587].

Rohdal et al. [597] used a continuum mechanic approach to solve the wave equation for a model of two viscoelastic layers absorbing on the surface of a piezoelectric plate, which is oscillating in pure shear mode in a bulk liquid (Figure 6.7b). The wave solution was obtained under the no-slip condition (no phase shift between the quartz crystal and the absorbed films) and the films were in contact with a semi-infinite Newtonian liquid. The change in frequency Δf and dissipation change ΔD are given as follows:

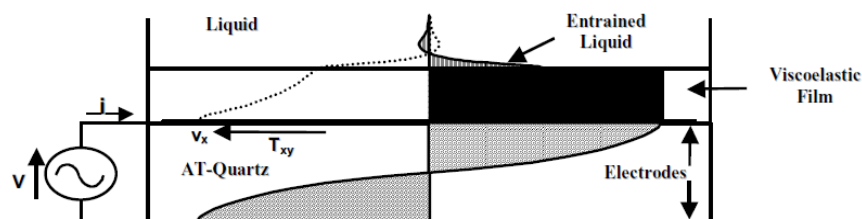
$$\Delta f \approx -\frac{1}{2\pi\rho_0 h_0} \left\{ \frac{\eta_3}{\delta_3} + \sum_{j=1,2} \left[h_j \rho_j \omega - 2h_j \left(\frac{\eta_3}{\delta_3} \right)^2 \frac{\eta_j \omega^2}{\mu_j + \omega^2 \eta_j^2} \right] \right\} \quad (5)$$

$$\Delta D \approx \frac{1}{2\pi f \rho_0 h_0} \left\{ \frac{\eta_3}{\delta_3} + \sum_{j=1,2} \left[2h_j \left(\frac{\eta_3}{\delta_3} \right)^2 \frac{\eta_j \omega^2}{\mu_j + \omega^2 \eta_j^2} \right] \right\} \quad (6)$$

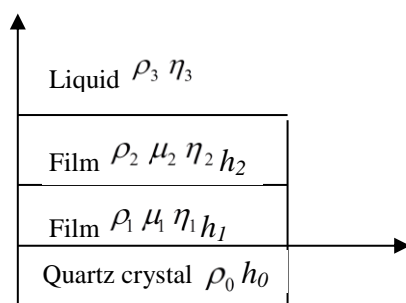
where h_j and h_0 are the thicknesses of the viscoelastic film and the quartz slab, ρ_j and ρ_0 are the densities of the film and the quartz, η_j and η_3 are the viscosities of the film and the liquid, μ_j is the shear modulus of the film, δ is the viscous penetration depth, and ω is the

angular frequency ($\omega = 2\pi f_n$). The mass of the attached film (m_j) is not determined directly but can be calculated from $\rho_j \cdot h_j$.

The results of this model enable the use of QCM as a mass and structural detector for viscoelastic materials such as lipids or peptides/proteins in the liquid phase. The structural change of a lipid bilayer upon the addition of a peptide was first demonstrated using $\Delta f - \Delta D$ plots [598].



(a)



(b)

Figure 6.7. (a) General configuration for a simultaneous mass and liquid loading. (b) A model of quartz chip with two film layers loaded in contact with bulk liquid.

6.2.3 Measurement of resonant frequency in QCM

Due to electromechanical coupling of piezoelectric material, the mechanical properties of a quartz crystal are reflected in its electrical properties. Thus, as a quartz resonator comes into contact with a medium, the mechanical interaction between the resonator and the contacting medium affects the electrical response of the device, and makes possible the use of the resonator as a sensor [585, 588, 599-600]. The sensor can then be treated as a component of an electronic circuit as it is represented by an electrical model which responds to an applied

voltage or current in the same way as the crystal itself. Among several models of such representations, the extended Butterworth Van Dyke (BVD) equivalent circuit is widely used to describe the electrical characteristics of loaded quartz (Figure 6.8). In this model, L_1 is the inductance representing the oscillating mass of the quartz, C_1 is the capacitance (a measure of the elasticity of the oscillating body representing the energy stored during oscillation) and R_1 is the resistance related to energy dissipation (due to internal friction, mechanical losses in the mounting system and acoustical losses to the surrounding environment). The electrical representation also includes a parallel C_0 capacitance resulting from the dielectric characteristic of the electrodes and the parasitic contributions of the wiring and crystal holder. The contribution of any surface load is represented by impedance Z_m . Z_m can be split to many components depending on properties of contacting media [588, 599, 601-602].

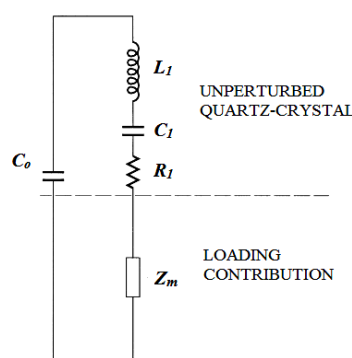


Figure 6.8. Extended Butterworth Van Dyke (BVD) equivalent circuit.

The resonator can be characterised electrically either under steady-state conditions (e.g. applying a steady radio frequency potential) or under transient conditions (e.g. a decay following an initial voltage-triggered resonance) [603]. The major representative of the steady-state method is impedance analysis or network analysis. In this setup, an rf voltage is applied across the crystal, which is then scanned over a range of frequencies around resonance [585, 603-605]. The impedance Z is obtained from the ratio of the voltage to the current. However, most applications of this technique use admittance Y (the reciprocal of impedance) instead of impedance. By monitoring both the magnitude and phase of the admittance at each frequency, the real part (conductance G) and imaginary part (susceptance B) of the admittance are measured. The BVD model is then fitted to these experimental data to determine the resonant frequencies and other related parameters such as resistance and parallel capacitance (Figure 6.9).

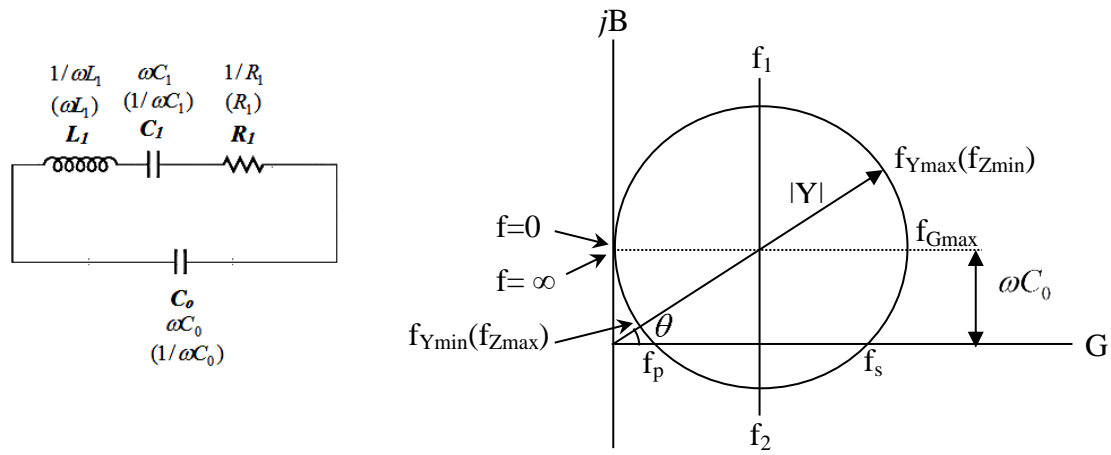


Figure 6.9. Admittance locus for the equivalent circuit of a quartz resonator. Note that AT-cut quartz as a piezoelectric material exhibits dual resonance at two frequencies, series frequency f_s and parallel frequency f_p . The resonance occurs as the phase angle $\theta = 0$ where the admittance locus crosses the real axis G . The series frequency f_s is monitored normally.

The series frequency of an unloaded resonator is given by equation:

$$f_s = \frac{1}{2\pi\sqrt{L_1 C_1}} \quad (7)$$

On the other hand, the decay method uses a signal generator to excite the resonator device. The frequency of the applied voltage is varied until the frequency of largest current is reached. The driving power of the resonator is then switched off (at $t = 0$) leaving the current or voltage to decay as an exponentially damped sinusoid, mathematically expressed by equation (8).

$$A(t) = A_0 e^{-t/\tau} \sin(2\pi f t + \varphi) + C \quad (8)$$

Where A_0 is the amplitude of the magnitude at $t = 0$, τ is the decay time constant, φ is the phase and C is the dc offset and f is the oscillating frequency

In a QCM-D instrument, the driving AC voltage is removed once every second. The amplitude of current or voltage as a function of time is recorded and the recorded curve is fitted to equation (8) to determine τ and f . The sensor is designed such that the decay currents for the various harmonics can be sequentially recorded [606-607].

6.2.4 Measurement of the dissipation factor

In terms of wave propagation, the acoustic wave generated by a resonator has a finite decay-distance due to energy loss in dissipating media. The driving voltage keeps the inherent decaying wave unchanged. However, if the voltage is shorted, not only the portion distant from the surface but also the entire wave will experience a time-dependent dissipation towards zero amplitude (Figure 6.10).

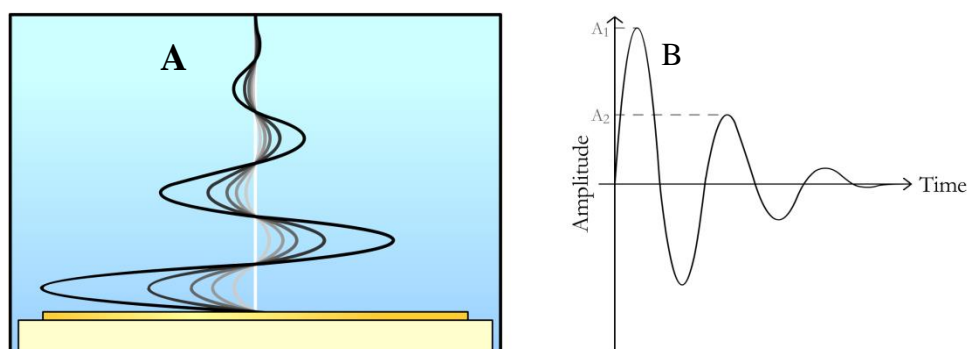


Figure 6.10. (A) The entire wave, (B) (A1–A2) is the change in the amplitude of the wave over one period.

The dissipation factor (D) of a resonator is a measure of how quickly the chip loses energy after removing the driving voltage:

$$D = \frac{E_{dissipated}}{2\pi E_{stored}} \quad (9)$$

where $E_{dissipated}$ is the energy lost during a single oscillation after removing voltage (Figure 6.10B) and E_{stored} is the initial energy of the chip.

In the decay technique, the dissipation value can be determined using equation (10).

$$D = \frac{2}{\omega\tau} \quad (10)$$

In most cases, not only the fluid medium but the film attached on the chip’s surface is also energy-dissipating. Thus, the structural properties (e.g. viscosity, elasticity) of the adhered mass and the interaction between the film and the quartz’s surface influence the way the chip loses energy. Since dissipation D describes the energy damping profile of the coated quartz, any change in structural properties of the film is reflected in the change of dissipation value

and hence, structural changes can be monitored throughout the experiment. In general, if the dissipation increases, the chip loses energy faster indicating that the added layer is softer or less rigid. Conversely, a decrease in dissipation indicates an increase in rigidity of the added mass (Figure 6.11).

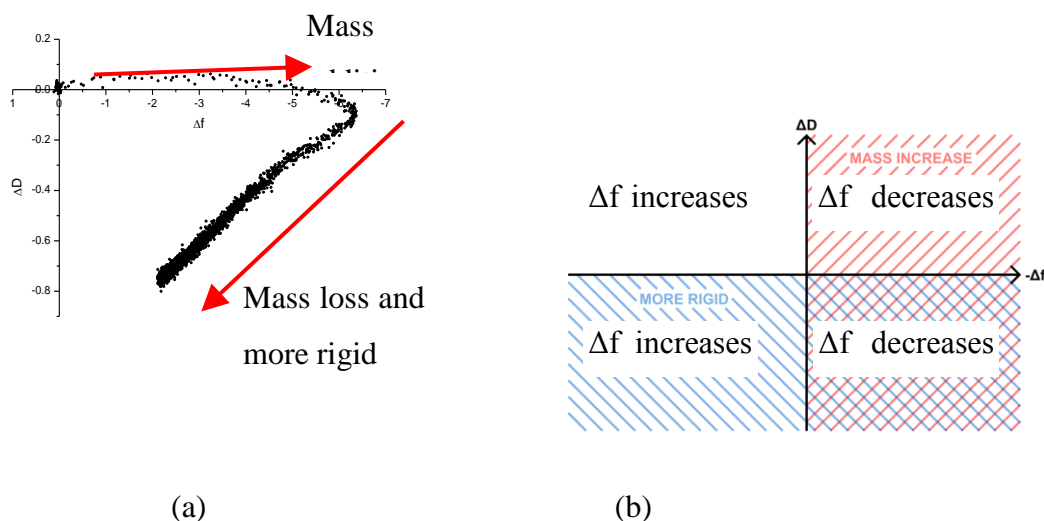


Figure 6.11. (a) A typical analysed $\Delta f - \Delta D$ plot. (b) The general assumptions associated with the shift in frequency and dissipation factor.

6.3 Results and discussion

Interaction between tested neuropeptides and biomimetic membranes were monitored *in situ* by QCM-D. The data were analysed to give insight into the mechanism of the interaction of each peptide with the corresponding membranes.

6.3.1 Riparin 1 and signiferin 1

All experiments with riparin 1 and signiferin 1 were carried out using eukaryotic mimicking membranes (DMPC or DMPC-C (C: cholesterol)). A concentration study of the two peptides at 1, 10, 20, 50 and 75 μM on DMPC lipid membranes revealed that the binding of the two

peptides is concentration-dependent and saturated at 75 μM . The peptides began interaction with the lipid at the minimum concentration of 10 μM . Binding appears proportional to concentration as increasing peptide concentration causes an increase in the change of frequency corresponding to a growth in binding mass (Figure 6.12).

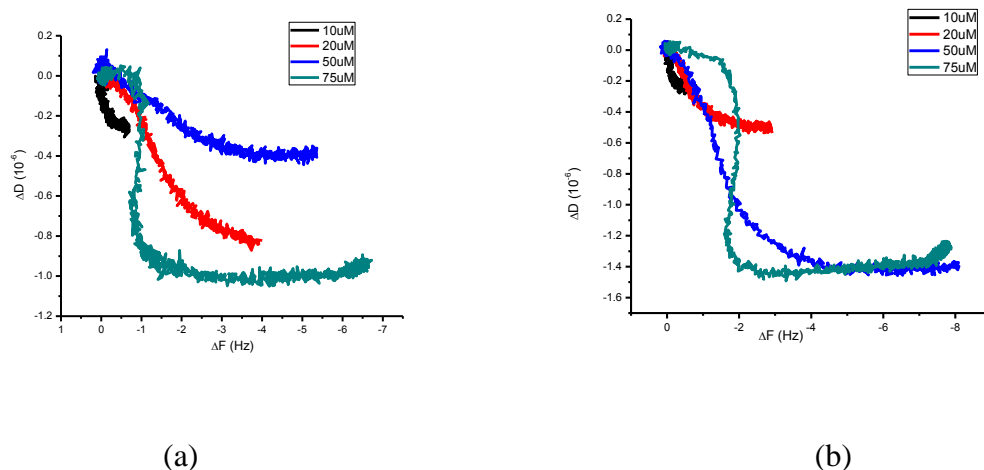


Figure 6.12. ΔD vs. Δf plot of (a) riparin 1 and (b) signiferin 1 at concentrations of 10, 20, 50 and 75 μM with DMPC lipid recorded on the 7th harmonic.

In general, riparin 1 and signiferin 1 interacted with the DMPC lipid bilayer in a three-state process (Figure 6.13). Firstly, they quickly bound to the membranes superficially and did not cause any change in dissipation. This was followed by a decrease in dissipation for both peptides which indicates that the insertion of each peptide or the peptide’s arrangement in the DMPC phospholipid layers makes the lipid more rigid. This coincided with a very small mass removal on the lipid surface as the frequency shift showed an increase only on the third harmonic in this stage. This may be a result of the removal of hydrating water molecules on the lipid surface due to the interaction of the peptides with the phosphate head groups of DMPC [608]. The final state revealed a deeper insertion of each peptide, characterised by the largest decrease in frequency for the ninth harmonic (larger harmonic probes closer to the surface of the chip).

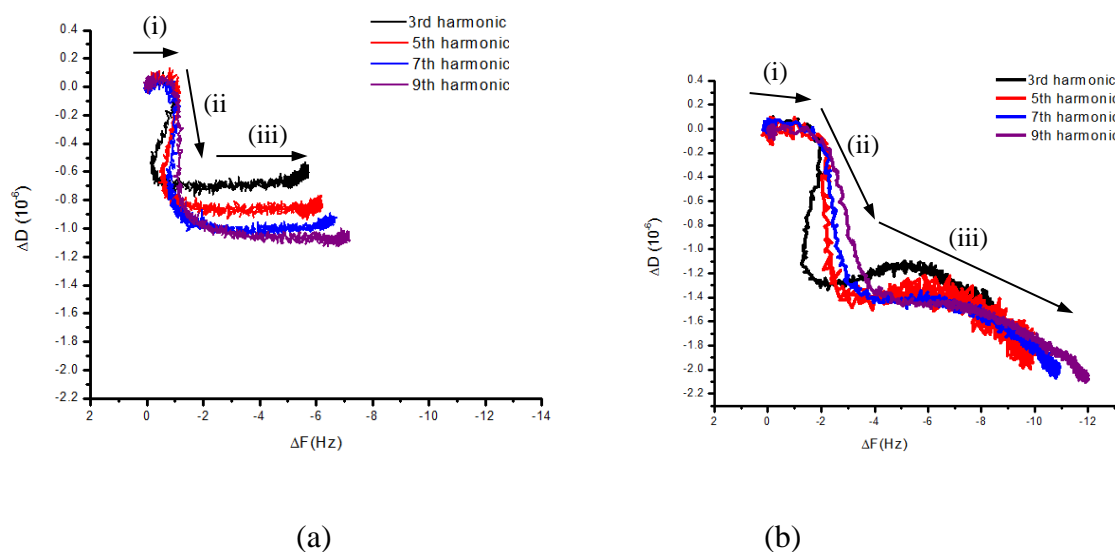


Figure 6.13. (a). ΔD vs. Δf plot of (a) riparin 1 and (b) signiferin 1 at a concentration $75 \mu\text{M}$ with DMPC lipid recorded on 3rd, 5th, 7th and 9th harmonics.

Although the disulfide containing peptides riparin 1 and signiferin 1 behaved quite similarly on the DMPC lipid bilayer, a detailed analysis of the data indicates some differences in their behaviour toward this lipid membrane. Since different overtones sense the change in frequency (and dissipation) at different distances from the surface of the quartz, frequency shifts at different harmonics provide a means to characterise mass change as a function of distance from the chip surface [609-611]. Both riparin 1 and signiferin 1 started interaction with a vertical transmembrane insertion in the first stage as the frequency shift measured by all harmonics was the same (no difference in binding mass for all overtones Figure 6.14 (i)). However, the second stage (indicated by two-end arrows Figure 6.14 (ii)) showed a mass removal with diverging harmonics for both peptides indicating that the mass disruption at different distances from the chip surface was not the same. While riparin 1 caused a mass loss only for the 3rd and 5th harmonic, signiferin 1 was observed to cause a mass loss for all harmonics. This suggests that riparin 1 only expelled solvent molecules coupled to the lipid's surface, whereas signiferin 1 experienced an asymmetrical mass disruption throughout its insertion thickness. The frequency shift of signiferin 1 descends from the 3rd to 9th overtone indicating that the mass disruption of signiferin 1 was a maximum on the membrane surface and declines as the distance from the quartz surface decreases. Even though the second stage was followed by a further mass deposition for both peptides (Figure 6.14 (iii)), after that, the frequency discrepancy between overtone 3rd and 9th of signiferin 1 was much larger than that of riparin 1. This means that signiferin 1 interacted strongly with

not only solvent molecules but also phosphate head groups of the lipid bilayer in the second step. Thus, the interaction between signiferin 1 and the surface of the DMPC bilayer is more pronounced than that of riparian 1.

In addition, signiferin 1 binds to DMPC lipid faster than riparian 1 in both stage 1 and stage 3 since the maximum frequency change for signiferin 1 is nearly 2 Hz/min, while that for riparian 1 is nearly 1 Hz/min (Figure 6.15). At the same concentration, signiferin 1 causes slightly more change in dissipation than riparian 1. This implies that signiferin 1 makes the DMPC bilayer more rigid upon its binding than riparian 1 does.

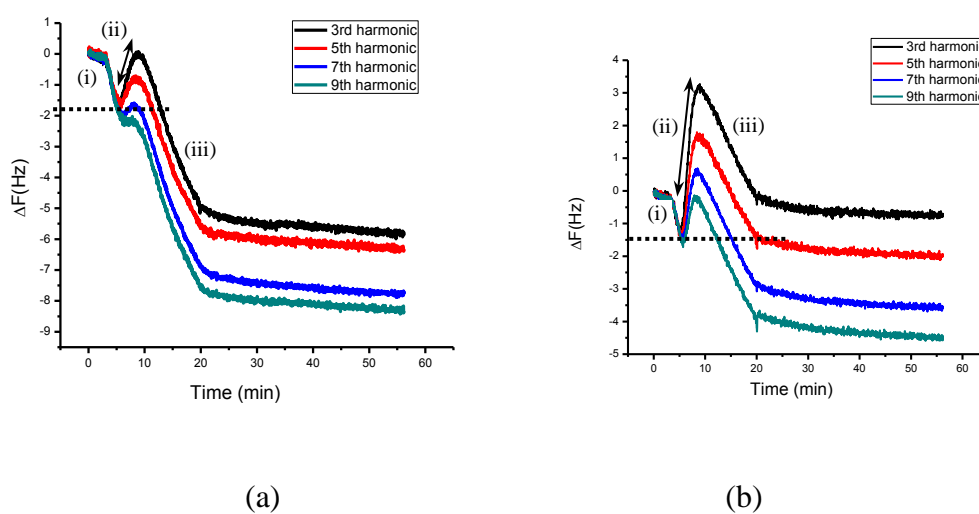
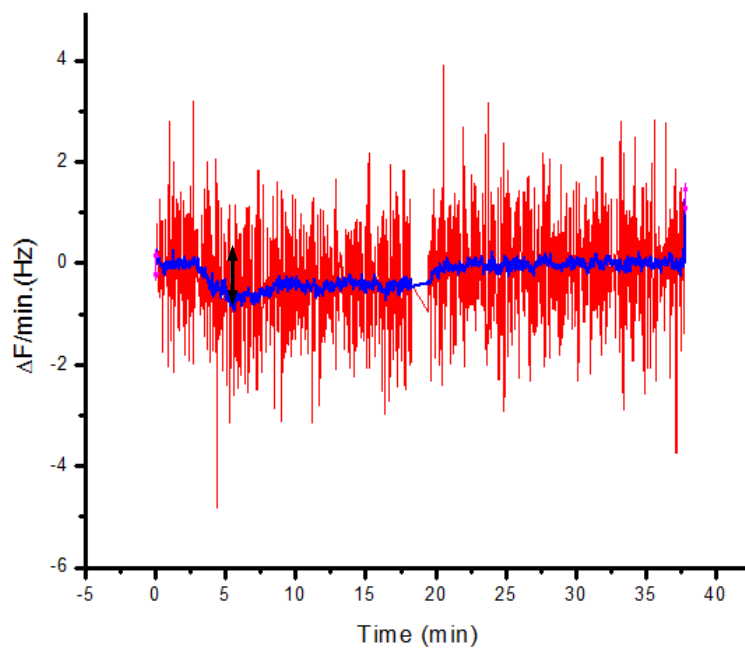
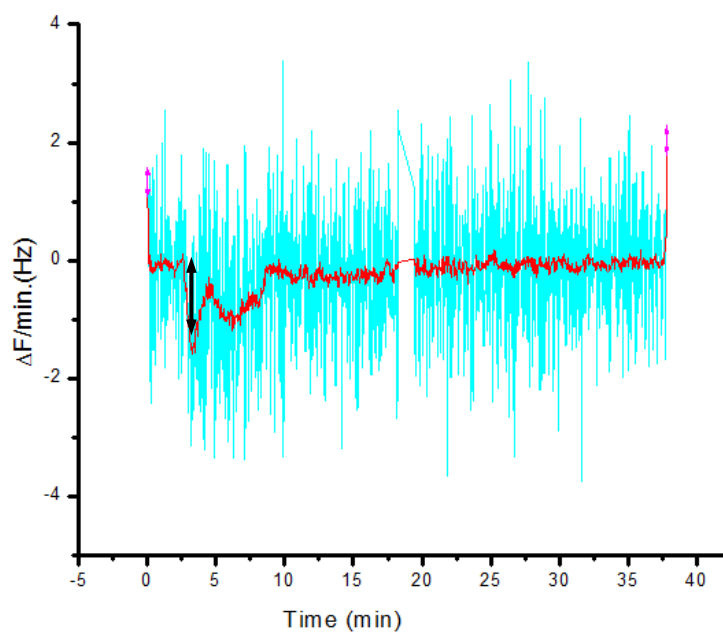


Figure 6.14. Change in Δf versus time on introduction of 75 μM of (a) riparian 1 and (b) signiferin 1 to DMPC membrane.



(a)



(b)

Figure 6.15. Binding rate of (a) riparin 1 and (b) signiferin 1 at a concentration of 75 μM . The maximum binding rates in the first stage of the binding are shown by two-end arrows.

On the other hand, the two peptides interacted with a DMPC-C bilayer in very simple mode. The frequencies increased by the same amount for all four harmonics, suggesting a trans-membrane binding of the two peptides to the DMPC-C bilayer (Figure 6.16). The dissipation was almost unchanged throughout the whole binding process. The incorporation of cholesterol into DMPC lipid bilayers made the bilayer more condensed as phospholipid molecules are more oriented and ordered in the presence of cholesterol [612-614], and thus the peptide binding could not change the membrane viscoelasticity significantly. Again, signiferin 1 produced a slightly more pronounced effect on dissipation than did riparin 1.

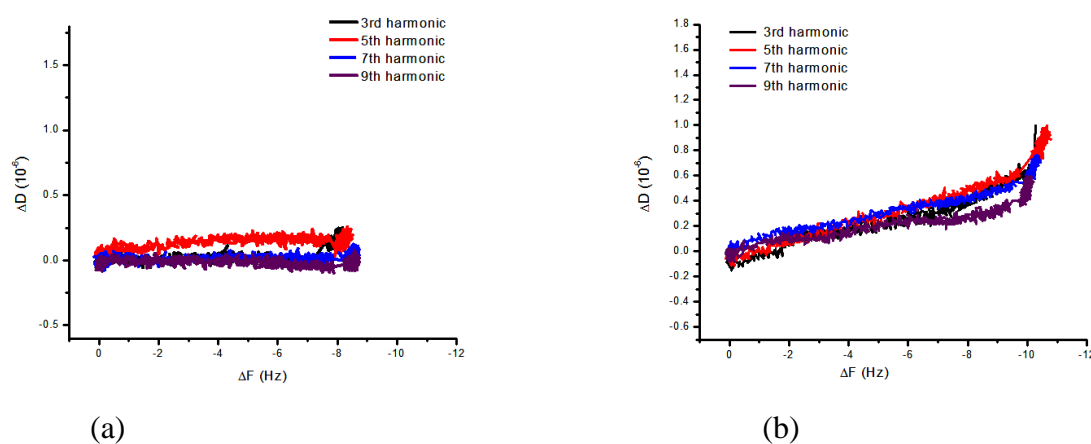


Figure 6.16. Interaction of riparin 1 (a) and signiferin 1 (b) with DMPC-C on different overtones.

In summary, both riparin 1 and signiferin 1 bound to DMPC in a 3-step process: (i) superficial binding, (ii) dispersion of energy in the environment (more rigid) occurring with mass removal and (iii) more mass absorption onto the bilayer. The surface mass removal in the second stage of signiferin 1 binding is more pronounced than that of riparin 1, suggesting that signiferin 1 has more interaction with the surface of the lipid bilayer than does riparin 1. On the other hand, both peptides bind to DMPC-C without changing the properties of the lipid bilayer.

The QCM results show some agreement with the conclusion drawn by a solid state NMR study [615] which reported that signiferin 1 interacted more with the phosphate head groups of a phospholipid bilayer than riparin 1. In contrast, riparin 1 inserted further into *one leaflet* of the bilayer than did signiferin 1. The QCM results cannot unambiguously define how deep each peptide inserts into the DMPC/DMPC-C lipid bilayer. In addition,

experimental conditions and lipid materials used are not identical for the QCM and NMR techniques. In solid state NMR, the peptides were mixed with the DMPC lipid (in 1:10 molar ratio) and then the solvent was evaporated to leave the mixture of the peptides and lipid in solid state, while in this study, the peptides were continuously passing through the DMPC lipid which were deposited on the surface of the chips. In addition, 19.1°C was the temperature used for QCM experiments instead of 25°C as mentioned in the NMR study. The transition temperature of DMPC is 23°C, so if the QCM experiments were carried out at 25°C, DMPC lipid would be in liquid crystalline form making the lipid deposition difficult and ineffective [616]. Finally, the DMPC lipid has been used in the form of multi-lamellar vesicles in the NMR study, whereas for QCM lipid bilayers are deposited on the surface of the chips.

6.3.2 Tryptophyllin 3.1 [FPWP(NH₂)] and kynurenine-tetrapeptide [FPKynL(NH₂)]

No binding was found when tryptophyllin 3.1 and kynurenine tetrapeptide were tested on the two mammalian membrane mimicking materials DMPC and DMPC-C for a range of concentrations up to 75 µM. Experiments have therefore been carried out on the model bacterial membrane containing DMPC and DMPG (4:1 v/v). Both peptides showed modest binding with DMPC:DMPG with the maximum frequency shift for tryptophyllin 3.1 and kynurenine tetrapeptide around 5 and 10 Hz, respectively (Figure 6.17). The change in frequency varied slightly for different harmonics with the largest frequency shift corresponding to the third overtone (detecting furthest from the chip's surface). The mass distribution of the peptides across the thickness of the lipid bilayer was not very different and largest at the membrane surface. This suggests that the peptides bind to the membrane surface and insert partially into the lipid bilayer. The PBS buffer wash, denoted by the star to the end of the process in Figure 6.19, removed some 20% of the peptide from the membrane indicating that the binding is partly reversible [617-618]. Replacing the peptide solution with PBS solution caused 30% of the membrane-bound peptides to diffuse to solution to compensate for the concentration lost.

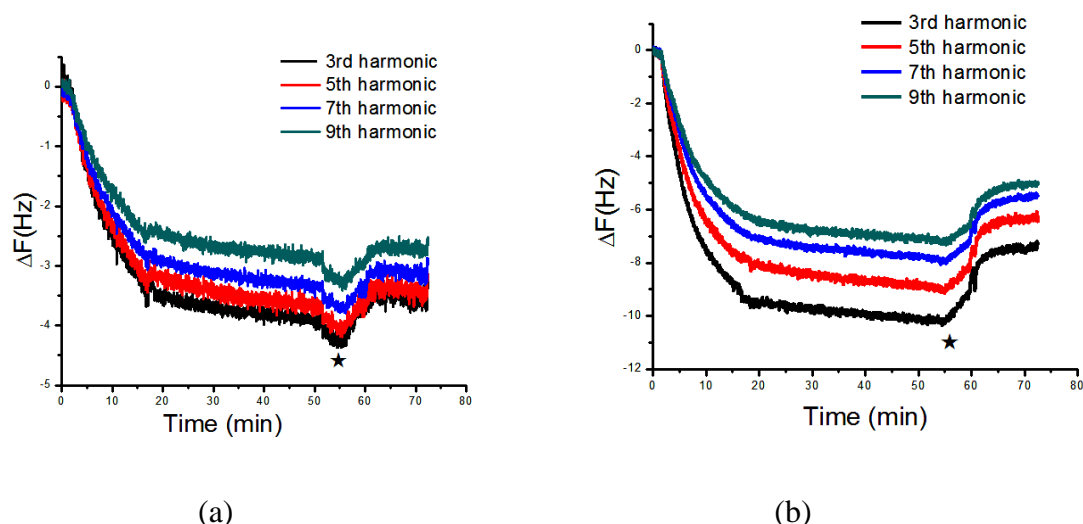


Figure 6.17. Change in frequency with time on introduction of 50 μM solution of (a) tryptophyllin 3.1 and (b) kynurenine tetrapeptide into the DMPC:DMPG lipid.

Binding of the peptides to the lipid bilayers was accompanied by an increase in dissipation indicating that the addition of peptides makes the membrane less dense (Figure 6.18). In terms of interaction mechanism, tryptophyllin 3.1 and kynurenine tetrapeptide acted similarly towards DMPC:DMPG lipid bilayers but the binding capacities were different as the kynurenine tetrapeptide showed twice the change in frequency compared to tryptophyllin 3.1 at the same concentration (Figure 6.19).

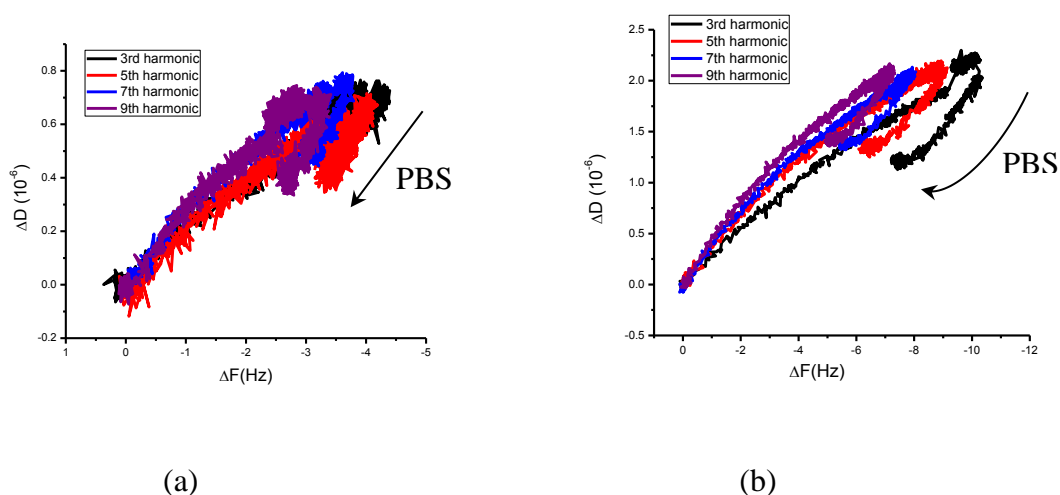


Figure 6.18. ΔD vs. Δf plot of (a) tryptophyllin 3.1 and (b) kynurenin tetrapeptide (50 μM) bound to bacterial membrane recorded on 3rd, 5th, 7th and 9th harmonics.

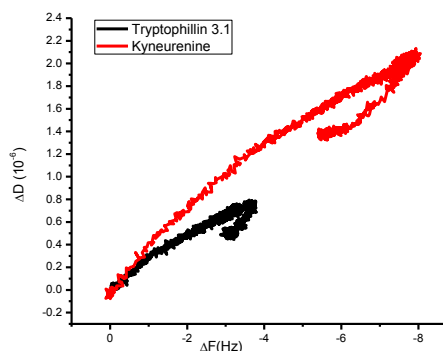
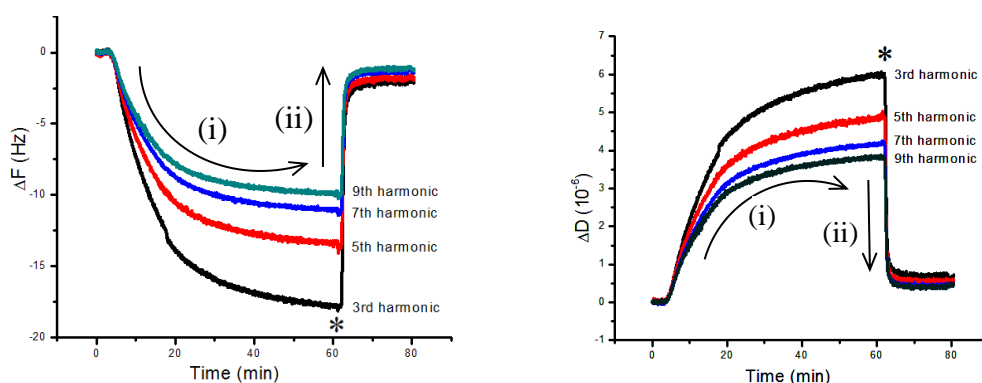


Figure 6.19. Interactions of tryptophillin 3.1 and kyneurenine tetrapeptide (50 μM) with DMPC:DMPG lipid recorded on 7th harmonic.

6.3.3 Tachykinin peptides: *iso*-Asp uperin 1.1 [pEA*iso*-DPNAFYGLM(NH₂)] and uperolein [pEPDPNAFYGLM(NH₂)]

The *iso*-Asp3 modification of uperin 1:1 (*iso*-Asp3 uperin 1.1) and uperolein are respectively the most smooth-muscle-contracting active synthetic and natural of all known tachykinin peptides [536]. They showed negligible interaction with DMPC membranes but better interaction with DMPC-C. *iso*-Asp3 uperin 1.1 interacted with DMPC-C in a simple mechanism with the binding of the peptide accompanied by a decrease in rigidity of the lipid membrane (increase in dissipation factor) (Figure 6.20c). The mass distribution of *iso*-Asp3 uperin 1.1 was very different across the membrane. The spreading of the overtones with frequency change decreased from the third harmonic to the ninth harmonic indicates a surface binding mode (Figure 6.20a (i)). This binding was reversible since 90% of the membrane-bound peptide was removed if a PBS wash was performed after peptide loading (Figure 6.20a (ii)). This reversible process was observed for all concentrations of *iso*-Asp3 uperin 1.1 tested (Figure 6.20d).



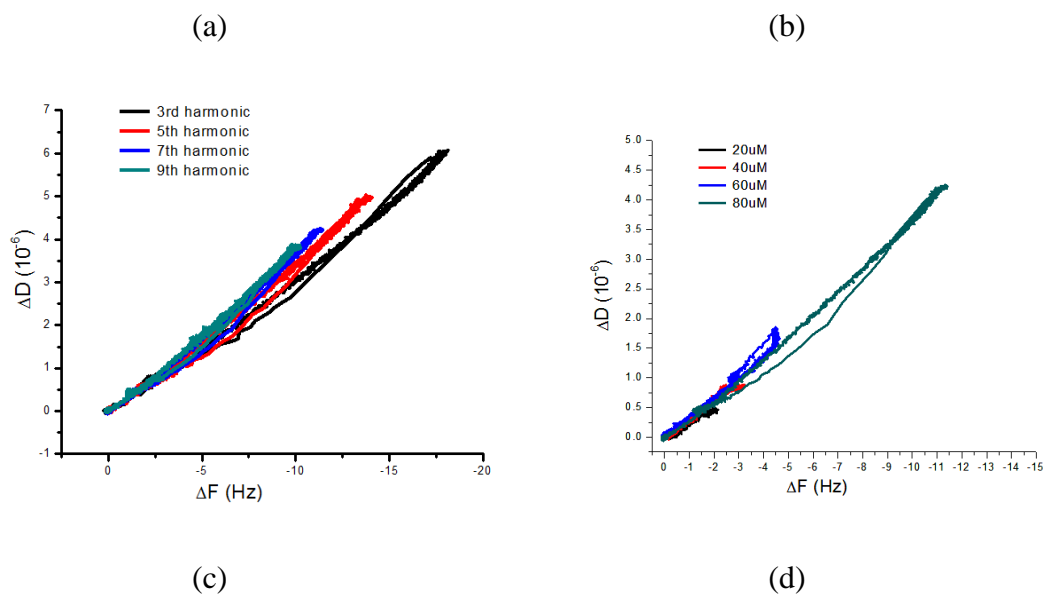


Figure 6.20. Interactions of *iso*-Asp3 uperin 1.1 with a DMPC-C membrane. Δf vs. time (a), ΔD vs. time (b), ΔD vs. Δf (c) of a 80 μM solution; and ΔD vs. Δf (d) of *iso*-Asp3 uperin 1.1 at 4 different concentrations (20, 40, 60 and 80 μM).

On the other hand, uperolein displayed a quite complicated mode of action on the mammalian DMPC-C membrane model. At low concentration, it showed a transmembrane insertion since the frequency changes for all overtones were slightly different. The third overtone recorded the least change, suggesting mass removal of solvent on the surface of the lipid (Figure 6.21a). However, at higher concentrations (above 50 μM), uperolein interacted with the DMPC-C membrane in a surface mode similar to that of *iso*-Asp3 uperin 1.1 (Figure 6.21b). The change in dissipation was different from low to high peptide concentrations (Figure 6.21c). Low concentrations caused a light decrease in dissipation indicating the insertion of uperolein made the lipid membrane more rigid, while high concentration showed a growth in dissipation suggesting a loss in rigidity of the lipid membrane.

Uperolein seemed not to behave with a concentration dependence on the DMPC-C membrane if the PBS wash was not included. However, the Δf - ΔD plots for a range of concentrations with PBS wash included revealed that the binding at all concentrations was highly reversible and the *overall* mass addition of peptide was proportional to the peptide concentration (Figure 6.21d).

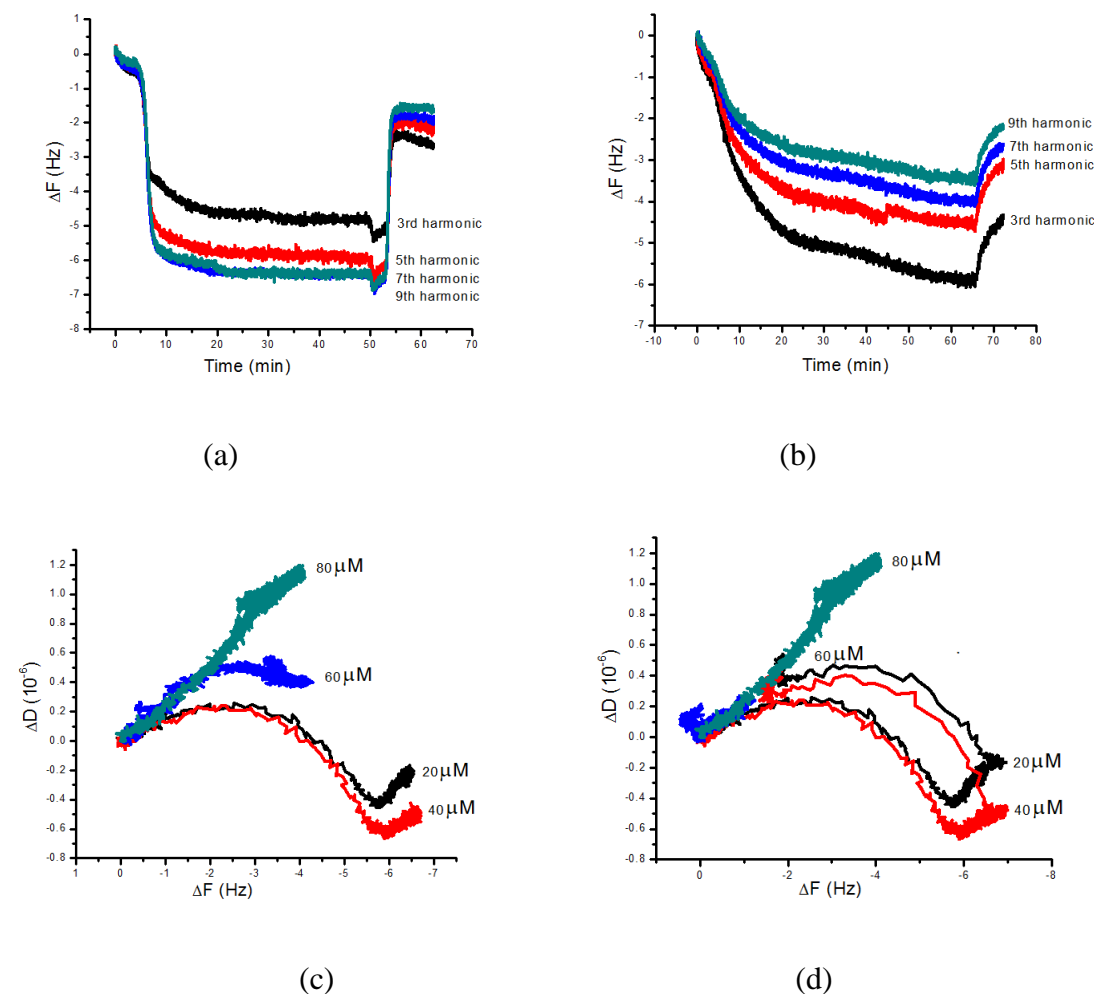


Figure 6.21. Interactions of uperolein with a DMPC-C membrane. Δf vs. time at concentration of 20 μM (a) and 80 μM (b). ΔD vs. Δf at 4 different concentrations (20, 40, 60 and 80 μM) without PBS wash (c) and with PBS wash (d).

6.3.4 Rothein 1 and its synthetic modifications

The experiments involving rothein 1 and its synthetic modifications were only implemented with DMPC lipid. The maximum concentration of these peptides tested was 50 μM and even at this concentration the binding of these peptides to DMPC was negligible as the change of frequency was less than 3 Hz and there was a diminutive change of dissipation. This is in agreement with solid state NMR results which also indicated no binding to the model eukaryotic membrane.

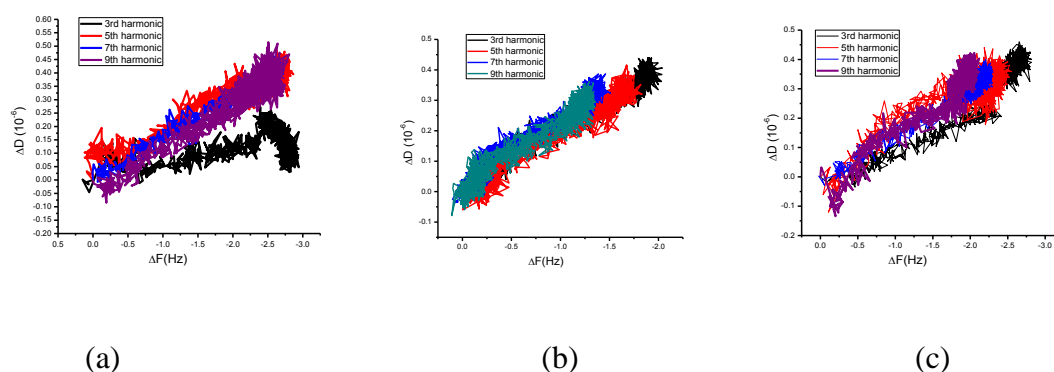


Figure 6.22. ΔD vs. Δf plot of rothein 1 (a), rothein 1.1 (b) and rothein 1.2 (c) at a concentration of 50 μM .

6.4 Discussion and conclusion

The Wimley-White experiment-based interfacial hydrophobicity scale [580-581] (see Table 6.2), which was extrapolated from studying membrane-binding of small monomeric peptides (< 30 amino acids) with unfolded structures in the aqueous phase, has provided a basis for explaining the difference in membrane-binding behaviour of the peptides observed by QCM-D. Considering Table 6.3, it is clear that, in general, riparin 1 and signiferin 1 possess the most favourable features to bind with lipid membranes. Both have a total net charge of +1 (while other peptides have total net charge of -1), which favours the interaction with negatively charged and zwitterionic phospholipids due to electrostatic attraction to the phosphate head groups.

The process of transferring riparin 1 and signiferin 1 from water to the water-membrane interface is exothermic by 4.22 and 5.02 kJ mol^{-1} respectively (Table 6.3), which are more favourable interface migrations than those of the other peptides. The free energies for transferring riparin 1 and signiferin 1 to the membrane hydrophobic core are -15.44 and -13.69 kJ mol^{-1} respectively (lowest ΔG values in Table 6.3). Thus, the hydrophobic interaction for these peptides is the most energetically favourable processes of all peptides investigated. Although the interface-association of signiferin 1 is slightly better than riparin 1, riparin 1 is transferred to the hydrophobic environment more readily (by 1.67 kJ mol^{-1}) than signiferin 1. This explains the higher tendency of signiferin 1 to interact with the membrane surface than riparin 1. In contrast, the penetration of riparin 1 into the

hydrophobic core of the mammalian model phosphate bilayers is more stable than that of signiferin 1.

Table 6.3. Free energies for transferring the studied peptides from water to 1-palmitoyl-2-oleoylphosphatidylcholine (POPC) interface (wif) and to hydrophobic environment n-octanol (woct) based on the Wimley-White hydrophobicity scale [580].

Peptide	Sequence	Charge	ΔG_{wif} (kJ mol ⁻¹)	ΔG_{woct} (kJ mol ⁻¹)
Riparin 1	RLCIPVIFPC(OH)	+1	-4.22	-15.11
Signiferin 1	RLCIPYIIPC(OH)	+1	-5.02	-13.69
Rothein 1:	SVSNIPESIGF(OH)	-1	+7.46	+11.47
Rothein 1.1:	AVSNIPESIGF(OH)	-1	+7.66	+11.64
Rothein 1.2:	SVANIPESIGF(OH)	-1	+7.66	+11.64
<i>Iso</i> -Asp3 uperin 1:1	pEA(isoD)PNAFYGLM(NH ₂)	-1	-1.76	+10.67
Uperolein	pEPDPNAFYGLM(NH ₂)	-1	-0.59	+9.14
Tryptophyllin 3.1	FPWP(NH ₂)	-1	+3.85	+6.19
Kynurenine-tetrapeptide	FPKynL(NH ₂)	-1	-0.37	+0.37

Structural studies of riparin 1 and signiferin 1 in TFE/H₂O 1:1 by 2D NMR showed that both belong to the β -turn class with the only difference being the direction of the N-termini (Figure 6.23) [534]. While the N-terminus in signiferin 1 is oriented toward the turn region, the situation is opposite for riparin 1. This renders signiferin 1 of higher charge density than riparin 1 as the former’s structure is more compact, which adds to the rationale of the better membrane-surface association of signiferin 1.

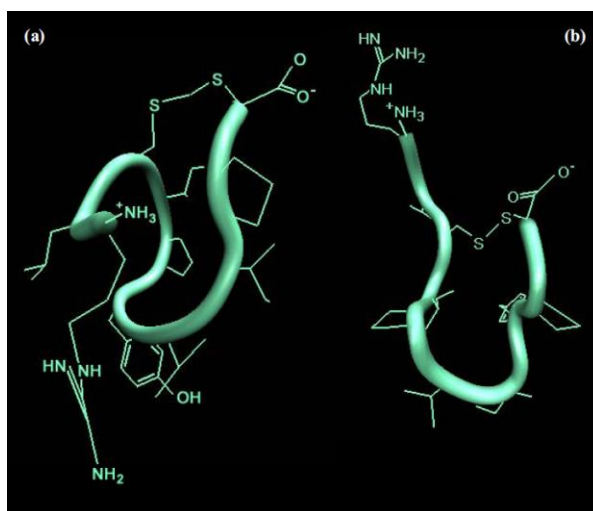


Figure 6.23. Signiferin 1 (a) and riparin 1 (b) in TFA/H₂O by 2D NMR. Adapted from [534].

The membrane binding of rothein and its modifications are least favourable since the total free energy costs for phase transfer of these peptides ΔG_{wif} and ΔG_{woct} are most positive (Table 6.3). The free energy to transfer any rothein from aqueous solution to the water-membrane interface and lipid hydrophobic phase are about $+7 \text{ kJ mol}^{-1}$ and $+11 \text{ kJ mol}^{-1}$, respectively. These data support the observation of no membrane binding of these peptides by solid state NMR and QCM-D.

The binding of the two tachykinin peptides to DMPC-C are insignificant because their interactions are weak to either the surface or to the hydrophobic core of the model membrane. This may be because each possesses a net charge of -1, a small negative free energy for water-membrane interface and a positive value for hydrophobic phase interaction. Therefore, they are easily washed off when a PBS wash is included. In addition, the difference in secondary structures of uperolein and *isoAsp3* uperin 1.1 in a lipid environment may contribute to the difference in their binding mechanisms to DMPC-C membranes. In dodecylphosphocholine (DPC) lipid micelles, *isoAsp3* uperin 1:1 is more random coiled and open [536] while uperolein was calculated to be 80% α helical [619]. The helical structure of uperolein enables a higher ability to associate with the water-membrane interface and membrane hydrophobic phase than *isoAsp3* uperin 1:1. Thus, at low concentrations this peptide partially penetrates into the model lipid bilayer while *isoAsp3* uperin 1:1 binds to the bilayer surface. However, uperolein aggregates readily at high concentration in PBS buffer (as mentioned in Experimental section 5.1). Thus, at the concentration of more than $60 \mu\text{M}$,

this effect may cause uperolein to accumulate more on the membrane surface, affecting the shift of membrane binding mechanism from insertion to surface association.

Finally, the tryptophyllins are the odd ones out since they show no interaction with the model mammalian membranes but associate with bacterial mimicking phospholipids to a small extent. The increase in total negative charge on the membrane surface, as DMPC is replaced by DMPC:DMPG, cannot be the reason for the preference of these peptides to bind to this model membrane since they both contain the total charge of -1. However, the introduction of DMPG into the lipid bilayers has been reported to cause changes in the mechanical properties of the model membranes, namely area compression/expansion modulus K_a , bending modulus K_b and the spontaneous radius of curvature R_o , which affect the binding abilities of these small peptides [620-621].

Even though all the studied peptides are known to exert their activities via G-coupled receptors located in the mammalian membrane, the binding of these peptides to eukaryotic mimicking membranes was not observed consistently. The peptide-membrane interaction thus may not be a prerequisite step for all the peptides to act on membrane receptors. For riparin 1, signiferin 1 and two tachykinin peptides, the difference in the overall charges, the charge densities, the secondary structures and the free energies of phase transferring (to the water-membrane interface and membrane interior) of these peptides can rationalise the difference in their lipid-bilayer binding behaviours observed by QCM. However, the contribution of the difference in membrane binding to the varied biological activities of the peptides is not certain.

Tryptophyllin and rothein peptides show bioactivity at eukaryotic receptors without interacting with the neutral model membranes. This suggests that these peptides may not follow the membrane-associated receptor binding pathway, or the models of mammalian lipid bilayers used in this study may not reflect fully the sophisticated properties of real eukaryotic membranes, which thus cannot facilitate the membrane binding of these peptides. Models of membranes are typically created by mixing main lipid components and neglect a level of micro-inhomogeneity of the corresponding real membranes, such as lipid raft, a small percentage of other lipids or cholesterol [622]. These contributions may change the features of the lipid membranes such as the membrane potential and the mechanical properties, thus affecting the interaction of peptides with the membrane.

Finally, other techniques such as AFM or SPR would be recommended to be used in concert with the QCM method in order to provide a more precise conclusion about membrane interaction of the selected neuropeptides.

6.5 Experimental

6.5.1 Peptides

All peptides were synthesised by GenScript, Piscataway, NJ, USA using L-amino acids. Synthetic peptides were all of more than 90% purity, and shown to be identical to their natural counterparts by high performance liquid chromatography and electrospray ionization mass spectrometry.

All peptides were firstly dissolved in milliQ water to make up 1 mM stock solutions, which were diluted further to obtain desired concentrations by using high salt phosphate buffer saline (PBS) before introduction to QCM cells.

Due to the insolubility of tachykinins in milliQ water at high concentration, 100 μ M tachykinins stock solutions were prepared instead of 1 mM. Tachykinin solutions were sonicated for 3 minutes before use to ensure the complete dissolution.

6.5.2 Buffers and solvents

Sodium chloride, potassium phosphate monobasic and potassium phosphate dibasic were purchased from Sigma-Aldrich. Ultrapure water with a resistivity of 18.2 M Ω cm was used (Sartorius, Gottingen, Germany). Chloroform (ACS Reagent \geq 99.8%) and methanol (HPLC grade \geq 99.9%) were purchased from Sigma-Aldrich (Sydney, Australia).

Absolute ethanol, acetone, propan-2-ol, and hydrogen peroxide (30%) were purchased from Merck (Melbourne, Australia). Ammonia solution (28%) was purchased from Ajax Finechem (Sydney, Australia). 3-mercapto-propionic acid (MPA; HPLC grade \geq 99%) was purchased from Fluka, BioChimica (Buchs, Switzerland).

Phosphate saline buffer (PBS) high salt contains KH_2PO_4 0.013 M and K_2HPO_4 0.0065 M and NaCl 0.1 M.

Phosphate saline buffer (PBS) low salt contains KH_2PO_4 0.013 M and K_2HPO_4 0.0065 M and NaCl 0.03 M.

6.5.3 Liposome preparation

DMPC and cholesterol were dissolved in chloroform and DMPG in chloroform/methanol (75:25 v/v) to produce individual stock solutions of 5 mM concentration. These stock solutions were then mixed with the following ratios for the three model membrane types: mammalian model membrane (1) DMPC (100), (2) DMPC-C (80:20 w/w) and bacterial model membrane (3) DMPC-DMPG (80:20 v/v). 100 μl of each solution was then aliquoted into test tubes and evaporated under a gentle stream of nitrogen gas to yield a thin lipid film, which was dried in a vacuum desiccator for 40 minutes. The lipids were resuspended in 1 ml of high salt saline buffer (20 mM PBS + 100 mM NaCl at pH 6.9), vortexed and sonicated. PBS high salt buffer (4 ml) was added to each tube to make a total volume of 5 ml lipid solution before introduction to the QCM chip.

Although all the experiments have been done with great care, it was difficult to reproduce exactly the same conditions of sonication. Thus, variation of liposome size between batches produced at different times was not unusual. In addition, small vesicles of lipids are inherently unstable and will spontaneously fuse to form larger vesicles when stored below their phase transition temperature.

6.5.4 Chip cleaning and modification

Chips were cleaned by placing into a 1:1:3 mixture of ammonia, hydrogen peroxide and water at 75°C for 20 mins, rinsed with ultra-pure water and ethanol, then dried under a gentle stream of nitrogen gas and immediately assembled into the QCM chamber.

Surfaces of the gold-coated quartz chips were modified by 3-mercaptopropionic acid (MPA) (1 mM) in *isopropanol* for 20 mins to form a self-assembled monolayer of a uniform negatively charged surface. This enhances the interaction between the surface of the chip and hydrophilic parts of liposomes. The chips were then washed with *isopropanol* and dried with a stream of nitrogen gas before being assembled into QCM-D cells.

6.5.5 QCM experiments

A typical experiment taking place in the QCM-D instrument involves two basic steps: (i) lipid deposition on the modified chips and (ii) introduction of peptides and subsequent monitoring of the peptide-membrane interaction. Four different measurements on 4 quartz chips can take place simultaneously at the same temperature (19.1°C) with the lipid and peptide compositions for each chip varied.

Lipid deposition was achieved by purging 5 ml of lipid solutions (prepared as mentioned previously) through the system with a flow rate of 50 µl/min. The loaded lipids in liposome form were then ruptured to form lipid bilayers by applying PBS low salt buffer. The chips in QCM cells were flushed with PBS until the system reached equilibrium (no change in frequency and dissipation observed). The peptide solution (1 ml) was allowed to flow through the cells with a flow rate of 50 µl/min, and left to incubate with the lipid bilayer for 30 mins. Finally, the cells were washed with PBS to remove any peptide residue that did not bind to the lipid bilayer.

QCM experiments were repeated 3-4 times for each peptide and at each concentration. For the same lipid mass, the peptide response was reproducible within 1 Hz.

This study was carried out on the Q-SENSE E4 system. The sensor crystals used were 5 MHz, AT-cut, polished chips with evaporated gold sensor surface. The frequency and dissipation measurements were performed at the third (15 MHz), fifth (25 MHz), seventh (35 MHz) and the ninth (45 MHz) harmonics. The first harmonic was excluded because it is very sensitive to the flow changes within the cell and thus generates unreliable data.

Experimental data were analysed by graphing software Origin 7.5 (OriginLab, Northampton, MA). Three graphing methods were used to display and interpret QCM results. $\Delta f-t$ and $\Delta D-t$ were used to track the change in frequency and dissipation with time for all harmonics at a certain concentration. The y-axis is Δf (or ΔD) instead of f (or D) value as they are normalised by the values at the start of the experiment ($\Delta f_{\text{at time}=t} = f_{\text{at time}=t} - f_{\text{at time}=0}$). The $\Delta f-\Delta D$ plot presents the change in mass and structure of the base (lipid coated quartz chip) upon the addition of peptide. Each point on the plots represents the values of Δf and ΔD at a particular point in time. Δf values are plotted in reverse on the x-axis (+ \rightarrow -) to reflect mass increase and ΔD values are plotted on the y-axis corresponding to the change in viscoelasticity of the base. A typical $\Delta f - \Delta D$ plot is depicted in Figure 6.11 [617]. In this

study, some plots present the time window which starts when the peptide was introduced into the cell and ends before the PBS wash, while others include the PBS wash if the wash causes desorption of binding material.

REFERENCE

- [1] Grant, S. G. and Blackstock, W. P. Proteomics in neuroscience: from protein to network. *J. Neurosci.*, **2001**, 21, 8315-8318.
- [2] Cobon, G. S., Verrills, N., Papakostopoulos, P., Eastwood, H. and Linnane, A. W. The proteomics of ageing. *Biogerontology*, **2002**, 3, 133-136.
- [3] Dhingra, V., Gupta, M., Andacht, T. and Fu, Z. F. New frontiers in proteomics research: a perspective. *Int. J. Pharm.*, **2005**, 299, 1-18.
- [4] Walsh, C. T., Garneau-Tsodikova, S. and Gatto, G. J. Protein posttranslational modifications: the chemistry of proteome diversifications. *Angew. Chem. Int. Ed.*, **2005**, 44, 7342-7372.
- [5] Black, D. L. Mechanisms of alternative pre-messenger RNA splicing. *Annu. Rev. Biochem.*, **2003**, 72, 291-336.
- [6] Kannicht, C. and Fuchs, B., Post-Translational Modifications of Proteins. Springer, Totowa, USA, **2008**.
- [7] Walther, T. C. and Mann, M. Mass spectrometry-based proteomics in cell biology. *J. Cell Bio.*, **2010**, 190, 491-500.
- [8] Domon, B. and Aebersold, R. Mass spectrometry and protein analysis. *Science*, **2006**, 312, 212-217.
- [9] Aebersold, R. and Mann, M. Mass spectrometry-based proteomics. *Nature*, **2003**, 422, 198-207.
- [10] Barber, M., Bordoli, R. S., Elliott, G. J., Sedgwick, R. D. and Tyler, A. N. Fast atom bombardment mass spectrometry. *Anal. Chem.*, **1982**, 54, 645-657.
- [11] Dole, M., Mack, L., Hines, R., Mobley, R., Ferguson, L. and Alice, M. B. Molecular beams of macroions. *J. Chem. Phys.*, **1968**, 49, 2240.
- [12] Fenn, J. B., Mann, M., Meng, C. K., Wong, S. F. and Whitehouse, C. M. Electrospray ionization for mass spectrometry of large biomolecules. *Science*, **1989**, 246, 64-71.
- [13] Fenn, J. B., Mann, M., Meng, C. K., Wong, S. F. and Whitehouse, C. M. Electrospray ionization—principles and practice. *Mass Spectrom. Rev.*, **1990**, 9, 37-70.
- [14] Macfarlane, R. and Torgerson, D. Californium-252 plasma desorption mass spectroscopy. *Science*, **1976**, 191, 920-925.
- [15] Biemann, K. Mass spectrometry of peptides and proteins. *Annu. Rev. Biochem.*, **1992**, 61, 977-1010.

- [16] Marshall, A. G., Hendrickson, C. L. and Jackson, G. S. Fourier transform ion cyclotron resonance mass spectrometry: a primer. *Mass Spectrom. Rev.*, **1998**, 17, 1-35.
- [17] Griffin, T. J. and Aebersold, R. Advances in proteome analysis by mass spectrometry. *J. Biol. Chem.*, **2001**, 276, 45497-45500.
- [18] de Hoffmann, E. Tandem mass spectrometry: a primer. *J. Mass Spectrom.*, **1996**, 31, 129-137.
- [19] Han, X., Aslanian, A. and Yates III, J. R. Mass spectrometry for proteomics. *Curr. Opin. Chem. Biol.*, **2008**, 12, 483-490.
- [20] Yost, R. and Enke, C. Triple quadrupole mass spectrometry for direct mixture analysis and structure elucidation. *Anal. Chem.*, **1979**, 51, 1251-1264.
- [21] Morris, H. R., Paxton, T., Dell, A., Langhorne, J., Berg, M., Bordoli, R. S., Hoyes, J. and Bateman, R. H. High sensitivity collisionally-activated decomposition tandem mass spectrometry on a novel quadrupole/orthogonal-acceleration time-of-flight mass spectrometer. *Rapid Commun. Mass Spectrom.*, **1996**, 10, 889-896.
- [22] Medzihradzky, K. F., Campbell, J. M., Baldwin, M. A., Falick, A. M., Juhasz, P., Vestal, M. L. and Burlingame, A. L. The characteristics of peptide collision-induced dissociation using a high-performance MALDI-TOF/TOF tandem mass spectrometer. *Anal. Chem.*, **2000**, 72, 552-558.
- [23] Hager, J. W. A new linear ion trap mass spectrometer. *Rapid Commun. Mass Spectrom.*, **2002**, 16, 512-526.
- [24] Scigelova, M. and Makarov, A. Orbitrap mass analyzer-overview and applications in proteomics. *Proteomics*, **2006**, 6, 16-21.
- [25] Zubarev, R. A. and Makarov, A. Orbitrap mass spectrometry. *Anal. Chem.*, **2013**, 85, 5288-5296.
- [26] Perry, R. H., Cooks, R. G. and Noll, R. J. Orbitrap mass spectrometry: instrumentation, ion motion and applications. *Mass Spectrom. Rev.*, **2008**, 27, 661-699.
- [27] Schwartz, J. C., Senko, M. W. and Syka, J. E. A two-dimensional quadrupole ion trap mass spectrometer. *J. Am. Chem. Soc. Mass Spectrom.*, **2002**, 13, 659-669.
- [28] Yates, J. R., Ruse, C. I. and Nakorchevsky, A. Proteomics by mass spectrometry: approaches, advances, and applications. *Annu. Rev. Biomed. Eng.*, **2009**, 11, 49-79.
- [29] Mitchell, W. J. and McLuckey, S. A. Collision-Induced Dissociation (CID) of Peptides and Proteins. *Meth. Enzymol.*, **2005**, 402, 148-185.
- [30] Mabud, M. A., Dekrey, M. J. and Cooks, G. R. Surface-induced dissociation of molecular ions. *Int. J. Mass Spectrom* **1985**, 67, 285-294.

- [31] Brodbelt, J. S. and Wilson, J. J. Infrared multiphoton dissociation in quadrupole ion traps. *Mass Spectrom. Rev.*, **2009**, 28, 390-424.
- [32] Reilly, J. P. Ultraviolet photofragmentation of biomolecular ions. *Mass Spectrom. Rev.*, **2009**, 28, 425-447.
- [33] Kalcic, C. L., Gunaratne, T. C., Jones, A. D., Dantus, M. and Reid, G. E. Femtosecond laser-induced ionization/dissociation of protonated peptides. *J. Am. Chem. Soc.*, **2009**, 131, 940-942.
- [34] Cooper, H. J., Håkansson, K. and Marshall, A. G. The role of electron capture dissociation in biomolecular analysis. *Mass Spectrom. Rev.*, **2005**, 24, 201-222.
- [35] Zubarev, R. A., Kelleher, N. L. and McLafferty, F. W. Electron capture dissociation of multiply charged protein cations. A nonergodic process. *J. Am. Chem. Soc.*, **1998**, 120, 3265-3266.
- [36] McLafferty, F. W., Horn, D. M., Breuker, K., Ge, Y., Lewis, M. A., Cerda, B., Zubarev, R. A. and Carpenter, B. K. Electron capture dissociation of gaseous multiply charged ions by Fourier-transform ion cyclotron resonance. *J. Am. Chem. Soc. Mass Spectrom.*, **2001**, 12, 245-249.
- [37] Wiesner, J., Premisler, T. and Sickmann, A. Application of electron transfer dissociation (ETD) for the analysis of posttranslational modifications. *Proteomics*, **2008**, 8, 4466-4483.
- [38] Kim, M. S. and Pandey, A. Electron transfer dissociation mass spectrometry in proteomics. *Proteomics*, **2012**, 12, 530-542.
- [39] Fung, Y. E., Adams, C. M. and Zubarev, R. A. Electron ionization dissociation of singly and multiply charged peptides. *J. Am. Chem. Soc.*, **2009**, 131, 9977-9985.
- [40] Lioe, H. and Richard, A. Comparison of collision-induced dissociation and electron-induced dissociation of singly protonated aromatic amino acids, cystine and related simple peptides using a hybrid linear ion trap-FT-ICR mass spectrometer. *Anal. Bioanal. Chem.*, **2007**, 389, 1429-1437.
- [41] Palumbo, A. M., Smith, S. A., Kalcic, C. L., Dantus, M., Stemmer, P. M. and Reid, G. E. Tandem mass spectrometry strategies for phosphoproteome analysis. *Mass Spectrom. Rev.*, **2011**, 30, 600-625.
- [42] Wu, C., Tran, J. C., Zamdborg, L., Durbin, K. R., Li, M., Ahlf, D. R., Early, B. P., Thomas, P. M., Sweedler, J. V. and Kelleher, N. L. A protease for 'middle-down' proteomics. *Nat. Methods*, **2012**, 9, 822-824.
- [43] Fuerstenau, S. D., Benner, W. H., Thomas, J. J., Brugidou, C., Bothner, B. and Siuzdak, G. Mass spectrometry of an intact virus. *Angew. Chem. Int. Ed.*, **2001**, 40, 541-544.
- [44] Yamashita, M. and Fenn, J. B. Negative ion production with the electrospray ion source. *J. Phys. Chem.*, **1984**, 88, 4671-4675.

- [45] Yamashita, M. and Fenn, J. B. Electrospray ion source. Another variation on the free-jet theme. *J. Phys. Chem.*, **1984**, 88, 4451-4459.
- [46] Kebarle, P. and Verkerk, U. H., On the Mechanism of Electrospray Ionization Mass Spectrometry (ESIMS), in *Electrospray and MALDI Mass Spectrometry*, (ed. by Richard, B. C.), New York, John Wiley and Sons, **2010**, pp. 3-63.
- [47] Kebarle, P. A brief overview of the present status of the mechanisms involved in electrospray mass spectrometry. *J. Mass Spectrom.*, **2000**, 35, 804-817.
- [48] Kebarle, P. and Tang, L. From ions in solution to ions in the gas phase-the mechanism of electrospray mass spectrometry. *Anal. Chem.*, **1993**, 65, 972A-986A.
- [49] Felitsyn, N., Peschke, M. and Kebarle, P. Origin and number of charges observed on multiply-protonated native proteins produced by ESI. *Int. J. Mass Spectrom.*, **2002**, 219, 39-62.
- [50] Iribarne, J. and Thomson, B. On the evaporation of small ions from charged droplets. *J. Chem. Phys.*, **1976**, 64, 2287.
- [51] Griffiths, W., Jonsson, A., Liu, S., Rai, D. and Wang, Y. Electrospray and tandem mass spectrometry in biochemistry. *Biochem. J.*, **2001**, 355, 545-561.
- [52] Winger, B. E., Light-Wahl, K. J., Ogorzalek Loo, R. R., Udseth, H. R. and Smith, R. D. Observation and implications of high mass-to-charge ratio ions from electrospray ionization mass spectrometry. *J. Am. Chem. Soc.*, **1993**, 115, 536-545.
- [53] Amad, M. H., Cech, N. B., Jackson, G. S. and Enke, C. G. Importance of gas-phase proton affinities in determining the electrospray ionization response for analytes and solvents. *J. Mass Spectrom.*, **2000**, 35, 784-789.
- [54] Loo, R. R. O. and Smith, R. D. Proton transfer reactions of multiply charged peptide and protein cations and anions. *J. Mass Spectrom.*, **1995**, 30, 339-347.
- [55] Kebarle, P. and Verkerk, U. H. Electrospray: from ions in solution to ions in the gas phase, what we know now. *Mass Spectrom. Rev.*, **2009**, 28, 898-917.
- [56] Hautreux, M., Hue, N., Du Fou de Kerdaniel, A., Zahir, A., Malec, V. and Laprévotte, O. Under non-denaturing solvent conditions, the mean charge state of a multiply charged protein ion formed by electrospray is linearly correlated with the macromolecular surface. *Int. J. Mass Spectrom.*, **2004**, 231, 131-137.
- [57] Davidson, W. and Kebarle, P. Binding energies and stabilities of potassium ion complexes from studies of the gas phase ion equilibria $K^+ + M \rightleftharpoons K^+ \cdot M$. *J. Am. Chem. Soc.*, **1976**, 98, 6133-6138.
- [58] Hoyau, S., Norrman, K., McMahon, T. and Ohanessian, G. A quantitative basis for a scale of Na^+ affinities of organic and small biological molecules in the gas phase. *J. Am. Chem. Soc.*, **1999**, 121, 8864-8875.

- [59] McMahon, T. and Ohanessian, G. An experimental and *ab initio* study of the nature of the binding in gas-phase complexes of sodium ions. *Chem. Eur. J.*, **2000**, 6, 2931-2941.
- [60] Constantopoulos, T. L., Jackson, G. S. and Enke, C. G. Effects of salt concentration on analyte response using electrospray ionization mass spectrometry. *J. Am. Chem. Soc. Mass Spectrom.*, **1999**, 10, 625-634.
- [61] Tang, L. and Kebarle, P. Dependence of ion intensity in electrospray mass spectrometry on the concentration of the analytes in the electrosprayed solution. *Anal. Chem.*, **1993**, 65, 3654-3668.
- [62] Cech, N. B. and Enke, C. G. Relating electrospray ionization response to nonpolar character of small peptides. *Anal. Chem.*, **2000**, 72, 2717-2723.
- [63] Enke, C. G. A predictive model for matrix and analyte effects in electrospray ionization of singly-charged ionic analytes. *Anal. Chem.*, **1997**, 69, 4885-4893.
- [64] Ikonou, M. G., Blades, A. T. and Kebarle, P. Electrospray mass spectrometry of methanol and water solutions suppression of electric discharge with SF₆ gas. *J. Am. Chem. Soc. Mass Spectrom.*, **1991**, 2, 497-505.
- [65] Wampler, F. M., Blades, A. T. and Kebarle, P. Negative ion electrospray mass spectrometry of nucleotides: ionization from water solution with SF₆ discharge suppression. *J. Am. Chem. Soc. Mass Spectrom.*, **1993**, 4, 289-295.
- [66] Herskovits, T. T., Gadegbeku, B. and Jaillet, H. On the structural stability and solvent denaturation of proteins I. Denaturation by the alcohols and glycols. *J. Biol. Chem.*, **1970**, 245, 2588-2598.
- [67] Kaltashov, I. A. and Mohimen, A. Estimates of protein surface areas in solution by electrospray ionization mass spectrometry. *Anal. Chem.*, **2005**, 77, 5370-5379.
- [68] Wicar, S., Mulkerrin, M., Bathory, G., Khundkar, L. and Karger, B. Conformational changes in the reversed phase liquid chromatography of recombinant human growth hormone as a function of organic solvent: the molten globule state. *Anal. Chem.*, **1994**, 66, 3908-3915.
- [69] Iavarone, A. T. and Williams, E. R. Mechanism of charging and supercharging molecules in electrospray ionization. *J. Am. Chem. Soc.*, **2003**, 125, 2319-2327.
- [70] Šamalikova, M. and Grandori, R. Protein charge-state distributions in electrospray-ionization mass spectrometry do not appear to be limited by the surface tension of the solvent. *J. Am. Chem. Soc.*, **2003**, 125, 13352-13353.
- [71] Šamalikova, M. and Grandori, R. Testing the role of solvent surface tension in protein ionization by electrospray. *J. Mass Spectrom.*, **2005**, 40, 503-510.
- [72] Iavarone, A. T., Jurchen, J. C. and Williams, E. R. Supercharged protein and peptide ions formed by electrospray ionization. *Aal. Chem.*, **2001**, 73, 1455-1460.

- [73] Iavarone, A. T., Jurchen, J. C. and Williams, E. R. Effects of solvent on the maximum charge state and charge state distribution of protein ions produced by electrospray ionization. *J. Am. Chem. Soc. Mass Spectrom.*, **2000**, 11, 976-985.
- [74] Wilm, M. and Mann, M. Analytical properties of the nanoelectrospray ion source. *Anal. Chem.*, **1996**, 68, 1-8.
- [75] Wilm, M. S. and Mann, M. Electrospray and Taylor-Cone theory, Dole's beam of macromolecules at last?. *Int. J. Mass Spectrom. Ion Processes*, **1994**, 136, 167-180.
- [76] Juraschek, R., Dülcks, T. and Karas, M. Nanoelectrospray- more than just a minimized-flow electrospray ionization source. *J. Am. Chem. Soc. Mass Spectrom.*, **1999**, 10, 300-308.
- [77] Schmidt, A., Karas, M. and Dülcks, T. Effect of different solution flow rates on analyte ion signals in nano-ESI MS, or: when does ESI turn into nano-ESI? *J. Am. Chem. Soc. Mass Spectrom.*, **2003**, 14, 492-500.
- [78] Chernushevich, I., Bahr, U. and Karas, M. Nanospray 'taxation' and how to avoid it. *Rapid Commun. Mass Spectrom.*, **2004**, 18, 2479-2485.
- [79] Valaskovic, G. A., Utley, L., Lee, M. S. and Wu, J.-T. Ultra-low flow nanospray for the normalization of conventional liquid chromatography/mass spectrometry through equimolar response: standard-free quantitative estimation of metabolite levels in drug discovery. *Rapid Commun. Mass Spectrom.*, **2006**, 20, 1087-1096.
- [80] Warriner, R. N., Craze, A. S., Games, D. E. and Lane, S. J. Capillary electrochromatography/mass spectrometry- a comparison of the sensitivity of nanospray and microspray ionization techniques. *Rapid Commun. Mass Spectrom.*, **1998**, 12, 1143-1149.
- [81] Wysocki, V. H., Resing, K. A., Zhang, Q. and Cheng, G. Mass spectrometry of peptides and proteins. *Methods*, **2005**, 35, 211-222.
- [82] Downard, K., Mass Spectrometry A Foundation Course. The Royal Society of Chemistry, Cambridge, UK, **2004**.
- [83] Chernushevich, I. V., Loboda, A. V. and Thomson, B. A. An introduction to quadrupole-time-of-flight mass spectrometry. *J. Mass Spectrom.*, **2001**, 36, 849-865.
- [84] Gross, M. L., Chen, G. and Pramanik, B., Protein and Peptide Mass Spectrometry in Drug Discovery. John Wiley & Sons, **2011**.
- [85] Bruins, A. P., ESI source design and dynamic range considerations, in *Electrospray Ionization Mass Spectrometry, Fundamentals, Instrumentation & Applications*, (ed. by Cole, R. B.), New York, Wiley-Interscience, **1997**, pp. 107-136.
- [86] Gundry, R. L., White, M. Y., Murray, C. I., Kane, L. A., Fu, Q., Stanley, B. A. and Van Eyk, J. E. Preparation of Proteins and Peptides for Mass Spectrometry Analysis in a Bottom-Up Proteomics Workflow. *Curr. Protoc. Mol. Biol.*, **2009**, 10.25. 11-10.25. 23.

- [87] Meleady, P., 2D gel electrophoresis and mass spectrometry identification and analysis of proteins, in *Gene Expression Profiling*, Springer, **2011**, pp. 123-137.
- [88] O'Farrell, P. H. High resolution two-dimensional electrophoresis of proteins. *J. Biol. Chem.*, **1975**, 250, 4007-4021.
- [89] Gygi, S. P., Corthals, G. L., Zhang, Y., Rochon, Y. and Aebersold, R. Evaluation of two-dimensional gel electrophoresis-based proteome analysis technology. *Proc. Natl. Acad. Sci. U. S. A.*, **2000**, 97, 9390-9395.
- [90] Tal, M., Silberstein, A. and Nusser, E. Why does Coomassie Brilliant Blue R interact differently with different proteins? A partial answer. *J. Biol. Chem.*, **1985**, 260, 9976-9980.
- [91] Compton, S. J. and Jones, C. G. Mechanism of dye response and interference in the Bradford protein assay. *Anal. Biochem.*, **1985**, 151, 369-374.
- [92] Neuhoff, V., Stamm, R., Pardowitz, I., Arold, N., Ehrhardt, W. and Taube, D. Essential problems in quantification of proteins following colloidal staining with coomassie brilliant blue dyes in polyacrylamide gels, and their solution. *Electrophoresis*, **1990**, 11, 101-117.
- [93] Richert, S., Luche, S., Chevallet, M., Van Dorsselaer, A., Leize-Wagner, E. and Rabilloud, T. About the mechanism of interference of silver staining with peptide mass spectrometry. *Proteomics*, **2004**, 4, 909-916.
- [94] Patton, W. F. A thousand points of light: the application of fluorescence detection technologies to two-dimensional gel electrophoresis and proteomics. *Electrophoresis*, **2000**, 21, 1123-1144.
- [95] Mackintosh, J. A., Choi, H. Y., Bae, S. H., Veal, D. A., Bell, P. J., Ferrari, B. C., Van Dyk, D. D., Verrills, N. M., Paik, Y. K. and Karuso, P. A fluorescent natural product for ultra sensitive detection of proteins in one-dimensional and two-dimensional gel electrophoresis. *Proteomics*, **2003**, 3, 2273-2288.
- [96] Chevalier, F., Centeno, D., Rofidal, V., Tauzin, M., Martin, O., Sommerer, N. and Rossignol, M. Different impact of staining procedures using visible stains and fluorescent dyes for large-scale investigation of proteomes by MALDI-TOF mass spectrometry. *J. Proteome Res.*, **2006**, 5, 512-520.
- [97] Lauber, W. M., Carroll, J. A., Dufield, D. R., Kiesel, J. R., Radabaugh, M. R. and Malone, J. P. Mass spectrometry compatibility of two-dimensional gel protein stains. *Electrophoresis*, **2001**, 22, 906-918.
- [98] Wirth, P. J. and Romano, A. Staining methods in gel electrophoresis, including the use of multiple detection methods. *J. Chromatogr. A*, **1995**, 698, 123-143.
- [99] Rabilloud, T. and Lelong, C. Two-dimensional gel electrophoresis in proteomics: a tutorial. *J. Proteome.*, **2011**, 74, 1829-1841.
- [100] Hancock, W. S., Handbook of HPLC for the separation of amino acids, peptides, and proteins. CRC press, **1984**.

- [101] Mant, C. T. and Hodges, R. S., High-performance liquid chromatography of peptides and proteins: separation, analysis, and conformation. CRS Press, **1991**.
- [102] Garcia, M. The effect of the mobile phase additives on sensitivity in the analysis of peptides and proteins by high-performance liquid chromatography–electrospray mass spectrometry. *J. Chromatogr. B* **2005**, 825, 111-123.
- [103] Yoshida, T. Peptide separation by hydrophilic-interaction chromatography: a review. *J. Biochem. Biophys. Methods.*, **2004**, 60, 265-280.
- [104] Williams, D. H. a. F., I, Spectroscopic Methods in Organic Chemistry. McGraw-Hill Book Co., London, **1995**.
- [105] Shevchenko, A., Henrik Tomas, J. H., sbreve, Olsen, J. V. and Mann, M. In-gel digestion for mass spectrometric characterization of proteins and proteomes. *Nat. Protoc.* , **2007**, 1, 2856-2860.
- [106] Medzihradszky, K. F. In-Solution Digestion of Proteins for Mass Spectrometry. *Methods in enzymology*, **2005**, 405, 50-65.
- [107] Dunn, M. J., Electroelution of proteins from polyacrylamide gels, in *Protein Purification Protocols*, Springer, **1996**, pp. 357-362.
- [108] Jenö, P. and Horst, M., Electroelution of proteins from polyacrylamide gels, in *The Protein Protocols Handbook*, Springer, **1996**, pp. 207-214.
- [109] Smith, J. A. Electroelution of proteins from stained gels. *Curr. Protoc. Immuno.*, **2002**, 8.8. 1-8.8. 5.
- [110] Biringer, R. G., Amato, H., Harrington, M. G., Fonteh, A. N., Riggins, J. N. and Hühmer, A. F. Enhanced sequence coverage of proteins in human cerebrospinal fluid using multiple enzymatic digestion and linear ion trap LC-MS/MS. *Brief. Funct. Genomic Proteomic* **2006**, 5, 144-153.
- [111] Schlosser, A., Vanselow, J. T. and Kramer, A. Mapping of phosphorylation sites by a multi-protease approach with specific phosphopeptide enrichment and NanoLC-MS/MS analysis. *Anal. Chem.*, **2005**, 77, 5243-5250.
- [112] Wu, C., Tran, J. C., Zamdborg, L., Durbin, K. R., Li, M., Ahlf, D. R., Early, B. P., Thomas, P. M., Sweedler, J. V. and Kelleher, N. L. A protease for 'middle-down' proteomics. *Nat. Methods.*, **2012**, 9, 822-824.
- [113] Wada, Y. and Kadoya, M. In-gel digestion with endoproteinase LysC. *J. Mass Spectrom.*, **2003**, 38, 117-118.
- [114] Vermachova, M., Purkrtova, Z., Santrucek, J., Jolivet, P., Chardot, T. and Kodicek, M., Combining Chymotrypsin/Trypsin Digestion to Identify Hydrophobic Proteins from Oil Bodies, in *Plant Proteomics*, Springer, **2014**, pp. 185-198.

- [115] Medzihradzky, K., Maltby, D., Hall, S., Settineri, C. and Burlingame, A. Characterization of protein N-glycosylation by reversed-phase microbore liquid chromatography/electrospray mass spectrometry, complementary mobile phases, and sequential exoglycosidase digestion. *J. Am. Chem. Soc. Mass Spectrom.*, **1994**, 5, 350-358.
- [116] Pitt, J. J. Principles and applications of liquid chromatography-mass spectrometry in clinical biochemistry. *Clin. Biochem. Rev.*, **2009**, 30, 19.
- [117] McLafferty, F. W., Breuker, K., Jin, M., Han, X., Infusini, G., Jiang, H., Kong, X. and Begley, T. P. Top-down MS, a powerful complement to the high capabilities of proteolysis proteomics. *FEBS J.*, **2007**, 274, 6256-6268.
- [118] Kelleher, N. L., Lin, H. Y., Valaskovic, G. A., Aaserud, D. J., Fridriksson, E. K. and McLafferty, F. W. Top down versus bottom up protein characterization by tandem high-resolution mass spectrometry. *J. Am. Chem. Soc.*, **1999**, 121, 806-812.
- [119] Shaw, J. B., Li, W., Holden, D. D., Zhang, Y., Griep-Raming, J., Fellers, R. T., Early, B. P., Thomas, P. M., Kelleher, N. L. and Brodbelt, J. S. Complete protein characterization using top-down mass spectrometry and ultraviolet photodissociation. *J. Am. Chem. Soc.*, **2013**, 135, 12646-12651.
- [120] Yan, X., Essaka, D. C., Sun, L., Zhu, G. and Dovichi, N. J. Bottom-up proteome analysis of E. coli using capillary zone electrophoresis-tandem mass spectrometry with an electrokinetic sheath-flow electrospray interface. *Proteomics*, **2013**, 13, 2546-2551.
- [121] Zhang, Y., Cui, W., Zhang, H., Dewald, H. D. and Chen, H. Electrochemistry-Assisted Top-Down Characterization of Disulfide-Containing Proteins. *Anal. Chem.*, **2012**, 84, 3838-3842.
- [122] Kelleher, N. L. Top-down proteomics. *Anal. Chem.*, **2004**, 76, 196 A-203 A.
- [123] Kaltashov, I. A., Bobst, C. E., Abzalimov, R. R., Wang, G., Baykal, B. and Wang, S. Advances and challenges in analytical characterization of biotechnology products: mass spectrometry-based approaches to study properties and behavior of protein therapeutics. *Biotech. Adv.*, **2012**, 30, 210-222.
- [124] Hughes, C., Ma, B. and Lajoie, G. A., De novo sequencing methods in proteomics, in *Proteome Bioinformatics*, Springer, **2010**, pp. 105-121.
- [125] Ma, B., Zhang, K., Hendrie, C., Liang, C., Li, M., Doherty-Kirby, A. and Lajoie, G. PEAKS: powerful software for peptide de novo sequencing by tandem mass spectrometry. *Rapid Commun. Mass Spectrom.*, **2003**, 17, 2337-2342.
- [126] Horn, D. M., Zubarev, R. A. and McLafferty, F. W. Automated de novo sequencing of proteins by tandem high-resolution mass spectrometry. *Proc. Natl. Acad. Sci. USA*, **2000**, 97, 10313-10317.
- [127] Craig, R. and Beavis, R. C. Tandem: matching proteins with tandem mass spectra. *Bioinformatics*, **2004**, 20, 1466-1467.

- [128] Nesvizhskii, A. I., Keller, A., Kolker, E. and Aebersold, R. A statistical model for identifying proteins by tandem mass spectrometry. *Anal. Chem.*, **2003**, 75, 4646-4658.
- [129] Johnson, R. S., Davis, M. T., Taylor, J. A. and Patterson, S. D. Informatics for protein identification by mass spectrometry. *Methods*, **2005**, 35, 223-236.
- [130] Taylor, J. A. and Johnson, R. S. Sequence database searches via de novo peptide sequencing by tandem mass spectrometry. *Rapid Commun. Mass Spectrom.*, **1997**, 11, 1067-1075.
- [131] Mann, M. and Wilm, M. Error-tolerant identification of peptides in sequence databases by peptide sequence tags. *Anal. Chem.*, **1994**, 66, 4390-4399.
- [132] Eng, J. K., McCormack, A. L. and Yates, J. R. An approach to correlate tandem mass spectral data of peptides with amino acid sequences in a protein database. *J. Am. Chem. Soc. Mass Spectrom.*, **1994**, 5, 976-989.
- [133] Cottrell, J. and London, U. Probability-based protein identification by searching sequence databases using mass spectrometry data. *Electrophoresis*, **1999**, 20, 3551-3567.
- [134] Zhang, N., Aebersold, R. and Schwikowski, B. ProBID: a probabilistic algorithm to identify peptides through sequence database searching using tandem mass spectral data. *Proteomics*, **2002**, 2, 1406-1412.
- [135] Yates III, J. R., Eng, J. K., McCormack, A. L. and Schieltz, D. Method to correlate tandem mass spectra of modified peptides to amino acid sequences in the protein database. *Anal. Chem.*, **1995**, 67, 1426-1436.
- [136] Yates III, J. R., Eng, J. K. and McCormack, A. L. Mining genomes: correlating tandem mass spectra of modified and unmodified peptides to sequences in nucleotide databases. *Anal. Chem.*, **1995**, 67, 3202-3210.
- [137] Eng, J. K., Fischer, B., Grossmann, J. and MacCoss, M. J. A fast SEQUEST cross correlation algorithm. *J. Proteome Res.*, **2008**, 7, 4598-4602.
- [138] MacCoss, M. J., Wu, C. C. and Yates, J. R. Probability-based validation of protein identifications using a modified SEQUEST algorithm. *Anal. Chem.*, **2002**, 74, 5593-5599.
- [139] Geer, L. Y., Markey, S. P., Kowalak, J. A., Wagner, L., Xu, M., Maynard, D. M., Yang, X., Shi, W. and Bryant, S. H. Open mass spectrometry search algorithm. *J. Proteome Res.*, **2004**, 3, 958-964.
- [140] Papayannopoulos, I. A. The interpretation of collision-induced dissociation tandem mass spectra of peptides. *Mass Spectrom. Rev.*, **1995**, 14, 49-73.
- [141] Boyd, R. and Somogyi, Á. The mobile proton hypothesis in fragmentation of protonated peptides: a perspective. *J. Am. Chem. Soc. Mass Spectrom.*, **2010**, 21, 1275-1278.

- [142] Wysocki, V. H., Tsaprailis, G., Smith, L. L. and Breci, L. A. Mobile and localized protons: a framework for understanding peptide dissociation. *J. Mass Spectrom.*, **2000**, 35, 1399-1406.
- [143] Paizs, B. and Suhai, S. Fragmentation pathways of protonated peptides. *Mass Spectrom. Rev.*, **2005**, 24, 508-548.
- [144] Bleiholder, C., Osburn, S., Williams, T. D., Suhai, S., Van Stipdonk, M., Harrison, A. G. and Paizs, B. I. Sequence-scrambling fragmentation pathways of protonated peptides. *J. Am. Chem. Soc.*, **2008**, 130, 17774-17789.
- [145] Ambihapathy, K., Yalcin, T., Leung, H. W. and Harrison, A. G. Pathways to immonium ions in the fragmentation of protonated peptides. *J. Mass Spectrom.*, **1997**, 32, 209-215.
- [146] Falick, A., Hines, W., Medzihradszky, K., Baldwin, M. and Gibson, B. Low-mass ions produced from peptides by high-energy collision-induced dissociation in tandem mass spectrometry. *J. Am. Chem. Soc. Mass Spectrom.*, **1993**, 4, 882-893.
- [147] Bradford, A. M., Waugh, R. J. and Bowie, J. H. Characterization of underivatized tetrapeptides by negative-ion fast-atom bombardment mass spectrometry. *Rapid Commun. Mass Spectrom.*, **1995**, 9, 677-685.
- [148] Steinborner, S. T. and Bowie, J. H. A Comparison of the Positive-and Negative-ion Mass Spectra of Bio-active Peptides from the Dorsal Secretion of the Australian Red Tree Frog, *Litoria rubella*. *Rapid Commun. Mass Spectrom.*, **1996**, 10, 1243-1247.
- [149] Boontheung, P., Brinkworth, C. S., Bowie, J. H. and Baudinette, R. V. Comparison of the positive and negative ion electrospray mass spectra of some small peptides containing pyroglutamate. *Rapid Commun. Mass Spectrom.*, **2002**, 16, 287-292.
- [150] Brinkworth, C. S., Dua, S. and Bowie, J. H. Backbone cleavages of (M-H)⁻ anions of peptides. Cyclisation of citropin 1 peptides involving reactions between the C-terminal [CONH]⁻ residue and backbone amide carbonyl groups. A new type of β cleavage: a joint experimental and theoretical study. *Rapid Commun. Mass Spectrom.*, **2002**, 16, 713-721.
- [151] Chass, G. A., Marai, C. N., Setiadi, D. H., Csizmadia, I. G. and Harrison, A. G. A Hartree-Fock, MP2 and DFT computational study of the structures and energies of b2 ions derived from deprotonated peptides. A comparison of method and basis set used on relative product stabilities. *J. mol. struct. Theochem*, **2004**, 675, 149-162.
- [152] Harrison, A. Sequence-specific fragmentation of deprotonated peptides containing H or alkyl side chains. *J. Am. Chem. Soc. Mass Spectrom.*, **2001**, 12, 1-13.
- [153] Harrison, A. G. Effect of phenylalanine on the fragmentation of deprotonated peptides. *J. Am. Chem. Soc. Mass Spectrom.*, **2002**, 13, 1242-1249.
- [154] Harrison, A. G. and Young, A. B. Fragmentation of deprotonated N-benzoylpeptides: formation of deprotonated oxazolones. *J. Am. Chem. Soc. Mass Spectrom.*, **2004**, 15, 446-456.

- [155] Steinborner, S. T. and Bowie, J. H. The negative ion mass spectra of $[M-H]^-$ ions derived from caeridin and dynastin peptides. Internal backbone cleavages directed through Asp and Asn residues. *Rapid Commun. Mass Spectrom.*, **1997**, 11, 253-258.
- [156] Bowie, J. H., Brinkworth, C. S. and Dua, S. Collision-induced fragmentations of the $(M-H)^-$ parent anions of underivatized peptides: An aid to structure determination and some unusual negative ion cleavages. *Mass Spectrom. Rev.*, **2002**, 21, 87-107.
- [157] Brinkworth, C. S., Dua, S., McAnoy, A. M. and Bowie, J. H. Negative ion fragmentations of deprotonated peptides: backbone cleavages directed through both Asp and Glu. *Rapid Commun. Mass Spectrom.*, **2001**, 15, 1965-1973.
- [158] Wang, T., Tran, N. T. T., Calabrese, A. N. and Bowie, J. H. Backbone fragmentations of $[M-H]^-$ anions from peptides. Reinvestigation of the mechanism of the beta prime cleavage. *Rapid Commun. Mass Spectrom.*, **2012**, 26, 1832-1840.
- [159] Waugh, R., Bowie, J. H. and Gross, M. Collision-Induced Dissociations of Deprotonated Peptides. Dipeptides Containing Asn, Arg and Lys. *Aust. J. Chem.*, **1993**, 46, 693-702.
- [160] Waugh, R. J., Bowie, J. H., Gross, M. L. and Vollmer, D. Collision induced dissociations of deprotonated peptides. Dipeptides and tripeptides containing proline. *Int. J. Mass Spectrom. Ion Processes*, **1994**, 133, 165-174.
- [161] Mann, M. and Jensen, O. N. Proteomic analysis of post-translational modifications. *Nat. Biotech.*, **2003**, 21, 255-261.
- [162] Nørregaard Jensen, O. Modification-specific proteomics: characterization of post-translational modifications by mass spectrometry. *Curr. Opin. Chem. Biol.*, **2004**, 8, 33-41.
- [163] Witze, E. S., Old, W. M., Resing, K. A. and Ahn, N. G. Mapping protein post-translational modifications with mass spectrometry. *Nat. Methods.*, **2007**, 4, 798-806.
- [164] Porath, J., Carlsson, J., Olsson, I. and Belfrage, G. Metal chelate affinity chromatography, a new approach to protein fractionation. *Nature*, **1975**, 258, 598-599.
- [165] Cuatrecasas, P. Protein purification by affinity chromatography derivatizations of agarose and polyacrylamide beads. *J. Biol. Chem.*, **1970**, 245, 3059-3065.
- [166] Zhang, W., Zhou, G., Zhao, Y., White, M. A. and Zhao, Y. Affinity enrichment of plasma membrane for proteomics analysis. *Electrophoresis*, **2003**, 24, 2855-2863.
- [167] Blagoev, B., Ong, S.-E., Kratchmarova, I. and Mann, M. Temporal analysis of phosphotyrosine-dependent signaling networks by quantitative proteomics. *Nat. Biotech.*, **2004**, 22, 1139-1145.
- [168] Villén, J., Beausoleil, S. A., Gerber, S. A. and Gygi, S. P. Large-scale phosphorylation analysis of mouse liver. *Proc. Natl. Acad. Sci. USA*, **2007**, 104, 1488-1493.

- [169] Zhang, Y., Wolf-Yadlin, A., Ross, P. L., Pappin, D. J., Rush, J., Lauffenburger, D. A. and White, F. M. Time-resolved mass spectrometry of tyrosine phosphorylation sites in the epidermal growth factor receptor signaling network reveals dynamic modules. *Mol. Cell Proteomics*, **2005**, 4, 1240-1250.
- [170] Garcia, B. A., Shabanowitz, J. and Hunt, D. F. Characterization of histones and their post-translational modifications by mass spectrometry. *Curr. Opin. Chem. Biol.*, **2007**, 11, 66-73.
- [171] Vishwanathan, K., Tackett, R. L., Stewart, J. T. and Bartlett, M. G. Determination of arginine and methylated arginines in human plasma by liquid chromatography–tandem mass spectrometry. *J. Chromatogr. B*, **2000**, 748, 157-166.
- [172] Monigatti, F., Hekking, B. and Steen, H. Protein sulfation analysis—a primer. *Biochim. Biophys. Acta*, **2006**, 1764, 1904-1913.
- [173] Carr, S. A., Huddleston, M. J. and Bean, M. F. Selective identification and differentiation of N- and O-linked oligosaccharides in glycoproteins by liquid chromatography-mass spectrometry. *Protein Sci.*, **1993**, 2, 183-196.
- [174] Wu, S.-L., Hühmer, A. F., Hao, Z. and Karger, B. L. On-line LC-MS approach combining collision-induced dissociation (CID), electron-transfer dissociation (ETD), and CID of an isolated charge-reduced species for the trace-level characterization of proteins with post-translational modifications. *J. Proteome Res.*, **2007**, 6, 4230-4244.
- [175] Delom, F. and Chevet, E. Phosphoprotein analysis: from proteins to proteomes. *Proteome science*, **2006**, 4, 15.
- [176] Collins, M. O., Yu, L. and Choudhary, J. S. Analysis of protein phosphorylation on a proteome-scale. *Proteomics*, **2007**, 7, 2751-2768.
- [177] Cieśla, J., Frączyk, T. and Rode, W. Phosphorylation of basic amino acid residues in proteins: important but easily missed. *Acta. Biochim. Pol.*, **2011**, 58, 137-148.
- [178] Matthews, H. R. Protein kinases and phosphatases that act on histidine, lysine, or arginine residues in eukaryotic proteins: a possible regulator of the mitogen-activated protein kinase cascade. *Pharmacol. Ther.*, **1995**, 67, 323-350.
- [179] Klumpp, S. and Krieglstein, J. Phosphorylation and dephosphorylation of histidine residues in proteins. *Eur. J. Biochem.*, **2002**, 269, 1067-1071.
- [180] Collins, M. O., Yu, L. and Choudhary, J. S. Analysis of protein phosphorylation on a proteome scale. *Proteomics*, **2007**, 7, 2751-2768.
- [181] Johnson, L. The regulation of protein phosphorylation. *Biochem. Soc. Trans.*, **2009**, 37, 627.
- [182] Cohen, P. The role of protein phosphorylation in human health and disease. *Eur. J. Biochem.*, **2001**, 268, 5001-5010.

- [183] Boersema, P. J., Mohammed, S. and Heck, A. J. Phosphopeptide fragmentation and analysis by mass spectrometry. *J. Mass Spectrom.*, **2009**, 44, 861-878.
- [184] McLachlin, D. T. and Chait, B. T. Analysis of phosphorylated proteins and peptides by mass spectrometry. *Curr. Opin. Chem. Biol.*, **2001**, 5, 591-602.
- [185] Hoffert, J. D. and Knepper, M. A. Taking aim at shotgun phosphoproteomics. *Anal. Biochem.*, **2008**, 375, 1.
- [186] Paradela, A. and Albar, J. P. Advances in the analysis of protein phosphorylation. *J. Proteome Res.*, **2008**, 7, 1809-1818.
- [187] Ishihama, Y., Wei, F.-Y., Aoshima, K., Sato, T., Kuromitsu, J. and Oda, Y. Enhancement of the efficiency of phosphoproteomic identification by removing phosphates after phosphopeptide enrichment. *J. Proteome Res.*, **2007**, 6, 1139-1144.
- [188] Marcantonio, M., Trost, M., Courcelles, M., Desjardins, M. and Thibault, P. Combined Enzymatic and Data Mining Approaches for Comprehensive Phosphoproteome Analyses Application to Cell Signaling Events of Interferon- γ -Stimulated Macrophages. *Mol. Cell. Proteomics*, **2008**, 7, 645-660.
- [189] Arnott, D., Henzel, W. J. and Stults, J. T. Rapid identification of comigrating gel-isolated proteins by ion trap-mass spectrometry. *Electrophoresis*, **1998**, 19, 968-980.
- [190] Ficarro, S. B., McClelland, M. L., Stukenberg, P. T., Burke, D. J., Ross, M. M., Shabanowitz, J., Hunt, D. F. and White, F. M. Phosphoproteome analysis by mass spectrometry and its application to *Saccharomyces cerevisiae*. *Nat. Biotechnol.*, **2002**, 20, 301-305.
- [191] Beausoleil, S. A., Jedrychowski, M., Schwartz, D., Elias, J. E., Villén, J., Li, J., Cohn, M. A., Cantley, L. C. and Gygi, S. P. Large-scale characterization of HeLa cell nuclear phosphoproteins. *Proc. Nat. Acad. Sci. USA.*, **2004**, 101, 12130-12135.
- [192] Ruse, C. I., McClatchy, D. B., Lu, B., Cociorva, D., Motoyama, A., Park, S. K. and Yates III, J. R. Motif-specific sampling of phosphoproteomes. *J. Proteome Res.*, **2008**, 7, 2140-2150.
- [193] Zhang, X., Ye, J., Jensen, O. N. and Roepstorff, P. Highly efficient phosphopeptide enrichment by calcium phosphate precipitation combined with subsequent IMAC enrichment. *Mol. Cell. Proteomics*, **2007**, 6, 2032-2042.
- [194] Pandey, A., Podtelejnikov, A. V., Blagoev, B., Bustelo, X. R., Mann, M. and Lodish, H. F. Analysis of receptor signaling pathways by mass spectrometry: identification of vav-2 as a substrate of the epidermal and platelet-derived growth factor receptors. *Proc. Nat. Acad. Sci. USA.*, **2000**, 97, 179-184.
- [195] Oda, Y., Nagasu, T. and Chait, B. T. Enrichment analysis of phosphorylated proteins as a tool for probing the phosphoproteome. *Nat. Biotechnol.*, **2001**, 19, 379-382.

- [196] Zhou, H., Watts, J. D. and Aebersold, R. A systematic approach to the analysis of protein phosphorylation. *Nat. Biotechnol.*, **2001**, 19, 375-378.
- [197] Kalume, D. E., Molina, H. and Pandey, A. Tackling the phosphoproteome: tools and strategies. *Curr. Opin. Chem. Biol.*, **2003**, 7, 64-69.
- [198] Bateman, R., Carruthers, R., Hoyes, J., Jones, C., Langridge, J., Millar, A. and Vissers, J. A novel precursor ion discovery method on a hybrid quadrupole orthogonal acceleration time-of-flight (Q-TOF) mass spectrometer for studying protein phosphorylation. *J. Am. Chem. Soc. Mass Spectrom.*, **2002**, 13, 792-803.
- [199] Salek, M., Costagliola, S. and Lehmann, W. D. Protein tyrosine-O-sulfation analysis by exhaustive product ion scanning with minimum collision offset in a NanoESI Q-TOF tandem mass spectrometer. *Anal. Chem.*, **2004**, 76, 5136-5142.
- [200] Steen, H., Küster, B., Fernandez, M., Pandey, A. and Mann, M. Detection of tyrosine phosphorylated peptides by precursor ion scanning quadrupole TOF mass spectrometry in positive ion mode. *Anal. Biochem.*, **2001**, 73, 1440-1448.
- [201] Steen, H., Küster, B. and Mann, M. Quadrupole time-of-flight versus triple-quadrupole mass spectrometry for the determination of phosphopeptides by precursor ion scanning. *J. Mass Spectrom.*, **2001**, 36, 782-790.
- [202] Ekroos, K., Chernushevich, I. V., Simons, K. and Shevchenko, A. Quantitative profiling of phospholipids by multiple precursor ion scanning on a hybrid quadrupole time-of-flight mass spectrometer. *Anal. Chem.*, **2002**, 74, 941-949.
- [203] Niggeweg, R., Köcher, T., Gentzel, M., Buscaino, A., Taipale, M., Akhtar, A. and Wilm, M. A general precursor ion-like scanning mode on quadrupole-TOF instruments compatible with chromatographic separation. *Proteomics*, **2006**, 6, 41-53.
- [204] Louris, J. N., Wright, L. G., Cooks, R. G. and Schoen, A. E. New scan modes accessed with a hybrid mass spectrometer. *Anal. Chem.*, **1985**, 57, 2918-2924.
- [205] Schlosser, A., Pipkorn, R., Bossemeyer, D. and Lehmann, W. D. Analysis of protein phosphorylation by a combination of elastase digestion and neutral loss tandem mass spectrometry. *Anal. Chem.*, **2001**, 73, 170-176.
- [206] Hoffman, M. D., Sniatynski, M. J., Rogalski, J. C., Le Blanc, J. and Kast, J. Multiple neutral loss monitoring (MNM): a multiplexed method for post-translational modification screening. *J. Am. Soc. Mass Spectrom.*, **2006**, 17, 307-317.
- [207] Hopfgartner, G., Varesio, E., Tschäppät, V., Grivet, C., Bourgoigne, E. and Leuthold, L. A. Triple quadrupole linear ion trap mass spectrometer for the analysis of small molecules and macromolecules. *J. Mass Spectrom.*, **2004**, 39, 845-855.
- [208] Larsen, M. R., Sørensen, G. L., Fey, S. J., Larsen, P. M. and Roepstorff, P. Phosphoproteomics: evaluation of the use of enzymatic de-phosphorylation and differential mass spectrometric peptide mass mapping for site specific phosphorylation assignment in proteins separated by gel electrophoresis. *Proteomics*, **2001**, 1, 223-238.

- [209] Liao, P., Leykam, J., Andrews, P., Gage, D. and Allison, J. An approach to locate phosphorylation sites in a phosphoprotein: mass mapping by combining specific enzymatic degradation with matrix-assisted laser desorption/ionization mass spectrometry. *Anal. Biochem.*, **1994**, 219, 9-20.
- [210] Reid, G. E., Simpson, R. J. and O'Hair, R. A. Leaving group and gas phase neighboring group effects in the side chain losses from protonated serine and its derivatives. *J. Am. Soc. Mass Spectrom.*, **2000**, 11, 1047-1060.
- [211] Palumbo, A. M., Tepe, J. J. and Reid, G. E. Mechanistic insights into the multistage gas-phase fragmentation behavior of phosphoserine- and phosphothreonine-containing peptides. *J. Proteome Res.*, **2008**, 7, 771-779.
- [212] Tholey, A., Reed, J. and Lehmann, W. D. Electrospray tandem mass spectrometric studies of phosphopeptides and phosphopeptide analogues. *J. Mass Spectrom.*, **1999**, 34, 117-123.
- [213] DeGnore, J. and Qin, J. Fragmentation of phosphopeptides in an ion trap mass spectrometer. *J. Am. Soc. Mass Spectrom.*, **1998**, 9, 1175-1188.
- [214] Metzger, S. and Hoffmann, R. Studies on the dephosphorylation of phosphotyrosine-containing peptides during post-source decay in matrix-assisted laser desorption/ionization. *J. Mass Spectrom.*, **2000**, 35, 1165-1177.
- [215] Moyer, S. C., Cotter, R. J. and Woods, A. S. Fragmentation of phosphopeptides by atmospheric pressure MALDI and ESI/ion trap mass spectrometry. *J. Am. Soc. Mass Spectrom.*, **2002**, 13, 274-283.
- [216] Palumbo, A. M., Smith, S. A., Kalcic, C. L., Dantus, M., Stemmer, P. M. and Reid, G. E. Tandem mass spectrometry strategies for phosphoproteome analysis. *Mass Spectrom. Rev.*, **2011**, 30, 600-625.
- [217] Olsen, J. V., Blagoev, B., Gnad, F., Macek, B., Kumar, C., Mortensen, P. and Mann, M. Global, in vivo, and site-specific phosphorylation dynamics in signaling networks. *Cell*, **2006**, 127, 635-648.
- [218] Benschop, J. J., Mohammed, S., O'Flaherty, M., Heck, A. J., Slijper, M. and Menke, F. L. Quantitative phosphoproteomics of early elicitor signaling in Arabidopsis. *Mol. Cell. Proteomics*, **2007**, 6, 1198-1214.
- [219] Gruhler, A., Olsen, J. V., Mohammed, S., Mortensen, P., Færgeman, N. J., Mann, M. and Jensen, O. N. Quantitative phosphoproteomics applied to the yeast pheromone signaling pathway. *Mol. Cell. Proteomics*, **2005**, 4, 310-327.
- [220] Lemeer, S., Jopling, C., Gouw, J., Mohammed, S., Heck, A. J., Slijper, M. and den Hertog, J. Comparative phosphoproteomics of zebrafish Fyn/Yes morpholino knockdown embryos. *Mol. Cell. Proteomics*, **2008**, 7, 2176-2187.

- [221] Lemeer, S., Pinkse, M. W., Mohammed, S., van Breukelen, B., den Hertog, J., Slijper, M. and Heck, A. J. Online automated in vivo zebrafish phosphoproteomics: from large-scale analysis down to a single embryo. *J. Proteome Res.*, **2008**, 7, 1555-1564.
- [222] Schroeder, M. J., Shabanowitz, J., Schwartz, J. C., Hunt, D. F. and Coon, J. J. A neutral loss activation method for improved phosphopeptide sequence analysis by quadrupole ion trap mass spectrometry. *Anal. Chem.*, **2004**, 76, 3590-3598.
- [223] Beausoleil, S. A., Villén, J., Gerber, S. A., Rush, J. and Gygi, S. P. A probability-based approach for high-throughput protein phosphorylation analysis and site localization. *Nat. Biotechnol.*, **2006**, 24, 1285-1292.
- [224] Olsen, J. V. and Mann, M. Improved peptide identification in proteomics by two consecutive stages of mass spectrometric fragmentation. *Proc. Nat. Acad. Sci. USA.*, **2004**, 101, 13417-13422.
- [225] Palumbo, A. M. and Reid, G. E. Evaluation of gas-phase rearrangement and competing fragmentation reactions on protein phosphorylation site assignment using collision induced dissociation-MS/MS and MS3. *Anal. Chem.*, **2008**, 80, 9735-9747.
- [226] Syka, J. E., Coon, J. J., Schroeder, M. J., Shabanowitz, J. and Hunt, D. F. Peptide and protein sequence analysis by electron transfer dissociation mass spectrometry. *Proc. Nat. Acad. Sci. USA.*, **2004**, 101, 9528-9533.
- [227] Zubarev, R. A. Electron-capture dissociation tandem mass spectrometry. *Curr. Opin. Chem. Biol.*, **2004**, 15, 12-16.
- [228] Chi, A., Huttenhower, C., Geer, L. Y., Coon, J. J., Syka, J. E., Bai, D. L., Shabanowitz, J., Burke, D. J., Troyanskaya, O. G. and Hunt, D. F. Analysis of phosphorylation sites on proteins from *Saccharomyces cerevisiae* by electron transfer dissociation (ETD) mass spectrometry. *Proc. Nat. Acad. Sci. USA.*, **2007**, 104, 2193-2198.
- [229] Xia, Y., Gunawardena, H. P., Erickson, D. E. and McLuckey, S. A. Effects of cation charge-site identity and position on electron-transfer dissociation of polypeptide cations. *J. Am. Chem. Soc.*, **2007**, 129, 12232-12243.
- [230] Good, D. M., Wirtala, M., McAlister, G. C. and Coon, J. J. Performance characteristics of electron transfer dissociation mass spectrometry. *Mol. Cell. Proteomics*, **2007**, 6, 1942-1951.
- [231] Molina, H., Horn, D. M., Tang, N., Mathivanan, S. and Pandey, A. Global proteomic profiling of phosphopeptides using electron transfer dissociation tandem mass spectrometry. *Proc. Nat. Acad. Sci. USA.*, **2007**, 104, 2199-2204.
- [232] Swaney, D. L., McAlister, G. C. and Coon, J. J. Decision tree-driven tandem mass spectrometry for shotgun proteomics. *Nat. Methods*, **2008**, 5, 959-964.
- [233] van den Toorn, H. W., Mohammed, S., Gouw, J. W., van Breukelen, B. and Heck, A. J. Targeted scx based peptide fractionation for optimal sequencing by collision induced, and electron transfer dissociation. *J. Proteomics Bioinform*, **2008**, 1, 379-388.

- [234] Syrstad, E. A. and Tureček, F. Toward a general mechanism of electron capture dissociation. *J. Am. Soc. Mass Spectrom.*, **2005**, 16, 208-224.
- [235] Huddleston, M. J., Annan, R. S., Bean, M. F. and Carr, S. A. Selective detection of phosphopeptides in complex mixtures by electrospray liquid chromatography/mass spectrometry. *J. Am. Soc. Mass Spectrom.*, **1993**, 4, 710-717.
- [236] Ding, J., Burkhart, W. and Kassel, D. B. Identification of phosphorylated peptides from complex mixtures using negative-ion orifice-potential stepping and capillary liquid chromatography/electrospray ionization mass spectrometry. *Rapid Commun. Mass Spectrom.*, **1994**, 8, 94-98.
- [237] Edelson-Averbukh, M., Pipkorn, R. and Lehmann, W. D. Phosphate group-driven fragmentation of multiply charged phosphopeptide anions. Improved recognition of peptides phosphorylated at serine, threonine, or tyrosine by negative ion electrospray tandem mass spectrometry. *Anal. Chem.*, **2006**, 78, 1249-1256.
- [238] Andrezza, H. J., Fitzgerald, M., Bilusich, D., Hoffmann, R., Hoffmann, P., Eichinger, P. C. and Bowie, J. H. Characteristic negative ion fragmentations of deprotonated peptides containing post-translational modifications: mono-phosphorylated Ser, Thr and Tyr. A joint experimental and theoretical study. *Rapid Commun. Mass Spectrom.*, **2008**, 22, 3305-3312.
- [239] Tran, N. T. T., Wang, T., Hack, S. and Bowie, J. H. Diagnostic cyclisation reactions which follow phosphate transfer to carboxylate anion centres for energised $[M-H]^-$ anions of pTyr containing peptides. *Rapid Commun. Mass Spectrom.*, **2011**, 25, 2489-2499.
- [240] Edelson-Averbukh, M., Shevchenko, A., Pipkorn, R. d. and Lehmann, W. D. Gas-phase intramolecular phosphate shift in phosphotyrosine-containing peptide monoanions. *Anal. Chem.*, **2009**, 81, 4369-4381.
- [241] Wang, T., Andrezza, H. J., Bilusich, D. and Bowie, J. H. Negative ion fragmentations of deprotonated peptides containing post-translational modifications. An unusual cyclisation/rearrangement involving phosphotyrosine; a joint experimental and theoretical study. *Rapid Commun. Mass Spectrom.*, **2009**, 23, 1669-1677.
- [242] Andrezza, H. J., Wang, T., Bilusich, D., Hoffmann, P. and Bowie, J. H. Negative ion fragmentations of deprotonated peptides containing post-translational modifications: diphosphorylated systems containing Ser, Thr and Tyr. A characteristic phosphate/phosphate cyclisation. A joint experimental and theoretical study. *Rapid Commun. Mass Spectrom.*, **2009**, 23, 1825-1833.
- [243] Huttner, W. B. Tyrosine sulfation and the secretory pathway. *Annu. Rev. Physiol.*, **1988**, 50, 363-376.
- [244] Niehrs, C., Reißwanger, R. and Huttner, W. B. Protein tyrosine sulfation, 1993-an update. *Chem. Biol. Interact.*, **1994**, 92, 257-271.
- [245] Bettelheim, F. Tyrosine-O-sulfate in a peptide from fibrinogen. *J. Am. Chem. Soc.*, **1954**, 76, 2838-2839.

- [246] Hille, A., Rosa, P. and Huttner, W. Tyrosine sulfation: a post-translational modification of proteins destined for secretion? *FEBS Lett.*, **1984**, 177, 129-134.
- [247] Danielsen, E. M. Tyrosine sulfation, a post-translational modification of microvillar enzymes in the small intestinal enterocyte. *EMBO*, **1987**, 6, 2891.
- [248] Fong, A. M., Alam, S. M., Imai, T., Haribabu, B. and Patel, D. D. CX3CR1 tyrosine sulfation enhances fractalkine-induced cell adhesion. *J. Biol. Chem.*, **2002**, 277, 19418-19423.
- [249] Maiti, A., Maki, G. and Johnson, P. TNF- α induction of CD44-mediated leukocyte adhesion by sulfation. *Science*, **1998**, 282, 941-943.
- [250] Hortin, G. Sulfation of tyrosine residues in coagulation factor V. *Blood*, **1990**, 76, 946-952.
- [251] Lee, R. and Huttner, W. Tyrosine-O-sulfated proteins of PC12 pheochromocytoma cells and their sulfation by a tyrosylprotein sulfotransferase. *J. Biol. Chem.*, **1983**, 258, 11326-11334.
- [252] Hortin, G. L., Farries, T. C., Graham, J. P. and Atkinson, J. P. Sulfation of tyrosine residues increases activity of the fourth component of complement. *Proc. Natl. Acad. Sci. U.S.A.*, **1989**, 86, 1338-1342.
- [253] Costagliola, S., Panneels, V., Bonomi, M., Koch, J., Many, M.-C., Smits, G. and Vassart, G. Tyrosine sulfation is required for agonist recognition by glycoprotein hormone receptors. *EMBO*, **2002**, 21, 504-513.
- [254] Panksepp, J., Burgdorf, J., Beinfeld, M. C., Kroes, R. A. and Moskal, J. R. Regional brain cholecystokinin changes as a function of friendly and aggressive social interactions in rats. *Brain Res.* , **2004**, 1025, 75-84.
- [255] Moore, K. L. The biology and enzymology of protein tyrosine O-sulfation. *J. Biol. Chem.*, **2003**, 278, 24243-24246.
- [256] Beisswanger, R., Corbeil, D., Vannier, C., Thiele, C., Dohrmann, U., Kellner, R., Ashman, K., Niehrs, C. and Huttner, W. B. Existence of distinct tyrosylprotein sulfotransferase genes: molecular characterization of tyrosylprotein sulfotransferase-2. *Proc. Natl. Acad. Sci. U.S.A.*, **1998**, 95, 11134-11139.
- [257] Seibert, C. and Sakmar, T. P. Toward a framework for sulfoproteomics: Synthesis and characterization of sulfotyrosine containing peptides. *Pept. Sci.* , **2008**, 90, 459-477.
- [258] Kehoe, J. W. and Bertozzi, C. R. Tyrosine sulfation: a modulator of extracellular protein-protein interactions. *Chem. Biol.* , **2000**, 7, R57-R61.
- [259] Rosen, S. D. Ligands for L-selectin: homing, inflammation, and beyond. *Annu. Rev. Immunol.*, **2004**, 22, 129-156.

- [260] Farzan, M., Mirzabekov, T., Kolchinsky, P., Wyatt, R., Cayabyab, M., Gerard, N. P., Gerard, C., Sodroski, J. and Choe, H. Tyrosine sulfation of the amino terminus of CCR5 facilitates HIV-1 entry. *Cell*, **1999**, 96, 667-676.
- [261] Hemmerich, S., Paavola, C., Bloom, A., Bhakta, S., Freedman, R., Grunberger, D., Krstenansky, J., Lee, S., McCarley, D. and Mulkins, M. Identification of residues in the monocyte chemotactic protein-1 that contact the MCP-1 receptor, CCR2. *Biochemistry*, **1999**, 38, 13013-13025.
- [262] Leppänen, A., Mehta, P., Ouyang, Y.-B., Ju, T., Helin, J., Moore, K. L., van Die, I., Canfield, W. M., McEver, R. P. and Cummings, R. D. A novel glycosulfopeptide binds to P-selectin and inhibits leukocyte adhesion to P-selectin. *J. Biol. Chem.*, **1999**, 274, 24838-24848.
- [263] Medzihradzky, K., Darula, Z., Perlson, E., Fainzilber, M., Chalkley, R., Ball, H., Greenbaum, D., Bogyo, M., Tyson, D. and Bradshaw, R. O-sulfonation of serine and threonine Mass spectrometric detection and characterization of a new posttranslational modification in diverse proteins throughout the eukaryotes. *Mol. Cell. Proteomics*, **2004**, 3, 429-440.
- [264] Monigatti, F., Hekking, B. and Steen, H. Protein sulfation analysis-a primer. *Biochim. Biophys. Acta*, **2006**, 1764, 1904-1913.
- [265] Balsved, D., Bundgaard, J. R. and Sen, J. W. Stability of tyrosine sulfate in acidic solutions. *Anal. Biochem.*, **2007**, 363, 70-76.
- [266] Huttner, W. B. Determination and occurrence of tyrosine O-sulfate in proteins. *Meth. Enzymol.* , **1984**, 107, 200-223.
- [267] Seibert, C., Cadene, M., Sanfiz, A., Chait, B. T. and Sakmar, T. P. Tyrosine sulfation of CCR5 N-terminal peptide by tyrosylprotein sulfotransferases 1 and 2 follows a discrete pattern and temporal sequence. *Proc. Natl. Acad. Sci. U.S.A.*, **2002**, 99, 11031-11036.
- [268] Önnarfjord, P., Heathfield, T. F. and Heinegård, D. Identification of tyrosine sulfation in extracellular leucine-rich repeat proteins using mass spectrometry. *J. Biol. Chem.*, **2004**, 279, 26-33.
- [269] Monigatti, F., Gasteiger, E., Bairoch, A. and Jung, E. The Sulfinator: predicting tyrosine sulfation sites in protein sequences. *Bioinformatics*, **2002**, 18, 769-770.
- [270] PM, H., GW, K. and RC, S. The antral hormone gastrin. Structure of gastrin. *Nature*, **1964**, 204, 931-933.
- [271] Hoffhines, A. J., Damoc, E., Bridges, K. G., Leary, J. A. and Moore, K. L. Detection and purification of tyrosine-sulfated proteins using a novel anti-sulfo tyrosine monoclonal antibody. *J. Biol. Chem.*, **2006**, 281, 37877-37887.
- [272] Bundgaard, J. R., Sen, J. W., Johnsen, A. H. and Rehfeld, J. F., Analysis of tyrosine-O-sulfation, in *The Protein Protocols Handbook*, Springer, **2009**, pp. 1601-1621.

- [273] Hortin, G., Griest, T. and Benutto, B. Separations of sulfated and nonsulfated forms of peptides by capillary electrophoresis: comparison with reversed-phase HPLC. *BioChromatophapy*, **1990**, 5.
- [274] Amano, Y., Shinohara, H., Sakagami, Y. and Matsubayashi, Y. Ion-selective enrichment of tyrosine-sulfated peptides from complex protein digests. *Anal. Biochem.*, **2005**, 346, 124-131.
- [275] Drake, S. K. and Hortin, G. L. Improved detection of intact tyrosine sulfate-containing peptides by matrix-assisted laser desorption/ionization time-of-flight mass spectrometry in linear negative ion mode. *Int. J. Biochem. Cell Biol.*, **2010**, 42, 174-179.
- [276] Nemeth, C., Jennifer F, Karnik, S. and Rouse, J. C. Analysis of sulfated peptides using positive electrospray ionization tandem mass spectrometry. *J. Mass Spectrom.*, **2001**, 36, 1301-1311.
- [277] Yu, Y., Hoffhines, A. J., Moore, K. L. and Leary, J. A. Determination of the sites of tyrosine O-sulfation in peptides and proteins. *Nat. Methods*, **2007**, 4, 583-588.
- [278] Edelson-Averbukh, M., Shevchenko, A., Pipkorn, R. and Lehmann, W. D. Discrimination Between Peptide O-Sulfo-and O-Phosphotyrosine Residues by Negative Ion Mode Electrospray Tandem Mass Spectrometry. *J. Am. Chem. Soc.*, **2011**, 22, 2256-2268.
- [279] Cook, S. L. and Jackson, G. P. Metastable atom-activated dissociation mass spectrometry of phosphorylated and sulfonated peptides in negative ion mode. *J. Am. Chem. Soc.*, **2011**, 22, 1088-1099.
- [280] Kice, J. L. and Anderson, J. M. The Mechanism of the Acid Hydrolysis of Sodium Aryl Sulfates¹. *J. Am. Chem. Soc.*, **1966**, 88, 5242-5245.
- [281] Yagami, T., Kitagawa, K., Aida, C., Fujiwara, H. and Futaki, S. Stabilization of a tyrosine O-sulfate residue by a cationic functional group: formation of a conjugate acid–base pair. *J. Pept. Res.*, **2000**, 56, 239-249.
- [282] Taylor, S. W., Sun, C., Hsieh, A., Andon, N. L. and Ghosh, S. S. A sulfated, phosphorylated 7 kDa secreted peptide characterized by direct analysis of cell culture media. *J. Proteome Res.*, **2008**, 7, 795-802.
- [283] Loughnan, M. L., Nicke, A., Jones, A., Adams, D. J., Alewood, P. F. and Lewis, R. J. Chemical and Functional Identification and Characterization of Novel Sulfated α -Conotoxins from the Cone Snail *Conus a nemone*. *J. Med. Chem.*, **2004**, 47, 1234-1241.
- [284] Yagami, T., Kitagawa, K. and Futaki, S. Liquid secondary-ion mass spectrometry of peptides containing multiple tyrosine-O-sulfates. *Rapid Commun. Mass Spectrom.*, **1995**, 9, 1335-1341.
- [285] Zaia, J., Boynton, R., Heinegård, D. and Barry, F. Posttranslational modifications to human bone sialoprotein determined by mass spectrometry. *Biochemistry*, **2001**, 40, 12983-12991.

- [286] Gibson, B. W. and Cohen, P. Liquid secondary ion mass spectrometry of phosphorylated and sulfated peptides and proteins. *Meth. Enzymol.*, **1990**, 193, 480-501.
- [287] Bean, M. F., Annan, R. S., Hemling, M. E., Mentzer, M., Huddleston, M. J. and Carr, S. A. LC-MS methods for selective detection of posttranslational modifications in proteins: Glycosylation, phosphorylation, sulfation, and acylation. *Techniques in Protein Chemistry*, **1995**, 6, 107-116.
- [288] Jedrzejewski, P. T. and Lehmann, W. D. Detection of modified peptides in enzymatic digests by capillary liquid chromatography/electrospray mass spectrometry and a programmable skimmer CID acquisition routine. *Aal. Chem.*, **1997**, 69, 294-301.
- [289] Wolfender, J.-L., Chu, F., Ball, H., Wolfender, F., Fainzilber, M., Baldwin, M. A. and Burlingame, A. L. Identification of tyrosine sulfation in *Conus pennaceus* conotoxins α -PnIA and α -PnIB: further investigation of labile sulfo- and phosphopeptides by electrospray, matrix-assisted laser desorption/ionization (MALDI) and atmospheric pressure MALDI mass spectrometry. *J. Mass Spectrom.*, **1999**, 34, 447-454.
- [290] Bundgaard, J. R., Heterologous expression in endocrine cells for analysis of posttranslational modifications, in *Posttranslational Modifications of Proteins*, Springer, **2002**, pp. 291-299.
- [291] Talbo, G. and Roepstorff, P. Determination of sulfated peptides via prompt fragmentation by UV matrix-assisted laser desorption/ionization mass spectrometry. *Rapid Comm. Mass Spectrom.*, **1993**, 7, 201-204.
- [292] Tran, N. T. T., Wang, T., Hack, S., Hoffmann, P. and Bowie, J. H. Can collision-induced negative-ion fragmentations of $[M-H]^-$ anions be used to identify phosphorylation sites in peptides? *Rapid Commun. Mass Spectrom.*, **2011**, 25, 3537-3548.
- [293] Tran, N. T. T., Wang, T., Hack, S. and Bowie, J. H. Fragmentations of $[M-H]^-$ anions of peptides containing Ser sulfate. A joint experimental and theoretical study. *Rapid Commun. Mass Spectrom.*, **2013**, 27, 2287-2296.
- [294] Tran, N. T. T., Wang, T., Hack, S. and Bowie, J. H. Fragmentations of $[M-H]^-$ anions of peptides containing tyrosine sulfate. Does the sulfate group rearrange? A joint experimental and theoretical study. *Rapid Commun. Mass Spectrom.*, **2013**, 27, 1135-1142.
- [295] Torfs, P., Baggerman, G., Meeusen, T., Nieto, J., Nachman, R., Calderon, J., De Loof, A. and Schoofs, L. Isolation, identification, and synthesis of a disulfated sulfakinin from the central nervous system of an arthropods the white shrimp *Litopenaeus vannamei*. *Biochem. Biophys. Res. Commun.*, **2002**, 299, 312-320.
- [296] Kim, J. S., Song, S. U. and Kim, H. J. Simultaneous identification of tyrosine phosphorylation and sulfation sites utilizing tyrosine-specific bromination. *J. Am. Chem. Soc. Mass Spectrom.*, **2011**, 22, 1916-1925.
- [297] Zubarev, R. A. Reactions of polypeptide ions with electrons in the gas phase. *Mass Spectrom. Rev.*, **2003**, 22, 57-77.

- [298] Kelleher, N. L., Zubarev, R. A., Bush, K., Furie, B., Furie, B. C., McLafferty, F. W. and Walsh, C. T. Localization of labile posttranslational modifications by electron capture dissociation: the case of γ -carboxyglutamic acid. *Anal. Chem.*, **1999**, 71, 4250-4253.
- [299] Mikesch, L. M., Ueberheide, B., Chi, A., Coon, J. J., Syka, J. E., Shabanowitz, J. and Hunt, D. F. The utility of ETD mass spectrometry in proteomic analysis. *Biochem. Biophys. Acta*, **2006**, 1764, 1811-1822.
- [300] Liu, H. and Håkansson, K. Electron capture dissociation of tyrosine O-sulfated peptides complexed with divalent metal cations. *Anal. Chem.*, **2006**, 78, 7570-7576.
- [301] Medzihradzky, K., Guan, S., Maltby, D. and Burlingame, A. Sulfopeptide fragmentation in electron-capture and electron-transfer dissociation. *J. Am. Chem. Soc.*, **2007**, 129, 1617-1624.
- [302] Kweon, H. K. and Håkansson, K. Metal oxide-based enrichment combined with gas-phase ion-electron reactions for improved mass spectrometric characterization of protein phosphorylation. *J. Proteome Res.*, **2008**, 7, 749-755.
- [303] Coon, J. J., Shabanowitz, J., Hunt, D. F. and Syka, J. E. Electron transfer dissociation of peptide anions. *J. Am. Chem. Soc.*, **2005**, 127, 880-882.
- [304] Hersberger, K. E., Brant, A., Wang, N. and Hakansson, K., *ASMS Conference* (Salt Lake City, UT) **2010**.
- [305] Wang, T., Tran, N. T. T., Scanlon, D., Andreatza, H. J., Abell, A. D. and Bowie, J. H. Diagnostic di- and triphosphate cyclisation in the negative ion electrospray mass spectra of phosphoSer peptides. *Rapid Commun. Mass Spectrom.*, **2011**, 25, 2649-2656.
- [306] Bowie, J. H., Brinkworth, C. S. and Dua, S. Collision-induced fragmentations of the (M-H)⁻ parent anions of underivatized peptides: An aid to structure determination and some unusual negative ion cleavages. *Mass Spectrom. Rev.*, **2002**, 21, 87-107.
- [307] Bilusich, D. and Bowie, J. Fragmentations of (M-H)⁻ anions of underivatized peptides. Part 2: Characteristic cleavages of Ser and Cys and of disulfides and other post-translational modifications, together with some unusual internal processes. *Mass spectrometry reviews*, **2009**, 28, 20-34.
- [308] O'Hair, R. A., Bowie, J. H. and Gronert, S. Gas phase acidities of the α amino acids. *Int. J. Mass Spectrom.*, **1992**, 117, 23-36.
- [309] Jones, C. M., Bernier, M., Carson, E., Colyer, K. E., Metz, R., Pawlow, A., Wischow, E. D., Webb, I., Andriole, E. J. and Poutsma, J. C. Gas-phase acidities of the 20 protein amino acids. *Int. J. Mass Spectrom.*, **2007**, 267, 54-62.
- [310] Morris, R. A., Knighton, W., Viggiano, A., Hoffman, B. C. and Schaefer III, H. F. The gas-phase acidity of H₃PO₄. *J. Chem. Phys.*, **1997**, 106, 3545.

- [311] Wang, X. B., Nicholas, J. B. and Wang, L. S. Photoelectron spectroscopy and theoretical calculations of SO_4^- and HSO_4^- : Confirmation of high electron affinities of SO_4 and HSO_4 . *J. Chem. Phys.*, **2000**, 104, 504-508.
- [312] Frand, A. R. and Kaiser, C. A. Ero1p oxidizes protein disulfide isomerase in a pathway for disulfide bond formation in the endoplasmic reticulum. *Mol. Cell*, **1999**, 4, 469-477.
- [313] Pollard, M. G., Travers, K. J. and Weissman, J. S. Ero1p: a novel and ubiquitous protein with an essential role in oxidative protein folding in the endoplasmic reticulum. *Mol. Cell*, **1998**, 1, 171-182.
- [314] Tavender, T. J., Springate, J. J. and Bulleid, N. J. Recycling of peroxiredoxin IV provides a novel pathway for disulphide formation in the endoplasmic reticulum. *EMBO* **2010**, 29, 4185-4197.
- [315] Zito, E., Melo, E. P., Yang, Y., Wahlander, Å., Neubert, T. A. and Ron, D. Oxidative protein folding by an endoplasmic reticulum-localized peroxiredoxin. *Mol. Cell*, **2010**, 40, 787-797.
- [316] Wajih, N., Hutson, S. M. and Wallin, R. Disulfide-dependent protein folding is linked to operation of the vitamin K cycle in the endoplasmic reticulum. A protein disulfide isomerase-VKORC1 redox enzyme complex appears to be responsible for vitamin K1 2,3-epoxide reduction. *J. Biol. Chem.*, **2007**, 282, 2626-2635.
- [317] Nguyen, V. D., Saaranen, M. J., Karala, A.-R., Lappi, A.-K., Wang, L., Raykhel, I. B., Alanen, H. I., Salo, K. E., Wang, C.-c. and Ruddock, L. W. Two endoplasmic reticulum PDI peroxidases increase the efficiency of the use of peroxide during disulfide bond formation. *J. Mol. Biol.*, **2011**, 406, 503-515.
- [318] Kodali, V. K. and Thorpe, C. Oxidative protein folding and the quiescin-sulfhydryl oxidase family of flavoproteins. *Antiox. Redox Signal*, **2010**, 13, 1217-1230.
- [319] Raina, S. and Missiakas, D. Making and breaking disulfide bonds. *Annu. Rev. Microbiol.*, **1997**, 51, 179-202.
- [320] Kadokura, H., Katzen, F. and Beckwith, J. Protein disulfide bond formation in prokaryotes. *Annu. Rev. Biochem.*, **2003**, 72, 111-135.
- [321] Fass, D. Disulfide bonding in protein biophysics. *Annu. Rev. Biophys.*, **2012**, 41, 63-79.
- [322] Lioe, H. and O'Hair, R. A. A novel salt bridge mechanism highlights the need for nonmobile proton conditions to promote disulfide bond cleavage in protonated peptides under low-energy collisional activation. *J. Am. Chem. Soc.*, **2007**, 18, 1109-1123.
- [323] Gupta, K., Kumar, M. and Balaram, P. Disulfide bond assignments by mass spectrometry of native natural peptides: cysteine pairing in disulfide bonded conotoxins. *Anal. Chem.*, **2010**, 82, 8313-8319.

- [324] Thakur, S. S. and Balaram, P. Rapid mass spectral identification of contryphans. Detection of characteristic peptide ions by fragmentation of intact disulfide-bonded peptides in crude venom. *Rapid Commun. Mass Spectrom.*, **2007**, 21, 3420-3426.
- [325] Kim, H. I. and Beauchamp, J. Mapping disulfide bonds in insulin with the route 66 method: selective cleavage of SC bonds using alkali and alkaline earth metal enolate complexes. *J. Am. Soc. Mass Spectrom.*, **2009**, 20, 157-166.
- [326] Mentinova, M., Han, H. and McLuckey, S. A. Dissociation of disulfide-intact somatostatin ions: the roles of ion type and dissociation method. *Rapid Commun. Mass Spectrom.*, **2009**, 23, 2647-2655.
- [327] Gunawardena, H. P., O'Hair, R. A. J. and McLuckey, S. A. Selective disulfide bond cleavage in gold (I) cationized polypeptide ions formed via gas-phase ion/ion cation switching. *J. Proteome Res.*, **2006**, 5, 2087-2092.
- [328] Bhattacharyya, M., Gupta, K., Gowd, K. H. and Balaram, P. Rapid mass spectrometric determination of disulfide connectivity in peptides and proteins. *Mol. Biosyst.*, **2013**, 9, 1340-1350.
- [329] Gorman, J. J., Wallis, T. P. and Pitt, J. J. Protein disulfide bond determination by mass spectrometry. *Mass Spectrom. Rev.*, **2002**, 21, 183-216.
- [330] Murphy, R. C. and Clay, K. L. Preparation of labeled molecules by exchange with oxygen-18 water. *Methods enzymol.*, **1990**, 193, 338-348.
- [331] Wu, J. and Watson, J. T. A novel methodology for assignment of disulfide bond pairings in proteins. *Protein Sci.*, **1997**, 6, 391-398.
- [332] Gray, W. R. Disulfide structures of highly bridged peptides: a new strategy for analysis. *Protein Sci.*, **1993**, 2, 1732-1748.
- [333] Sechi, S. and Chait, B. T. Modification of cysteine residues by alkylation. A tool in peptide mapping and protein identification. *Anal. Chem.*, **1998**, 70, 5150-5158.
- [334] Qi, J., Wu, W., Borges, C. R., Hang, D., Rupp, M., Torng, E. and Watson, J. T. Automated data interpretation based on the concept of "negative signature mass" for mass-mapping disulfide structures of cystinyl proteins. *J. Am. Soc. Mass Spectrom.*, **2003**, 14, 1032-1038.
- [335] Borges, C. R., Qi, J., Wu, W., Torng, E., Hinck, A. P. and Throck Watson, J. Algorithm-assisted elucidation of disulfide structure: application of the negative signature mass algorithm to mass-mapping the disulfide structure of the 12-cysteine transforming growth factor β type II receptor extracellular domain. *Anal. Biochem.*, **2004**, 329, 91-103.
- [336] Zhang, M. and Kaltashov, I. A. Mapping of protein disulfide bonds using negative ion fragmentation with a broadband precursor selection. *Anal. Chem.*, **2006**, 78, 4820-4829.

- [337] Chrisman, P. A. and McLuckey, S. A. Dissociations of disulfide-linked gaseous polypeptide/protein anions: ion chemistry with implications for protein identification and characterization. *J. Proteome Res.*, **2002**, 1, 549-557.
- [338] Bilusich, D., Maselli, V. M., Brinkworth, C. S., Samguina, T., Lebedev, A. T. and Bowie, J. H. Direct identification of intramolecular disulfide links in peptides using negative ion electrospray mass spectra of underivatized peptides. A joint experimental and theoretical study. *Rapid Commun. Mass Spectrom.*, **2005**, 19, 3063-3074.
- [339] Bilusich, D. and Bowie, J. H. Identification of intermolecular disulfide linkages in underivatized peptides using negative ion electrospray mass spectrometry. A joint experimental and theoretical study. *Rapid Commun. Mass Spectrom.*, **2007**, 21, 619-628.
- [340] Andreatza, H. J. and Bowie, J. H. The application of negative ion electrospray mass spectrometry for the sequencing of underivatized disulfide-containing proteins: insulin and lysozyme. *Chem. Phys.*, **2010**, 12, 13400-13407.
- [341] Halling, K. C., Halling, A. C., Murray, E. E., Ladin, B. F., Houston, L. and Weaver, R. F. Genomic cloning and characterization of a ricin gene from *Ricinus communis*. *Nucleic Acids Res.*, **1985**, 13, 8019-8033.
- [342] Funatsu, G., Yoshitake, S. and Funatsu, M. Primary structure of Ile chain of ricin D. *Agric. Biol. Chem.*, **1978**, 42, 501-503.
- [343] Yoshitake, S., Funatsu, G. and Funatsu, M. Isolation and sequences of peptic peptides, and the complete sequence of Ile chain of ricin D [castor-oil plant]. *Agric. Biol. Chem.*, **1978**, 42, 1253.
- [344] Araki, T. and Funatsu, G. Revised amino acid sequence of the B-chain of ricin D due to loss of tryptophan in the cyanogen bromide cleavage. *FEBS letters*, **1985**, 191, 121-124.
- [345] Funatsu, G., Kimura, M. and Funatsu, M. Primary structure of Ala chain of ricin D. *Agric. Biol. Chem.*, **1979**, 43, 2221-2224.
- [346] Lamb, F. I., Roberts, L. M. and Lord, J. M. Nucleotide sequence of cloned cDNA coding for preproricin. *Eur. J. Biochem.*, **1985**, 148, 265-270.
- [347] Lord, J. M., Roberts, L. M. and Robertus, J. D. Ricin: structure, mode of action, and some current applications. *FASEB J.*, **1994**, 8, 201-208.
- [348] Kimura, Y., Hase, S., Kobayashi, Y., Kyogoku, Y., Ikenaka, T. and Funatsu, G. Structures of sugar chains of ricin D. *J. Biol. Chem.*, **1988**, 103, 944-949.
- [349] Kimura, Y., Kusuoku, H., Tada, M., Takagi, S. and Funatsu, G. Structural analyses of sugar chains from ricin A-chain variant. *Agric. Biol. Chem.*, **1990**, 54, 157-162.
- [350] Despeyroux, D., Walker, N., Pearce, M., Fisher, M., McDonnell, M., Bailey, S., Griffiths, G. and Watts, P. Characterization of ricin heterogeneity by electrospray mass spectrometry, capillary electrophoresis, and resonant mirror. *Anal. Biochem.*, **2000**, 279, 23-36.

- [351] Frigerio, L., Jolliffe, N. A., Di Cola, A., Felipe, D. H., Paris, N., Neuhaus, J.-M., Lord, J. M., Ceriotti, A. and Roberts, L. M. The internal propeptide of the ricin precursor carries a sequence-specific determinant for vacuolar sorting. *Plant Physiol.*, **2001**, 126, 167-175.
- [352] Frigerio, L. and Lord, J. M. Glycoprotein degradation: Do sugars hold the key? *Curr. Biol.*, **2000**, 10, R674-R677.
- [353] Katzin, B. J., Collins, E. J. and Robertus, J. D. Structure of ricin A-chain at 2.5 Å. *Proteins: Struct., Funct., Bioinf.*, **1991**, 10, 251-259.
- [354] Montfort, W., Villafranca, J. E., Monzingo, A. F., Ernst, S. R., Katzin, B., Rutenber, E., Xuong, N. H., Hamlin, R. and Robertus, J. D. The three-dimensional structure of ricin at 2.8 Å. *J. Biol. Chem.*, **1987**, 262, 5398-5403.
- [355] Rutenber, E. and Robertus, J. D. Structure of ricin B-chain at 2.5 Å resolution. *Proteins: Struct., Funct., Bioinf.*, **1991**, 10, 260-269.
- [356] Rutenber, E., Katzin, B. J., Ernst, S., Collins, E. J., Mlsna, D., Ready, M. P. and Robertus, J. D. Crystallographic refinement of ricin to 2.5 Å. *Proteins: Struct., Funct., Bioinf.*, **1991**, 10, 240-250.
- [357] Weston, S. A., Tucker, A. D., Thatcher, D. R., Derbyshire, D. J. and Pauptit, R. A. X-ray structure of recombinant ricin A-chain at 1.8 Å resolution. *J. Mol. Biol.*, **1994**, 244, 410-422.
- [358] Yan, X., Hollis, T., Svinth, M., Day, P., Monzingo, A. F., Milne, G. W. and Robertus, J. D. Structure-based identification of a ricin inhibitor. *J. Mol. Biol.*, **1997**, 266, 1043-1049.
- [359] Day, P. J., Ernst, S. R., Frankel, A. E., Monzingo, A. F., Pascal, J. M., Molina-Svinth, M. C. and Robertus, J. D. Structure and activity of an active site substitution of ricin A chain. *Biochemistry*, **1996**, 35, 11098-11103.
- [360] Kim, Y. and Robertus, J. D. Analysis of several key active site residues of ricin A chain by mutagenesis and X-ray crystallography. *Protein Eng.*, **1992**, 5, 775-779.
- [361] Ogasawara, T., Sawasaki, T., Morishita, R., Ozawa, A., Madin, K. and Endo, Y. A new class of enzyme acting on damaged ribosomes: ribosomal RNA apurinic site specific lyase found in wheat germ. *EMBO* **1999**, 18, 6522-6531.
- [362] Audi, J., Belson, M., Patel, M., Schier, J. and Osterloh, J. Ricin poisoning: a comprehensive review. *Jama*, **2005**, 294, 2342-2351.
- [363] Alexander, J., Benford, D., Cockburn, A., Cravedi, J., Dogliotti, E., Di Domenico, A., Fernández-Cruz, M., Fürst, P., Fink-Gremmels, J. and Galli, C. Scientific Opinion of the Panel on Contaminants in the Food Chain on a request from the European Commission on ricin (from *Ricinus communis*) as undesirable substances in animal feed. *EFSA J*, **2008**, 726, 1-38.

- [364] Fredriksson, S.-Å., Hulst, A. G., Artursson, E., de Jong, A. L., Nilsson, C. and van Baar, B. L. Forensic identification of neat ricin and of ricin from crude castor bean extracts by mass spectrometry. *Anal. Chem.*, **2005**, 77, 1545-1555.
- [365] Leith, A., Griffiths, G. and Green, M. Quantification of ricin toxin using a highly sensitive avidin/biotin enzyme-linked immunosorbent assay. *J. Forensic Sci. Soc.*, **1988**, 28, 227-236.
- [366] Poli, M. A., Rivera, V. R., Hewetson, J. F. and Merrill, G. A. Detection of ricin by colorimetric and chemiluminescence ELISA. *Toxicon*, **1994**, 32, 1371-1377.
- [367] Shyu, H.-F., Chiao, D.-J., Liu, H.-W. and Tang, S.-S. Monoclonal antibody-based enzyme immunoassay for detection of ricin. *Hybrid. Hybridomics*, **2002**, 21, 69-73.
- [368] Kalb, S. R. and Barr, J. R. Mass spectrometric detection of ricin and its activity in food and clinical samples. *Anal. Chem.*, **2009**, 81, 2037-2042.
- [369] Hines, H. B., Brueggemann, E. E. and Hale, M. L. High-performance liquid chromatography–mass selective detection assay for adenine released from a synthetic RNA substrate by ricin A chain. *Anal. Biochem.*, **2004**, 330, 119-122.
- [370] Sturm, M. B. and Schramm, V. L. Detecting ricin: sensitive luminescent assay for ricin A-chain ribosome depurination kinetics. *Anal. Chem.*, **2009**, 81, 2847-2853.
- [371] Darby, S. M., Miller, M. L. and Allen, R. O. Forensic determination of ricin and the alkaloid marker ricinine from castor bean extracts. *J. Forensic Sci.*, **2001**, 46, 1033.
- [372] Kanamori-Kataoka, M., Ohsawa, I. and Seto, Y. Analytical method for proteinous toxin ricin based on its molecular weight estimation. *Jpn. J. Forensic Sci. Technol*, **2006**, 11, 131.
- [373] Brinkworth, C. S., Pigott, E. J. and Bourne, D. J. Detection of intact ricin in crude and purified extracts from castor beans using matrix-assisted laser desorption ionization mass spectrometry. *Anal. Chem.*, **2009**, 81, 1529-1535.
- [374] Kanamori-Kataoka, M., Kato, H., Uzawa, H., Ohta, S., Takei, Y., Furuno, M. and Seto, Y. Determination of ricin by nano liquid chromatography/mass spectrometry after extraction using lactose-immobilized monolithic silica spin column. *J. Mass Spectrom.*, **2011**, 46, 821-829.
- [375] Duriez, E., Fenaille, F., Tabet, J.-C., Lamourette, P., Hilaire, D., Becher, F. and Ezan, E. Detection of ricin in complex samples by immunocapture and matrix-assisted laser desorption/ionization time-of-flight mass spectrometry. *J. Proteome Res.*, **2008**, 7, 4154-4163.
- [376] Brinkworth, C. S. Identification of ricin in crude and purified extracts from castor beans using on-target tryptic digestion and MALDI mass spectrometry. *Anal. Chem.*, **2010**, 82, 5246-5252.

- [377] Östin, A., Bergström, T., Fredriksson, S.-Å. and Nilsson, C. Solvent-assisted trypsin digestion of ricin for forensic identification by LC-ESI MS/MS. *Anal. Chem.*, **2007**, 79, 6271-6278.
- [378] Araki, T. and Funatsu, G. The complete amino acid sequence of the B-chain of ricin E isolated from small-grain castor bean seeds. Ricin E is a gene recombination product of ricin D and *ricinus communis* agglutinin. *Biochim. Biophys. Acta.*, **1987**, 911, 191-200.
- [379] Hartley, M. R., Chaddock, J. A. and Bonness, M. S. The structure and function of ribosome-inactivating proteins. *Trends Plant Sci.*, **1996**, 1, 252.
- [380] Roberts, L. M., Lamb, F., Pappin, D. and Lord, J. The primary sequence of *Ricinus communis* agglutinin. Comparison with ricin. *J. Biol. Chem.*, **1985**, 260, 15682-15686.
- [381] Harley, S. M. and Michael Lord, J. In vitro endoproteolytic cleavage of castor bean lectin presursors. *Plant Sci.*, **1985**, 41, 111-116.
- [382] Biemann, K. and Martin, S. A. Mass spectrometric determination of the amino acid sequence of peptides and proteins. *Mass Spectrom. Rev.*, **1987**, 6, 1-75.
- [383] Bilusich, D. and Bowie, J. Fragmentations of (M-H)⁻ anions of underivatized peptides. Part 2: Characteristic cleavages of Ser and Cys and of disulfides and other post-translational modifications, together with some unusual internal processes. *Mass Spectrom. Rev.*, **2009**, 28, 20-34.
- [384] Gergely, J., Gouvea, M. and Karibian, D. Fragmentation of myosin by chymotrypsin. *J. Biol. Chem.*, **1955**, 212, 165-177.
- [385] Drapeau, G. R. Substrate specificity of a proteolytic enzyme isolated from a mutant of *Pseudomonas fragi*. *J. Biol. Chem.*, **1980**, 255, 839-840.
- [386] Ingrosso, D., Fowler, A. V., Bleibaum, J. and Clarke, S. Specificity of endoproteinase Asp-N (*Pseudomonas fragi*): Cleavage at glutamyl residues in two proteins. *Biochem. Biophys. Res. Commun.*, **1989**, 162, 1528-1534.
- [387] Lazarus, L. H. and Attila, M. The toad, ugly and venomous, wears yet a precious jewel in his skin. *Prog. Neurobiol.*, **1993**, 41, 473-507.
- [388] Toledo, R. C. and Jared, C. Cutaneous granular glands and amphibian venoms. *Comp. Biochem. Physiol., A: Comp. Physiol.*, **1995**, 111, 1-29.
- [389] Savage, J. M., The geographic distribution of frogs: Patterns and predictions. . University of Missouri Press, Chicago, USA, **1973**.
- [390] Pounds, J. A., Fogden, M. P. and Campbell, J. H. Biological response to climate change on a tropical mountain. *Nature*, **1999**, 398, 611-615.
- [391] Kiesecker, J. M., Blaustein, A. R. and Belden, L. K. Complex causes of amphibian population declines. *Nature*, **2001**, 410, 681-684.

- [392] Berger, L., Speare, R., Daszak, P., Green, D. E., Cunningham, A. A., Goggin, C. L., Slocombe, R., Ragan, M. A., Hyatt, A. D. and McDonald, K. R. Chytridiomycosis causes amphibian mortality associated with population declines in the rain forests of Australia and Central America. *Proc. Natl. Acad. Sci. USA*, **1998**, 95, 9031-9036.
- [393] Tyler, M. J., Frog and cane toad skin secretions, in *Toxic plants and animals: a guide for Australia*, (ed. by Covacevich, J.), Brisbane, Queensland Museum, **1987**, pp. 329-339.
- [394] Clarke, B. T. The natural history of amphibian skin secretions, their normal functioning and potential medical applications. *Bio. Rev.*, **1997**, 72, 365-379.
- [395] Daly, J. W. The chemistry of poisons in amphibian skin. *Proc. Natl. Acad. Sci.*, **1995**, 92, 9-13.
- [396] Daly, J. W., Caceres, J., Moni, R. W., Gusovsky, F., Moos, M., Seamon, K. B., Milton, K. and Myers, C. W. Frog secretions and hunting magic in the upper Amazon: identification of a peptide that interacts with an adenosine receptor. *Proc. Natl. Acad. Sci.*, **1992**, 89, 10960-10963.
- [397] Erspamer, V., Erspamer, G. F., Severini, C., Potenza, R. L., Barra, D., Mignogna, G. and Bianchi, A. Pharmacological studies of 'sapo' from the frog *Phyllomedusa bicolor* skin: A drug used by the Peruvian Matsigenka Indians in shamanic hunting practices. *Toxicon*, **1993**, 31, 1099-1111.
- [398] Cei, J. M., Erspamer, V. and Roseghini, M. Taxonomic and evolutionary significance of biogenic amines and polypeptides occurring in amphibian skin. I. Neotropical leptodactylid frogs. *Syst. Zool.*, **1967**, 16, 328-342.
- [399] Cunha Filho, G. A., Schwartz, C. A., Resck, I. S., Murta, M. M., Lemos, S. S., Castro, M. S., Kyaw, C., Pires Jr, O. R., Leite, J. R. S. and Bloch Jr, C. Antimicrobial activity of the bufadienolides marinobufagin and telocinobufagin isolated as major components from skin secretion of the toad *Bufo rubescens*. *Toxicon*, **2005**, 45, 777-782.
- [400] Daly, J. W., Myers, C. W. and Whittaker, N. Further classification of skin alkaloids from neotropical poison frogs (*Dendrobatidae*), with a general survey of toxic/noxious substances in the amphibia. *Toxicon*, **1987**, 25, 1023-1095.
- [401] Daly, J. W. Thirty years of discovering arthropod alkaloids in amphibian skin. *J. Nat. Prod.*, **1998**, 61, 162-172.
- [402] Erspamer, V. and Melchiorri, P. Active polypeptides: from amphibian skin to gastrointestinal tract and brain of mammals. *Trends Pharmacol. Sci.*, **1980**, 1, 391-395.
- [403] Pukala, T. L., Bowie, J. H., Maselli, V. M., Musgrave, I. F. and Tyler, M. J. Host-defence peptides from the glandular secretions of amphibians: structure and activity. *Nat. Prod. Rep.*, **2006**, 23, 368-393.
- [404] Wabnitz, P. A., Walters, H., Tyler, M. J., Wallace, J. C. and Bowie, J. H. First record of host defence peptides in tadpoles. The magnificent tree frog *Litoria splendida*. *J. Pep. Res.*, **1998**, 52, 477-481.

- [405] Zasloff, M., Martin, B. and Chen, H.-C. Antimicrobial activity of synthetic magainin peptides and several analogues. *Proc. Natl. Acad. Sci.*, **1988**, 85, 910-913.
- [406] Zasloff, M. Magainins, a class of antimicrobial peptides from *Xenopus* skin: isolation, characterization of two active forms, and partial cDNA sequence of a precursor. *Proc. Natl. Acad. Sci.*, **1987**, 84, 5449-5453.
- [407] Vanhoye, D., Bruston, F., Nicolas, P. and Amiche, M. Antimicrobial peptides from hylid and ranin frogs originated from a 150-million-year-old ancestral precursor with a conserved signal peptide but a hypermutable antimicrobial domain. *Eur. J. Biochem.*, **2003**, 270, 2068-2081.
- [408] Nicolas, P., Vanhoye, D. and Amiche, M. Molecular strategies in biological evolution of antimicrobial peptides. *Peptides*, **2003**, 24, 1669-1680.
- [409] Apponyi, M. A., Pukala, T. L., Brinkworth, C. S., Maselli, V. M., Bowie, J. H., Tyler, M. J., Booker, G. W., Wallace, J. C., Carver, J. A. and Separovic, F. Host-defence peptides of Australian anurans: structure, mechanism of action and evolutionary significance. *Peptides*, **2004**, 25, 1035-1054.
- [410] Stone, D. J., Blumenthal, T., Bowie, J. H. and Tyler, M. J. Detection of plasticers in skin and glandular extracts of the green tree frog *Litoria splendida*. *Rapid Commun. Mass Spectrom.*, **1992**, 6, 400-402.
- [411] Stone, D. J. M., Waugh, R. J., Bowie, J. H., Wallace, J. L. and Tyler, M. J. Peptides from Australian frogs. Structures of the caeridins from *Litoria caerulea*. *J. Chem. Soc. Perkin Trans. 1*, **1993**, 573-576.
- [412] Erspamer, V., Bioactive secretions of the amphibian integument, in *Amphibian biology*, (ed. by Heatwole, H.), NSW, Australia, Surrey Beatty and Sons, **1994**, pp. 178-350.
- [413] Erspamer, V., Melchiorri, P., Nakajima, T., Yasuhara, T. and Endean, R. Amino acid composition and sequence of crinia-angiotensin, an angiotensin II-like endecapeptide from the skin of the Australian frog *Crinia georgiana*. *Experientia*, **1979**, 35, 1132-1133.
- [414] Erspamer, G. F., Nakajima, T. and Yasuhara, T. Pharmacological data on crinia-angiotensin II. *J. Pharm. Pharmacol.*, **1979**, 31, 720-720.
- [415] Araki, K., Tachibana, S., Uchiyama, M., Nakajima, T. and Yasuhara, T. Isolation and structure of a new active peptide "Xenopsin" on the smooth muscle, especially on a strip of fundus from a rat stomach, from the skin of *Xenopus laevis*. *Chem. Pharm. Bull. (Japan)*, **1973**, 21, 2801-2804.
- [416] Araki, K., Tachibana, S., Uchiyama, M., Nakajima, T. and Yasuhara, T. Isolation and structure of a new active peptide xenopsin on rat stomach strip and some biogenic amines in the skin of *Xenopus laevis*. *Chem. Pharm. Bull.*, **1975**, 23, 3132-3140.
- [417] Carraway, R. and Leeman, S. E. The isolation of a new hypotensive peptide, neurotensin, from bovine hypothalami. *J. Biol. Chem.*, **1973**, 248, 6854-6861.

- [418] Carraway, R. and Leeman, S. E. The amino acid sequence of a hypothalamic peptide, neurotensin. *J. Biol. Chem.*, **1975**, 250, 1907-1911.
- [419] Steinborner, S. T. The observation of Evolutionary trends in Amphibians and the Analysis of Negative Ion Fragmentations in Large Peptide Systems by Mass Spectrometry. PhD Thesis. The university of Adelaide. Adelaide, SA. **1997**, pp. 43-62.
- [420] Barker, J., Grigg, G. C. and Tyler, M. J., A field guide to Australian frogs. Surrey Beatty & Sons Sydney, Australia, **1995**.
- [421] Erspamer, V., Erspamer, G. F., Mazzanti, G. and Endean, R. Active peptides in the skins of one hundred amphibian species from Australia and Papua New Guinea. *Comp. Biochem. Physiol. C.*, **1984**, 77, 99-108.
- [422] Steinborner, S. T., Wabnitz, P. A., Waugh, R. J., Bowie, J. H., Gao, C., Tyler, M. J. and Wallace, J. C. The structures of new peptides from the Australian Red Tree Frog '*Litoria rubella*'. The skin peptide profile as a probe for the study of evolutionary trends of amphibians. *Aust. J. Chem.*, **1996**, 49, 955-963.
- [423] Rozek, T., Wegener, K. L., Bowie, J. H., Olver, I. N., Carver, J. A., Wallace, J. C. and Tyler, M. J. The antibiotic and anticancer active aurein peptides from the Australian Bell Frogs *Litoria aurea* and *Litoria raniformis*. *Eur. J. Biochem.*, **2000**, 267, 5330-5341.
- [424] Wabnitz, P. A., Bowie, J. H., Tyler, M. J., Wallace, J. C. and Smith, B. P. Differences in the skin peptides of the male and female Australian tree frog *Litoria splendida*. *Eur. J. Biochem.*, **2000**, 267, 269-275.
- [425] Stone, D. J. M., Waugh, R. J., Bowie, J. H., Wallace, J. C. and Tyler, M. J. Peptides from Australian frogs. The structures of the caerins from *Litoria caerulea*. *J. Chem. Res.*, S, 1993, 138; M, 1993, 910-935.
- [426] Waugh, R., Stone, D., Bowie, J., Wallace, J. and Tyler, M. Peptides from Australian frogs. The structures of the caerins and caeridins from *Litoria gilleni*. *J. Chem. Res.*, S, 1993, 139; M, 1993, 937-961.
- [427] Steinborner, S. T., Waugh, R. J., Bowie, J. H., Wallace, J. C., Tyler, M. J. and Ramsay, S. L. New caerin antibacterial peptides from the skin glands of the Australian tree frog *Litoria xanthomera*. *J. Pep. Sci.*, **1997**, 3, 181-185.
- [428] Steinborner, S. T., Currie, G. J., Bowie, J. H., Wallace, J. C. and Tyler, M. J. New antibiotic caerin 1 peptides from the skin secretion of the Australian tree frog *Litoria chloris*. Comparison of the activities of the caerin 1 peptides from the genus *Litoria*. *J. Pep. Res.*, **1998**, 51, 121-126.
- [429] Brinkworth, C. S., Bowie, J. H., Tyler, M. J. and Wallace, J. C. A comparison of the antimicrobial skin peptides of the new guinea tree frog (*Litoria genimaculata*) and the fringed tree frog (*Litoria eucnemis*). *Aust. J. Chem.*, **2002**, 55, 605-610.

- [430] Wegener, K. L., Wabnitz, P. A., Carver, J. A., Bowie, J. H., Chia, B., Wallace, J. C. and Tyler, M. J. Host defence peptides from the skin glands of the Australian Blue Mountains tree-frog *Litoria citropa*. *Eur. J. Biochem.*, **1999**, 265, 627-637.
- [431] Wegener, K. L., Brinkworth, C. S., Bowie, J. H., Wallace, J. C. and Tyler, M. J. Bioactive dahlein peptides from the skin secretions of the Australian aquatic frog *Litoria dahlii*: sequence determination by electrospray mass spectrometry. *Rapid Commun. Mass Spectrom.*, **2001**, 15, 1726-1734.
- [432] Raftery, M., Bradford, A., Bowie, J., Wallace, J. and Tyler, M. Peptides from Australian frogs. The structures of the dynastins from the banjo frogs *Limnodynastes interioris*, *Limnodynastes dumerilii* and *Limnodynastes terraereginae*. *Aust. J. Chem.*, **1993**, 46, 833-842.
- [433] Bradford, A., Raftery, M., Bowie, J., Wallace, J. and Tyler, M. Peptides from Australian Frogs. The structures of the Dynastins from *Limnodynastes salmini* and Fletcherin from *Limnodynastes fletcheri*. *Aust. J. Chem.*, **1993**, 46, 1235-1244.
- [434] Wabnitz, P. A., Bowie, J. H., Wallace, J. C. and Tyler, M. J. Peptides from the skin glands of the Australian buzzing tree frog *Litoria electrica*. Comparison with the skin peptides of the red tree frog *Litoria rubella*. *Aust. J. Chem.*, **1999**, 52, 639-646.
- [435] Raftery, M. J., Waugh, R. J., Bowie, J. H., Wallace, J. C. and Tyler, M. J. The structures of the frenatin peptides from the skin secretion of the giant tree frog *Litoria infrafrenata*. *J. Pep. Sci.*, **1996**, 2, 117-124.
- [436] Doyle, J., Llewellyn, L. E., Brinkworth, C. S., Bowie, J. H., Wegener, K. L., Rozek, T., Wabnitz, P. A., Wallace, J. C. and Tyler, M. J. Amphibian peptides that inhibit neuronal nitric oxide synthase. *Eur. J. Biochem.*, **2002**, 269, 100-109.
- [437] Rozek, T., Waugh, R. J., Steinborner, S. T., Bowie, J. H., Tyler, M. J. and Wallace, J. C. The maculatin peptides from the skin glands of the tree frog *Litoria genimaculata*: a comparison of the structures and antibacterial activities of maculatin 1.1 and caerin 1.1. *J. Pep. Sci.*, **1998**, 4, 111-115.
- [438] Steinborner, S. T., Gao, C., Raftery, M. J., Waugh, R. J., Blumenthal, T., Bowie, J. H., Wallace, J. C. and Tyler, M. J. The structures of four tryptophyllin and three rubellidin peptides from the Australian red tree frog *Litoria rubella*. *Aust. J. Chem.*, **1994**, 47, 2099-2108.
- [439] Anastasi, A., Erspamer, V. and Exdean, R. Isolation and amino acid sequence of caerulein, the active decapeptide of the skin of *Hyla caerulea*. *Arch. Biochem. Biophys.*, **1968**, 125, 57-68.
- [440] Dockray, G. J. and Hopkins, C. R. Caerulein secretion by dermal glands in *Xenopus laevis*. *J. Cell Biol.*, **1975**, 64, 724-733.
- [441] Iwamuro, S., Kuwagaki, D. and Kikuyama, S. Effect of Arginine Vasotocin (AVT) and AVT-Related Peptide on Skin Gland Secretion in *Xenopus laevis* (Endocrinology). *Zoo. Sci.*, **1991**, 8, 743-746.

- [442] Giovannini, M. G., Poulter, L., Gibson, B. W. and Williams, D. H. Biosynthesis and degradation of peptides derived from *Xenopus laevis* prohormones. *J. Biol. Chem.*, **1987**, 243, 113-120.
- [443] Seki, T., Kikuyama, S. and Yanaihara, N. Development of *Xenopus laevis* skin glands producing 5-hydroxytryptamine and caerulein. *Cell Tissue Res.*, **1989**, 258, 483-489.
- [444] Terry, A. S., Poulter, L., Williams, D. H., Nutkins, J. C., Giovannini, M., Moore, C. and Gibson, B. The cDNA sequence coding for prepro-PGS (prepro-magainins) and aspects of the processing of this prepro-polypeptide. *J. Biol. Chem.*, **1988**, 263, 5745-5751.
- [445] Bevins, C. L. and Zasloff, M. Peptides from frog skin. *Annu. Rev. Biochem.*, **1990**, 59, 395-414.
- [446] Roseghini, M., Erspamer, V. and Endean, R. Indole-, imidazole- and phenyl-alkylamines in the skin of one hundred amphibian species from Australia and Papua New Guinea. *Comp. Biochem. Physiol. C.*, **1976**, 54, 31-43.
- [447] Tyler, M. J., Stone, D. J. and Bowie, J. H. A novel method for the release and collection of dermal, glandular secretions from the skin of frogs. *J. Pharm. Toxicol. Methods*, **1992**, 28, 199-200.
- [448] Bodanszky, M., Sequence determination, in *Peptide chemistry: a practical textbook*, German, Springer Berlin Heidelberg, **1988**, pp. 16-38.
- [449] Edman, P. and Begg, G. A protein sequenator. *Eur. J. Biochem.*, **1967**, 1, 80-91.
- [450] Hunkapiller, M. W., Hewick, R. M., Dreyer, W. J. and Hood, L. E. High-sensitivity sequencing with a gas-phase sequenator. *Methods Enzymol.*, **1982**, 91, 399-413.
- [451] Hovgaard, L., Frøkjær, S. and van-de-Weert, M., Pharmaceutical formulation development of peptides and proteins. CRC Press, US, **2012**.
- [452] Gevaert, K. and Vandekerckhove, J. Protein identification methods in proteomics. *Electrophoresis*, **2000**, 21, 1145-1154.
- [453] Steinborner, S. T., Wabnitz, P. A., Bowie, J. H. and Tyler, M. J. The application of mass spectrometry to the study of evolutionary trends in amphibians. *Rapid Commun. Mass Spectrom.*, **1996**, 10, 92-95.
- [454] Jackway, R. J., Maselli, V. M., Musgrave, I. F., Maclean, M. J., Tyler, M. J. and Bowie, J. H. Skin peptides from anurans of the *Litoria rubella* Group: sequence determination using electrospray mass spectrometry. Opioid activity of two major peptides. *Rapid Commun. Mass Spectrom.*, **2009**, 23, 1189-1195.
- [455] Ellis-Steinborner, S. T., Scanlon, D., Musgrave, I. F., Tran, N. T. T., Hack, S., Wang, T., Abell, A. D., Tyler, M. J. and Bowie, J. H. An unusual kynurenine-containing opioid tetrapeptide from the skin gland secretion of the Australian red tree frog *Litoria rubella*. Sequence determination by electrospray mass spectrometry. *Rapid Commun. Mass Spectrom.*, **2011**, 25, 1735-1740.

- [456] Opitz, C. A., Litzenburger, U. M., Sahn, F., Ott, M., Tritschler, I., Trump, S., Schumacher, T., Jestaedt, L., Schrenk, D. and Weller, M. An endogenous tumour-promoting ligand of the human aryl hydrocarbon receptor. *Nature*, **2011**, 478, 197-203.
- [457] Simat, T. and Steinhart, H. Oxidation of free tryptophan and tryptophan residues in peptides and proteins. *J. Agric. Food Chem.*, **1998**, 46, 490-498.
- [458] Chen, Y. and Guillemin, G. J. Kynurenine pathway metabolites in humans: disease and healthy states. *Int. J. Tryptophan Res.*, **2009**, 2, 1.
- [459] Aquilina, J. and Truscott, R. Kynurenine binds to the peptide binding region of the chaperone α B-crystallin. *Biochem. Biophys. Res. Commun.*, **2001**, 285, 1107-1113.
- [460] Aquilina, J. A. and Truscott, R. J. W. Cysteine is the initial site of modification of α -crystallin by kynurenine. *Biochem. Biophys. Res. Commun.*, **2000**, 276, 216-223.
- [461] Garner, B., Shaw, D. C., Lindner, R. A., Carver, J. A. and Truscott, R. J. Non-oxidative modification of lens crystallins by kynurenine: a novel post-translational protein modification with possible relevance to ageing and cataract. *Biochim. Biophys. Acta - Prot. Struct. Mol. Enzym.*, **2000**, 1476, 265-278.
- [462] Staniszewska, M. and Nagaraj, R. H. Detection of kynurenine modifications in proteins using a monoclonal antibody. *J. Immunol. Methods*, **2007**, 324, 63-73.
- [463] Vazquez, S., Aquilina, J. A., Jamie, J. F., Sheil, M. M. and Truscott, R. J. Novel protein modification by kynurenine in human lenses. *J. Biol. Chem.*, **2002**, 277, 4867-4873.
- [464] Zhang, H., Joseph, J., Crow, J. and Kalyanaraman, B. Mass spectral evidence for carbonate-anion-radical-induced posttranslational modification of tryptophan to kynurenine in human Cu, Zn superoxide dismutase. *Free Radical Biol. Med.*, **2004**, 37, 2018-2026.
- [465] Bringans, S. D., Dyer, J. M., Plowman, J. E. and Bryson, W. G. Kynurenine located within keratin proteins isolated from photoyellowed wool fabric. *Textile Res.*, **2006**, 76, 288-294.
- [466] Dyer, J. M., Bringans, S. D. and Bryson, W. G. Determination of Photo-oxidation Products Within Photoyellowed Bleached Wool Proteins. *Photochem. Photobiol.*, **2006**, 82, 551-557.
- [467] Dalsgaard, T. K., Otzen, D., Nielsen, J. H. and Larsen, L. B. Changes in structures of milk proteins upon photo-oxidation. *J. Agric. Food Chem.*, **2007**, 55, 10968-10976.
- [468] Si, S. and Mandal, T. K. Tryptophan-Based Peptides to Synthesize Gold and Silver Nanoparticles: A Mechanistic and Kinetic Study. *Chem. Eur. J.*, **2007**, 13, 3160-3168.
- [469] Yang, C.-y., Gu, Z.-W., Yang, M., Lin, S.-N., Siuzdak, G. and Smith, C. V. Identification of modified tryptophan residues in apolipoprotein B-100 derived from copper ion-oxidized low-density lipoprotein. *Biochem.*, **1999**, 38, 15903-15908.

- [470] Helland, R., Fjellbirkeland, A., Karlsen, O. A., Ve, T., Lillehaug, J. R. and Jensen, H. B. An oxidized tryptophan facilitates copper binding in *Methylococcus capsulatus*-secreted protein MopE. *J. Biol. Chem.*, **2008**, 283, 13897-13904.
- [471] Yambe, H., Kitamura, S., Kamio, M., Yamada, M., Matsunaga, S., Fusetani, N. and Yamazaki, F. L-Kynurenine, an amino acid identified as a sex pheromone in the urine of ovulated female masu salmon. *Proc. Nat. Acad. Sci. USA*, **2006**, 103, 15370-15374.
- [472] Amirkhani, A., Heldin, E., Markides, K. E. and Bergquist, J. Quantitation of tryptophan, kynurenine and kynurenic acid in human plasma by capillary liquid chromatography–electrospray ionization tandem mass spectrometry. *J. Chromatogr. B Anal. Tech. Biomed. Life Sci.*, **2002**, 780, 381-387.
- [473] Arvidsson, B., Johannesson, N., Citterio, A., Righetti, P. G. and Bergquist, J. High throughput analysis of tryptophan metabolites in a complex matrix using capillary electrophoresis coupled to time-of-flight mass spectrometry. *J. Chromatogr.*, **2007**, 1159, 154-158.
- [474] Perdivara, I., Deterding, L. J., Przybylski, M. and Tomer, K. B. Mass spectrometric identification of oxidative modifications of tryptophan residues in proteins: chemical artifact or post-translational modification? *J. Am. Soc. Mass Spectrom.*, **2010**, 21, 1114-1117.
- [475] Schey, K. L., Little, M., Fowler, J. G. and Crouch, R. K. Characterization of human lens major intrinsic protein structure. *Invest. Ophthalmol. Vis. Sci.*, **2000**, 41, 175-182.
- [476] Todorovski, T., Fedorova, M. and Hoffmann, R. Mass spectrometric characterization of peptides containing different oxidized tryptophan residues. *J. Mass Spectrom.*, **2011**, 46, 1030-1038.
- [477] Vazquez, S., Truscott, R. J., O'Hair, R. A., Weimann, A. and Sheil, M. M. A study of kynurenine fragmentation using electrospray tandem mass spectrometry. *J. Am. Soc. Mass Spectrom.*, **2001**, 12, 786-794.
- [478] Krogull, M. K. and Fennema, O. Oxidation of tryptophan in the presence of oxidizing methyl linoleate. *J. Agric. Food Chem.*, **1987**, 35, 66-70.
- [479] Kanner, J. D. and Fennema, O. Photooxidation of tryptophan in the presence of riboflavin. *J. Agric. Food Chem.*, **1987**, 35, 71-76.
- [480] Mous, L., Silajdzic, E., Haroune, N., Spickett, C. M. and Pitt, A. R. Development of novel mass spectrometric methods for identifying HOCl-induced modifications to proteins. *Proteomics*, **2009**, 9, 1617-1631.
- [481] Todorovski, T., Fedorova, M. and Hoffmann, R. Identification of isomeric 5-hydroxytryptophan-and oxindolylalanine-containing peptides by mass spectrometry. *J. Mass Spectrom.*, **2012**, 47, 453-459.
- [482] Simat, T., Meyer, K. and Steinhart, H. Synthesis and analysis of oxidation and carbonyl condensation compounds of tryptophan. *J. Chromatogr. A.*, **1994**, 661, 93-99.

- [483] Taylor, S. W., Fahy, E., Murray, J., Capaldi, R. A. and Ghosh, S. S. Oxidative post-translational modification of tryptophan residues in cardiac mitochondrial proteins. *J. Biol. Chem.*, **2003**, 278, 19587-19590.
- [484] Finley, E. L., Dillon, J., Crouch, R. K. and Schey, K. L. Identification of tryptophan oxidation products in bovine α -crystallin. *Protein Sci.*, **1998**, 7, 2391-2397.
- [485] Anderson, L. B., Maderia, M., Ouellette, A. J., Putnam-Evans, C., Higgins, L., Krick, T., MacCoss, M. J., Lim, H., Yates, J. R. and Barry, B. A. Posttranslational modifications in the CP43 subunit of photosystem II. *Proc. Natl. Acad. Sci. USA*, **2002**, 99, 14676-14681.
- [486] Johnson, S., Costa, M., Humphreys, C. and Shearman, R. Inhibitory effects of opioids in a circular muscle-myenteric plexus preparation of guinea-pig ileum. *Naunyn Schmiedeberg's Arch Pharmacol.*, **1987**, 336, 419-424.
- [487] Lord, J. A., Waterfield, A. A., Hughes, J. and Kosterlitz, H. W. Endogenous opioid peptides: multiple agonists and receptors. *Nature*, **1977**, 267, 495-499.
- [488] Goldstein, A. and Naidu, A. Multiple opioid receptors: ligand selectivity profiles and binding site signatures. *Mol. Pharmacol.*, **1989**, 36, 265-272.
- [489] Kromer, W. Endogenous and exogenous opioids in the control of gastrointestinal motility and secretion. *Pharmacol. Rev.*, **1988**, 40, 121-162.
- [490] Yao, K., Fang, J., Yin, Y., Feng, Z., Tang, Z. and Wu, G. Tryptophan metabolism in animals: important roles in nutrition and health. *Front. Biosci.*, **2011**, 3, 286.
- [491] Funakoshi, H., Kanai, M. and Nakamura, T. Modulation of tryptophan metabolism, promotion of neurogenesis and alteration of anxiety-related behavior in tryptophan 2, 3-dioxygenase-deficient mice. *Int. J. Tryptophan Res.*, **2011**, 4, 7.
- [492] Schmid, L. Excretion of Tryptophan Metabolites after Physical Effort. *Nature*, **1961**, 189, 64-65.
- [493] Wu, G. Amino acids: metabolism, functions, and nutrition. *Amino acids*, **2009**, 37, 1-17.
- [494] Giuliani, S., Lecci, A., Tramontana, M. and Maggi, C. A. Role of K opioid receptors in modulating cholinergic twitches in the circular muscle of guinea-pig colon. *Br. J. Pharmacol.*, **1996**, 119, 985-989.
- [495] Loh, H. H. and Law, P. The role of membrane lipids in receptor mechanisms. *Annu. Rev. Pharmacol. Toxicol.*, **1980**, 20, 201-234.
- [496] Sargent, D. and Schwyzer, R. Membrane lipid phase as catalyst for peptide-receptor interactions. *Proc. Natl. Acad. Sci. USA*, **1986**, 83, 5774-5778.
- [497] Zerbe, O., Neumoin, A., Mares, J., Walser, R. and Zou, C. Recognition of neurohormones of the NPY family by their receptors. *J. Recept. Sig.*, **2006**, 26, 487-504.

- [498] Franklin, T. J. Binding energy and the activation of hormone receptors. *Biochem. Pharm.*, **1980**, 29, 853.
- [499] Herschlag, D. The role of induced fit and conformational changes of enzymes in specificity and catalysis. *Bioorg. Chem.*, **1988**, 16, 62-96.
- [500] Page, M. I., The chemistry of enzyme action. Elsevier Science, **1983**.
- [501] Kaiser, E. and Kezdy, F. Secondary structures of proteins and peptides in amphiphilic environments.(A review). *Proc. Natl. Acad. Sci. USA*, **1983**, 80, 1137-1143.
- [502] Kaiser, E. and Kezdy, F. Amphiphilic secondary structure: design of peptide hormones. *Science*, **1984**, 223, 249-255.
- [503] Schwyzer, R. Peptide–membrane interactions and a new principle in quantitative structure–activity relationships. *Biopolymers*, **1991**, 31, 785-792.
- [504] Schwyzer, R. 100 Years lock-and-key concept: Are peptide keys shaped and guided to their receptors by the target cell membrane?. *Biopolymers*, **1995**, 37, 5-16.
- [505] Heijne, G. V. On the hydrophobic nature of signal sequences. *Eur. J. Biochem.*, **1981**, 116, 419-422.
- [506] Schwyzer, R. Molecular mechanism of opioid receptor selection. *Biochemistry*, **1986**, 25, 6335-6342.
- [507] Schwyzer, R. Estimated conformation, orientation, and accumulation of dynorphin A-(1-13)-tridecapeptide on the surface of neutral lipid membranes. *Biochemistry*, **1986**, 25, 4281-4286.
- [508] Erne, D., Sargent, D. F. and Schwyzer, R. Preferred conformation, orientation, and accumulation of dynorphin A-(1-13)-tridecapeptide on the surface of neutral lipid membranes. *Biochemistry*, **1985**, 24, 4261-4263.
- [509] Gremlich, H. U., Fringeli, U. P. and Schwyzer, R. Interaction of adrenocorticotropin-(11-24)-tetradecapeptide with neutral lipid membranes revealed by infrared attenuated total reflection spectroscopy. *Biochemistry*, **1984**, 23, 1808-1810.
- [510] Gremlich, H.-U., Sargent, D. and Schwyzer, R. The adsorption of adrenocorticotropin-(1-24)-tetracosapeptide to lecithin bilayer membranes formed from liposomes. *Biophys. Struct. Mech.*, **1981**, 8, 61-65.
- [511] Gysin, B. and Schwyzer, R. Head group and structure specific interactions of enkephalins and dynorphin with liposomes: investigation by hydrophobic photolabeling. *Arch. Biochem. Biophys.*, **1983**, 225, 467-474.
- [512] Gysin, B. and Schwyzer, R. Liposome-mediated labeling of adrenocorticotropin fragments parallels their biological activity. *FEBS Lett.*, **1983**, 158, 12-16.

- [513] Schoch, P., Sargent, D. and Schwyzer, R. Hormone-receptor interactions: corticotropin-(1-24)-tetracosapeptide spans artificial lipid-bilayer membranes. *Biochem. Soc. Trans.*, **1979**, 7, 846.
- [514] Bader, R., Bettio, A., Beck-Sickinger, A. G. and Zerbe, O. Structure and dynamics of micelle-bound neuropeptide Y: comparison with unligated NPY and implications for receptor selection. *J. Mol. Biol.*, **2001**, 305, 307.
- [515] Bader, R., Rytz, G., Lerch, M., Beck-Sickinger, A. G. and Zerbe, O. Key motif to gain selectivity at the Neuropeptide Y5-receptor: structure and dynamics of micelle-bound [Ala31, Pro32]-NPY. *Biochemistry*, **2002**, 41, 8031-8042.
- [516] Bader, R. and Zerbe, O. Are Hormones from the Neuropeptide Y Family Recognized by Their Receptors from the Membrane-Bound State? *ChemBioChem*, **2005**, 6, 1520-1534.
- [517] Lerch, M., Gafner, V., Bader, R., Christen, B., Folkers, G. and Zerbe, O. Bovine pancreatic polypeptide (bPP) undergoes significant changes in conformation and dynamics upon binding to DPC micelles. *J. Mol. Biol.*, **2002**, 322, 1117-1133.
- [518] Lerch, M., Kamimori, H., Folkers, G., Aguilar, M.-I., Beck-Sickinger, A. G. and Zerbe, O. Strongly altered receptor binding properties in PP and NPY chimeras are accompanied by changes in structure and membrane binding. *Biochemistry*, **2005**, 44, 9255-9264.
- [519] Lerch, M., Mayrhofer, M. and Zerbe, O. Structural similarities of micelle-bound peptide YY (PYY) and neuropeptide Y (NPY) are related to their affinity profiles at the Y receptors. *J. Mol. Biol.*, **2004**, 339, 1153-1168.
- [520] Zdobinsky, T., Scherkenbeck, J., Zerbe, O., Antonicek, H. and Chen, H. Structures of Micelle-Bound Selected Insect Neuropeptides and Analogues: Implications for Receptor Selection. *ChemBioChem*, **2009**, 10, 2644-2653.
- [521] Blondelle, S. E., Lohner, K. and Aguilar, M.-I. Lipid-induced conformation and lipid-binding properties of cytolytic and antimicrobial peptides: determination and biological specificity. *Biochim. Biophys. Acta.*, **1999**, 1462, 89-108.
- [522] de Jongh, H. H., Goormaghtigh, E. and Killian, J. A. Analysis of circular dichroism spectra of oriented protein-lipid complexes: toward a general application. *Biochemistry*, **1994**, 33, 14521-14528.
- [523] Picard, F., Paquet, M.-J., DuFourc, E. J. and Auger, M. Measurement of the lateral diffusion of dipalmitoylphosphatidylcholine adsorbed on silica beads in the absence and presence of melittin: a ³¹P twodimensional exchange solid state NMR study. *Biophys. J.*, **1998**, 74, 857-868.
- [524] Haris, P. I. and Chapman, D. The conformational analysis of peptides using Fourier transform IR spectroscopy. *Biopolymers*, **1995**, 37, 251-263.
- [525] Mingeot-Leclercq, M.-P., Deleu, M., Brasseur, R. and Dufrêne, Y. F. Atomic force microscopy of supported lipid bilayers. *Nat. Protoc.*, **2008**, 3, 1654-1659.

- [526] Mozsolits, H. and Aguilar, M. I. Surface plasmon resonance spectroscopy: an emerging tool for the study of peptide–membrane interactions. *J. Pept. Sci.*, **2002**, 66, 3-18.
- [527] Erspamer, V., Bioactive secretions of the amphibian integument, in *Amphibian Biology. The Integument*,(ed. by Heatwole, H. and Bartholameus, G.), Chipping Norton, N. S. W., Beatty and Sons, **1994**, pp. 178-350.
- [528] Maselli, V. M., Bilusich, D., Bowie, J. H. and Tyler, M. J. Host-defence skin peptides of the Australian Streambank Froglet *Crinia riparia*: isolation and sequence determination by positive and negative ion electrospray mass spectrometry. *Rapid Commun. Mass Spectrom.*, **2006**, 20, 797-803.
- [529] Maselli, V. M., Brinkworth, C. S., Bowie, J. H. and Tyler, M. J. Host-defence skin peptides of the Australian Common Froglet *Crinia signifera*: sequence determination using positive and negative ion electrospray mass spectra. *Rapid Commun. Mass Spectrom.*, **2004**, 18, 2155-2161.
- [530] Brinkworth, C. S., Bowie, J. H., Bilusich, D. and Tyler, M. J. The rothein peptides from the skin secretion of Roth's tree frog *Litoria rothii*. Sequence determination using positive and negative ion electrospray mass spectrometry. *Rapid Commun. Mass Spectrom.*, **2005**, 19, 2716-2724.
- [531] Erspamer, V., Negri, L., Erspamer, G. F. and Endean, R. Uperolein and other active peptides in the skin of the Australian leptodactylid frogs *Uperoleia* and *Taudactylus*. *Naunyn-Schmiedeberg's Arch. Pharmacol.*, **1975**, 289, 41-54.
- [532] Bradford, A. M., Raftery, M. J., Bowie, J. H., Tyler, M. J., Wallace, J. C., Adams, G. W. and Severini, C. Novel uperin peptides from the dorsal glands of the Australian floodplain toadlet *Uperoleia inundata*. *Aust. J. Chem.*, **1996**, 49, 475-484.
- [533] Ellis-Steinborner, S. T., Scanlon, D., Musgrave, I. F., Tran, T. T., Hack, S., Wang, T., Abell, A. D., Tyler, M. J. and Bowie, J. H. An unusual kynurenine-containing opioid tetrapeptide from the skin gland secretion of the Australian red tree frog *Litoria rubella*. Sequence determination by electrospray mass spectrometry. *Rapid Commun. Mass Spectrom.*, **2011**, 25, 1735-1740.
- [534] Jackway, R. J., Pukala, T. L., Maselli, V. M., Musgrave, I. F., Bowie, J. H., Liu, Y., Surinya-Johnson, K. H., Donnellan, S. C., Doyle, J. R. and Llewellyn, L. E. Disulfide-containing peptides from the glandular skin secretions of froglets of the genus *Crinia*: structure, activity and evolutionary trends. *Regul. peptides*, **2008**, 151, 80.
- [535] Sherman, P. J., Jackway, R. J., Nicholson, E., Musgrave, I. F., Boontheung, P. and Bowie, J. H. Activities of seasonably variable caerulein and rothein skin peptides from the tree frogs *Litoria splendida* and *Litoria rothii*. *Toxicon*, **2009**, 54, 828-835.
- [536] Calabrese, A. N., Markulic, K., Musgrave, I. F., Guo, H., Zhang, L. and Bowie, J. H. Structural and activity changes in three bioactive anuran peptides when Asp is replaced by isoAsp. *Peptides*, **2012**.

- [537] Severini, C., Salvadori, S., Guerrini, R., Falconieri-Erspamer, G., Mignogna, G. and Erspamer, V. Parallel bioassay of 39 tachykinins on 11 smooth muscle preparations. Structure and receptor selectivity/affinity relationship. *Peptides*, **2000**, 21, 1587-1595.
- [538] Shai, Y. Mode of action of membrane active antimicrobial peptides. *Pept. Sci.*, **2002**, 66, 236-248.
- [539] Yeaman, M. R. and Yount, N. Y. Mechanisms of antimicrobial peptide action and resistance. *Pharmacol. Rev.*, **2003**, 55, 27-55.
- [540] Bieri, C., Ernst, O. P., Heyse, S., Hofmann, K. P. and Vogel, H. Micropatterned immobilization of a G protein-coupled receptor and direct detection of G protein activation. *Nat. Biotechnol.*, **1999**, 17, 1105-1108.
- [541] Chan, Y.-H. M. and Boxer, S. G. Model membrane systems and their applications. *Curr. Opin. Chem. Biol.*, **2007**, 11, 581-587.
- [542] Kung, L. A., Kam, L., Hovis, J. S. and Boxer, S. G. Patterning hybrid surfaces of proteins and supported lipid bilayers. *Langmuir*, **2000**, 16, 6773-6776.
- [543] Lee, T.-H. and Aguilar, M.-I. Trends in the development and application of functional biomembrane surfaces. *Biotechnol. Annu. Rev.*, **2006**, 12, 85-136.
- [544] Salafsky, J., Groves, J. T. and Boxer, S. G. Architecture and function of membrane proteins in planar supported bilayers: a study with photosynthetic reaction centers. *Biochemistry*, **1996**, 35, 14773-14781.
- [545] Sapuri, A. R., Baksh, M. M. and Groves, J. T. Electrostatically targeted intermembrane lipid exchange with micropatterned supported membranes. *Langmuir*, **2003**, 19, 1606-1610.
- [546] Brian, A. A. and McConnell, H. M. Allogeneic stimulation of cytotoxic T cells by supported planar membranes. *Proc. Natl. Acad. Sci. USA*, **1984**, 81, 6159-6163.
- [547] Keller, C., Glasmästar, K., Zhdanov, V. and Kasemo, B. Formation of supported membranes from vesicles. *Phys. Rev. Lett.*, **2000**, 84, 5443-5446.
- [548] Rädler, J., Strey, H. and Sackmann, E. Phenomenology and kinetics of lipid bilayer spreading on hydrophilic surfaces. *Langmuir*, **1995**, 11, 4539-4548.
- [549] Richter, R., Mukhopadhyay, A. and Brisson, A. Pathways of lipid vesicle deposition on solid surfaces: a combined QCM-D and AFM study. *Biophys. J.*, **2003**, 85, 3035-3047.
- [550] Reimhult, E., Hook, F. and Kasemo, B. Vesicle adsorption on SiO₂ and TiO₂: Dependence on vesicle size. *J. Chem. Phys.*, **2002**, 117, 7401-7404.
- [551] Reimhult, E., Höök, F. and Kasemo, B. Intact vesicle adsorption and supported biomembrane formation from vesicles in solution: influence of surface chemistry, vesicle size, temperature, and osmotic pressure. *Langmuir*, **2003**, 19, 1681-1691.

- [552] Richter, R. P., Bérat, R. and Brisson, A. R. Formation of solid-supported lipid bilayers: an integrated view. *Langmuir*, **2006**, 22, 3497-3505.
- [553] Johnson, J. M., Ha, T., Chu, S. and Boxer, S. G. Early steps of supported bilayer formation probed by single vesicle fluorescence assays. *Biophys. J.*, **2002**, 83, 3371-3379.
- [554] Jiang, F. Y., Bouret, Y. and Kindt, J. T. Molecular dynamics simulations of the lipid bilayer edge. *Biophys. J.*, **2004**, 87, 182-192.
- [555] Kasson, P. M. and Pande, V. S. Molecular dynamics simulation of lipid reorientation at bilayer edges. *Biophys. J.*, **2004**, 86, 3744-3749.
- [556] Reviakine, I. and Brisson, A. Formation of supported phospholipid bilayers from unilamellar vesicles investigated by atomic force microscopy. *Langmuir*, **2000**, 16, 1806-1815.
- [557] Richter, R. P. and Brisson, A. R. Following the formation of supported lipid bilayers on mica: a study combining AFM, QCM-D, and ellipsometry. *Biophys. J.*, **2005**, 88, 3422-3433.
- [558] Zhdanov, V., Keller, C., Glasmästar, K. and Kasemo, B. Simulation of adsorption kinetics of lipid vesicles. *J. Chem. Phys.*, **2000**, 112, 900.
- [559] Cha, T., Guo, A. and Zhu, X.-Y. Formation of supported phospholipid bilayers on molecular surfaces: role of surface charge density and electrostatic interaction. *Biophys. J.*, **2006**, 90, 1270-1274.
- [560] Cremer, P. S. and Boxer, S. G. Formation and spreading of lipid bilayers on planar glass supports. *J. Phys. Chem. B*, **1999**, 103, 2554-2559.
- [561] Nollert, P., Kiefer, H. and Jähnig, F. Lipid vesicle adsorption versus formation of planar bilayers on solid surfaces. *Biophys. J.*, **1995**, 69, 1447-1455.
- [562] Mechler, A., Praporski, S., Piantavigna, S., Heaton, S. M., Hall, K. N., Aguilar, M.-I. and Martin, L. L. Structure and homogeneity of pseudo-physiological phospholipid bilayers and their deposition characteristics on carboxylic acid terminated self-assembled monolayers. *Biomaterials*, **2009**, 30, 682-689.
- [563] Lasic, D. D., Liposomes in gene delivery. CRC press, **1997**.
- [564] Olsson, U. and Wennerström, H. On the ripening of vesicle dispersions. *J. Phys. Chem. B*, **2002**, 106, 5135-5138.
- [565] Cho, N.-J., Frank, C. W., Kasemo, B. and Höök, F. Quartz crystal microbalance with dissipation monitoring of supported lipid bilayers on various substrates. *Nat. Protoc.*, **2010**, 5, 1096-1106.
- [566] Reviakine, I., Simon, A. and Brisson, A. Effect of Ca^{2+} on the morphology of mixed DPPC-DOPS supported phospholipid bilayers. *Langmuir*, **2000**, 16, 1473-1477.

- [567] Beneš, M., Billy, D., Benda, A., Speijer, H., Hof, M. and Hermens, W. T. Surface-dependent transitions during self-assembly of phospholipid membranes on mica, silica, and glass. *Langmuir*, **2004**, 20, 10129-10137.
- [568] Ekeröth, J., Konradsson, P. and Höök, F. Bivalent-ion-mediated vesicle adsorption and controlled supported phospholipid bilayer formation on molecular phosphate and sulfate layers on gold. *Langmuir*, **2002**, 18, 7923-7929.
- [569] Cho, W. Membrane targeting by C1 and C2 domains. *J. Biol. Chem.*, **2001**, 276, 32407-32410.
- [570] Das, S., Dixon, J. E. and Cho, W. Membrane-binding and activation mechanism of PTEN. *Proc. Natl. Acad. Sci. U. S. A.*, **2003**, 100, 7491-7496.
- [571] DiNitto, J. P., Cronin, T. C. and Lambright, D. G. Membrane recognition and targeting by lipid-binding domains. *Sci. Signal.*, **2003**, 2003, re16.
- [572] Kutateladze, T. G., Capelluto, D. G., Ferguson, C. G., Cheever, M. L., Kutateladze, A. G., Prestwich, G. D. and Overduin, M. Multivalent mechanism of membrane insertion by the FYVE domain. *J. Biol. Chem.*, **2004**, 279, 3050-3057.
- [573] Ladokhin, A. S. and White, S. H. Protein chemistry at membrane interfaces: non-additivity of electrostatic and hydrophobic interactions. *J. Mol. Biol.*, **2001**, 309, 543-552.
- [574] McLaughlin, S. The electrostatic properties of membranes. *Annu. Rev. Biophys. Biophys. Chem.*, **1989**, 18, 113-136.
- [575] Murray, D., Arbuzova, A., Hangyás-Mihályiné, G., Gambhir, A., Ben-Tal, N., Honig, B. and McLaughlin, S. Electrostatic properties of membranes containing acidic lipids and adsorbed basic peptides: theory and experiment. *Biophys. J.*, **1999**, 77, 3176-3188.
- [576] Mulgrew-Nesbitt, A., Diraviyam, K., Wang, J., Singh, S., Murray, P., Li, Z., Rogers, L., Mirkovic, N. and Murray, D. The role of electrostatics in protein-membrane interactions. *Biochim. Biophys. Acta.*, **2006**, 1761, 812-826.
- [577] Sharp, K. A. and Honig, B. Electrostatic interactions in macromolecules: theory and applications. *Annu. Rev. Biophys. Biophys. Chem.*, **1990**, 19, 301-332.
- [578] Honig, B. and Nicholls, A. Classical electrostatics in biology and chemistry. *Science*, **1995**, 268, 1144-1149.
- [579] Davis, M. E. and McCammon, J. A. Electrostatics in biomolecular structure and dynamics. *Chem. Rev.*, **1990**, 90, 509-521.
- [580] White, S. H. and Wimley, W. C. Hydrophobic interactions of peptides with membrane interfaces. *Biochim. Biophys. Acta.*, **1998**, 1376, 339-352.
- [581] Wimley, W. C. and White, S. H. Experimentally determined hydrophobicity scale for proteins at membrane interfaces. *Nat. Struct. Biol.*, **1996**, 3, 842-848.

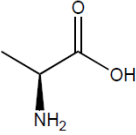
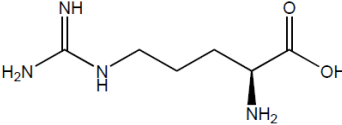
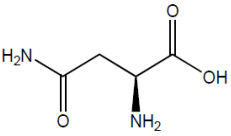
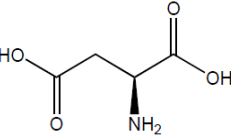
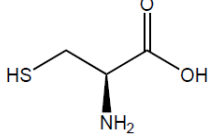
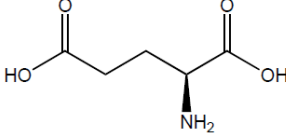
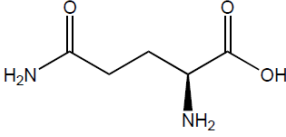
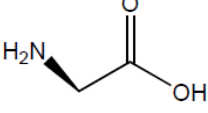
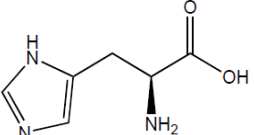
- [582] de Planque, M. R., Kruijtzter, J. A., Liskamp, R. M., Marsh, D., Greathouse, D. V., Koepe, R. E., de Kruijff, B. and Killian, J. A. Different membrane anchoring positions of tryptophan and lysine in synthetic transmembrane α -helical peptides. *J. Biol. Chem.*, **1999**, 274, 20839-20846.
- [583] Killian, J. A. and von Heijne, G. How proteins adapt to a membrane–water interface. *Trends in biochem. Sci.*, **2000**, 25, 429-434.
- [584] Strandberg, E., Morein, S., Rijkers, D. T., Liskamp, R. M., van der Wel, P. C. and Killian, J. A. Lipid dependence of membrane anchoring properties and snorkeling behavior of aromatic and charged residues in transmembrane peptides. *Biochemistry*, **2002**, 41, 7190-7198.
- [585] Buttry, D. A. and Ward, M. D. Measurement of interfacial processes at electrode surfaces with the electrochemical quartz crystal microbalance. *Chem. Rev.*, **1992**, 92, 1355-1379
- [586] Goka, S., Okabe, K., Watanabe, Y. and Sekimoto, H. Multimode quartz crystal microbalance. *Jpn. J. Appl. Phys.*, **2000**, 39, 3073.
- [587] Martin, S. J., Granstaff, V. E. and Frye, G. C. Characterization of a quartz crystal microbalance with simultaneous mass and liquid loading. *Am. Chem. Soc.*, **1991**, 63, 2272-2281.
- [588] Wegener, J., Janshoff, A. and Steinem, C. The quartz crystal microbalance as a novel means to study cell-substrate interactions in situ. *Cell Biochem. Biophys.*, **2001**, 34, 121-151.
- [589] Sauerbrey, G. The use of quartz oscillators for weighing thin layers and for microweighing. *Z Phys.*, **1959**, 155.
- [590] Nomura, T. and Okuhara, M. Frequency shifts of piezoelectric quartz crystals immersed in organic liquids. *Anal. Chim. Acta.*, **1982**, 142, 281-284.
- [591] Bailey, C. A., Fiebor, B., Yen, W., Vodyanoy, V., Cernosek, R. V. and Chin, B. A. Thickness shear mode (TSM) resonators used for biosensing. *Proc.*, **2002**, 4575, 138-149.
- [592] Behling, C., Lucklum, R. and Hauptmann, P. Possibilities and limitations in quantitative determination of polymer shear parameters by TSM resonators. *Sensor. Actuat. A*, **1997**, 61, 260–266.
- [593] Kanazawa, K. K. and Gordon, J. G. Frequency of a quartz microbalance in contact with liquids. *Anal. Chem.*, **1985**, 57, 1770-1771.
- [594] Voinova, M. V., Jonson, M. and Kasemo, B. ‘Missing mass’ effect in biosensor’s QCM applications. *Biosens. Bioelectron.*, **2002**, 17, 835-841.
- [595] Martin, S. J., Frye, G. G. and Rico, A. J. Effect of surface roughness on the response of thickness-shear mode resonators in liquids. *Anal. Chem.*, **1993**, 65, 2910-2922.

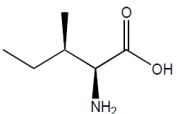
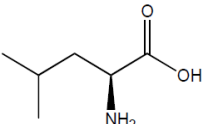
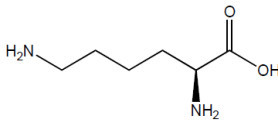
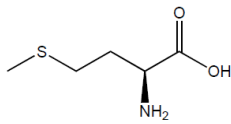
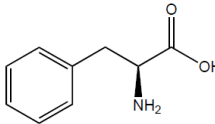
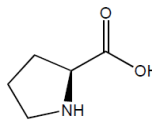
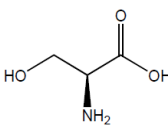
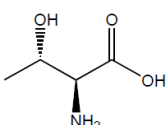
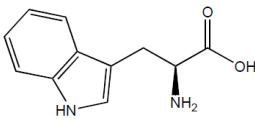
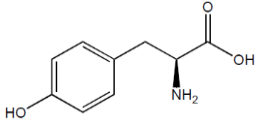
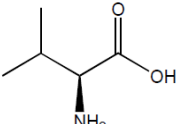
- [596] Ferrante, F., Kipling, A. L. and Thompson, M. Molecular slip at the solid-liquid interface of an acoustic-wave sensor *Jour. Appl. Physiol.*, **1994**, 76, 3448–3462.
- [597] Voinova, M. V., Rodahl, M., Jonson, M. and Kasemo, B. Viscoelastic acoustic response of layered polymer films at fluid-solid interfaces: Continuum mechanics approach. *Physica. Scripta.*, **1999**, 59, 391.
- [598] Rodahl, M., Höök, F., Fredriksson, C., Keller, C. A., Krozer, A., Brzezinski, P., Voinova, M. and Kasemo, B. Simultaneous frequency and dissipation factor QCM measurements of biomolecular adsorption and cell adhesion. *Farad. Discuss.*, **1997**, 107, 229-246.
- [599] Arnau, A., Sogorb, T. and Jimenez, Y. Circuit for continuous motional series resonant frequency and motional resistance monitoring of quartz crystal resonators by parallel capacitance compensation. *Rev. Sci. Instr.*, **2002**, 73, 2724- 2737.
- [600] Barnes, C. Development of quartz crystal oscillators for under-liquid sensing. *Sensor. Actuat. A*, **1991**, 29, 59-69.
- [601] Arnau, A. A Review of Interface Electronic Systems for AT-cut Quartz Crystal Microbalance Applications in Liquids. *Sensors*, **2008**, 8, 370-411.
- [602] Bandey, H. L., Martin, S. J. and Cemosek, R. W. Modelling the responses of thickness shear mode resonators under various loading conditions. *Anal. Chem.*, **1999**, 71, 2205- 2214.
- [603] Kanazawa, K. and Cho, N. J. Quartz Crystal Microbalance as a Sensor to Characterize Macromolecular Assembly Dynamics. *Sensors*, **2009**, 2009.
- [604] Kipling, A. L. and Thompson, M. Network analysis applied to liquid-phase acoustic wave sensors. *Anal. Chem.*, **1990**, 62, 1514-1519.
- [605] S.M. Yoon, N.J. Cho and K. Kanazawa. Analyzing spur-distorted impedance spectra for the QCM. *Sensors*, **2009**, 2009.
- [606] Rodahl, M., Hook, F., Krozer, A., Brzezinski, P. and Kasemo, B. Quartz crystal microbalance setup for frequency and Q-factor measurements in gaseous and liquid environments. *Rev. Sci. Instrum.*, **1995**, 66, 3924- 3930.
- [607] Rodahl, M. and Kasemo, B. A simple setup to simultaneously measure the resonant frequency and the absolute dissipation factor for a quartz crystal microbalance. *Rev. Sci. Instrum.*, **1996**, 67, 2338- 3240.
- [608] Mechler, A., Praporski, S., Atmuri, K., Boland, M., Separovic, F. and Martin, L. L. Specific and selective peptide-membrane interactions revealed using quartz crystal microbalance. *Biophys. J.*, **2007**, 93, 3907-3916.
- [609] Du, B. Y. and Johannsmann, D. Operation of the quartz crystal microbalance in liquids: derivation of the elastic compliance of a film from the ratio of bandwidth shift and frequency shift. *Langmuir*, **2004**, 20, 2809-2812.

- [610] Hook, F., Kasemo, B., Nylander, T., Fant, C., Sott, K. and Elwing, H. Variations in coupled water, viscoelastic properties and film thickness of a Mefp-1 protein film during adsorption and cross-linking: a quartz crystal microbalance with dissipation monitoring, ellipsometry and surface plasmon resonance study. *Anal. Chem.*, **2001**, 73, 5796-5804.
- [611] Wolff, O., Seydel, E. and Johannsmann, D. Viscoelastic properties of thin films studied with quartz crystal resonators. *Farad. Discuss.*, **1997**, 107, 91-104.
- [612] Mannock, D. A., Lewis, R. N., McMullen, T. P. and McElhaney, R. N. The effect of variations in phospholipid and sterol structure on the nature of lipid-sterol interactions in lipid bilayer model membranes. *Chem. Phys. Lipids*, **2010**, 163, 403-448.
- [613] Mannock, D. A., Lewis, R. N. and McElhaney, R. N. A calorimetric and spectroscopic comparison of the effects of ergosterol and cholesterol on the thermotropic phase behavior and organization of dipalmitoylphosphatidylcholine bilayer membranes. *Biochim. Biophys. Acta.*, **2010**, 1798, 376-388.
- [614] McMullen, T. P., Lewis, R. N. and McElhaney, R. N. Calorimetric and spectroscopic studies of the effects of cholesterol on the thermotropic phase behavior and organization of a homologous series of linear saturated phosphatidylglycerol bilayer membranes. *Biochim. Biophys. Acta.*, **2009**, 1788, 345-357.
- [615] Patrick. The isolation, structure and membrane interaction of biologically active peptide. PhD thesis. The University of Adelaide. **2012**, pp. 153-190.
- [616] Jing, Y., Trefna, H., Persson, M., Kasemo, B. and Svedhem, S. Formation of supported lipid bilayers on silica: relation to lipid phase transition temperature and liposome size. *Soft Matter*, **2014**, 10, 187-195.
- [617] McCubbin, G. A., Praporski, S., Piantavigna, S., Knappe, D., Hoffmann, R., Bowie, J. H., Separovic, F. and Martin, L. L. QCM-D fingerprinting of membrane-active peptides. *Eur. Biophys. J.*, **2011**, 40, 437-446.
- [618] Piantavigna, S., Czihal, P., Mechler, A., Richter, M., Hoffmann, R. and Martin, L. L. Cell penetrating apidaecin peptide interactions with biomimetic phospholipid membranes. *Int. J. Pept. Res. Ther.*, **2009**, 15, 139-146.
- [619] Dike, A. and Cowsik, S. M. Solution structure of amphibian tachykinin Uperolein bound to DPC micelles. *J. Struct. Biol.*, **2006**, 156, 442-452.
- [620] McIntosh, T. J. and Simon, S. A. Roles of bilayer material properties in function and distribution of membrane proteins. *Annu. Rev. Biophys. Biomol. Struct.*, **2006**, 35, 177-198.
- [621] Garcia, M. L. Ion channels: gate expectations. *Nature*, **2004**, 430, 153-155.
- [622] Sanderson, J. M. Peptide-lipid interactions: insights and perspectives. *Org. Biomol. Chem.*, **2005**, 3, 201-212.

APPENDIX

20 common amino acids

Amino acid Abbreviation	Structure	Integral Mass
Alanine		71
Ala/A		
Arginine		156
Arg/R		
Asparagine		114
Asn/N		
Aspartic acid		115
Asp/D		
Cysteine		103
Cys/C		
Glutamic acid		129
Glu/E		
Glutamine		128
Gln/Q		
Glycine		57
Gly/G		
Histidine		137
His/H		
Amino acid	Structure	Integral Mass

Abbreviation		
Isoleucine		113
Ileu/I		
Leucine		113
Leu/L		
Lysine		128
Lys/K		
Methionine		131
Met/M		
Phenylalanine		147
Phe/F		
Proline		97
Pro/P		
Serine		87
Ser/S		
Threonine		101
Thr/T		
Tryptophan		186
Trp/W		
Tyrosine		163
Tyr/Y		
Valine		99
Val/V		

PUBLICATIONS

1. T T N. Tran, T. Wang, S. Hack and J. H. Bowie. Fragmentations of $[M - H]^-$ anions of peptides containing Ser sulfate. A joint experimental and theoretical study. *Rapid Commun. Mass Spectrom.*, 2013 , 27, 2287-96.
2. T T N. Tran, T. Wang, S. Hack and J. H. Bowie. Fragmentations of $[M - H]^-$ anions of peptides containing tyrosine sulfate. Does the sulfate group rearrange? A joint experimental and theoretical study. *Rapid Commun. Mass Spectrom.*, 2013, 27,1135-1142.
3. T. Wang, T. T. N. Tran, A. N. Calabrese, J. H. Bowie. Backbone fragmentations of $[M-H]^-$ anions from peptides. Reinvestigation of the mechanism of the beta prime cleavage. *Rapid Commun. Mass Spectrom.*, 2012, 26, 1832-1840.
4. T. T. N. Tran, T. Wang, S. Hack, P. Hoffmann, J. H. Bowie. Can collision-induced negative-ion fragmentations of $[M-H]^-$ anions be used to identify phosphorylation sites in peptides? *Rapid Commun. Mass Spectrom.*, 2011, 25, 3537-3548.
5. T. Wang, T. T. N. Tran, D. Scanlon, H. J. Andrezza, A. D. Abell, J. H. Bowie. Diagnostic di- and triphosphate cyclisation in the negative ion electrospray mass spectra of phosphoSer peptides. *Rapid Commun. Mass Spectrom.*, 2011, 25, 2649-2656.
6. T. T. N. Tran, T. Wang, S. Hack, J. H. Bowie. Diagnostic cyclisation reactions which follow phosphate transfer to carboxylate anion centres for energised $[M-H]^-$ anions of pTyr-containing peptides. *Rapid Commun. Mass Spectrom.*, 2011, 25, 2489-99.
7. S. T. E. Steinborner, D. Scanlon, I. F. Musgrave, T. T. N. Tran, S. Hack, T. Wang, A. D. Abell, M. J. Tyler, J. H. Bowie. An unusual kynurenine-containing opioid tetrapeptide from the skin gland secretion of the Australian red tree frog *Litoria rubella*. Sequence determination by electrospray mass spectrometry. *Rapid Commun. Mass Spectrom.*, 2011, 25, 1735-1740.

Ellis-Steinborner, S.T., Scanlon, D., Musgrave, I.F., Tran, T.T.N., Hack, S., Wang, T., Abell, A.D.
Tyler, M.J. & Bowie, J.H. (2011) An unusual kynurenine-containing opioid tetrapeptide from the skin
gland secretion of the Australian red tree frog *Litoria rubella*. Sequence determination by electrospray
mass spectrometry.
Rapid Communications in Mass Spectrometry, v. 25(12), pp. 1735-1740

NOTE:

This publication is included on pages 252-257 in the print copy
of the thesis held in the University of Adelaide Library.

It is also available online to authorised users at:

<http://doi.org/10.1002/rcm.5041>

Tran, T.T.N., Wang, T., Hack, S. & Bowie, J.H. (2011) Diagnostic cyclisation reactions which follow phosphate transfer to carboxylate anion centres for energised [M-H]⁻ anions of pTyr-containing peptides.

Rapid Communications in Mass Spectrometry, v. 25(17), pp. 2489-2499

NOTE:

This publication is included on pages 258-268 in the print copy of the thesis held in the University of Adelaide Library.

It is also available online to authorised users at:

<http://doi.org/10.1002/rcm.5150>

Tran, T.T.N., Wang, T., Hack, S., Hoffmann, P. & Bowie, J.H. (2011) Can collision-induced negative-ion fragmentations of [M-H]⁻ anions be used to identify phosphorylation sites in peptides?. *Rapid Communications in Mass Spectrometry*, v. 25(23), pp. 3537-3548

NOTE:

This publication is included on pages 269-281 in the print copy of the thesis held in the University of Adelaide Library.

It is also available online to authorised users at:

<http://doi.org/10.1002/rcm.5261>

Wang, T., Tran, T.T.N., Calabrese, A.N. & Bowie, J.H. (2012) Backbone fragmentations of [M-H]⁻ anions from peptides. Reinvestigation of the mechanism of the beta prime cleavage. *Rapid Communications in Mass Spectrometry*, v. 26(16), pp. 1832-1840

NOTE:

This publication is included on pages 282-290 in the print copy of the thesis held in the University of Adelaide Library.

It is also available online to authorised users at:

<http://doi.org/10.1002/rcm.6297>

Wang, T., Tran, T.T.N., Scanlon, D., Andrezza, H.J., Abell, A.D. & Bowie, J.H. (2011) Diagnostic di- and triphosphate cyclisation in the negative ion electrospray mass spectra of phosphoSer peptides. *Rapid Communications in Mass Spectrometry*, v. 25(18), pp. 2649-2656

NOTE:

This publication is included on pages 291-298 in the print copy of the thesis held in the University of Adelaide Library.

It is also available online to authorised users at:

<http://doi.org/10.1002/rcm.5171>

Tran, T.T.N., Wang, T., Hack, S. & Bowie, J.H. (2013) Fragmentations of [M-H]⁻ anions of peptides containing tyrosine sulfate. Does the sulfate group rearrange? A joint experimental and theoretical study.

Rapid Communications in Mass Spectrometry, v. 27(10), pp. 1135-1142

NOTE:

This publication is included on pages 299-306 in the print copy of the thesis held in the University of Adelaide Library.

It is also available online to authorised users at:

<http://doi.org/10.1002/rcm.6547>

Tran, T.T.N., Wang, T., Hack, S. & Bowie, J.H. (2013) Fragmentations of [M-H]⁻ anions of peptides containing Ser sulfate. A joint experimental and theoretical study.
Rapid Communications in Mass Spectrometry, v. 27(21), pp. 2287-2296

NOTE:

This publication is included on pages 307-316 in the print copy of the thesis held in the University of Adelaide Library.

It is also available online to authorised users at:

<http://doi.org/10.1002/rcm.6686>